

*Science Applications International Corporation*

ANALYSIS OF FRACTURING MECHANISMS  
IN NATURALLY FRACTURED ROCKS  
FINAL REPORT

August 5, 1987

By:

T. L. Blanton  
T. W. Thompson  
K. L. Mann  
B. J. Zeigler

Submitted to:

Albert Yost  
U. S. Department of Energy  
Morgantown Energy Technical Center  
P. O. Box 880  
Morgantown, WV 26505

Contract Number: DE-AC21-83MC20289



Science Applications International Corporation 3349 South Highland Drive, Suite 403, Las Vegas, Nevada 89109

Albuquerque, Chicago, Dayton, Denver, Huntsville, Los Angeles, Oak Ridge, Orlando, San Diego, San Francisco, Tucson and Washington, D. C.

TABLE OF CONTENTS

Introduction.....	1
Task 1. Hydraulic/Natural Fracture Interaction.....	4
Objective.....	4
Work Performed.....	4
Scaling of Laboratory Experiments.....	4
Fracture Interaction Experiments.....	8
Fracture Interaction Criterion.....	18
Conclusions.....	24
Task 2. Dynamic/Natural Fracture Interaction.....	25
Objective.....	25
Work Performed.....	25
Charge Development.....	25
Interaction Tests.....	33
Conclusions.....	36
Task 3. Flow Characteristics of Natural Fractures.....	37
Objective.....	37
Work Performed.....	37
Core Examination.....	37
Permeability Testing.....	37
Experimental Results.....	39
Task 4. In Situ Stresses in the Appalachian Basin.....	56
Objective.....	56
Work Performed.....	56
State of Stress in the Appalachian Basin.....	56
Evaluation of Stress Measuring Techniques.....	58
Task 5. Tectonics of the Appalachian Basin.....	83
Objective.....	83
Work Performed.....	83
Tectonic Models: Existing Hypotheses.....	83
Natural Fracture System.....	85
Fracture Data.....	87
Tectonic Models: Plate Tectonics.....	91
Devonian Decollements.....	109
Current Regional Stress Field.....	114
Other Fracture Trends.....	114
Task 6. Induced/Natural Fracture Interaction In Devonian Shales of the Appalachian Basin.....	117
Objective.....	117
Limits Defined by Interaction Criteria.....	117
Application of Interaction Criterion in the Appalachian Basin.....	118

Appendix A.	Results of Hydraulic Fracture	
	Interaction Tests (Task 1).....	123
	Test PT-1.....	124
	Test PT-3.....	125
	Test PT-4.....	127
	Test PT-5.....	130
	Test PT-6.....	133
	Test PT-7.....	136
	Test PT-8.....	138
	Test PT-9.....	141
	Test PT-10.....	144
	Test PT-11.....	147
	Test PT-12.....	150
	Test PT-13.....	153
	Test PT-14.....	156
	Test PT-15.....	159
	Test PT-16.....	162
	Test PT-17.....	165
	Test PT-18.....	168
	Test PT-19.....	170
Appendix B.	Results of Dynamic Fracture Tests.....	172
	Solid Block Tests.....	173
	Test DB-1.....	175
	Test DB-2.....	177
	Test DB-3.....	178
	Test DB-4.....	180
	Test DB-5.....	182
	Test DB-6.....	184
	Test DB-7.....	186
	Split Block Tests.....	188
	Test DS-1.....	190
	Test DS-2.....	192
	Test DS-3.....	194
	Test DS-4.....	196
References.....		198

LIST OF FIGURES

FIGURE 0-1.	Interdependence of Three Major Task Areas.....	3
FIGURE 1-1.	Device Used to Initiate Fracture in Central Wellbore.....	9
FIGURE 1-2.	Vertical Cross Section of Triaxial Compression Apparatus.....	10
FIGURE 1-3.	Horizontal Cross Section of Triaxial Compression Apparatus.....	11
FIGURE 1-4.	Schematic Diagram of Hydraulic Fracturing Test System.....	12
FIGURE 1-5.	Typical Crossing Behavior.....	16
FIGURE 1-6.	Typical Opening Behavior.....	17
FIGURE 1-7.	Options for Hydraulic Fracture Growth in Presence of a Natural Fracture.....	19
FIGURE 1-8.	Comparison of Fracture Interaction Criterion with Experimental Results.....	22
FIGURE 1-9.	Sensitivity of Fracture Interaction Criterion to Variations in B.....	23
FIGURE 2-1.	Typical Pipe Test With Fracture Initiator Present	30
FIGURE 2-2.	Typical Pipe Test Without Fracture Initiator.....	30
FIGURE 2-3.	Fracture Running Parallel to Maximum Stress for Test DB-1.....	32
FIGURE 2-4.	Fracture Running Parallel to Minimum Stress for Test DB-6.....	32
FIGURE 2-5.	Fractures Near Mid-Plane for Test DS-2 Showing Pulverized Zone and Dynamic Fracture Parallel to Minimum Stress Intersecting Pre-Fracture.....	35
FIGURE 2-6.	Fractures at a Place Four Inches Between the Center for Test DS-2.....	35
FIGURE 3-1.	Schematic Diagram of Pulse-Decay Gas Permeameter.	38
FIGURE 3-2.	Test K-1. Raw Data.....	45
FIGURE 3-3.	Test K-1. Comparison of Measured and Calculated Values.....	47

FIGURE 3-4.	Test K-1. Comparison of Measured and Calculated Values.....	48
FIGURE 3-5.	Test K-7. Raw Data.....	49
FIGURE 3-6.	Test K-7. Comparison of Measured and Calculated Values.....	50
FIGURE 3-7.	Test K-9. Raw Data.....	51
FIGURE 3-8.	Test K-9. Comparison of Measured and Calculated Values.....	52
FIGURE 3-9.	Test K-10 Flow Rate Determination.....	53
FIGURE 3-10.	Test K-11 Flow Rate Determination.....	55
FIGURE 4-1.	Directions of Maximum Horizontal Stress.....	57
FIGURE 4-2.	Differential Stresses.....	59
FIGURE 5-1.	Relation Between Principal Stress Directions and Orientations of Extension and Shear Fractures....	86
FIGURE 5-2.	Rose Diagram of Orientations of Type One and Two Fracture Sets.....	86
FIGURE 5-3.	Location of Different Fracture Sets on a Typical Fold.....	89
FIGURE 5-4.	All Fracture Orientations from EGSP Wells.....	90
FIGURE 5-5.	Dominant Fracture Trends.....	102
FIGURE 5-6.	Dominant Trends of High Angle Faults.....	103
FIGURE 5-7.	Stratigraphic Distribution of Low Angle Faults...	104
FIGURE 5-8.	Evidence for a Failed Rift System.....	107
FIGURE 5-9.	Fractures and Faults That May Be Associated with the Failed Rift System.....	108
FIGURE 5-10.	Model of a Decollement.....	110
FIGURE 5-11.	Construction of Devonian Shale Decollement.....	111
FIGURE 5-12.	Devonian Shale Decollement.....	112
FIGURE 5-13.	Fractures and Faults That May Be Associated with the Appalachian Orogeny.....	113
FIGURE 5-14.	Fractures and Faults That May Be Associated with the Current Stress Field.....	115

FIGURE 5-15.	Fractures and Faults Not Clearly Associated with Any of the Tectonic Features Discussed.....	116
FIGURE 6-1.	Number of Fractures with Type I and II Orientations, and Boundaries of Type I and II Regions.....	120
FIGURE 6-2.	Domain of the Failed Rift System Divided into Type I and II Regions.....	121
FIGURE 6-3.	Domain of Appalachian Orogeny Divided into Type I and II Regions.....	122
FIGURE A-1.	Solid Block Test PT-3 Showing "Shut-In Rings"....	126
FIGURE A-2.	Interaction Test PT-4.....	128
FIGURE A-3.	Pressure Time Record for Test PT-4.....	129
FIGURE A-4.	Interaction Test PT-5.....	131
FIGURE A-5.	Pressure Time Record for Test PT-5.....	132
FIGURE A-6.	Interaction Test PT-6.....	134
FIGURE A-7.	Pressure Time Record for Test PT-6.....	135
FIGURE A-8.	Pressure Time Record for Test PT-7.....	137
FIGURE A-9.	Interaction Test PT-8.....	139
FIGURE A-10.	Pressure Time Record for Test PT-8.....	140
FIGURE A-11.	Interaction Test PT-9.....	142
FIGURE A-12.	Pressure Time Record for Test PT-9.....	143
FIGURE A-13.	Interaction Test PT-10.....	145
FIGURE A-14.	Pressure Time Record for Test PT-10.....	146
FIGURE A-15.	Interaction Test PT-11.....	148
FIGURE A-16.	Pressure Time Record for Test PT-11.....	149
FIGURE A-17.	Interaction Test PT-12.....	151
FIGURE A-18.	Pressure Time Record for Test PT-12.....	152
FIGURE A-19.	Interaction Test PT-13.....	154
FIGURE A-20.	Pressure Time Record for Test PT-13.....	155
FIGURE A-21.	Interaction Test PT-14.....	157

FIGURE A-22.	Pressure Time Record for Test PT-14.....	158
FIGURE A-23.	Interaction Test PT-15.....	160
FIGURE A-24.	Pressure Time Record for Test PT-15.....	161
FIGURE A-25.	Interaction Test PT-16.....	163
FIGURE A-26.	Pressure Time Record for Test PT-16.....	164
FIGURE A-27.	Interaction Test PT-17.....	166
FIGURE A-28.	Pressure Time Record for Test PT-17.....	167
FIGURE A-29.	Solid Block Test PT-18 Showing Extension of Hydraulic Fracture From an Open Hole After Initial Breakdown.....	169
FIGURE A-30.	Solid Block Test PT-19 Showing Extension of Hydraulic Fracture from a Paddle After Initial Breakdown.....	171
FIGURE B-1.	Test DB-1.....	176
FIGURE B-2.	Test DB-3.....	179
FIGURE B-3.	Test DB-4.....	181
FIGURE B-4.	Test DB-5.....	183
FIGURE B-5.	Test DB-6.....	185
FIGURE B-6.	Test DB-7.....	187
FIGURE B-7A.	Test DS-1.....	191
FIGURE B-7B.	Test DS-1.....	191
FIGURE B-8A.	Test DS-2.....	193
FIGURE B-8B.	Test DS-2.....	193
FIGURE B-9A.	Test DS-3.....	195
FIGURE B-9B.	Test DS-3.....	195
FIGURE B-10.	Test DS-4.....	197

LIST OF TABLES

TABLE 1-1.	Results of Mechanical Property Tests.....	7
TABLE 1-2.	Initial Test Matrix.....	14
TABLE 1-3.	Results of Fracture Interaction Tests.....	15
TABLE 2-1.	Pipe Tests.....	28
TABLE 2-2.	Block Tests.....	31
TABLE 2-3.	Interaction Tests.....	34
TABLE 3-1.	Permeability Tests.....	43
TABLE 3-2.	Permeability Results.....	44
TABLE 4-1.	Critical Stress Ratios Above Which the Well- bore Diameter Will Increase with Time.....	80
TABLE 5-1.	Kentucky Core Data.....	92
TABLE 5-2.	New York Core Data.....	93
TABLE 5-3.	Ohio Core Data.....	94
TABLE 5-4.	Pennsylvania Core Data.....	97
TABLE 5-5.	Tennessee and Virginia Core Data.....	99
TABLE 5-6.	West Virginia Core Data.....	100
TABLE 5-7.	Tectonic History of Appalachian Basin.....	105
TABLE 6-1.	Division of Fracture Systems into Type I and II Areas.....	119
TABLE B-1.	Block Tests.....	174
TABLE B-2.	Interaction Tests.....	189

## INTRODUCTION

This project was motivated by a desire to reduce the gap between potential and actual gas production from Devonian Shales in the Appalachian Basin. Estimates are difficult to make, but the drillable resource is usually considered to be between thirty and fifty times the reserves that are recoverable using conventional methods. The magnitude of the gap becomes apparent only when one considers that most estimates of the drillable resource are in excess of one thousand TCF. (See e.g., Mound, 1982.).

One way of increasing the part of the resource that can be counted as recoverable reserves is by tapping a larger portion of the reservoir through fractures induced by well stimulation. This is important since production from the shales is controlled by diffusion of the gas through the matrix to free surfaces (for example, fractures or wellbores). Fracturing a well increases the production rate not only by creating a new surface area to which the gas can migrate, but also by connecting the potentially much larger pre-existing surface area of the natural fractures to the wellbore.

In order to be most effective, fractures induced by well stimulation should cross and connect as much of the natural fracture system to the wellbore as possible. In many cases, however, natural fractures can arrest and divert the induced fractures, thus limiting the degree of connection to the natural fracture system. In an effort to improve well stimulation, a variety of techniques have been developed and promoted, but no single one has emerged as the best for Devonian shale reservoirs. It is likely that in different parts of the basin varying in situ conditions are producing different types of induced/natural fracture interactions, favorable in some areas but not in others. What is needed is a rational basis for predicting what types of interactions can be expected for different treatments in different parts of the basin.

The overall goal of this project was to provide a basis for selecting fracturing treatments that give the most constructive interaction with the natural fracture system. In order to achieve this goal the proposed program was divided into three general work areas, as illustrated in Figure 0-1. The first of these areas was concerned with understanding the induced/natural fracture interaction process. Fractures induced hydraulically and dynamically were treated in Tasks 1 and 2, respectively. The second work area which is comprised of Tasks 3, 4, and 5, was concerned with methods of predicting or measuring the conditions that determine the type of interaction that will occur. In Task 3 experimental work was attempted which would form a basis for identifying those fracture sets that provide essential reservoir permeability and with which the induced fractures should interact. In Task 4 the in situ stress data required for applying the results of the first three experimental studies to particular field situation was collected and analyzed. In Task 5 a tectonic model has been developed

as a basis for extrapolating and/or interpolating site-specific data on in situ stresses and fracture systems. The third work area, covered by Task 6, synthesized the results from the first two areas in a way that will allow prediction of the type of induced/natural fracture interaction on an area-by-area basis throughout the Appalachian Basin.

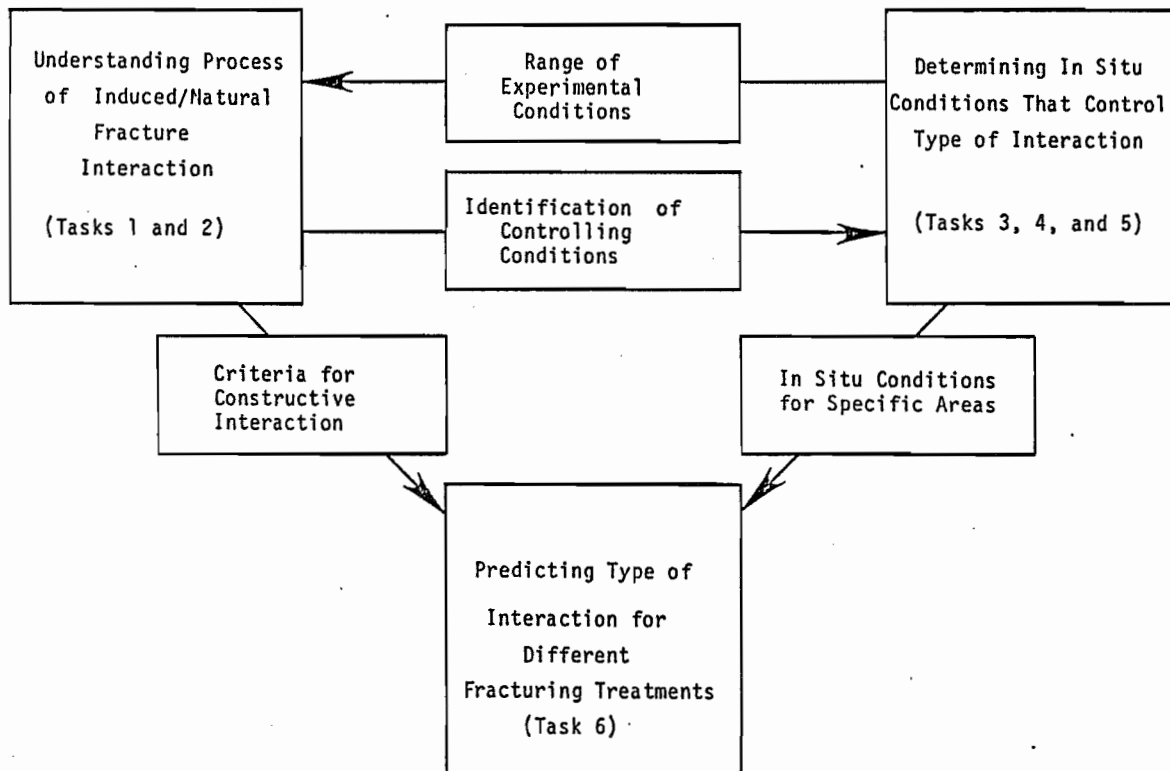


FIGURE O-1. Interdependence of three major task areas.

## TASK 1. HYDRAULIC/NATURAL FRACTURE INTERACTION

### OBJECTIVE

The objective of this task was to perform scaled laboratory experiments from which criteria could be developed for predicting the type of interaction which would occur between hydraulically induced and natural fractures.

### WORK PERFORMED

Dimensional analysis has been performed as a basis for scaling the laboratory experiments. The resulting dimensionless groups were used to select a material for laboratory testing whose properties are appropriate for modeling field situations in Devonian Shales. Fracture interaction experiments have been run in a triaxial compression apparatus capable of placing a 12x12x15-inch block under triaxial states of stress of up to 3000 psi. A series of tests has been run in which blocks were stressed and a hydraulic fracture was propagated from a central 1/8-inch hole toward pre-existing fractures three inches on either side of the hole. In this way the type of interaction for different states of stress and angles of approach was observed and recorded. Based on these results, interaction criteria have been developed.

### SCALING OF LABORATORY EXPERIMENTS

Dimensional analysis forms the basis for selecting appropriate test variables for laboratory experiments so that the results can be scaled to the field. The generalized approach to dimensional analysis is through the Buckingham "PI" Theorem, which states that if there are  $n$  dimensional variables in a dimensionally homogeneous equation, described by  $m$  fundamental dimensions, then the equation can be expressed as a relation between  $(n-m)$  dimensionless groups.

Dimensional analysis has been performed on fracture interaction equations developed as part of an earlier DOE-sponsored project (Blanton, 1982). The dimensional terms in these equations are listed with their fundamental dimensions below:

Term	Fundamental Dimension
$\Delta\sigma$	$ML^{-1}T^{-2}$
E	$ML^{-1}T^{-2}$
G	$MT^{-2}$
L	L

where  $\Delta\sigma$  is differential stress, E is Young's modulus, G is strain energy release rate, L is length (or, in particular, the distance between the wellbore and the pre-existing fracture), M is mass, and T is time. In this case there are four dimensionless variables and only two fundamental dimensions since M and T never appear independent of each other, and thus act together as a single fundamental dimension,  $MT^{-2}$ . According to the "PI" Theorem we should be able to form two dimensionless groups from the dimensional terms.

First, a general equation is written with the products of powers of the four dimensional terms, as follows:

$$\Delta\sigma^a E^b G^c L^d = F \quad (1-1)$$

where F is a function of dimensionless terms such as Poisson's ratio, coefficient of friction, and angle of approach. The dimensions of the left side of equation (1-1) are as follows:

$$\left(\frac{M}{LT^2}\right)^a \left(\frac{M}{LT^2}\right)^b \left(\frac{M}{T^2}\right)^c L^d$$

or

$$\left(\frac{M}{T^2}\right)^{a+b+c} (L)^{-a-b+d}$$

The problem now is to find exponents that will make the left side of equation (1-1) dimensionless. This condition is met when:

$$a + b + c = 0$$

$$a + b - d = 0$$

Solving these equations for b and c and substituting the results in equation (1-1) yields:

$$\left(\frac{\Delta\sigma}{E}\right)^a \left(\frac{EL}{G}\right)^d = F \quad (1-2)$$

This is equivalent to the equations in Blanton (1982) when  $a/d = 2$ .

The dimensionless fracture interaction equation (1-2) can be reformulated in terms of the critical mode-I stress intensity factor,  $K_{IC}$ , rather than the strain energy release rate. The new equation is as follows:

$$\left(\frac{\Delta\sigma}{E}\right)^a \left(\frac{E^2 L}{K_{IC}^2}\right)^d = F \quad (1-3)$$

In order to choose laboratory materials characterization of potential model materials has been carried out. This involved running twenty-eight triaxial compression tests for elastic properties and thirteen burst tests for determining fracture toughness. Seven different materials were examined: hydrostone (HS), hydrocal (HC), ceramical (CC), hydrostone plus 60-mesh sand (HSS), hydrocal plus 60-mesh sand (HCS), hydrocal plus 90-mesh sand, and ceramical plus 60-mesh sand (CCS).

The results of the material characterization tests are shown in Table 1-1. The material that best models Devonian shale for our purposes is the one with the highest  $E/K_{IC}$  ratio since this will give us the lowest model length,  $L$ . As can be seen in the table, this is hydrostone, which has been used on all subsequent tests. The values shown in Table 1-1 can be used to calculate the wellbore-to-natural-fracture distance in the field that is effectively being modeled by the 3-inch distance used in the laboratory. Thus, the second term in Equation 1-3 must be equivalent for the field and the laboratory, which results in the following equation:

$$\begin{aligned} L_D &= \left(\frac{K_D}{E_D}\right)^2 \left(\frac{E_H}{K_H}\right)^2 L_H \\ &= \frac{26.41 \times 10^7}{.91 \times 10^7} \times 3 = 87" = 7.26' \end{aligned}$$

Where the subscript D refers to field applications for Devonian Shale and H refers to laboratory tests with hydrostone.

TABLE 1-1  
RESULTS OF MECHANICAL PROPERTY TESTS

MATERIAL	YOUNG'S MODULUS (E, psi)	CRITICAL STRESS INTENSITY FACTOR ( $K_{IC}$ , psi $\sqrt{\text{in}}$ )	( $E/K_{IC}$ ) <sup>2</sup>
Dev. Sh.*	4.48x10E6 (24)	1485 (27)	.91x10E7
HS	2.26x10E6 (7)	139 (2)	26.41x10E7
HC	1.25x10E6 (4)	226 (2)	3.06x10E7
CC	1.02x10E6 (2)	179 (2)	3.25x10E7
HSS	.66x10E6 (2)	223 (2)	.88x10E7
HCS	1.01x10E6 (6)	253 (3)	1.59x10E7
CCS	.69x10E6 (2)	159 (2)	1.88x10E7

\*Average values for black shales from Blanton et al., (1981).

## FRACTURE INTERACTION EXPERIMENTS

For the fracture interaction experiments hydrostone blocks were prepared in three sections from a mold 12x12x15-inches. To create each outer section, the mold is placed with its long dimension parallel to the floor and then tilted to provide the desired fracture angle. Hydrostone is then poured to a level that is about three inches from where the central wellbore will eventually be located. After the outer sections have set, they are arranged in the mold with the long axis perpendicular to the floor.

In preparation for running the hydraulic/natural fracture interaction tests, two solid blocks were hydraulically fractured to determine exactly how far the hydraulic fracture was extending for different amount of fluid displaced. It was found that upon initial breakdown the fracture could extend more than three inches from the wellbore. In order to avoid this, a device was constructed to initiate a short crack that could then be hydraulically extended (Figure 1-1). This consisted of a 1x0.25x0.002 inch steel paddle cast into the hydrostone block. This steel paddle was epoxied to the end of a length of 1/8-inch diameter steel tubing and the central section of the block poured with the central wellbore hydraulic tube clamped in place. The "paddle" was well-lubricated to provide a path for the fracturing fluid to enter the block and initiate a fracture.

The testing procedure included assembly of a block in the triaxial testing apparatus, pressure application, test execution, and documentation of the results. The following paragraphs explain each of these procedures.

The apparatus used for this experiment consists of a 500,000-pound triaxial load frame and two hydraulic systems. The load frame is capable of subjecting a 12x12x15-inch block to stresses of up to 3000 psi with independent control in each of three directions. Cross-sectional diagrams of the load frame are shown in Figures 1-2 and 1-3. One hydraulic system provides fracturing pressure and the other applies pressure to the flatjacks. Fracturing pressure is generated by a pressure intensifier with eight-inch and four-inch diameter pistons giving a pressure intensification of 4:1. The intensifier is actuated by a closed-loop servo-control system that has as its feedback the output of an LVDT which measures the movement of the intensifier pistons. Since the diameter of the pistons is constant the LVDT essentially measures volume changes. A ramp voltage was used for a reference signal causing the intensifier to displace fracturing fluid at a constant flow rate. Fracturing pressures versus time were recorded in analog and digital form. The digital record was stored on magnetic disk for subsequent analysis and plotting with an HP-85 desktop computer. The entire hydraulic fracturing test system is illustrated schematically in Figure 1-4.

For testing a block is positioned on the bottom flatjack in the triaxial load frame and surrounded by the flatjacks used to apply horizontal pressure. All surfaces are adequately lubricated to

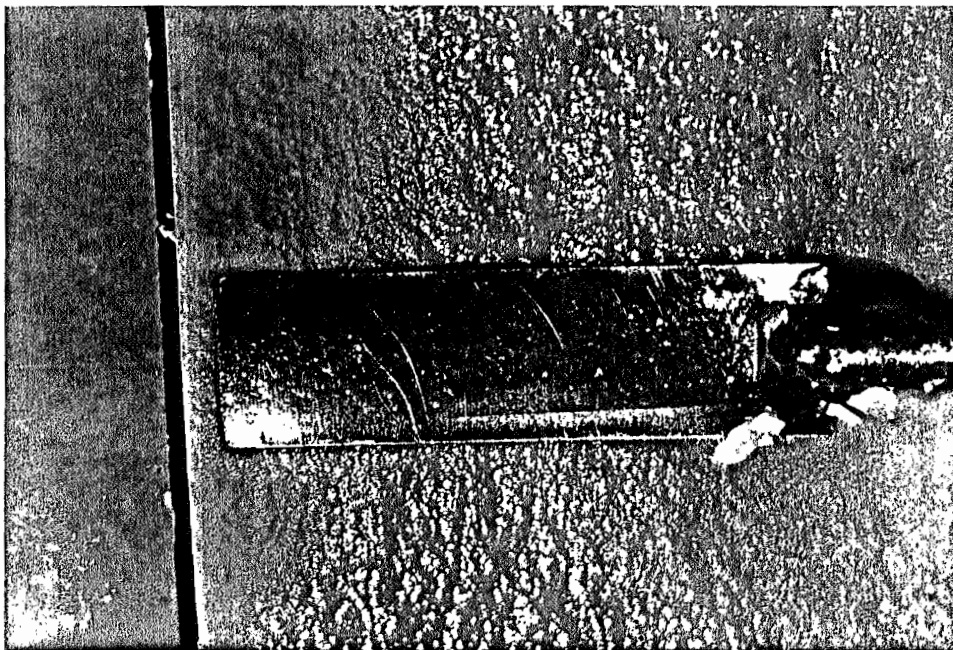


FIGURE 1-1. Device used to initiate fracture in central wellbore.

VERTICAL CROSS SECTION OF  
TRIAXIAL COMPRESSION APPARATUS

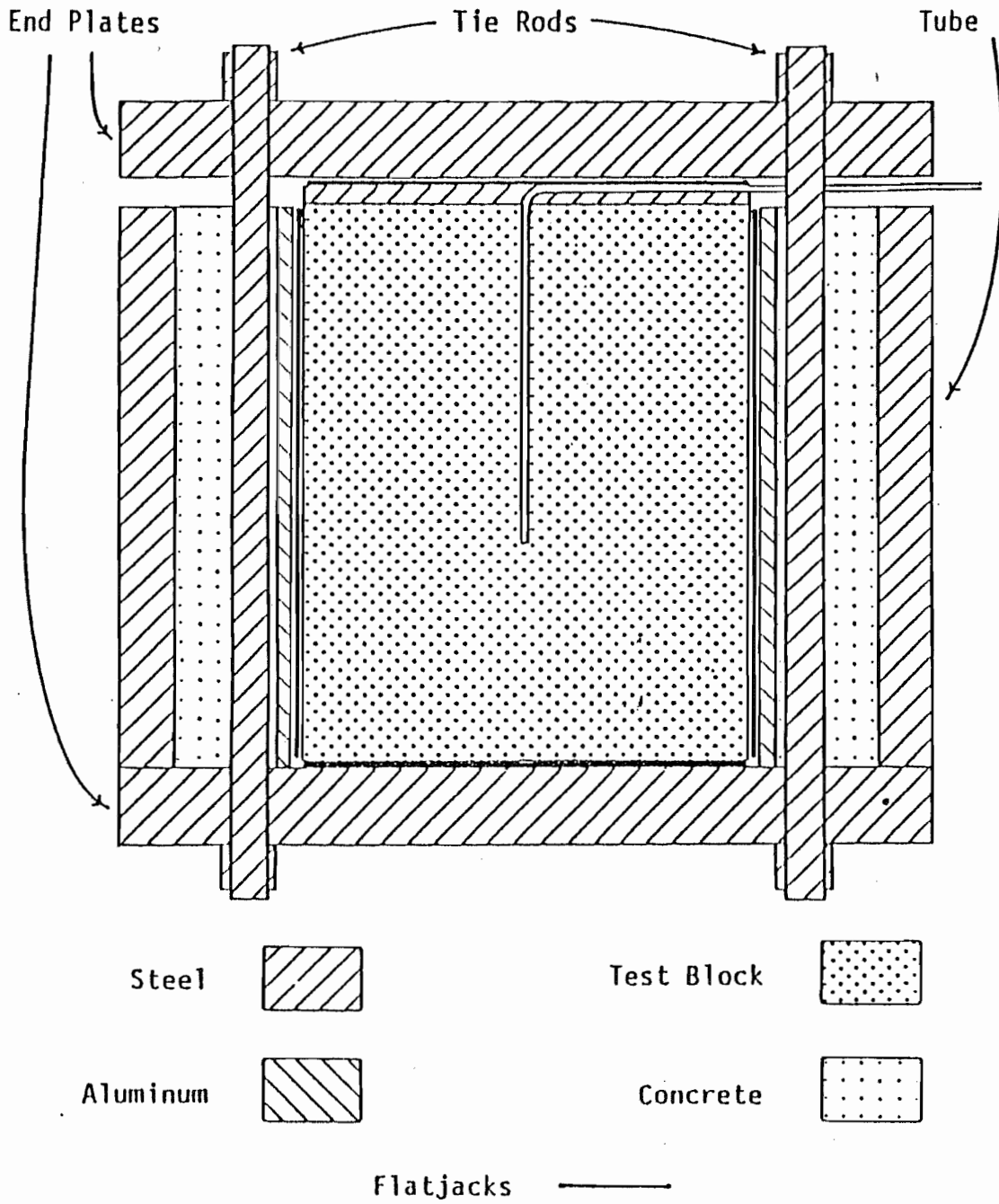


FIGURE 1-2. Vertical cross section of triaxial compression apparatus.

HORIZONTAL CROSS SECTION OF  
 TRIAXIAL COMPRESSION APPARATUS

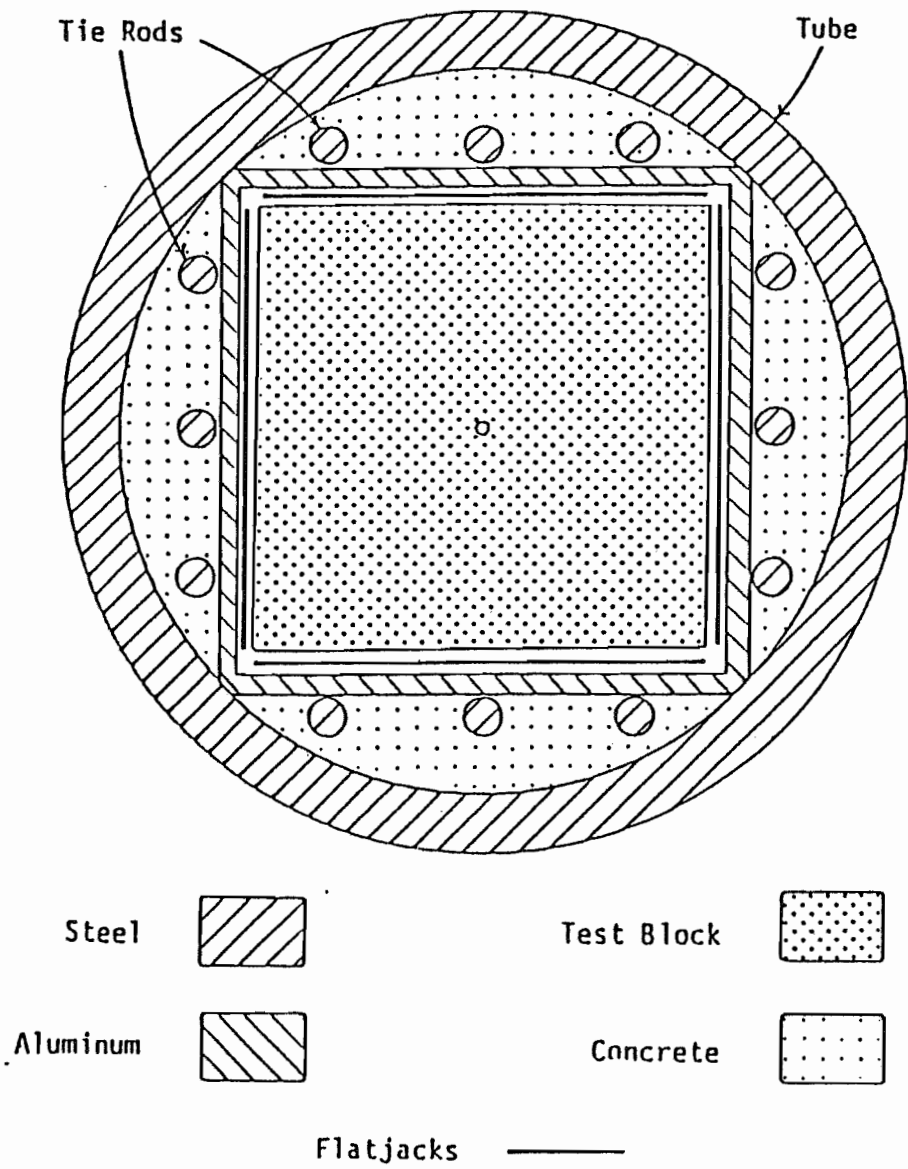


FIGURE 1-3. Horizontal cross section of triaxial compression apparatus.

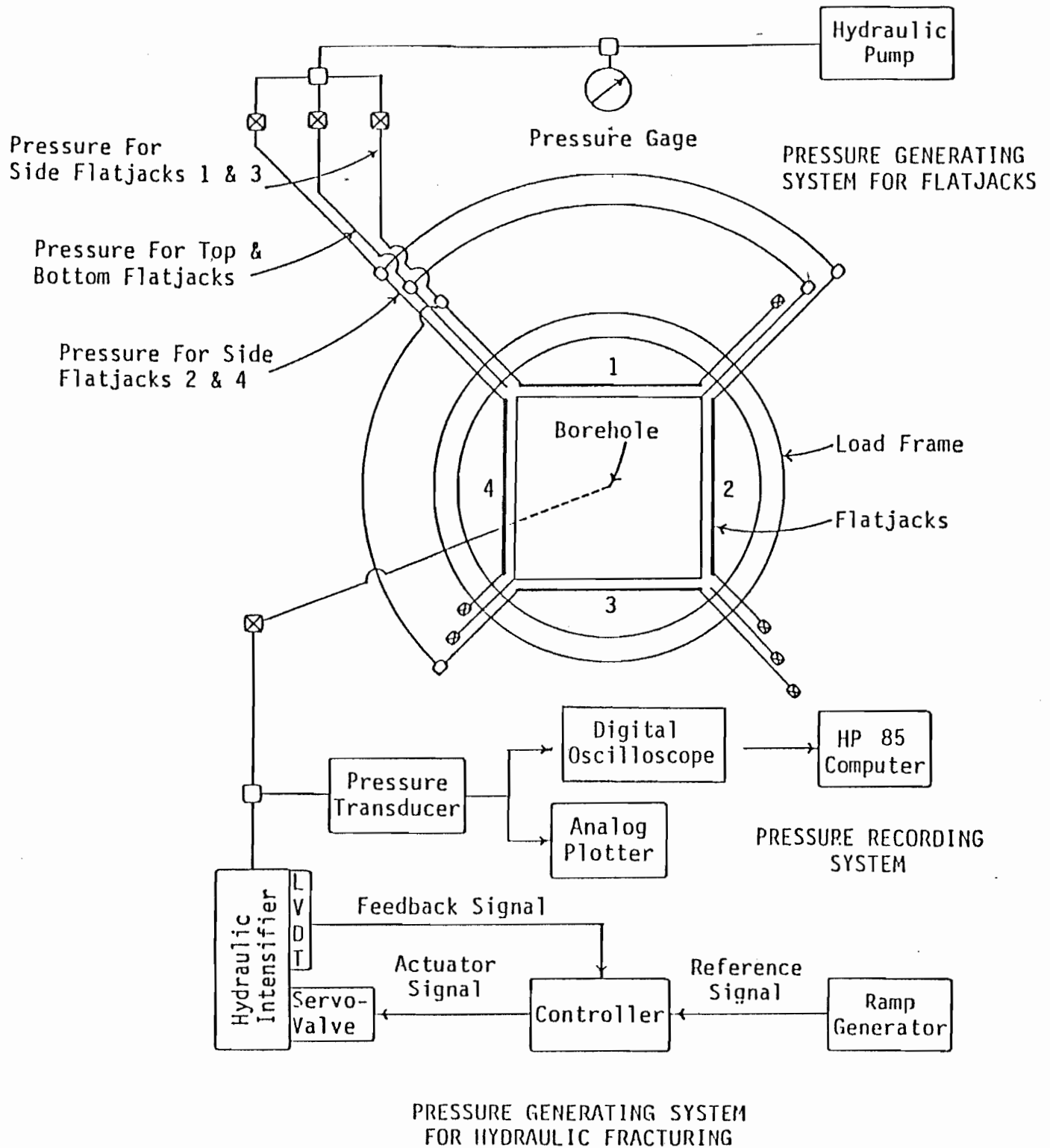


FIGURE 1-4. Schematic diagram of hydraulic fracturing test system.

minimize friction on the block surface and to allow easy disassembly. Steel spacers are slid into the opening between the load frame and flatjack to decrease the amount of flatjack expansion. When the assembly is sufficiently "tight", hydrostone is poured to approximately one quarter inch on the top surface of the block. This cement spacer provides a surface without asperities on which the top spacer is placed. The top flatjack is positioned on the top spacer, and the end plate is tightened down. Hydraulic connections are made, and air is purged from both the hydraulic lines and the flatjacks.

Each pair of flatjacks is pressurized independently using a hydraulic pump. When pressure has stabilized at the prescribed differential and vertical stresses, the test is begun by starting the intensifier ramp. The end of the ramp cycle, which occurred at approximately 250 seconds, signifies the end of the test, and pressure is released. After completing a test, the block is removed and sectioned with a circular diamond saw in order to examine the fracture. Horizontal cross-sections, hydraulic fracture surfaces, and interactions are photographed to help illustrate the results.

The initial test matrix for the fracture interaction tests is shown in Table 1-2. The plan was to run the end-member tests indicated by X's first, and then run tests at intermediate conditions indicated tentatively by the O's. The end-member at 2400 psi differential stress could not be run, however, because of apparent frictional sliding on the pre-fractures. In order to examine this further two friction tests were run under confining pressure on pre-cut samples of hydrostone to determine the coefficients of friction. The results gave coefficients of 0.65 and 0.75. Using an average of 0.7 it was found that instability in the pre-fractured block could be predicted. This is discussed in more detail in the following section on interaction criteria.

The plans for intermediate tests were modified based on the results of the end-member tests. The specific test conditions and associated results are summarized in Table 1-3. The pressure-time records for these tests, as well as a complete description of each test and photographs of the results are included in Appendix A.

The most significant difference between the results of these tests and those run in the previous study (Blanton, 1982) is the occurrence of much more crossing behavior. Figure 1-5 shows typical crossing behavior as viewed parallel and perpendicular to the fracture. Figure 1-6 shows opening behavior. Arrest behavior, which occurred at conditions intermediate to crossing and opening in the earlier study, appeared to be replaced by crossing behavior in this study. Also, crossing behavior was observed at lower differential stresses for the ninety and sixty degree approaches than in the earlier study.

TABLE 1-2.

## INITIAL TEST MATRIX

<u>PRINCIPAL STRESSES, psi</u>			<u>DIFFERENTIAL STRESS, psi</u>	<u>ANGLE OF APPROACH, DEGREES</u>		
$\sigma_1$	$\sigma_2$	$\sigma_3$	$\Delta\sigma$	90	60	30
900	750	600	300	X	0	
1200	900	600	600			X
1500	1050	600	900	0		
1800	1200	600	1200		0	
2100	1350	600	1500	X		0
2400	1500	600	1800			
2700	1650	600	2100		0	
3000	1800	600	2400			X

TABLE 1-3.

## RESULTS OF FRACTURE INTERACTION TESTS

PRINCIPAL STRESSES, psi			DIFFERENTIAL STRESS, psi	ANGLE OF APPROACH, DEGREES		
$\sigma_1$	$\sigma_2$	$\sigma_3$	$\Delta\sigma$	90	60	30
700	650	600	100	cross		
800	700	600	200	cross(2)		
900	750	600	300	cross	open(2)	
1200	900	600	600		cross	open
1500	1050	600	900	cross	cross	
1800	1200	600	1200			
2100	1350	600	1500	cross	cross	open
2200	1400	600	1600			open

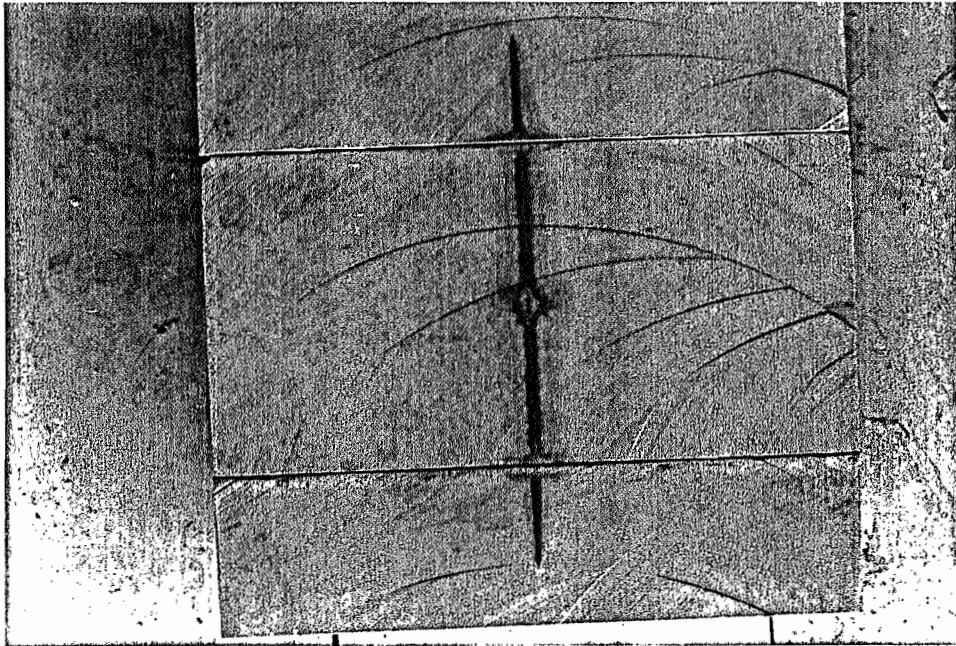


FIGURE 1-5. Typical crossing behavior.

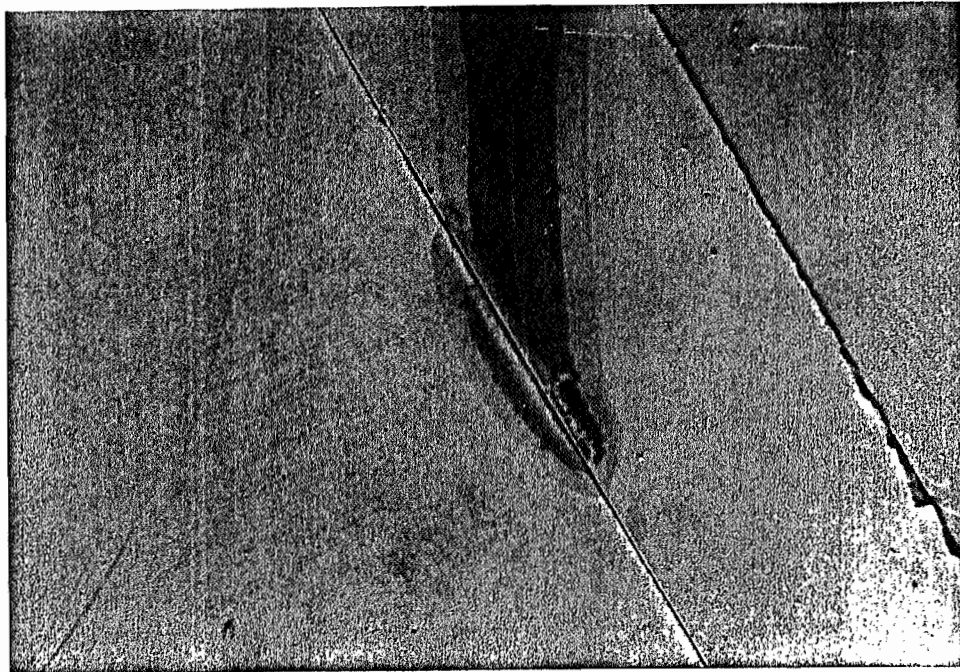
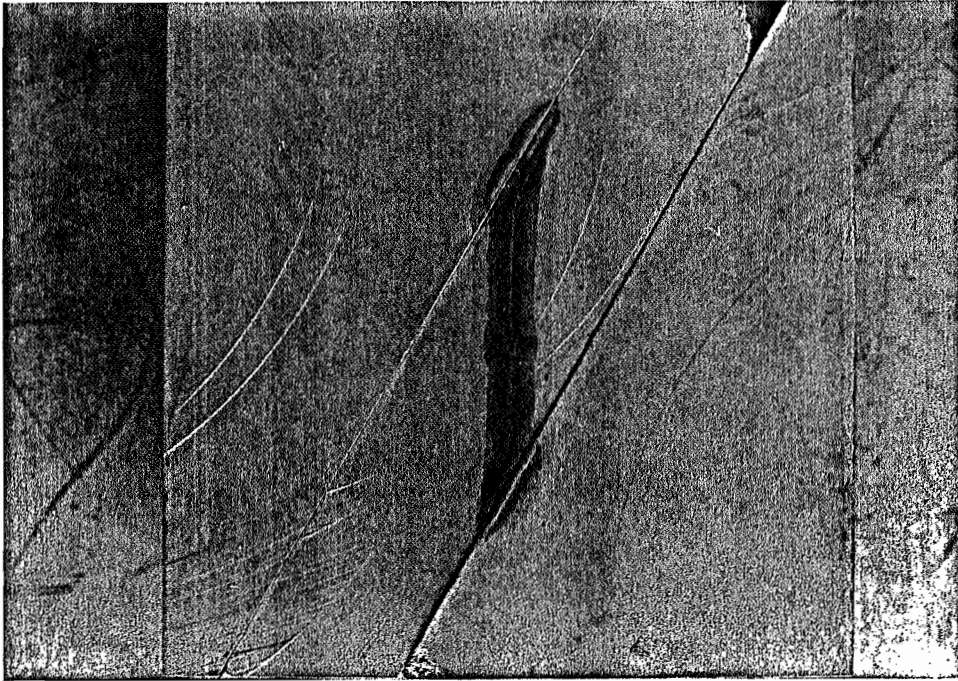


FIGURE 1-6. Typical opening behavior.

## FRACTURE INTERACTION CRITERION

The fracture interaction criteria suggested in an earlier study (Blanton, 1982) cannot be applied to the current work because the configuration of the experiment is different. In the earlier study a pre-existing fracture was placed on only one side of the wellbore, as shown in Figure 1-7A. In such a situation, when fracture growth was inhibited in the a (crossing) or b (opening) directions the fracture was free to grow in the opposing c direction. In the current study, an attempt has been made to model more realistic conditions with fractures on both sides of the wellbore, as shown in Figure 1-7B. With such a configuration, when growth is inhibited in the a and b direction, the other alternative is vertical growth. However, as the fracture grows vertically, the pressure will continue to increase at the points of intersection until either crossing (a) or opening (b) occurs. The arrest type interaction observed in the earlier study is eliminated when there are pre-existing fractures on both sides of the wellbore. This is exactly what has been observed in the experiments reported on here.

The first step in trying to predict whether crossing or opening will occur is to consider the initial interaction. It was argued in the earlier study that based on theoretical work by Hansen et al, (1981) the initial interaction of a crack approaching an unbonded interface at right angles will be an opening interaction. This argument is extended here for an arbitrary angle of approach,  $\theta$ , as shown in Figure 1-7C. The energy release rate as a function of  $\theta$  is given by Hussain et al. (1974) as follows:

$$G(\theta) = \frac{4(1 - \nu^2)}{E} \left( \frac{1}{3 + \cos^2\theta} \right) \left( \frac{\pi - \theta}{\pi + \theta} \right)^{\theta/\pi} [(1 + 3\cos^2\theta)(\pi L)(P - \sigma_3)^2] \quad (1-4)$$

From this equation it follows that for propagation across the interface in the direction a ( $\theta = 0$ ) the pressure in the fracture must be greater than:

$$P_a = \sigma_3 + \left( \frac{G_c E}{(1 - \nu^2) \pi L} \right)^{1/2} \quad (1-5)$$

where  $G_c$  is the critical strain energy release rate. For the direction of the pre-existing fracture the  $G$  will be zero, and thus it follows from equation 1-4 that the pre-existing fracture will open when the pressure becomes greater than:

$$P_b = \sigma_3 \quad (1-6)$$

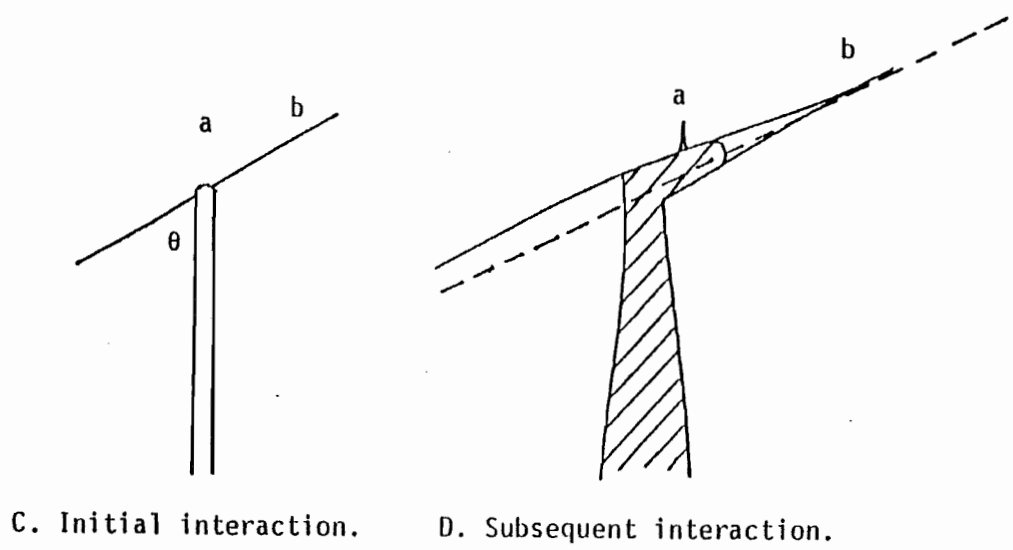
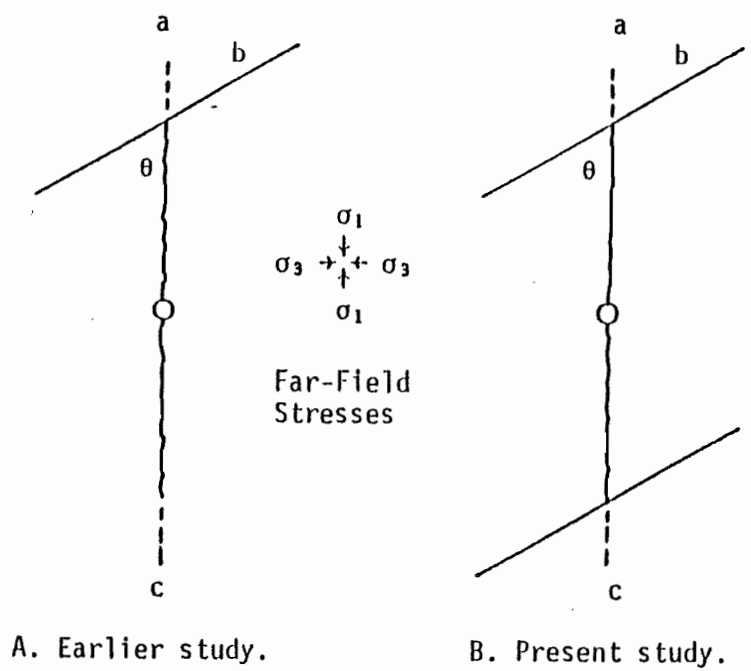


FIGURE 1-7. Options for hydraulic fracture growth in presence of a natural fracture: (a) crossing, (b) opening, and (c) unimpeded growth.

Since this will always be less than the pressure given by equation 1-5, opening of the pre-fracture will be preferred over crossing, at least initially.

Initial opening will not necessarily continue beyond the immediate vicinity of the interaction point, since this opening was due to the stress concentration caused by the crack tip. When the situation reaches the point shown in Figure 1-7D, whether continued opening or crossing occurs will depend more on the far field stresses. An exact solution for the state of stress associated with the situation shown in Figure 1-7D required a numerical approach because of its complexity. Numerical work has been done for similar situations and results have been published for a fracture approaching a pre-fracture at right angles (Lam and Cleary, 1982, and Lee and Keer 1984), however particular numerical solutions will not yield the kind of general criterion sought in this study.

Based on their numerical work, Lam and Cleary (1982) do suggest a simple criterion for re-initiation or crossing in the situation of a right angle approach. They contend the re-initiation should occur when the pressure in the fracture exceeds the following:

$$P_a = \sigma_3 + \sigma_T \quad (1-7)$$

where  $\sigma_T$  is the tensile strength of the rock. In the present study, equation 1-7 has been extended for other angles of approach by substituting for  $\sigma_3$  an expression for the stress acting parallel to the pre-fracture. This substitution result in the following condition for crossing:

$$\begin{aligned} P_a &= \sigma_t + \sigma_T \\ &= \frac{1}{2}(\sigma_1 + \sigma_3) + \frac{1}{2}(\sigma_1 - \sigma_3)\cos 2\theta + \sigma_T \end{aligned} \quad (1-8)$$

To determine whether crossing or opening is preferred the pressure given by equation 1-8 must be compared to the pressure required to open the pre-fracture which will be equal to the normal stress on the pre-fracture, as follows:

$$P_b = \frac{1}{2}(\sigma_1 + \sigma_3) - \frac{1}{2}(\sigma_1 - \sigma_3)\cos 2\theta \quad (1-9)$$

By setting equation 1-8 and 1-9 equal, an expression for the boundary between the two types of behavior can be derived. The result is:

$$\Delta\sigma = -\sigma_T \sec 2\theta \quad (1-10)$$

A plot of this criterion is compared to the experimental results in Figure 1-8. As can be seen it divides the regions where crossing and opening behavior were observed experimentally.

Equation 1-10 can be written in the form resulting from the dimensional analysis (Equation 1-3) by taking advantage of the relation between the critical stress intensity factor and tensile strength:

$$\sigma_T = (\pi l)^{-1/2} K_{1C} \quad (1-11)$$

where  $l$  is the length of critical microflaws in the material. The function,  $F$ , of dimensionless terms in Equation 1-3 becomes:

$$F = -(\pi B)^{-1/2} \sec 2\theta$$

where  $B = l/L$  (1-12)

$$B = l/L$$

$B$  is the only undetermined parameter in the criterion and it must be between zero and one. In Figure 1-9, the sensitivity of the criterion to variations in  $B$  is shown to be relatively small. The values of  $B$  used for these curves are from left to right 1, 0.5, 0.2, 0.1 and 0.05. The value used in Figure 1-8 is 0.05.

$B$  can be thought of as a blunting factor in the present context. When  $B$  is equal to one, the critical flaw length is equal to the length of the hydraulic fracture; i.e., the hydraulic fracture is the critical flaw and the stress concentration at its tip dominates. As  $B$  gets smaller the effectiveness of the length of the hydraulic fracture is reduced. When  $B$  equals the ratio between the critical flaw length in virgin material and the hydraulic fracture length then the influence of the length of the hydraulic fracture on failure in the opposing block is removed completely, and the virgin tensile strength will control the interaction as originally suggested by Lam and Cleary (1982).

Finally an explanation of the unstable region indicated in Figure 1-8 needs to be made. This indicates a region in which frictional sliding will occur on the pre-fractures. The curve plotted is for the following equation:

$$\Delta\sigma = \frac{2\mu\sigma_3}{\sin 2\theta (1 - \mu \tan \theta)} \quad (1-13)$$

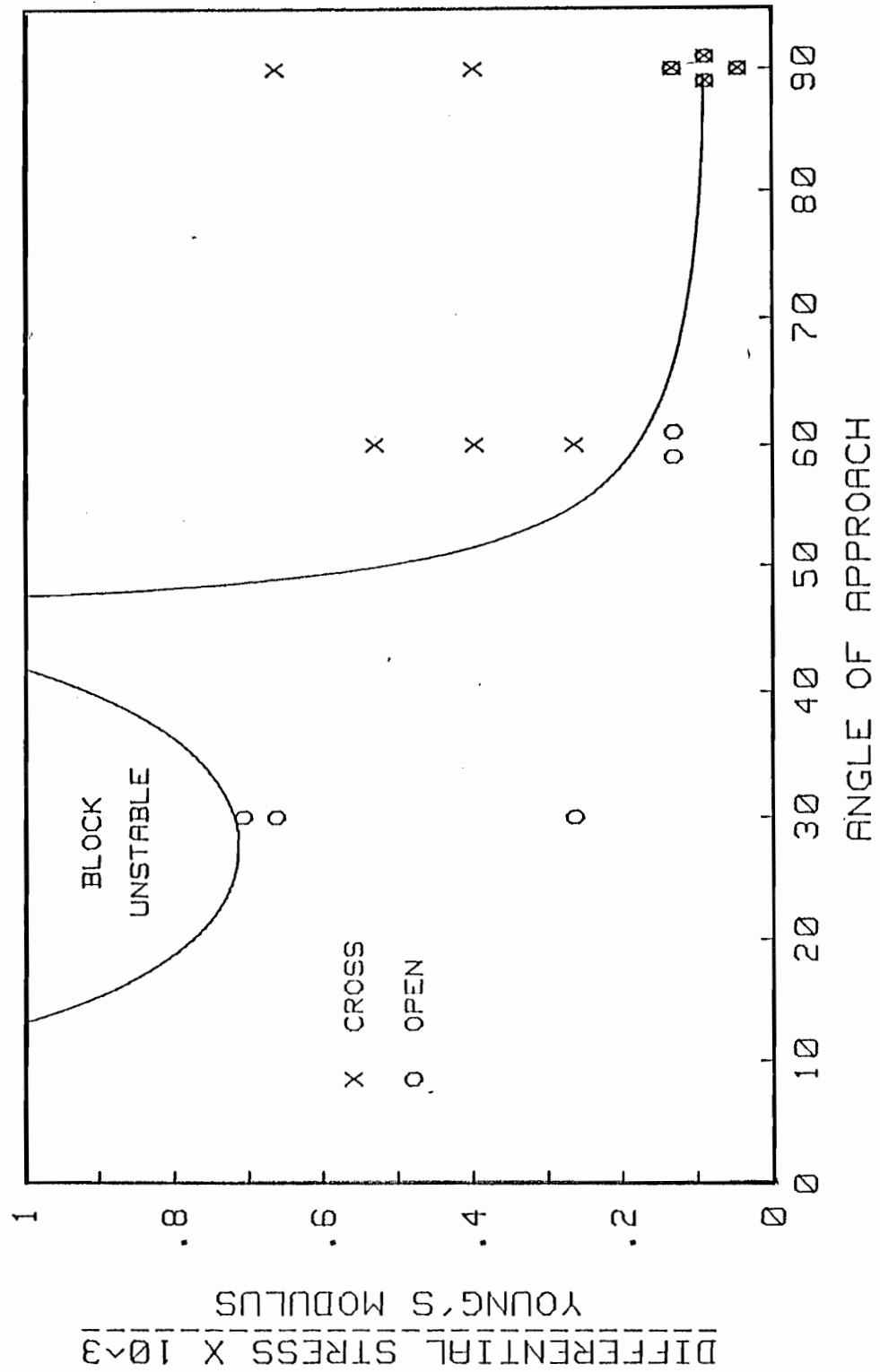


FIGURE 1-8. Comparison of fracture interaction criterion (Equation 1-10) with experimental results.

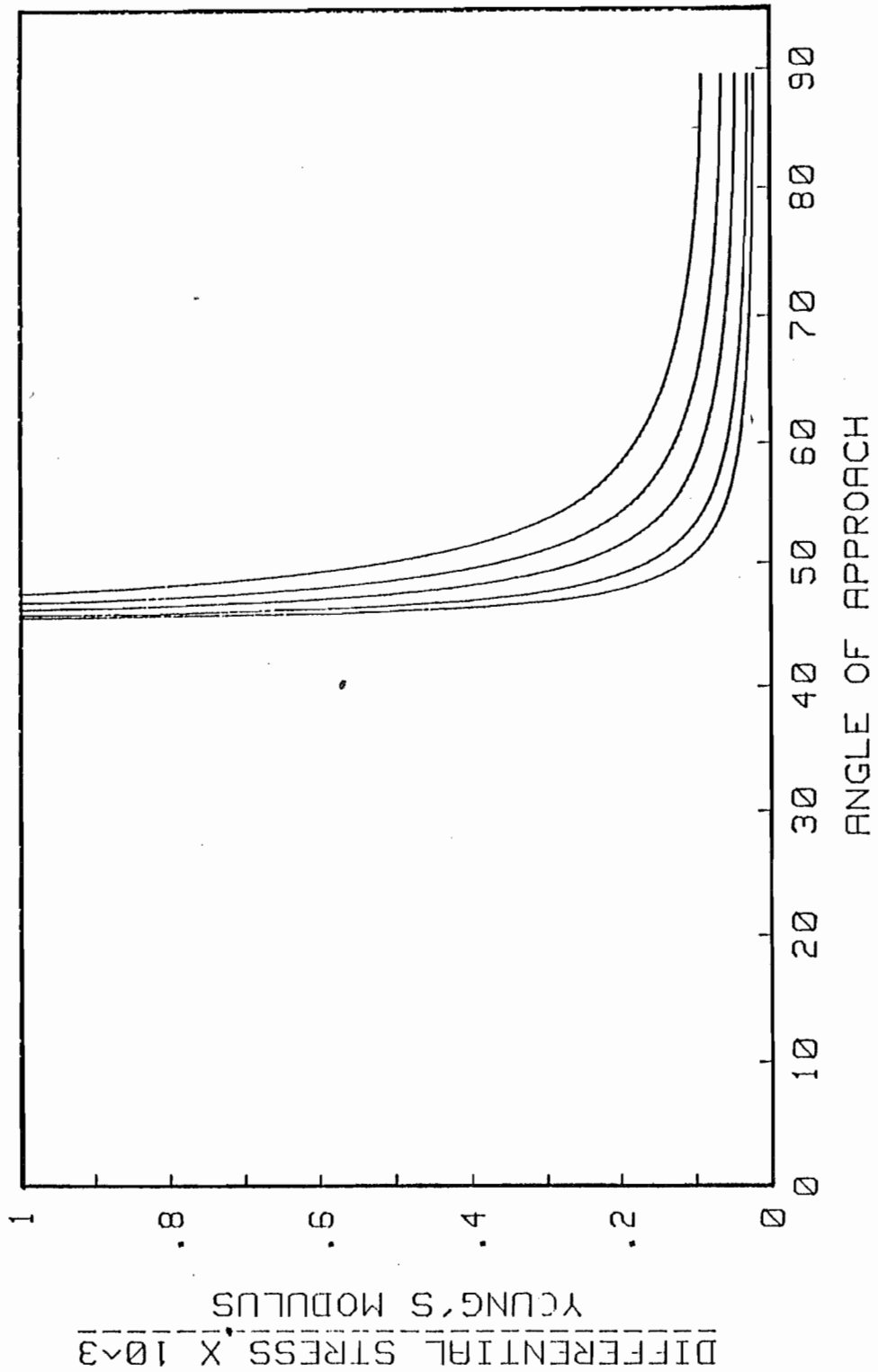


FIGURE 1-9. Sensitivity of fracture interaction criterion (equation 10) to variations in B. B equals 1, 0.5, 0.2, 0.1, 0.05 from left to right.

with the coefficient of friction equal to 0.7, as discussed in the previous section. Equation 1-13 has been derived directly from a simple linear law for sliding on a cohesionless surface as follows:

$$\tau = \mu \sigma_n \quad (1-14)$$

That this was indeed an unstable region was confirmed by our experiments.

## CONCLUSIONS

Two types of hydraulic/natural fracture interaction were observed: (1) the pre-fracture opened diverting fluid and preventing crossing or (2) the hydraulic fracture crossed the pre-fracture. Intermediate arrest behavior that was observed in earlier studies (Blanton, 1982, Warpinski and Teufel, 1984) did not occur in this study. This was probably a result of the configuration used with pre-fractures on both sides of the wellbore. Under these conditions arrest was probably only a temporary condition with either opening or crossing occurring with continued pumping.

Another significant difference found in the current study is that in a plot of differential stress versus angle of approach, the domain of crossing interaction is greater than in earlier work, suggesting that more constructive interaction can be expected than was previously believed.

A fracture interaction criterion that can be used to predict the type of interaction expected in Devonian shale reservoirs has been developed as an extension of a criterion suggested by Lam and Cleary (1982). An important characteristic of this criterion is that the sensitivity to differential stress is primarily confined to angles of approach between forty-five and sixty degrees. Below forty-five degrees opening interaction is preferred; above sixty degrees crossing is preferred, at least for differential stresses greater than about 400 psi.

## TASK 2. DYNAMIC/NATURAL FRACTURE INTERACTION

### OBJECTIVE

The objective of this task was to qualitatively and quantitatively examine in the laboratory the interaction between dynamically induced and pre-existing fractures.

### WORK PERFORMED

The experiments in this task have been performed in the same apparatus as used in Task 1. There were two important differences, however. First, the method of loading the wellbore was such that fractures were propagated dynamically. Second, particular attention was given to those conditions under which an unfavorable interaction was obtained with hydraulic fracturing.

An important precursor to the interaction experiments was the development of charges which would drive fractures a reasonable distance within the test block, and which would propagate fractures in a direction which is parallel to the minimum principal stress. The approach taken in developing the charge was firstly to experiment with different charge variables in unstressed cylinders of the test material which allowed different charges to be examined at minimum cost. These were followed by verification tests performed on solid blocks under the same stress states as planned for the interaction tests. During these tests some adjustment of the charges was carried out. Finally, a series of interaction tests were performed.

### CHARGE DEVELOPMENT

The initial intention in this task was to perform a dimensionless analysis similar to that conducted in Task 1 as an aid to experimental design. To this end a literature review of dynamic/natural fracture interaction was conducted. The conclusion of this review was that the process is not well enough understood to list the critical parameters with any certainty. However, based on unpublished reports to DOE/METC by Fourney and others at the University of Maryland, three dimensionless terms seem to stand out as being critical; the ratio of peak wellbore pressure to far field stresses, dynamic frictional properties of the natural fracture, and the angle of approach.

Since the dimensional analysis could not be carried out at this time charge development proceeded largely empirically. The aim of the development was to find a charge which would drive fractures at least three inches in the test blocks and oriented parallel to the least principal stress.

Pipe Tests. During charge development a series of thirteen tests were performed in cylindrical samples of hydrostone, the samples being formed by casting hydrostone, with the same composition as used in Task 1, in a six inch diameter one foot long steel cylinder with a quarter-inch wall. The sample diameter was chosen to demonstrate that fractures could be driven for at least three inches, to remove the sample boundary a reasonable distance from the borehole and yet to avoid the additional cost and handling difficulty of larger tubing. The sample length was chosen to minimize end effects in the central charged region. A central hole was prepared by casting-in a central quarter-inch diameter greased rod which was removed before final setting of the hydrostone, this hole size being chosen to match that planned for the block tests.

The samples were left in the steel tubing during testing to maintain some confinement of the samples, and thus to prevent the samples from breaking due to the action of tensile waves reflected from the outer surface. Stress calculations were performed to verify that the quarter-inch wall thickness for the outer steel tube was sufficient to contain the charge without failure. In some of the tests a "fracture initiator", that is a thin steel sheet one-quarter inch by one inch, was cast on both sides at the center of the central hole. The purpose of this was to investigate its effect on fracture orientation in case such a device were needed in later tests. After each test, the samples were split perpendicular to their axis by first cutting the steel tube, then by loading the sample across the split in a test frame.

In selecting charges for trial, several requirements were considered. Firstly, the charges needed to be formulated to give a pressure rise time fast enough to develop multiple fractures rather than the bi-wing fracture characteristic of slow rise times, such as those used in hydraulic fracturing, but slow enough to prevent pulverization of the wellbore region. Secondly the charge size should be sufficient to provide enough gas to drive the fractures the required distance. Finally a charge configuration was required which would give repeatable results.

There are several variables which will influence rise time. These include composition, grain size, hole size, method of initiation, and confinement. It was decided that the initial charge should consist of a propellant such as black powder, since this has a relatively slow rise time and is easily available. In the early tests the reaction speed would be adjusted by varying grain size and possibly by varying the method of initiation.

In determining charge size it was decided to start with rather small sizes, mainly for reasons of safety, and to increase these as needed. Some thought was given to the method of initiation, since this could effect both the repeatability of the results, and the speed of the reaction. Consideration was given to using either end initiation using blasting caps or center initiation using an MDF. It was decided to start the tests using end initiation with Exploding Bridge Wire (EBW) detonators, primarily because of their ready availability and safety in use, as well as because of some uncertainty of the reliability of MDF in such a small hole. The detonators used were RP2 EBW without explosives, manufactured by Reynolds Industries. Two principal propellants were used, FFFF (4F) superfine black rifle powder manufactured by Goex, Inc. and Hercules 2400 smokeless powder manufactured by Hercules, Inc. The charges were packed in a thin walled plastic tube, inserted into the central hole and stemmed with epoxy. The epoxy was used to contain the explosive energy and the gas products in the region of the charge and thus ensure that most of the energy was used to drive fractures through the sample.

A list of the pipe tests performed and their results is given in Table 2-1. Early tests with varying charge sizes, powder types and initiation methods (Tests DP-1 - DP-8) indicated that 4F black powder initiated with a single EBW (end initiation) gave the most reliable results. Charge sizes of from 0.56 gm to 1.75 gm, corresponding to charge lengths of from 1-3/8 to 4 inches, would consistently give at least three fractures and as many as five. A charge size of 1.0 gm, or 3 inch length in the 1/4 inch hole, was settled upon as the optimum value in this configuration since it gave fairly consistent results while the larger charges tended to lead to excessive venting of reaction gases at the hydrostone/pipe interface. The presence of fracture initiators seemed to have little effect on the results. When present they would tend to control the direction of initial fractures, but these fractures would typically curve away from that direction as soon as the initiator was passed (Figure 2-1). Results both with and without initiators tended to give fairly equally distributed fractures (Figure 2-2).

Block Tests. Following the pipe tests a series of seven block tests were performed to verify, and if need be modify, the charges. These tests were performed on 12x12x15-inch block samples of hydrostone placed under polyaxial stress. The material, preparation methods and loading methods were the same as those used in Task 1, while the charge loading and epoxy stemming methods were the same as in the pipe tests, except where noted in the test descriptions. Two stress configurations were used, the first was with horizontal stresses of 600 and 900 psi and a vertical stress of 750 psi, the second had horizontal stresses of 600 and 1200 psi and a vertical stress of 900 psi. These values gave ratios of minimum to maximum principal stress of 1.5 and 2. After testing, the samples were cut approximately in the center of the sample and in a plane perpendicular to the hole. The tests are summarized in Table 2-2, and described in detail in Appendix B. Typical results are shown in Figures 2-3 and 2-4.

TABLE 2-1.

## PIPE TESTS

TEST FRACTURE	CHARGE	FRACTURES/ INITIATOR	FRACTURES/ COMMENTS
DP-1	0.3 gm powder	None	None
DP-2	1.3 gm powder 3 inches	None	None
DP-3	1.0 gm flake powder	None	
DP-4	1.2 gm (3 in) smokeless IMR 4198, 4F black powder initiator		Black powder ignited smokeless did not
DP-5	1.75 gm (4 in) 4F black powder	Present	Five (-60, 0, 80, 125, 180: all 3 in)
DP-6	0.56 gm (1.375 in) 4F black powder	Present	Four (0:2 in, 30:2 in, 130:2.375 in, 240:3 in)
DP-7	1.2 gm (3 in) 4F black powder	Present	Three (-10, 90, 195: all 3 in)/gas vented through fracture
DP-8	1.72 gm (4 in) 4F black powder	Present	Three (0, 30, 180: all 3 in)
DP-9	1.0 gm (2.25 in) 4F black powder	None	Four (-20:3 in, 90:1 in, 195:2 in, 200:3 in)

TABLE 2-1. CONT.

PIPE TESTS

TEST FRACTURE	CHARGE	FRACTURES/ INITIATOR	FRACTURES/ COMMENTS
DP-10	1.0 gm (2.25 in) 4F black powder	None	Five (0:2.5 in, 140:0.75 in, 145:2.5 in, 225:1.5 in, 245:1.5 in)
DP-11	1.0 gm (2.25 in)	None	Three (0:2.5 in, 70:1.75 in, 195:3 in)
DP-12	1.0 gm (2.25 in) 4F black powder	Present	Three (-20:1 in, 80:1 in, 110:1.5 in)
DP-13	1.0 gm (2.25 in) 4F black powder	Present	Three (-20:1.5 in, 90:1.75 in, 200:1.75 in)

NOTES: Charge size given as gm and length (all in 1/4-inch hole)  
Fractures are given by (orientation:length,...).  
Orientation is angle of trace to fracture initiator.

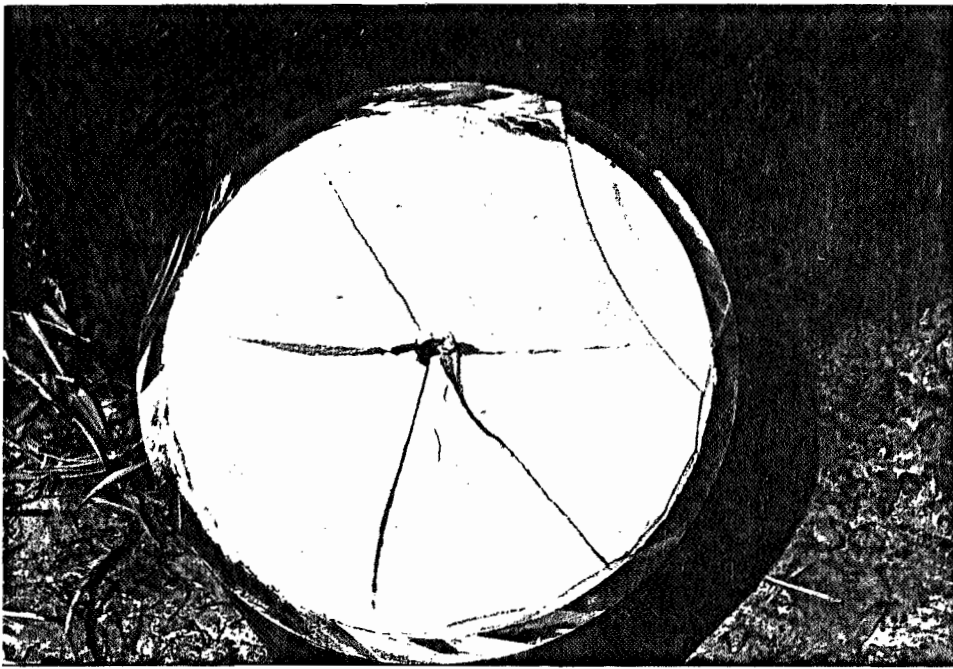


FIGURE 2-1. Typical pipe test with fracture initiator present.  
(Test DP-5).

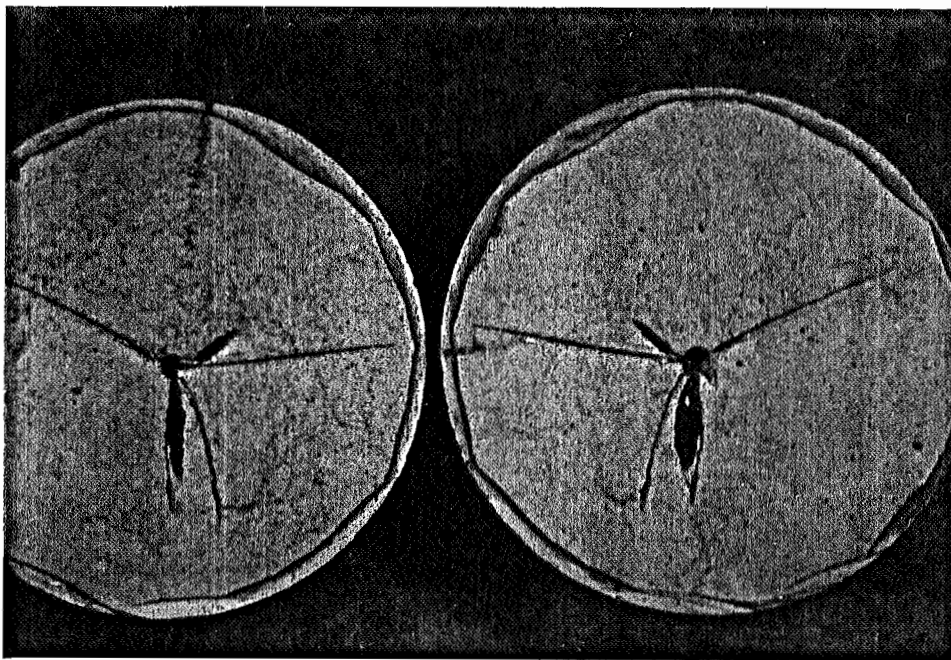


FIGURE 2-2. Typical pipe test without fracture initiator.  
(Test DP-10).

TABLE 2-2.

## BLOCK TESTS

TEST	STRESS (MIN,MAX,VERT) (PSI)	HOLE DIAM (IN)	CHARGE TYPE SIZE (GM)	INITIATOR	FRACTURES/COMMENTS
DB-1	600,1200,900	0.25	4F 1.70	1xRP-2 EBW	Two (90:1 in, 270:1 in)
DB-2	600,900,750	0.375	4F 1.70	1xRP-2 EBW	One (80:3/8 in)/ double hole
DB-3	600,900,750	0.375	4F 2.50	1xRP-2 EBW	Two (90:2.5 in, 270:2 in)
DB-4	600,900,750	0.375	RDX 1.07 4F 0.25	1xRP-83 EBW	Two (90:1.5 in, 270:1 in) Curved fractures
DB-5	600,900,750	0.375	RDX 2.14 4F 0.25	2xRP-83 EBW	Five (0:1 in, 130:7 in, 200:1 in, 250:1 in, 310:3.25 in)/ Multiple at the hole
DB-6	600,900,750	0.375	RDX 2.14 4F 0.25	2xRP-83 EBW	Two (-10:0.75 in, 170:3.75 in)/Multiple at the hole
DB-7	600,1200,750	0.375	RDX 2.14 4F 0.25	2xRP-83 EBW	Two (80:2.25 in, 180:2.25 in)

Note: Stresses are principal with minimum and maximum perpendicular to hole.

Fractures given as (Orientation: Length, .....). Orientation is angle of trace to minimum principal stress

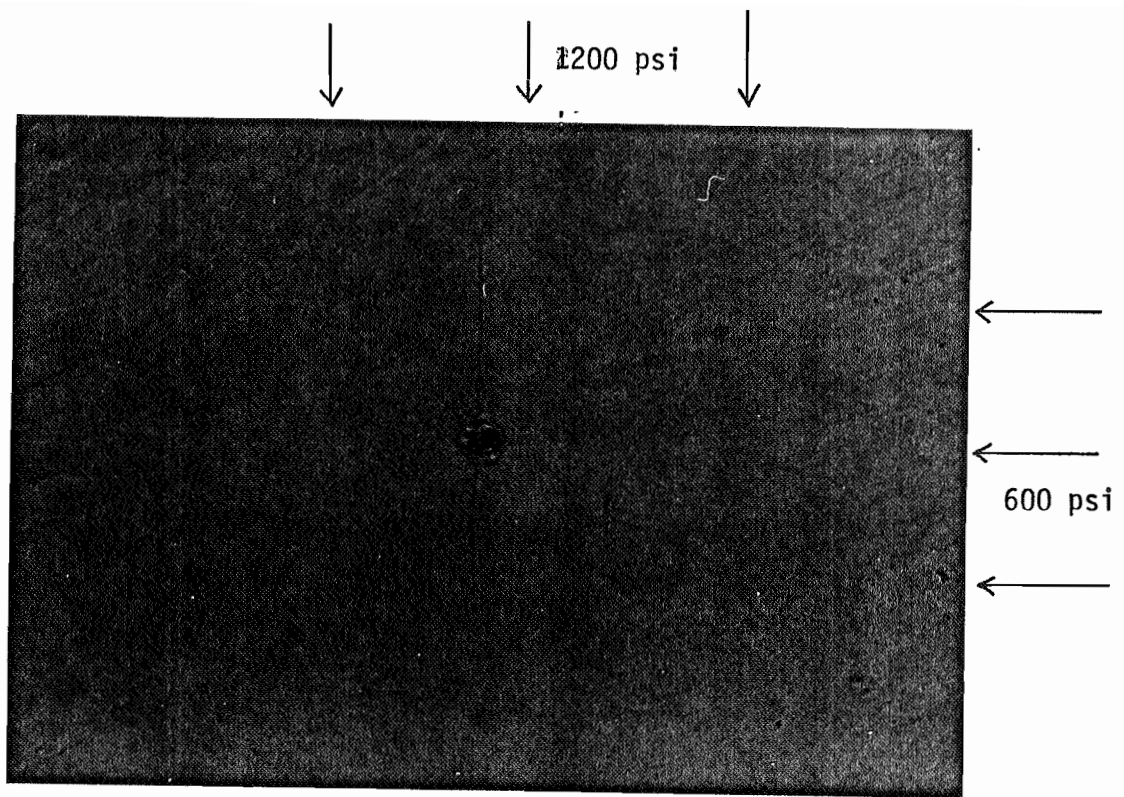


FIGURE 2-3. Fracture running parallel to maximum stress for Test DB-1.

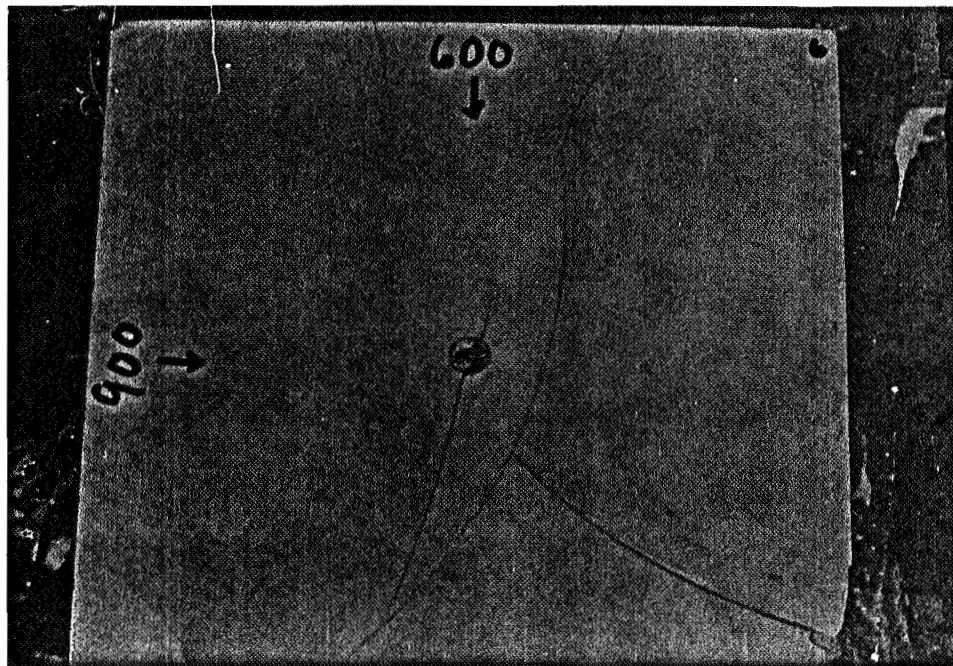


FIGURE 2-4. Fracture running parallel to minimum stress for Test DB-6.

Conclusions. The block tests showed that the effects of non-uniform stress were to alter the results of the unstressed pipe tests by changing the consistent long multiple fractures of the pipe tests to shorter bi-wing fractures parallel to the maximum stress when the same charge configuration was used (Figure 2-3). These fractures could be lengthened by firstly increasing the hole size, and thus concentrating the charge in the central section, and by increasing the charge size.

A decrease in the rise time of the charge was necessary to produce multiple fractures which were not parallel to the maximum principal stress. This was achieved by changing the principal component of the charge to RDX, and by using simultaneous initiation at both ends of the charge. This led to some pulverization near the hole, but did produce fractures of the desired orientations, particularly in planes closer to the ends of the charge than the center (Figure 2-4). However, increase of the differential stress, and of the value of the maximum stress, returned the fractures to the by-wing type parallel to the maximum stress.

#### INTERACTION TESTS

Four interaction tests have been performed, two with simulated natural fractures perpendicular to the least principal stress and two with the simulated fractures at thirty degrees to this stress. The material, the methods of block preparation and application of stress were the same as in Task 1. The charge configuration was the same as in the last solid block tests, that is, a 2.14 gm charge of RDX with 0.25 gm of black powder in a 3/8-inch hole and double end initiation by EBW's. The charges were again contained by filling the hole with epoxy.

Tests were only run at the lower differential stress, that is, the case with 600 and 900 psi horizontally and 750 psi vertically. This was due to the inability to drive fractures parallel to the least stress in the solid block tests at the higher stress differentials. Two additional tests were planned initially with simulated fractures at thirty degrees to the least stress. However, it was found that the dynamic fractures did not cross the natural fractures at the higher angles of approach so these tests were abandoned. After testing, the fractures were examined by cutting the block at several levels in planes perpendicular to the hole. Typical results are shown in Figures 2-5 and 2-6. The tests are described in detail in Appendix B.

In no cases did the dynamic fractures cross the simulated natural fractures, even though hydraulic fractures consistently crossed at the high angles of approach used here. In retrospect, this result is not very surprising, and is probably a function of the charges used. Thus, in all cases the fractures had to be of a reasonable length when they encountered the simulated fractures, and were in all probability close to the end of their propagation. At this point the gas pressure would

TABLE 2-3.

## INTERACTION TESTS

TEST	STRESS (MIN, MAX, VERT) (PSI)	NATURAL FRACTURE ORIENTATION	COMMENTS
DS-1	600, 900, 750	Perpendicular	Two fractures @ 45 and 135 deg. intersected natural fractures. Did not cross.
DS-2	600, 900, 750	Perpendicular	Two/three fractures. One @ 15 deg. intersected natural fracture. Did not cross.
DS-3	600, 900, 750	60 degrees	Three fractures. One @ 45 deg. intersected natural fracture. Did not cross.
DS-4	600, 900, 750	60 Degrees	Pulverization and multiple short fraction. No intersection with natural fractures.

Note: All tests were conducted with 2.14 gm RDX and 0.25 gm 4F black powder in a 3/8 inch hole with double ended RP-83 EBW initiation.

Stresses are principal with minimum and maximum perpendicular to hole.

Natural and dynamic fracture orientation is angle of trace to relative to minimum principal stress axis.

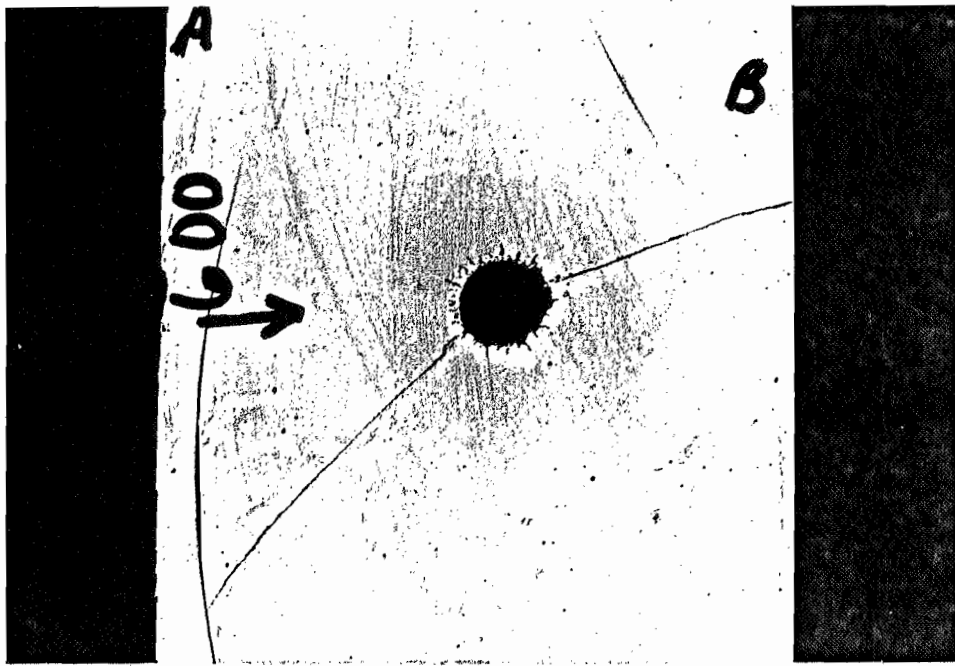


FIGURE 2-5. Fractures near mid-plane for Test DS-2 showing pulverized zone and dynamic fracture parallel to minimum stress intersecting pre-fracture.

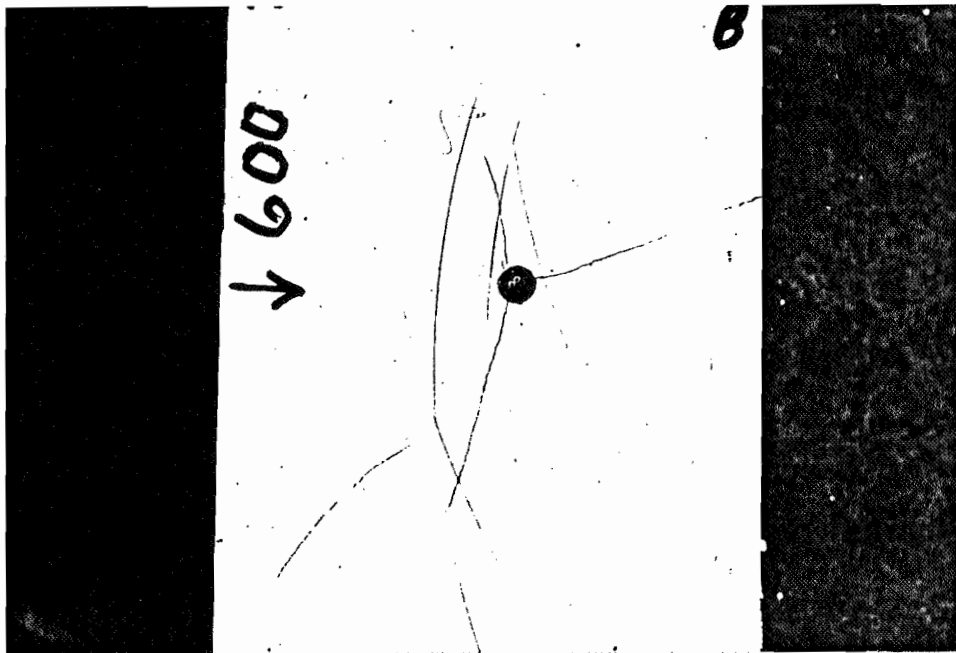


FIGURE 2-6. Fractures at a place four inches between the center for Test DS-2.

be dropping and the energy available for further propagation would be minimal. This, combined with the low viscosity of the gases and the rather low stress across the natural fractures would tend to make the gases leak off into the void of the natural fracture. Results with larger charges may be quite different.

## CONCLUSIONS

The work repeated in this task represents the first time, to our knowledge, that propellants have been used successfully in the laboratory to produce the full spectrum from "hydraulic" bi-wing fractures to wellbore pulverization in a simulated rock material. Nevertheless it is apparent from this work that the development of dynamic fractures in the laboratory is imperfectly understood at this time. Thus, the reproducibility of results in this task has not been very good, and this has undoubtedly influenced the results. It is true that with the final charge configuration multiple fractures were consistently produced, but the details of their number and orientation were not so consistent. It is believed that most of the variations were the result of variations in the, nominally identical, charges. It is also clear that stress has a large effect on the results of dynamic fracturing. This is particularly evident in the marked difference between the results at a differential stress of 300 and those at 600 psi. The use of unstressed pipe tests for preliminary charge design was useful for initial scoping, but, in retrospect have very little value for the final tailoring of charges for fracture design.

In summary, the results of this task must be taken as being very preliminary. The ability to drive multiple fractures against the preferred stress orientation has been demonstrated, but it is also apparent that an anisotropic stress field strongly suppresses propagation against the preferred direction. It has been shown that the ability of dynamic fractures to cross natural fractures can be limited, at least under the conditions examined in this study. It is also apparent that much more work is needed in the development of suitable charges for producing reproducible dynamic fractures before a truly systematic study of the interactions with natural fractures is possible.

TASK 3. FLOW CHARACTERISTICS  
OF NATURAL FRACTURES

OBJECTIVE

The objective of this task was to measure in the laboratory the influence of stress on natural fracture conductivity and the flow interaction between natural fractures and the matrix.

WORK PERFORMED

Core from various locations in the Appalachian Basin has been examined for the presence of natural fractures. No samples with natural macroscopic fractures were found. A pulse-permeameter has been constructed and a total of eleven preliminary tests and system check out tests performed on three samples with bedding plane partings.

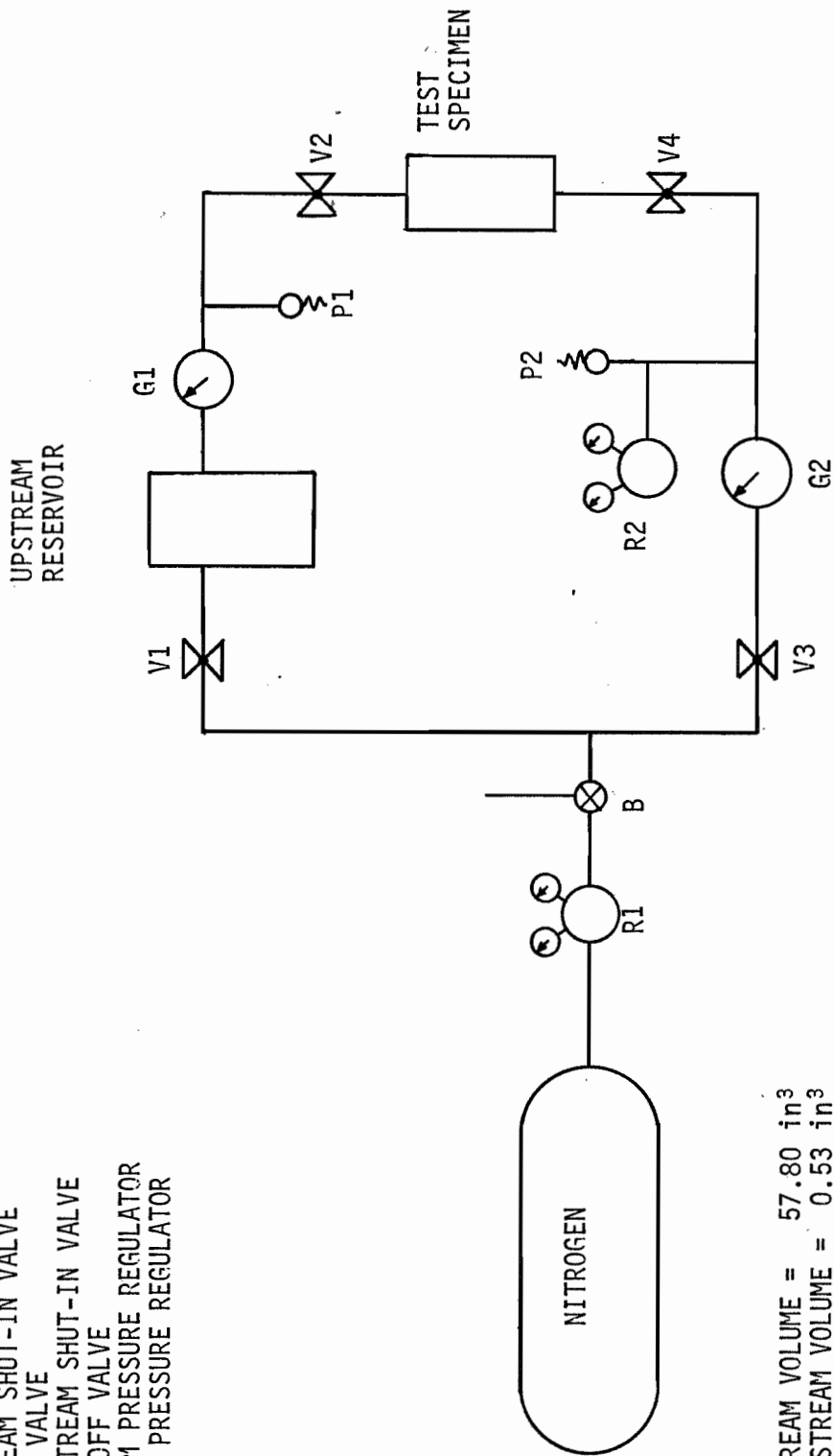
CORE EXAMINATION

About one-hundred and fifty feet of core from wells in Ohio and Pennsylvania have been examined, the wells being OH7, OH8, OH9 and PA2. In addition, about fourteen feet of core samples, preserved in cans from well OH9, has been examined. No natural macroscopic fractures were found in any of this core, although several had bedding plane separations. These were chosen for later testing.

PERMEABILITY TESTING

A pulse decay gas permeameter has been constructed for measurements on one inch diameter, two inch long samples which are jacketed and contained in a high pressure triaxial cell. This cell can contain confining pressures of up to 10,000 psi, and is placed in a 300,000 lbf load frame so that axial stress can be applied to the sample. The pore space of the sample is connected through porous end pieces, tubing and valves V2 and V4 to two gas reservoirs (Figure 3-1), the upstream reservoir (P1) having a volume of 57.80 cubic inches and

- B = SYSTEM BLEED VALVE
- G1 = UPSTREAM PRESSURE GAGE
- G2 = DOWNSTREAM PRESSURE GAGE
- P1 = UPSTREAM PRESSURE TRANSDUCER
- P2 = DOWNSTREAM PRESSURE TRANSDUCER
- V1 = UPSTREAM SHUT-IN VALVE
- V2 = PULSE VALVE
- V3 = DOWNSTREAM SHUT-IN VALVE
- V4 = SHUT-OFF VALVE
- R1 = SYSTEM PRESSURE REGULATOR
- R2 = BLEED PRESSURE REGULATOR



UPSTREAM VOLUME = 57.80 in<sup>3</sup>  
 DOWNSTREAM VOLUME = 0.53 in<sup>3</sup>

FIGURE 3-1. SCHEMATIC DIAGRAM OF PULSE-DECAY GAS PERMEAMETER.

the downstream reservoir with a volume of 0.53 cubic inches. These reservoirs are connected through valves V1 and V3 and a pressure regulator to a Nitrogen cylinder.

Permeability testing is performed in the following way. The sample is inserted into the vessel and the required confining pressure and axial stress applied. The Nitrogen regulator is adjusted to the required base pressure, valves V1 and V2 are opened and the pore gas pressure allowed to stabilize. Valves V3 and V2 are then closed isolating the sample and reservoir P2. The regulator is then reset to a new, higher pressure value and reservoir P1 allowed to reach this value.

Two principle types of tests have been performed. In build up tests, valve V1 is left open and valve V2 opened to allow the higher pressure to flow through the sample to reservoir P2. The pressure build up is monitored in P2 using a Dynisco Model APT 320 JA Pressure Transducer and the build up with time used to determine the permeability of the sample. In pulse decay tests, V1 is opened with V2 closed allowing P1 to come to the new pressure. V1 is then closed and V2 opened. As gas flows through the sample the decay of pressure in P1 and the build up in P2 are monitored and used to determine the permeability of the sample. In addition, two flowrate tests have been performed as a check of results. In these, the upstream pressure is maintained constant using the Nitrogen regulator and the downstream reservoir is opened to the atmosphere. Flow rate was determined by allowing gas to flow into an inverted, water filled, graduated cylinder.

## EXPERIMENTAL RESULTS

Before discussing the results of testing the following points should be brought out:

- 1.) The results of the test are sensitive to the volume of the downstream reservoir. Thus, a smaller reservoir will give more rapid pressure build up, and is best suited for very low permeability samples, while a larger reservoir will give slower pressure build up and is best suited to higher permeability samples. This can lead to problems when samples have a wide range of permeabilities, such as very low permeability shales with high conductivity fractures.
- 2.) The calculation of permeability can be quite sensitive to the ratio of the storage volume in the core (and hence its porosity) to the volume of the downstream reservoir.
- 3.) Since tests can run for a fairly long time the system is very sensitive to leaks, particularly in the downstream reservoir and associated tubing, and to temperature changes.

- 4.) In the tests described here the resulting "permeability" is a composite of the matrix permeability and the fracture conductivity. Given the very low permeability of the shale matrix it would be expected that flow through fractures would dominate.
- 5.) Any matrix permeability measured here will be a composite of flow due to Darcian flow and that, due to absorption/desorption mechanisms.

A total of nine permeability tests and two system checks have been run on three samples of Devonian shale. In all cases, the samples were prepared as one-inch diameter and two-inch long plugs cut parallel to bedding. Since no natural fractures were found in the available core these samples were chosen on the basis of having bedding plane partings, approximately parallel to the core axis. The presence of these partings is assumed to be a result of core handling after retrieval. The various tests are summarized in Table 3-1.

#### Data Analysis

Data from these tests has been analyzed on the basis of the techniques given by Chen and Stagg, 1984, and Brace et al, 1968. The test data were outside of the time domain in which an error function solution (Walls et al., 1982) would be applicable (i.e., dimensionless time is less than 0.6).

Chen and Stagg quote the solution for the transient pressure problem in the form:

$$P_D(x_D, t_D) = \sum_{n=1}^{\infty} \frac{2 \exp(-\alpha_n^2 t_D) \sin \alpha_n}{\alpha_n \{1 + \gamma / (\gamma^2 + \alpha_n^2)\}} \quad (3-1)$$

where 
$$P_d(x_D, t_D) = \frac{P_1 - P(x, t)}{P_1 - P_2(0, 0)}$$

$P_1$  is the upstream pressure,

$P(x, t)$  is the pressure at position  $x$  and time  $t$ ,

$$x_D = x/L,$$

$L$  is the length of the sample,

$$t_D = \frac{kt}{\phi\mu cL^2},$$

$k$  is the permeability,

$\phi$  is the porosity,

$\mu$  is the gas viscosity,

$c$  is the gas compressibility,

$$\gamma = \frac{\phi AL}{V_2},$$

$A$  is the area of the core,

$V_2$  is the volume of the downstream reservoir,

$\alpha_n$  is the  $n$ th root of:

$$\alpha \tan \alpha = \gamma.$$

This solution is taken from the analogous result for heat conduction given by Carslaw and Jaeger, 1959. For large values of time ( $t_D > 0.3$ ) terms above the first of this series can be neglected, and a straight line relationship should occur between the logarithm of dimensionless pressure and time. This line has a slope,  $M$ , given by:

$$M = \frac{\alpha^2 kt}{\phi\mu cL^2},$$

and an intercept,  $C$ , given by:

$$C = \log_e \frac{2 \sin \alpha}{\alpha \{1 + \gamma / (\gamma^2 + \alpha^2)\}},$$

The intercept may be used to determine values for  $\gamma$  (and hence  $\phi$ ) and  $\alpha$ . These values, together with the slope, are used to determine  $k$ .

Brace et al., give a simplified relationship which is suitable for  $\gamma \ll 1$  and  $\alpha \approx 1$ :

$$P_D(x_D, t_D) = \exp(-\gamma t_D). \quad (3-2)$$

Again a plot of the logarithm of  $P_D$  against time should have a straight line with a slope,  $m$  of:

$$m = Ak/(V_2 \mu c L).$$

As a check of the results of the analysis the series result of Chen and Stagg (Equation 3-1) has been used to compute dimensionless pressure as a function of time. In performing this computation using results from Equation 3-2 a porosity of one percent was used, this being a fairly typical value for Devonian Shale (i.e., Klyoncu et al., 1977).

### Test Results

Data from Tests K-1 (Sample 1) and K-7, K-9, K-10, K-11 (Sample 3) have been analyzed, and these tests are discussed below. Data for Tests K-2, K-4, K-5 and K-6 (Sample 2) are not analyzed since no detectable pressure changes were noted in ten minutes for K-2 and K-4 or in sixty minutes for K-5 and K-6. The results of these tests are shown in Table 3-2, and are discussed in more detail in the following paragraphs.

Test K-1 (Sample 1). This was a buildup tests with a base pressure established at a nominal 180 psig, and the upstream reservoir held constant during the test at 200 psig. A record of the test is shown in Figure 3-2. After about 100 seconds valve V2 was opened and a buildup observed. The downstream reservoir was then bled to about 18 psig and valve V2 reopened at about 170 seconds. Buildup occurred up to 290 seconds when the downstream pressure had reached nearly the same value as the upstream pressure.

Data from this second buildup have been analyzed, using both the semi-log analysis technique described by Chen and Stagg, and that based on the exponential relationship of Brace et al. The analysis after Chen and Stagg gave a straight line on semi-log paper with a slope of 0.0667/seconds and an intercept of 0.0896. These give a porosity of 19.05 percent and a permeability of 1.16 mD. The analysis based on Brace et al., gave a permeability of 0.692 mD.

TABLE 3-1

## PERMEABILITY TESTS

TEST NO.	SAMPLE NO.	CORE	AXIAL STRESS PSI	CONFINING PRESSURE PSI	TYPE OF TEST	DOWNSTREAM OR BASE PRESSURE PSIG	UPSTREAM PRESSURE PSIG
K-1	1	OH7	6000	3000	Buildup	0	200
K-2	2	OH7	6000	3000	Buildup	0	200
K-3	2	OH7	System Check				
K-4	2	OH7	6000	3000	Buildup	0	200
K-5	2	OH7	6000	3000	Decay	200	220
K-6	2	OH7	6000	3000	Decay	100	200
K-7	3	OH7	6000	3000	Buildup	0	200
K-8	3	OH7	System Check				
K-9	3	OH7	6000	3000	Buildup	180	200
K-10	3	OH7	6000	3000	Flowrate	0	20
K-11	3	OH7	6000	3000	Flowrate	0	20

TABLE 3-2  
PERMEABILITY RESULTS

TEST SAMPLE NO.	FLOW TIME SECS	MAXIMUM DIMENSIONLESS TIME	SEMILOG CHEN & STAGG		SEMILOG BRACE ET AL.	STEADY STATE
			PERM mD	POR	PERM mD	PERM mD
K-1	1	230	9	1.16	0.190	0.692
K-7	3	20	139			3.513
K-9	3	590	16			0.0091
K-10	3					0.0197
K-11	3					0.0676

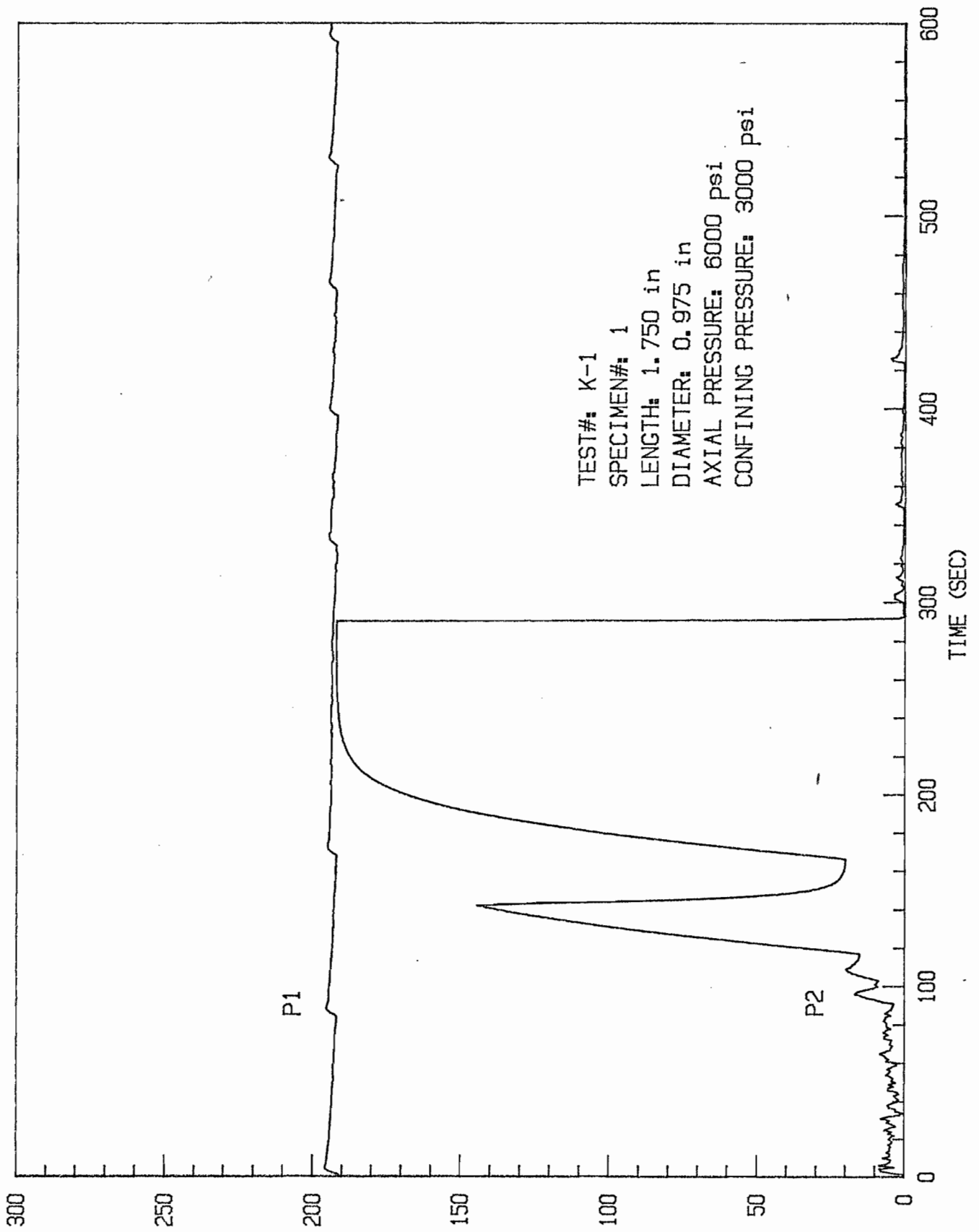


FIGURE 3-2.

Of these two sets of results those from the Brace et al., solution are preferred for two reasons. Firstly, the Chen and Stagg result gives a very high value for porosity - the porosity of the shale samples would be expected to be of the order of one percent rather than twenty percent (Klyoncu et al., 1977). Secondly, the back-calculated values of the dimensionless pressure are closer to the measured values for the lower permeability and (assumed) lower porosity of the Brace et al., results, (Figures 3-3 and 3-4).

Test K-7 (Sample 3). This was again a buildup tests with a base pressure established at a nominal 200 psig, and the upstream reservoir held constant during the test at 218 psig. A record of the test is shown in Figure 3-5. Buildup was rapid, occurring in about ten to fifteen seconds, suggesting a high permeability.

Analysis based on the Chen and Stagg equations gave negative porosities and was abandoned. The analysis based on the exponential relationship of Brace et al., gave a permeability of 3.56 mD. Back-calculated values of the dimensionless pressure are very close to the measured values for this permeability and an (assumed) porosity of one percent, (Figure 3-6).

Test K-9 (Sample 3). This buildup test, carried out on the same sample as Test K-7, had a base pressure established at a nominal 180 psig, and an upstream pressure of 200 psig. A record of the test is shown in Figure 3-7. In contrast to the earlier test, buildup was slow, with only about fifty percent of build up occurring in 600 seconds, suggesting a low permeability.

Analysis based on the Chen and Stagg equations again gave negative porosities and was abandoned. The analysis based on the exponential relationship of Brace et al., gave a permeability of 0.0091 mD. Back-calculated values of the dimensionless pressure are not very close to the measured values for this permeability and an (assumed) porosity of one percent, (Figure 3-8).

Tests K-10 and K-11 (Sample 3). In these tests measurements were made of flow volume rates under conditions of constant upstream and downstream pressures. An upstream pressure of 20 psig and downstream of 0 psig were used. In Test K-10 steady flow was reached after about 400 seconds, and a permeability of 0.0197 mD was calculated. In Test K-11 steady flow was achieved after about 250 seconds and a permeability of 0.0676 mD was calculated, (Figure 3-9, 3-10).

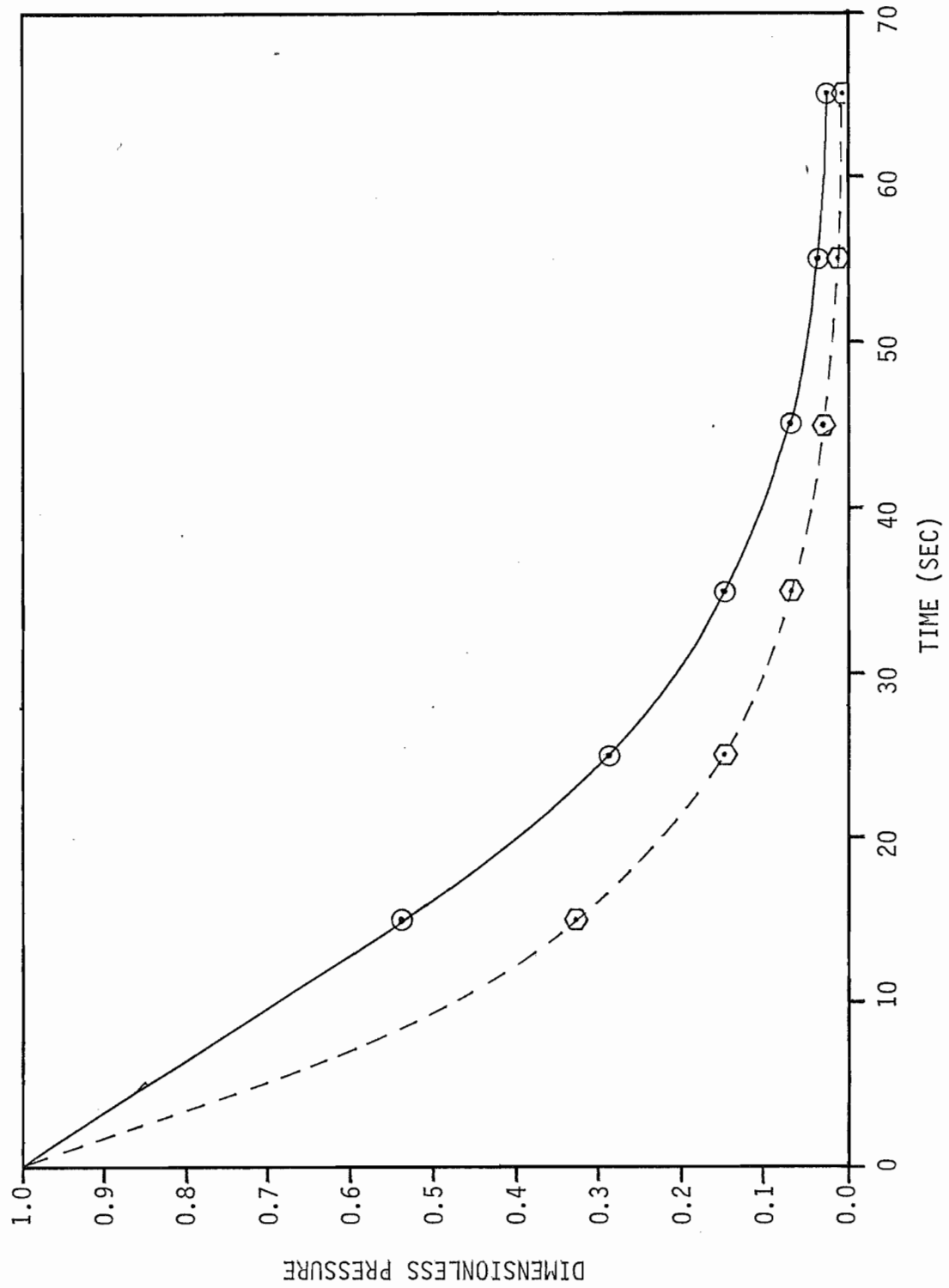


FIGURE 3-3. TEST K-1. PERMEABILITY = 1.16 mD  
POROSITY = 19%

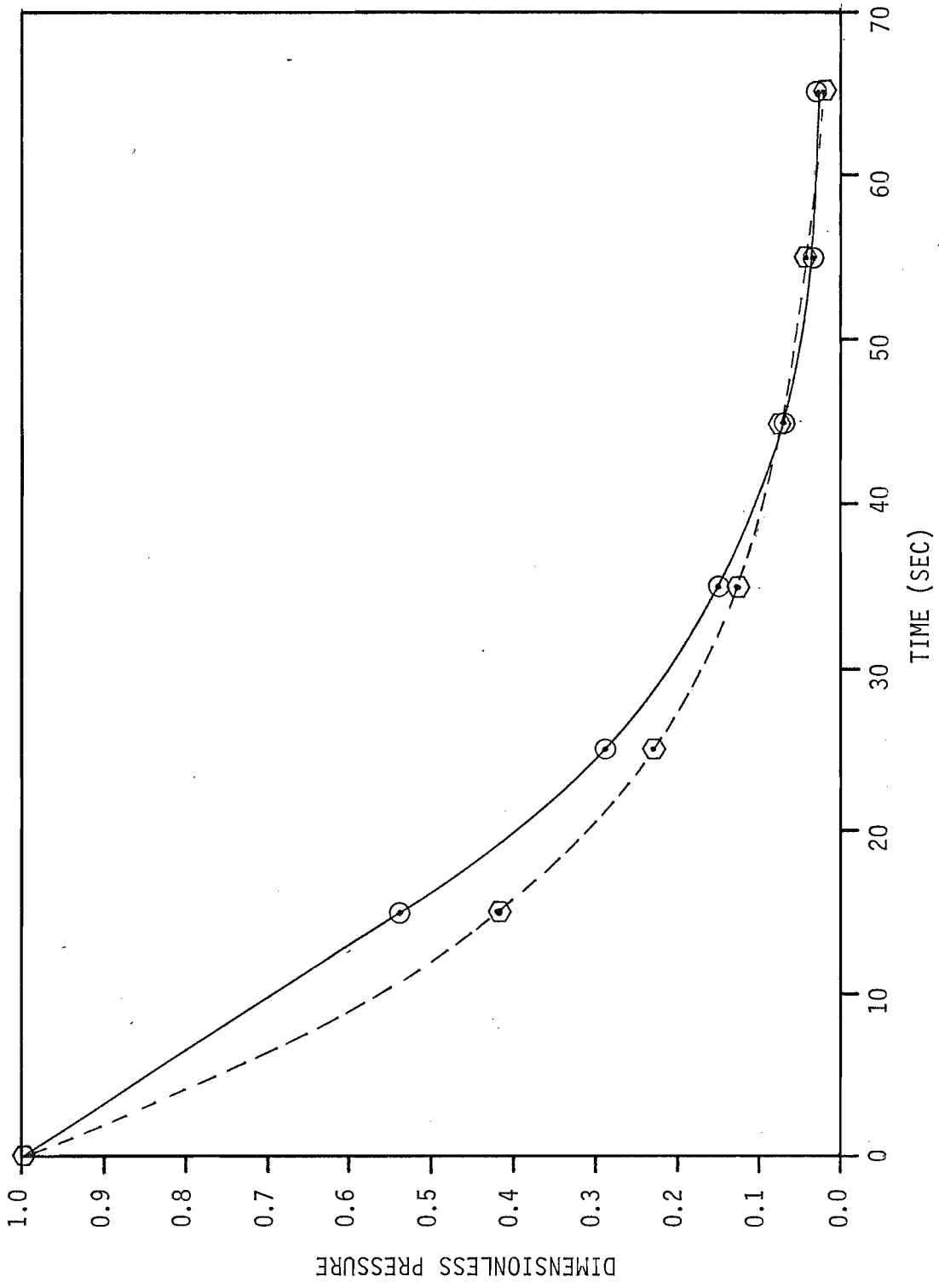


FIGURE 3-4. TEST K-1. PERMEABILITY = 0.692 mD  
POROSITY = 1%

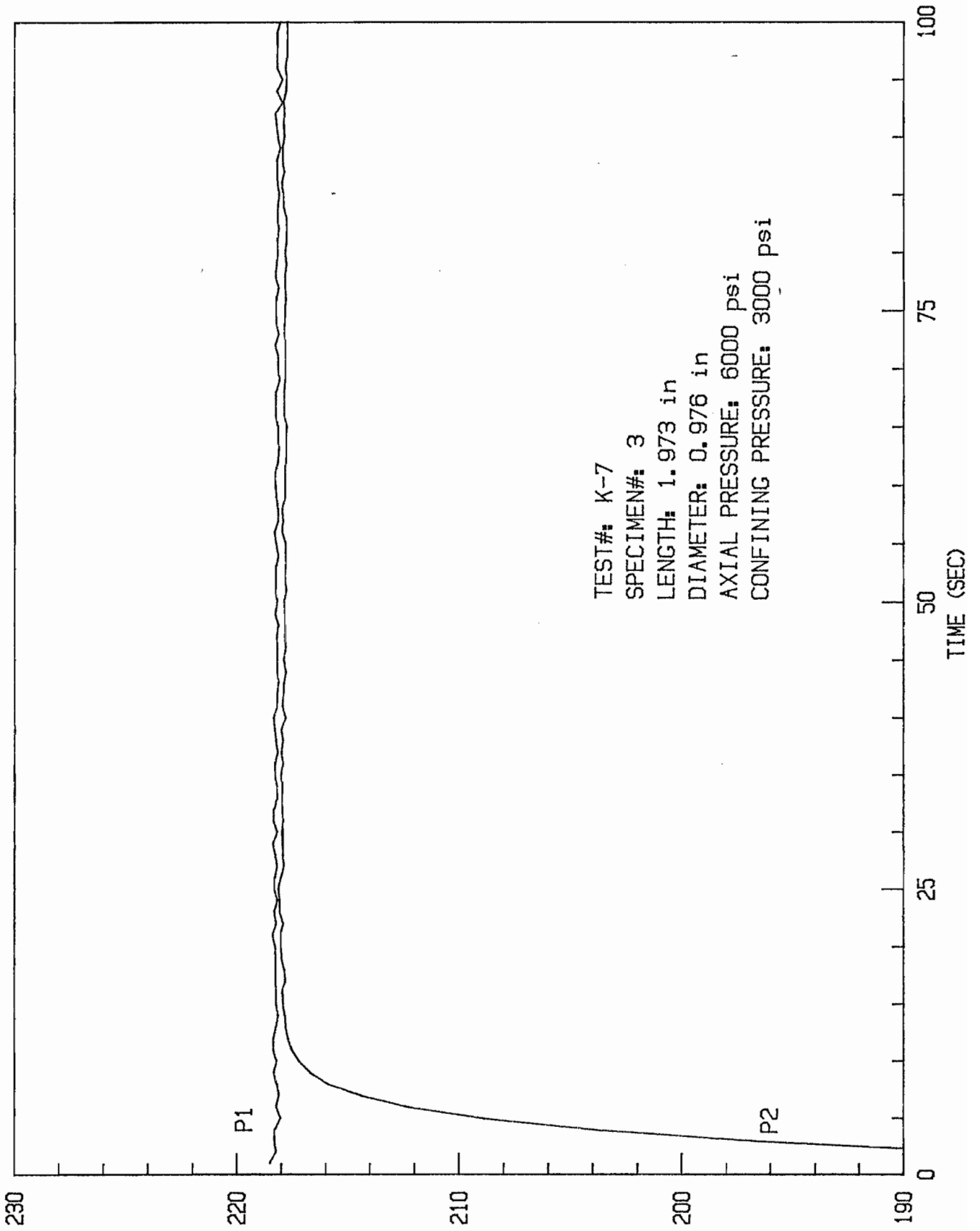


FIGURE 3-5.  
 PRESSURE (PSI)

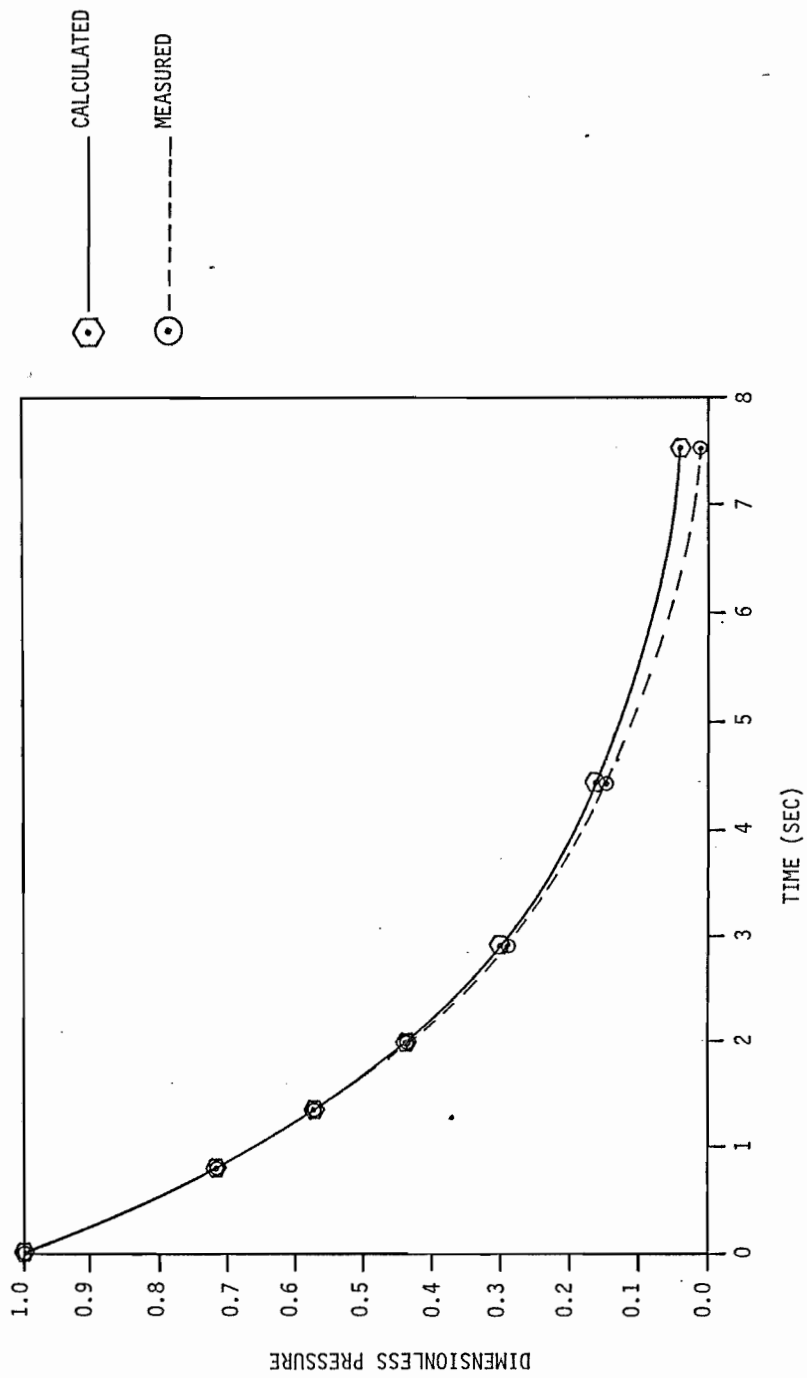


FIGURE 3-6. Test K-7. Permeability = 3.56 mD and Porosity = 1%.

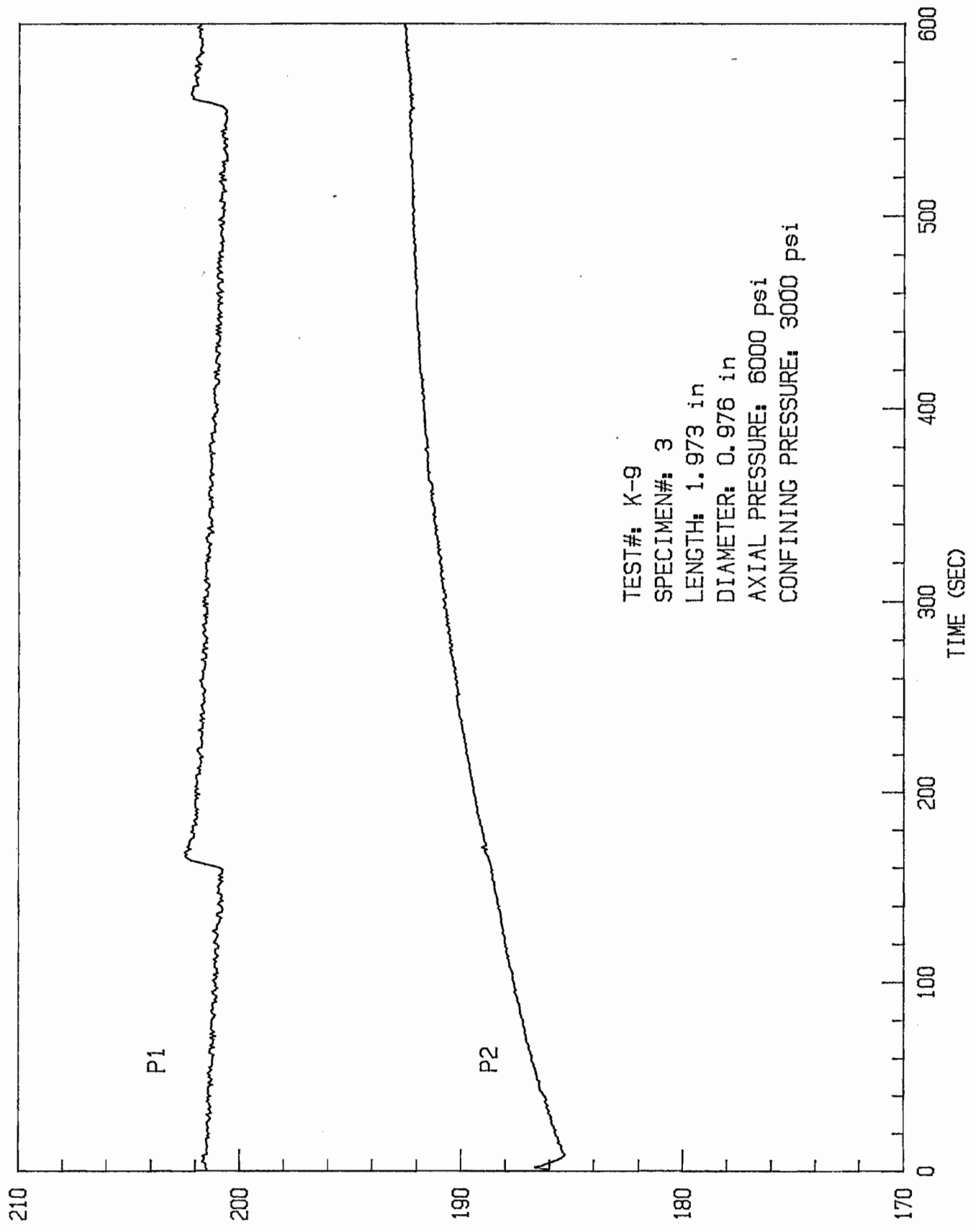


FIGURE 3-7.

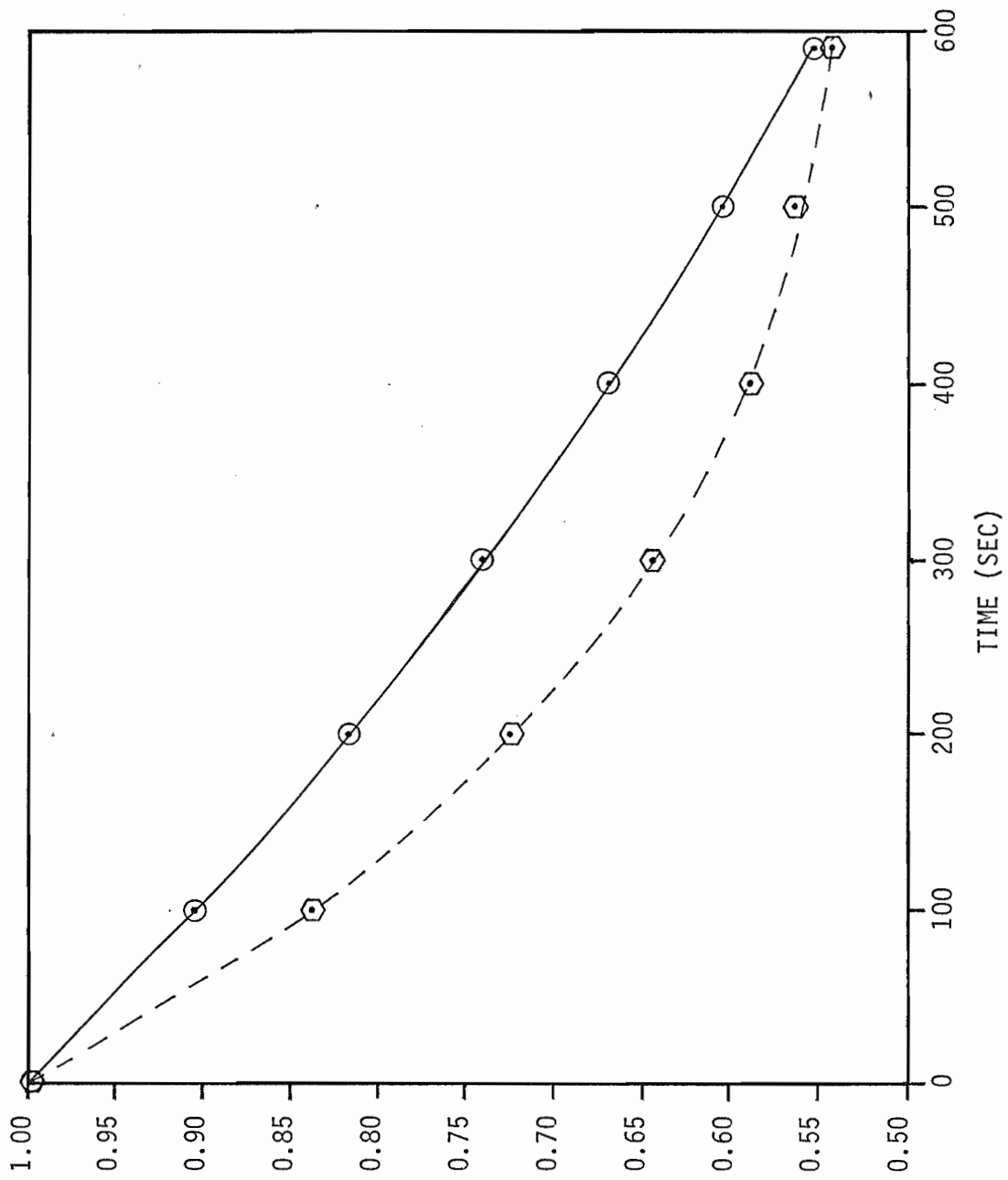
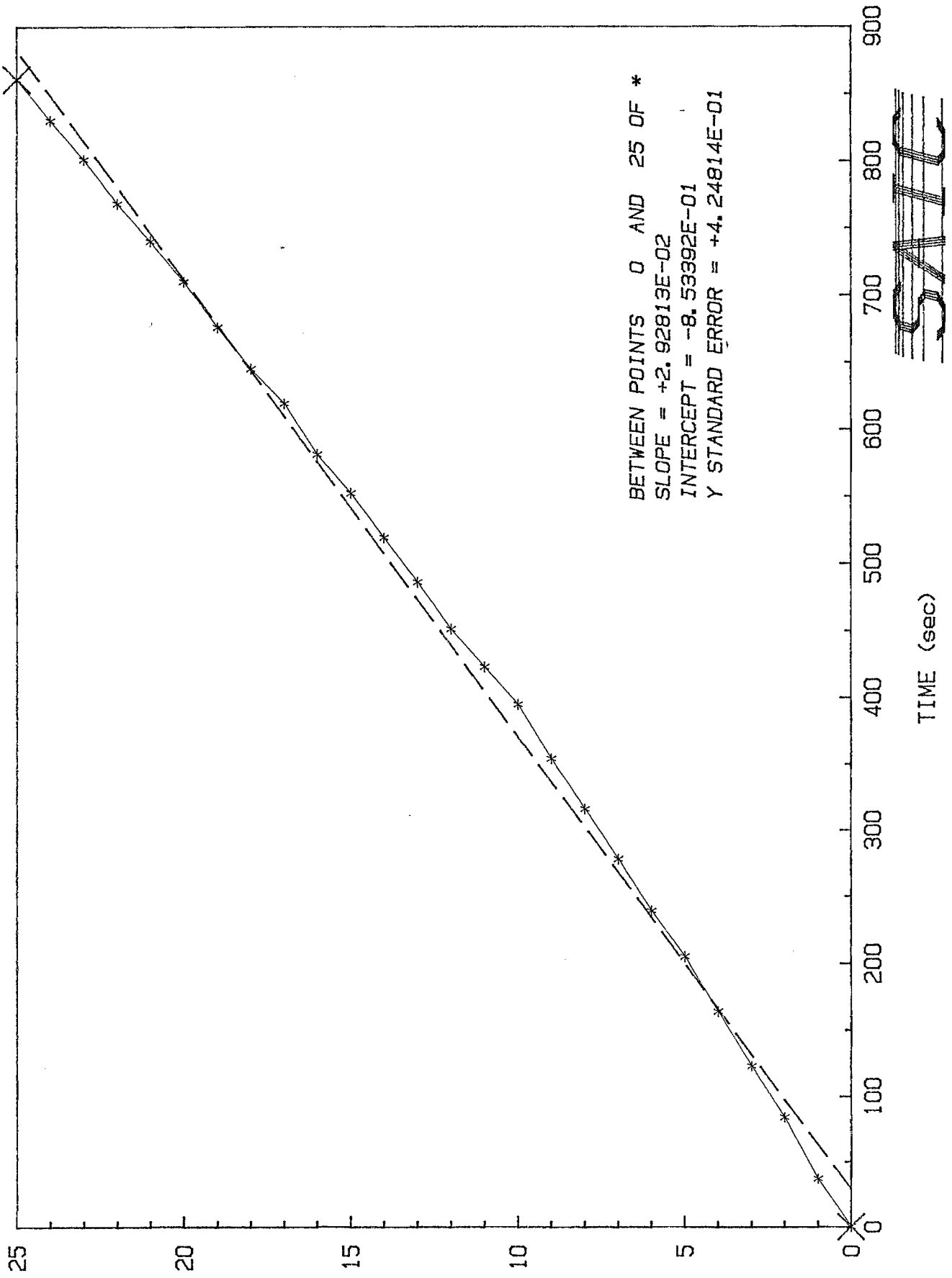


FIGURE 3-8. TEST K-9. PERMEABILITY = 0.0091 mD  
POROSITY = 1%

TEST#: K-10

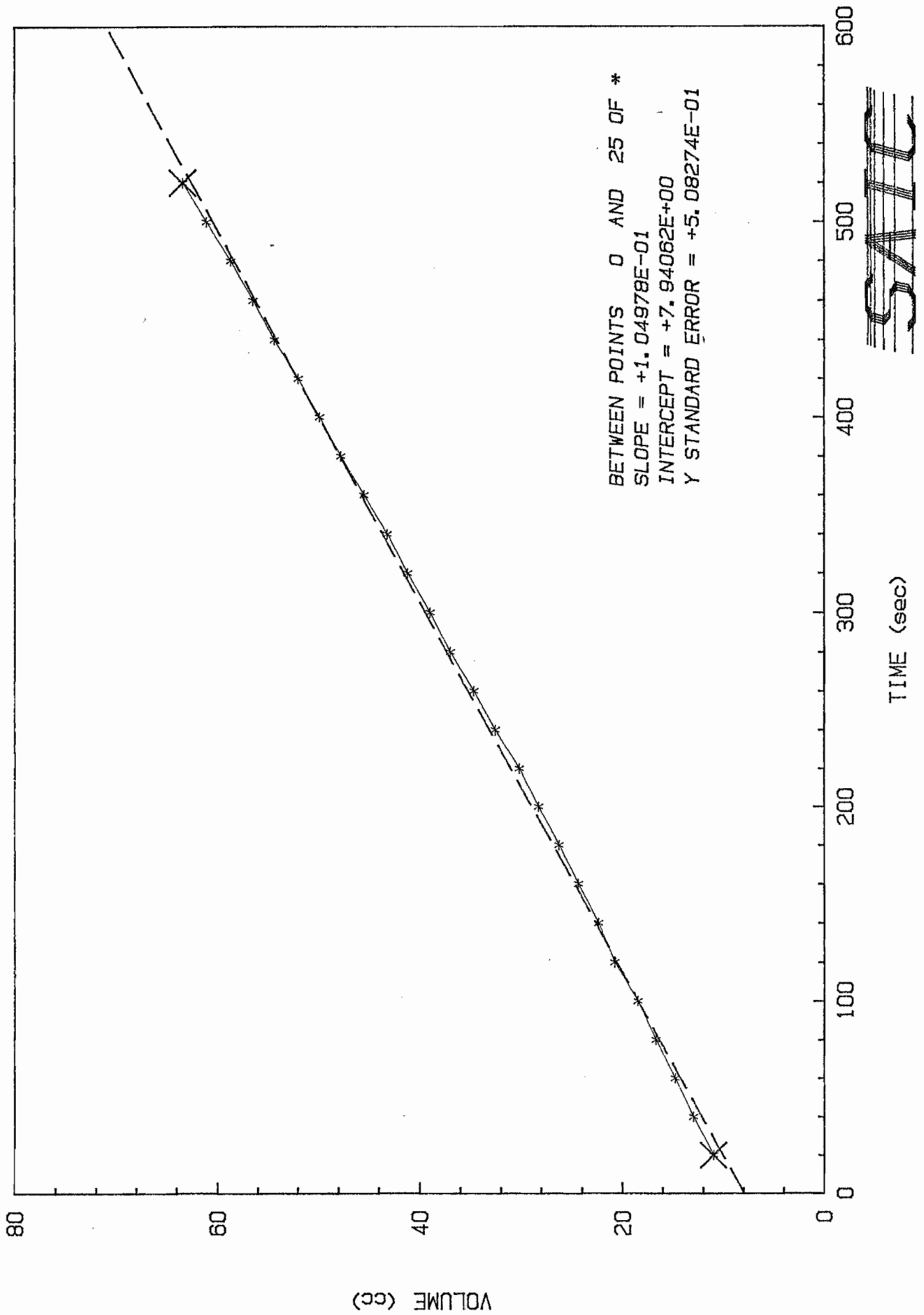
FLOW RATE DETERMINATION



VOLUME (cc)  
FIGURE 3-9.

TEST#: K-11

FLOW RATE DETERMINATION



VOLUME (cc)

FIGURE 3-10.

## CONCLUSIONS

The following conclusions were made on the basis of these early tests:

- 1.) The equipment as designed was not sufficiently sensitive to allow permeability measurements of the unfractured shale as evidenced by the lack of build up for Sample 2. It should be noted here that permeabilities of the order of  $10^{-2}$  to  $10^{-1}$  mD were determined without any problems for Sample 3.
- 2.) The equipment would need modification for measurements of higher permeability fractures, as demonstrated by the very rapid buildup in Test K-7.
- 3.) The data were not reproducible. Thus, the same sample, Sample 3, tested under nominally identical conditions gave permeabilities of from 0.009 to 2.14 mD for the buildup tests and from 0.0197 to 0.0676 mD under steady state flow. This extreme variability is presumably a result of variations in connection to the fracture in the different tests. This highlights the problems in the determination of the conductivity of natural fractures. In addition, more careful control of thermal effects could help the reproducibility.
- 4.) There were no suitable natural fractures suitable for testing in the core examined.

As a result of these conclusions, in particular the lack of reproducibility and the consequent difficulty in interpreting the results of permeability measurements in terms of flow regimes and mechanisms, it was concluded that a thorough study would be outside of the scope of the task as originally proposed. As a result further testing was suspended.

## TASK 4. IN SITU STRESSES IN THE APPALACHIAN BASIN

### OBJECTIVE

The objective of this task was to collect and analyze existing stress data for the Appalachian Basin and to study new techniques for stress measurement.

### WORK PERFORMED

Work in this task consisted of collecting stress data from as many sources as possible for the Appalachian Basin and plotting the results on maps to be used in applying the results of Tasks 1 and 2. A detailed evaluation of techniques available for determining stresses was also performed. Some development work was done on wellbore elongation, a technique that was only in the conceptual stage at the start of this study.

### STATE OF STRESS IN THE APPALACHIAN BASIN

In situ stress data for the Northeastern United States has been collected from a large number of sources (Lindner and Halpern, 1978, Haimson, 1978 & 1982, Zoback and Zoback, 1980, McKetta, 1980, Komar and Bolyard, 1981, Yang et al., Cliffs, 1981, Engelder, 1982, Zoback and Zoback, 1985, and Plumb, 1986.). The techniques used to make these measurements are hydraulic fracturing, focal mechanism solutions, wellbore breakouts, and recovery strain measurements. Surface measurements have been excluded because they are more influenced by local topography than regional stresses. Measurements based on core-induced fractures have also been excluded because there is a strong possibility that they are as much influenced by rock fabric as in situ stresses.

The orientations of the maximum compressive stresses have been plotted in Figure 4-1. In general they show an ENE trend in the north and south parts of the basin with a more east and west trend in the central part of Eastern Ohio and Western Pennsylvania.

The data on stress magnitudes is less comprehensive and, where it is available, tends to show more variation. This variability is illustrated by hydraulic fracturing measurements that are being made at

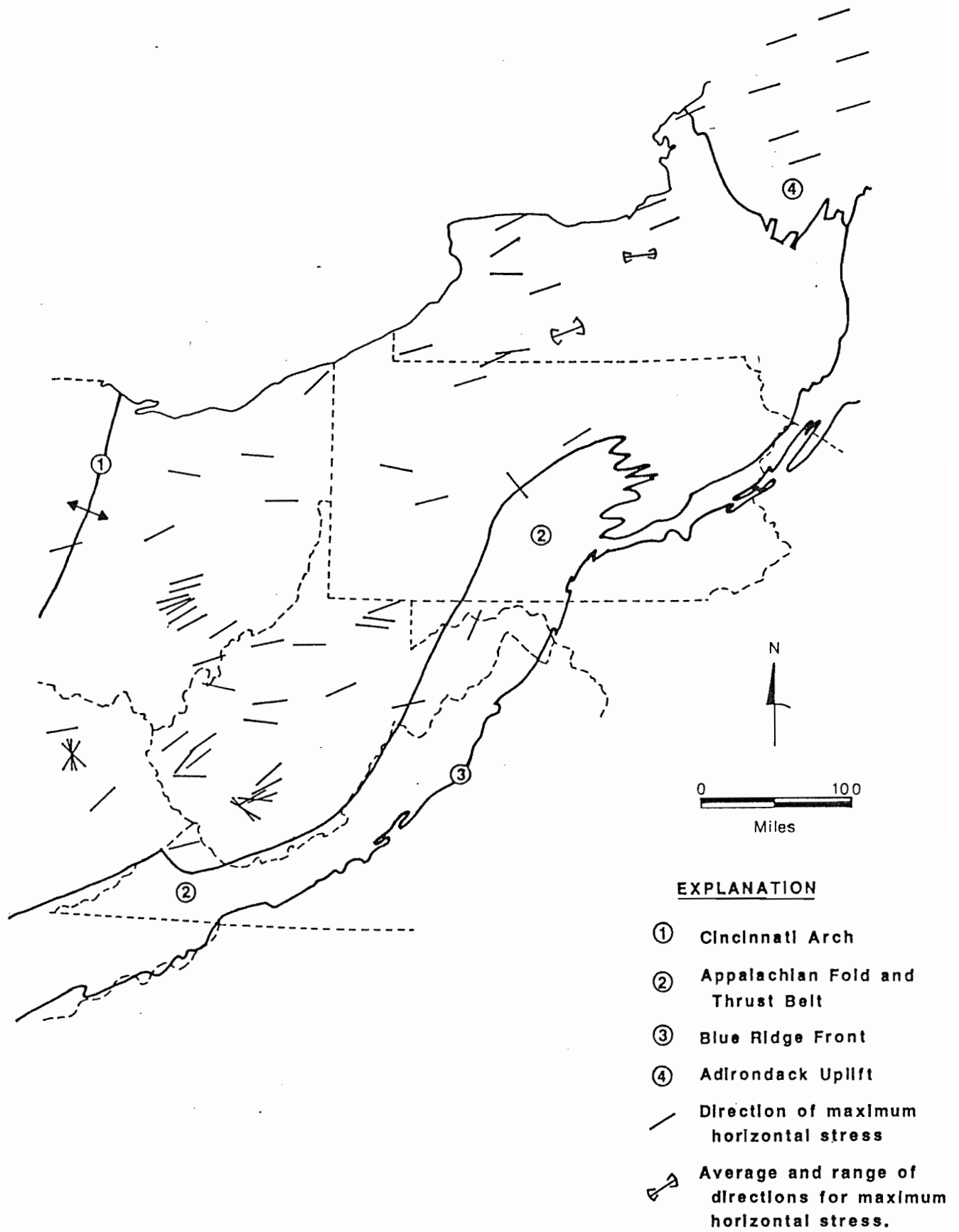


FIGURE 4-1. Directions of maximum horizontal stress.

two sites in New York by Evans and Engelder (1986). Over one thirty foot interval the fracture gradient dropped from 1.15 to 0.8 psi/ft. When this much variation can be found at one site over such a small interval, it is difficult to establish trends on a regional scale. There have been some efforts to delineate areas of high and low stress ratios (minimum horizontal stress/overburden) in the basin. McKetta (1980) suggested that the ratios of minimum horizontal to vertical stress were lower in the eastern part of the basin. It should be pointed out that the measurements in the eastern part of the basin were also deeper and the ratio of minimum horizontal to vertical stress is in most cases lower for deeper measurements. In any case, stress ratio data does not give the maximum stress, nor the stress differential which is needed for the applications being considered here.

Some generalizations can be drawn about stresses in the basin. In every case examined in this study, the maximum compressive stress was horizontal. In most cases the minimum principal stress was found to be horizontal and the intermediate principal stress was vertical, although in some of the shallower measurements the least principal stress was vertical.

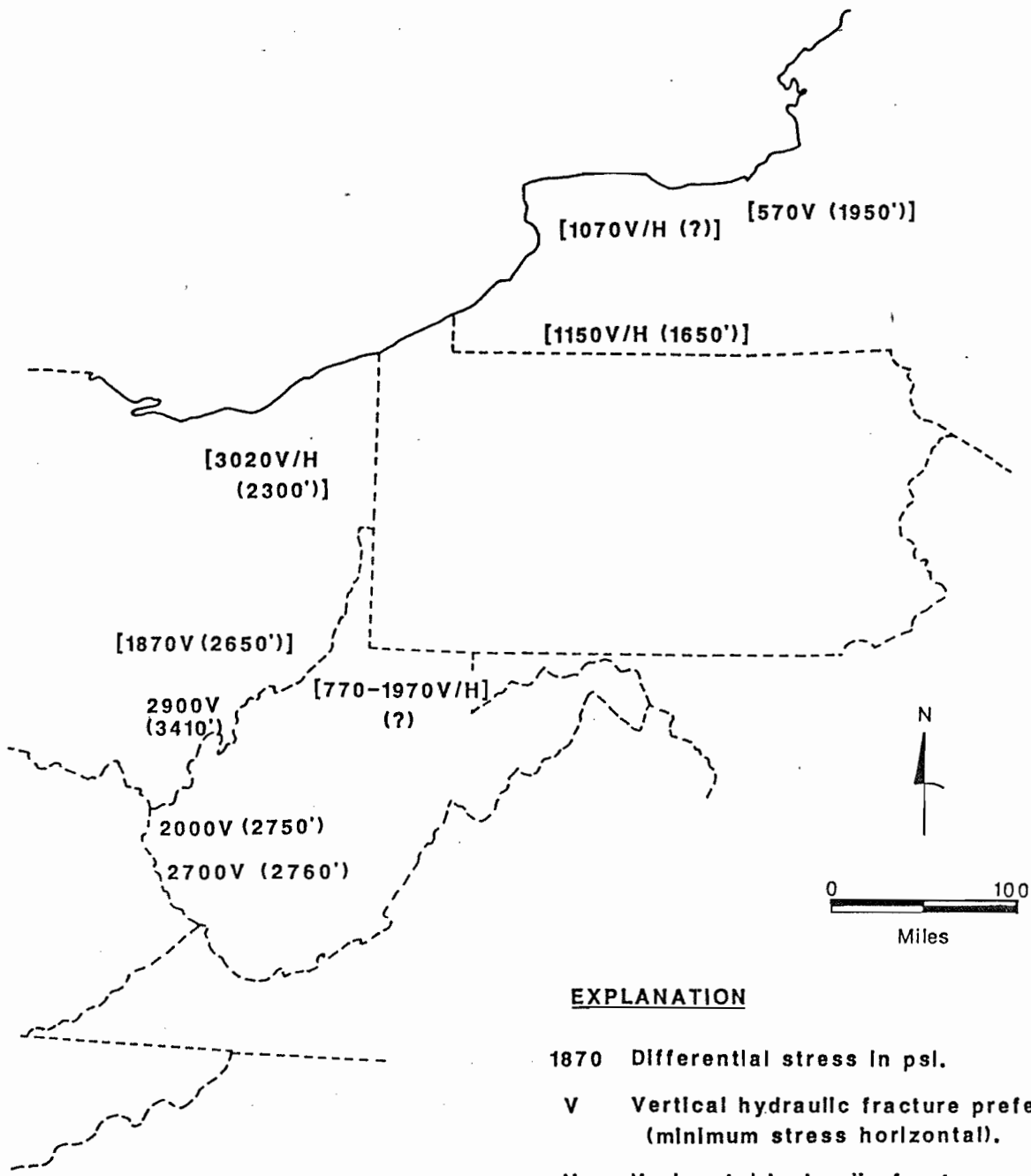
For the purposes of this study, it is the difference between the maximum and minimum principal stresses that is needed. However, some techniques used, such as focal mechanism solutions and wellbore breakouts, give only orientations. Even in cases where hydraulic fracturing was used, it was sometimes only possible to determine the least principal stress with any accuracy. The few cases where reliable magnitude data for calculating differential stress was available are plotted in Figure 4-2. The variety in values for stress difference makes it difficult to draw any generalizations. For the purposes of applying the results of Tasks 1 and 2, however, it may be enough to say that the differential stresses will always be greater than about 500 psi and in most cases will be greater than 1000 psi.

A more detailed discussion of the state of stress in the Appalachian basin, its relationship to the tectonic history of the basin, and its influence on the presence of fractures is given under Task 5.

#### EVALUATION OF STRESS MEASURING TECHNIQUES

Techniques for measuring in situ stresses fall into the following three groups according to the principle on which they are based: (1) those that relate rock fabric to in situ stresses, (2) those that depend on failure of the rock, and (3) those that measure viscoelastic recovery deformation.

##### Fabric



**EXPLANATION**

- 1870 Differential stress in psi.
- V Vertical hydraulic fracture preferred (minimum stress horizontal).
- H Horizontal hydraulic fracture preferred (minimum stress vertical).
- (2300') Depth of measurement in feet.
- [ ] Measurement not in Devonian Shale.

FIGURE 4-2. Differential stresses.

Techniques that measure some aspect of the fabric in the rock believed to have been caused by the in situ stresses are; differential strain analysis or DSA (Strickland and Ren, 1980), ultrasonics (Peng et al., 1980), twin lamellea analysis (Friedman and Heard, 1974), and the bifurcation technique (Gangareo et al., 1981).

1. DSA and ultrasonics are both based on the same principle. The idea is that when stresses are removed by coring, part of the recovery deformation experienced by the rock is due to the formation of microcracks and that the degrees of crack opening along a given axis will be proportional to the stress along that axis. DSA and ultrasonics are simply two different techniques that can be used to measure the crack population in different directions. The main advantage of the technique is that as long as a piece of core has been reasonably preserved, one should be able to determine its state of stress prior to coring. The main weakness in the technique is the assumption that microcrack opening will accurately reflect the in situ stresses.

There are two reasons why this might not be true. First there may be other mechanisms of recovery deformation, such as intracrystalline deformation, operative in the rock so that crack opening would not represent all or even a significant part of the recovery of the core. The second problem is that crack opening will be strongly influenced by the fabric of the rock. If the fabric is anisotropic, then it will distort the effect that the stresses have on crack opening. The fabric could be due to cracks that developed under a paleostress, and thus the technique would be a measure of the past stresses rather than the current stresses. Another source of distortion of the results by fabric could come from a preferred orientation of grain boundaries. In this case, the crack population may tell more about conditions of diagenesis or metamorphism than the current in situ stresses. In a rock that has undergone as many periods of deformation as the Devonian shales (see following section on tectonics), fabric could influence DSA and ultrasonics more than in situ stresses.

2. Twin lamellea analysis only applies to rocks composed of minerals, such as calcite, that undergo intracrystalline twinning at the stress conditions experienced by the rock. This approach is not applicable to Devonian shales.

3. The bifurcation technique is discussed in particular detail here because questions have been raised as to the difference between it and differential strain analysis (DSA) and the strain recovery method (SRM).

The method uses a prismatic sample of rock which has a strain gage rosette cemented to the face perpendicular to bedding. The sample is loaded along an axis in the bedding plane parallel to this face and clamped across the remaining two faces. A plot of strain from the rosette against stress is made. The technique then involves detecting a change in slope of the stress-strain curve and relating this to the in situ stress. As further background for the following discussion the

reader is urged to review pages 73-86 of Gangarao et al., (1981).

While there are some superficial similarities between this method, DSA and SRM, the techniques are distinct. DSA involves measuring a steepening of stress-strain curves, whereas the bifurcation technique involves picking a point at which the slope of a stress-strain curve decreases. Also, the DSA theory explicitly states the mechanism by which measurements are related to the in situ stresses; i.e., microcracks that develop during unloading. In the report on the bifurcation technique, no clear link between a mechanism and the observed behavior is presented. There is mention of the rock having a "memory" and "defect growth", but how these would cause the observed behavior is not discussed. Inelastic deformation would cause a lowering of the slope of the stress-strain curve, but Gangarao et al., makes a point of showing that the strains measured are elastic. Finally, the DSA theory clearly states the method of calculation of stresses and why the method is believed to work. As will be seen in later discussions the method of calculation in the bifurcation technique is vague.

The primary difference between the bifurcation technique and the SRM is that the SRM involves active measurement of recovery strains immediately after removal of core from the wellbore, whereas the bifurcation technique involves measuring deformation caused by loading the rock in the laboratory. Also, calculation of the stresses in the SRM employs equations derived from modern viscoelasticity for the appropriate unloading conditions.

The following points need to be addressed in order for the bifurcation technique to be considered viable.

- A. A clear relation between the bifurcation points and the in situ stresses needs to be established.

Such a relation is suggested by the statement on page 74 of Gangareo et. al that "the state of stress at the second bifurcation point should be nearly identical to the state of stress of the material before it was cored out of the formation." Actually, the state of stress at the second bifurcation point is quite different from the in situ state of stress for three reasons.

1. The state of stress produced in the laboratory involves a free face which does not exist in situ. The state of stress in the laboratory can be characterized as follows: the maximum principal stress is equal to the axial load in the bedding plane, the intermediate stress is equal to the clamping stress perpendicular to the bedding pane, and the least principal stress is equal to atmospheric pressure (about 14.7 psi) on the free face. It is unlikely that for every sample tested in this study, one of the in situ principal stresses was equal to atmospheric pressure.
2. On page 73 of Gangareo et. al the clamping forces are said to simulate the overburden pressure, but this cannot be verified

by referring to the actual tests in Tables E.6.1 - E.6.3 of the Appendix. The following table illustrates the variances between the actual overburdens and the clamping stresses.

Location	Depth	Clamping Stress		
		Direction	Overburden	From Tables
MI2	1478	Y	1642	760
MI2	1623	X	1860	748
OH8	3311	X	3570	920
OH8	4131	Y	4628	660

It appears from the values given that the laboratory clamping stress does simulate the overburden stress.

3. In the laboratory tests, the principal stresses in the bedding plane (X and Y directions) do not appear to correspond to the in situ principal stresses in the bedding plane. The orientations of X and Y directions in the laboratory specimens are apparently the same for each specimen and are chosen to be parallel and perpendicular to a particular compass direction (magnetic meridian, see page 16 of Gangareo et al.). It is doubtful that the in situ stress directions are the same.

- B. The idea that there will be a maximum and a minimum horizontal stress and that they can and often do have very different magnitudes does not seem to have been considered in developing and applying the bifurcation technique.

Horizontal stresses are measured in an X and Y direction. The method of choosing X and Y directions parallel and perpendicular to a compass direction insures that they will not necessarily be aligned with the maximum and minimum stress directions. The problem of distinguishing maximum and minimum horizontal stress also occurs in the comparisons with hydraulic fracturing measurements presented in Table 4.3 of Gangareo et al. The column is simply labeled Horizontal Pressure with no idea given as to whether these are maximum or minimum stresses. The methods of calculating maximum and minimum stresses from hydraulic fracturing data are quite distinct and there should not be any confusion as to which is which.

- C. The method for calculating horizontal stresses is not always clear.

With the exception of the first value, which corresponds to an individual test, it is difficult to determine how the horizontal stresses were calculated. They do not seem to correspond to an average for the X direction or the Y direction or an overall average for any individual test. As for the individual tests, it seems clear that the horizontal stresses were calculated by subtracting the stress at the

first bifurcation point from that at the second. This being the case, it is uncertain why the equation on page 74 of Gangareo et al., is presented as the means of calculating horizontal stresses. Attempts to use this equation to calculate stress resulted in numbers that did not correlate with anything.

D. A material responds to the resultant of the different stress field superposed at any given time, but it cannot distinguish the individual fields that have been superposed.

The idea behind the bifurcation technique seems to be that a material can indeed distinguish between different stresses that have been superposed in a single direction and even retains a memory of them.

## Failure

Techniques that depend on failure of the rock are; hydraulic fracturing, coring-induced fractures such as petal fractures and core discing (Obert and Duvall, 1967), and wellbore breakouts (Babcock, 1978, Bell and Gough, 1979).

1. Hydraulic Fracturing is the most widely accepted conventional technique for measuring in situ stresses, but it still has significant limitations. Calculation of the maximum horizontal stress is based on the assumption of a perfectly circular hole. Since this rarely occurs in most practical situations the maximum principal stress cannot be determined. This limitation is a particular problem for the applications being considered here, because it is the difference between the maximum and minimum stresses that is needed. The technique also assumes that the axis of the borehole is closely aligned with one of the principal stresses. This would present problems in deviated wells, which are now being considered for Devonian shales. Also, the treatment should be performed in open hole for best results. In addition to these technical limitations, hydraulic fracturing involves enough logistical complications to make any simpler technique look attractive. Even a small fracturing treatment requires considerable surface and downhole equipment (pumps, pressure and flow measuring devices, rig, inflatable straddle and impression packers, orienting survey, etc.).

2. Coring Induced Fractures. The primary limitation to using coring-induced fractures such as petal fractures and core discing in determining in situ stresses is that a direct cause-effect relationship that is independent of rock fabric has not been established. Thus, fabric could be influencing these features as much as stresses. Also, both techniques would require relatively high in situ stresses or very weak rock. Assuming that they do accurately reflect the state of stress downhole, petal fractures still only give information on stress orientation, which is not enough for the applications being considered here.

3. Wellbore Breakouts appear to give reliable information on the orientation of principal stresses, but they require relatively high differential stresses before they occur. Also, they do not give information on magnitudes.

Recovery Deformation

Techniques that measure viscoelastic deformation caused by removal of in situ stresses are; strain recovery method (Blanton, 1983, Blanton and Teufel, 1983) and wellbore elongation (Blanton and Teufel 1985).

1. The Strain Recovery Method has been used successfully in Devonian shales (Blanton and Teufel, 1983). Its main limitation is that it requires intact, oriented core. In situations where coring is already planned, however, it is an efficient approach since the additional costs and logistics are minimal, and it does not interfere with continued drilling and well completion. Also, in most cases it gives information of the complete stress tensor.

2. Wellbore Elongation. At the beginning of this study, wellbore elongation was only an idea. The concept involved applying the same principles used in the recovery strain method to deformation of the wellbore. The idea was particularly attractive because the technique only required an accurate caliper log of the hole, and it had the potential of providing information on the state of stress throughout the logged portion of the hole. Therefore, an effort has been made, as part of this task, to develop the equations required for calculating in situ stresses from wellbore deformation measurements. The development is divided into three parts. First, the basic constitutive theory for porous viscoelastic material is derived from elastic equations using the correspondence principle. Second, a stress history is formulated for the introduction of a vertical pressurized wellbore into a horizontal layer. Third, the solution for viscoelastic deformation around a wellbore is presented along with various ways of formulating the relation between this deformation and in situ stresses.

2a. Theoretical Development of Constitutive Equations. In modern viscoelasticity, constitutive relations may be based on hereditary integrals, which are a way of mathematically describing history-dependent behavior. This approach allows treatment of a broad range of materials and mechanisms and is also easier to use than many of the classical approaches based on springs and dashpots or on a particular mechanism. The general constitutive relation used in this study is given below:

$$\epsilon_{ij}(t) = \int_0^t [S_{ijkl}(t-\tau) \frac{\partial \sigma_{kl}(\tau)}{\partial \tau} - R_{ij}(t-\tau) \frac{\partial p(\tau)}{\partial \tau}] d\tau \quad (4-1)$$

where

$$\begin{aligned}\epsilon_{ij}(t) &= \text{strain tensor at time } t \\ S_{ijkl}(t) &= \text{creep compliance tensor} \\ \sigma_{ij}(t) &= \text{history of the stress tensor} \\ R_{ij}(t) &= \text{pore pressure compliance tensor} \\ p(t) &= \text{history of pore pressure} \\ \tau &= \text{time variable of integration}\end{aligned}$$

This equation is based on several assumptions that require discussion because they have special significance in the derivations that follow and the conditions under which the resulting formulas can be applied. These assumptions concern linearity, aging, and the effect of pore pressure and temperature.

The linearity condition gives definite mathematical form to a very broad definition of viscoelasticity. In the most general sense a viscoelastic material is one whose current state depends on its history. For example, here the concern is with the current state of strain as it depends on stress history. The linearity conditions for such a relation are as follows:

$$\text{Homogeneity:} \quad \epsilon\{c\sigma_a\} = c\epsilon\{\sigma_a\} \quad (4-2)$$

$$\text{Superposition:} \quad \epsilon\{\sigma_a + \sigma_b\} = \epsilon\{\sigma_a\} + \epsilon\{\sigma_b\} \quad (4-3)$$

where

$$\begin{aligned}\sigma_a, \sigma_b &= \text{different stress histories} \\ c &= \text{a constant}\end{aligned}$$

The behavior of a system that meets these restrictions can be described mathematically by hereditary integrals. For example, the strain response to a varying stress history is determined by:

$$\epsilon(t) = \int_{-\infty}^t S(t, \tau) \frac{\partial \sigma(\tau)}{\partial \tau} d\tau \quad (4-4)$$

where  $S(t, T)$  is the strain response to a unit step in stress applied at time  $T$ . These conditions are not as restrictive as other approaches to viscoelasticity based on a particular mechanism or on mechanical models composed of springs and dashpots. The standard response functions can take a variety of forms including power laws and modified power laws. The linearity conditions also allow the response to be dependent on several histories, such as different components of the stress tensor, pore pressure, and temperature.

If the material is non-aging, at least over the period of interest, then the viscoelastic properties will depend only on the time elapsed since the application of stress independent of the age of the material. Thus  $S(t, T)$  in Equation 4-4 becomes  $S(t-T)$ , and the integral becomes a convolution integral. The non-aging assumption, together with taking the lower bound of integration as zero, allows use of the Laplace transform method to solve viscoelastic problems and perhaps more importantly provides the basis for a particular form of Biot's (1954) correspondence principle which has been developed by Schapery (1974). This principle allows viscoelastic solutions to be derived from elastic results by performing the inverse transformation of the Laplace transform of the elastic solution in which the elastic coefficients are replaced with their Carson transforms.

The correspondence principle can be used to derive Equation 4-1 from equations for a porous anisotropic elastic material given by Carroll (1979). The resulting pore pressure compliance in Equation 4-1 becomes:

$$R_{ij}(t) = S_{ijkk}(t) - S_{ijkk}^*(t) \quad (4-5)$$

where the \* indicates properties of the matrix material. The compliances as they appear in Equation 4-5 with repeated indices are equivalent to the linear compressibility calculated from a hydrostatic creep test as follows:

$$K_{ij}(t) = \epsilon_{ij}(t)/\sigma' \quad (4-6)$$

where the stress history is:  $\sigma_{ij} = \delta_{ij}\sigma' H(t)$

and  $\sigma'$  = magnitude of hydrostatic creep stress  
 $H(t)$  = Heaviside step function

It will be convenient to use this form later in equations with more familiar engineering mechanical properties.

The normal approach to handling pore pressure effects is through an effective stress law, but this approach is not quite as simple for viscoelasticity because of the time dependence of  $R_{ij}(t)$ . However, if  $R_{ij}(t)$  can be written in the form below:

$$R_{ij}(t) = S_{ijkl}(t)\beta_{kl} \quad (4-7)$$

and can be shown to be independent of time, then Equation 4-1 can be written in terms of effective stresses as follows:

$$\epsilon_{ij}(t) = \int_0^t S_{ijkl}(t-\tau) \frac{\partial \hat{\sigma}_{kl}(\tau)}{\partial \tau} d\tau \quad (4-8)$$

where effective stress is:

$$\hat{\sigma}_{ij}(t) = \sigma_{ij}(t) - \beta_{ij}p(t)$$

It will now be shown that these conditions hold for an isotropic material with a Poisson's ratio that does not depend on time. The creep compliance tensor for an isotropic material takes the following form:

$$S_{ijkl}(t) = (\delta_{ik}\delta_{jl} + \delta_{il}\delta_{jk}) S_1(t) + \delta_{ij}\delta_{kl} S_2(t) \quad (4-9)$$

where  $\delta_{ij}$  = the Kronecker delta  
 The linear compressibility as defined by Equation 4-6 is related to their terms in Equation 4-9 by:

$$K_{ij}(t) = S_{ijkk}(t) = \delta_{ij}K(t) \quad (4-10)$$

where 
$$K(t) = 2S_1(t) + 3S_2(t)$$

The pore pressure compliance then becomes:

$$R_{ij}(t) = \delta_{ij}[K(t) - K^*(t)] \quad (4-11)$$

Equation 4-11 can easily be put in the form of Equation 4-7 by factoring out the  $K(t)$  and using Equation 4-10. To show that the resulting  $\beta_{ij}$  is independent of time, first consider Equation 4-9 in terms of the more familiar engineering properties:

$$S_1(t) = \frac{1}{3}D(t)[1 + \nu_c(t)] \quad (4-12)$$

$$S_2(t) = -D(t)\nu_c(t)$$

where  $D(t)$  and  $\nu_c(t)$  are the creep compliance and creep Poisson's ratio determined by the strain response in a uniaxial creep test as follows:

$$D(t) = \epsilon_{11}(t)/\sigma|_1 \quad (4-13)$$

$$\nu_c(t) = -\epsilon_{22}(t)/\epsilon_{11}(t)$$

where

$$\sigma'_{11} = \text{a constant stress}$$

For many materials the creep Poisson's ratio is constant relative to other time dependencies, and it will be assumed so here. While the creep Poisson's ratio will not in general be equal to Poisson's ratio measured in a relaxation test or a constant strain rate test, if it is constant in any one of these tests, then it will be constant and equal to that measured in the other two tests. This can be proved by assuming that  $\nu_c$  is constant and then calculating a Poisson's ratio from the isotropic constitutive equations with loading conditions appropriate for either a relaxation test or a constant strain rate test. This means that for the equations that follow, data from the more routine constant strain rate tests can be used for Poisson's ratio.

Assuming a constant Poisson's ratio also allows use of the effective stress law, because it means that  $\beta_{ij}$  will also be constant. For the isotropic case,  $\beta_{ij}$  as defined by equations 4-7 and 4-11 has the following form:

$$\beta_{ij} = \delta_{ij} \beta \quad (4-14)$$

where

$$\beta = 1 - \frac{K^*(t)}{K(t)} = 1 - \frac{D^*(t)(1-2\nu^*)}{D(t)(1-2\nu)}$$

Dimensional analysis implies that the bulk compliance,  $D(t)$ , equals the matrix compliance,  $D^*(t)$ , times a term that can depend on only dimensionless parameters like geometry, distribution of pore space, and Poisson's ratio. Since none of these dimensionless parameters are time dependent the ratio of creep compliances in the second Equation 4-14 above must be constant, and thus  $\beta$  is a constant.

Temperatures can influence behavior through both thermal expansion and a temperature effect on the viscoelastic coefficients. The expansion can be corrected by defining the strains in Equation 4-1 as strains due to stresses, which are given by:

$$\epsilon_{ij}(t) = e_{ij}(t) - \alpha_{ij} \Delta T \quad (4-15)$$

where

$$e_{ij}(t) = \text{true strain tensor}$$

$$\alpha_{ij} = \text{thermal coefficient of expansion tensor}$$

$$\Delta T = \text{change in temperature}$$

If the material is a thermorheologically simple material (TSM) then the influence of temperature on the viscoelastic coefficients can be

accounted for by substituting the following for t:

$$\xi = \int_0^t \frac{dt'}{a_{\tau}} \quad (4-16)$$

where

$\xi$  = is reduced time

$a_{\tau}$  = is the horizontal shift factor, which can be a function of temperature.

While the TSM assumption is not widely established for rocks, it has been used for modeling subsidence (Lee et al., 1984).

2b. Stress History. The drilling of a vertical well into the crust of the earth can be modeled as the instantaneous introduction of a pressurized hole into a horizontal bed of homogeneous and isotropic rock. The principal stresses in the bed prior to drilling the well will be taken as  $S_1$ ,  $S_2$ , and  $S_3$ , with  $S_3$  being in the vertical direction. The effective stress law, as given by Equations 4-8 and 4-14, can be used to include the effect of pore pressure in the derivations that follow.

After the well is drilled, the stresses are, of course, changed. The usual two dimensional solutions used for stresses around a wellbore are limited in that they do not allow stress to vary along the axis of the wellbore. These variations are particularly important to the logging applications being considered in this study, and therefore a three dimensional solution will be derived here.

The components of stress acting in the horizontal plane in the vicinity of a wellbore are given in cylindrical coordinates by the following well-known formulae (see e.g., Oberle Duvall, 1967):

$$\sigma_{rr} = \frac{1}{2} \left[ \left( 1 - \frac{r_w^2}{r^2} \right) (S_1 + S_2) + \left( 1 - 4 \frac{r_w^2}{r^2} + 3 \frac{r_w^4}{r^4} \right) (S_1 - S_2) \cos 2\theta \right] + \frac{r_w^2}{r^2} p_w$$

$$\sigma_{\theta\theta} = \frac{1}{2} \left[ \left( 1 + \frac{r_w^2}{r^2} \right) (S_1 + S_2) - \left( 1 + 3 \frac{r_w^4}{r^4} \right) (S_1 - S_2) \cos 2\theta \right] - \frac{r_w^2}{r^2} p_w \quad (4-17)$$

$$\sigma_{r\theta} = -\frac{1}{2} \left( 1 + 2 \frac{r_w^2}{r^2} - 3 \frac{r_w^4}{r^4} \right) (S_1 - S_2) \sin 2\theta$$

where

$r_w$  = wellbore radius

$P_w$  = wellbore pressure

The direction of the principal stress,  $S_1$ , is parallel to  $\theta = 0$ .

The components of stress that involve the vertical dimension are usually determined by restricting the problem to plane stress or plane strain, but as mentioned above this is too limiting for the purposes of this study. To determine the restrictions placed on the vertical components of stress by Equations 4-17, first consider the equilibrium conditions:

$$\left(\frac{\partial}{\partial r} + \frac{1}{r}\right) \sigma_{rr} + \frac{1}{r} \frac{\partial}{\partial \theta} \sigma_{r\theta} + \frac{\partial}{\partial z} \sigma_{rz} - \frac{1}{r} \sigma_{\theta\theta} = 0$$

$$\left(\frac{\partial}{\partial r} + \frac{2}{r}\right) \sigma_{r\theta} + \frac{1}{r} \frac{\partial}{\partial \theta} \sigma_{\theta\theta} + \frac{\partial}{\partial z} \sigma_{\theta z} = 0 \quad (4-18)$$

$$\left(\frac{\partial}{\partial r} + \frac{1}{r}\right) \sigma_{rz} + \frac{1}{r} \frac{\partial}{\partial \theta} \sigma_{\theta z} + \frac{\partial}{\partial z} \sigma_{zz} - \rho g = 0$$

where

$\rho$  = density

$g$  = acceleration due to gravity

Using Equation 4-17 in the first two equilibrium equations places the following restrictions on the vertical shear stresses:

$$\frac{\partial}{\partial z} \sigma_{rz} = \frac{\partial}{\partial z} \sigma_{\theta z} = 0 \quad (4-19)$$

Differentiating the third equilibrium equation with respect to  $z$  and taking advantage of Equation 4-19 results in the following restriction on the vertical normal stress:

$$\frac{\partial^2}{\partial z^2} \sigma_{zz} = g \frac{\partial}{\partial z} \rho \quad (4-20)$$

Integrating Equation 4-20 with respect to  $z$  gives the form that the vertical normal stress must have:

$$\sigma_{zz} = \rho g z + A_3 z + B_3 \quad (4-21)$$

$A_3$  and  $B_3$  are functions of  $r$  and  $\theta$  and can be determined by the remaining field equations: compatibility equations, Hooke's law, and the boundary conditions. The compatibility equations in cylindrical coordinates are as follows:

$$\frac{2}{r} \frac{\partial}{\partial \theta} \left( \frac{\partial}{\partial r} + \frac{1}{r} \right) \epsilon_{r\theta} = \left( \frac{\partial^2}{\partial r^2} + \frac{2}{r} \frac{\partial}{\partial r} \right) \epsilon_{\theta\theta} + \left( -\frac{1}{r} \frac{\partial}{\partial r} + \frac{1}{r^2} \frac{\partial^2}{\partial \theta^2} \right) \epsilon_{rr}$$

$$2 \frac{\partial^2}{\partial r \partial z} \epsilon_{rz} = \frac{\partial^2}{\partial r^2} \epsilon_{zz} + \frac{\partial^2}{\partial z^2} \epsilon_{rr}$$

$$\frac{2}{r} \frac{\partial}{\partial z} \left( \frac{\partial}{\partial \theta} \epsilon_{\theta z} + \epsilon_{rz} \right) = \left( \frac{1}{r} \frac{\partial}{\partial r} + \frac{1}{r^2} \frac{\partial^2}{\partial \theta^2} \right) \epsilon_{zz} + \frac{\partial^2}{\partial z^2} \epsilon_{\theta\theta} \quad (4-22)$$

$$\frac{1}{r} \frac{\partial}{\partial z} \left( \frac{\partial}{\partial \theta} \epsilon_{rr} - 2\epsilon_{r\theta} \right) = \frac{\partial}{\partial r} \left[ -\left( \frac{\partial}{\partial r} + \frac{1}{r} \right) \epsilon_{\theta z} + \frac{1}{r} \frac{\partial}{\partial \theta} \epsilon_{rz} + \frac{\partial}{\partial z} \epsilon_{r\theta} \right]$$

$$\frac{\partial}{\partial z} \left[ \left( \frac{\partial}{\partial r} + \frac{1}{r} \right) \epsilon_{\theta\theta} - \frac{1}{r} \epsilon_{rr} \right] = \frac{1}{r} \frac{\partial}{\partial \theta} \left[ \left( \frac{\partial}{\partial r} + \frac{1}{r} \right) \epsilon_{\theta z} - \frac{1}{r} \frac{\partial}{\partial \theta} \epsilon_{rz} + \frac{\partial}{\partial z} \epsilon_{r\theta} \right]$$

$$\frac{1}{r} \frac{\partial}{\partial \theta} \left( \frac{\partial}{\partial r} - \frac{1}{r} \right) \epsilon_{zz} = \frac{\partial}{\partial z} \left[ \left( \frac{\partial}{\partial r} - \frac{1}{r} \right) \epsilon_{\theta z} + \frac{1}{r} \frac{\partial}{\partial \theta} \epsilon_{rz} - \frac{\partial}{\partial z} \epsilon_{r\theta} \right]$$

The second compatibility equation can be used to complete the solution

for the vertical normal stress. The first term in this equation can be shown to be zero by using Hooke's law to write it in terms of stresses and then considering Equation 4-19. The term on the far right will also be zero if  $S_1$  and  $S_2$  have at most a first order variation in  $z$ , as given by:

$$S_1 = A_1 z + B_1 \quad (4-23)$$

$$S_2 = A_2 z + B_2$$

Equation 4-23 becomes part of the specified boundary conditions required to solve the problem. To prove that the far right term in the second of Equations 4-22 is zero, first use Hooke's law to write the strain in terms of stress, as follows:

$$\epsilon_{rr} = D[\sigma_{rr} - \nu(\sigma_{\theta\theta} + \sigma_{zz})] \quad (4-24)$$

Substituting Equations 4-17, 4-21 and 4-23 in Equation 4-24 and differentiating with respect to  $z$ , gives:

$$\frac{\partial^2}{\partial z^2} \epsilon_{rr} = 0 \quad (4-25)$$

At this point, it is also assumed that density does not vary with depth. The equations can be formulated so that this needs to hold true only through the zone of interest.

Now the second compatibility equation is reduced to the following:

$$\frac{\partial^2}{\partial r^2} \epsilon_{zz} = 0 \quad (4-26)$$

Using Hooke's law together with Equations 4-17, 4-21 and 4-23 to write the vertical component of strain in Equation 4-26 in terms of stresses, and differentiating with respect to  $r$  gives the following equation involving two unknowns,  $A_3$  and  $B_3$ :

$$\frac{\partial^2}{\partial r^2} (A_3 z + B_3) = -12\nu \frac{r^2}{r^4} (S_1 - S_2) \cos 2\theta \quad (4-27)$$

Integrating this equation with respect to  $r$  and using the boundary condition,

$$r = \infty \qquad \sigma_{zz} = \rho gz \qquad (4-28)$$

to determine the constants of integration, the functions  $A_3$  and  $B_3$  can be found. Using the result in Equation 4-21 gives the vertical normal stress, as follows:

$$\sigma_{zz} = \rho gz - 2\nu \frac{r^2}{r^2} (S_1 - S_2) \cos 2\theta \qquad (4-29)$$

This result is only good as long as Equations 4-23 hold true. Higher order variations in  $z$  would alter the vertical normal component as given by Equation 4-29 and thus would change the final results.

Using Equation 4-29 in the third equilibrium (See Equations 4-18), places the following restrictions on the remaining shear stress components:

$$\left(\frac{\partial}{\partial r} + \frac{1}{r}\right) \sigma_{rz} + \frac{1}{r} \frac{\partial}{\partial \theta} \sigma_{\theta z} = 2\nu \frac{r^2}{r^2} (A_1 - A_2) \cos 2\theta \qquad (4-30)$$

Equation 4-30 together with the remaining compatibility conditions can be used to find these last two shear components. The result is:

$$\sigma_{rz} = (1 - \nu) \frac{r^2}{r} (A_1 - A_2) \cos 2\theta \qquad (4-31)$$

$$\sigma_{\theta z} = \nu \frac{r^2}{r} (A_1 - A_2) \sin 2\theta$$

The fact that these components are non-zero when the rates of change in  $S_1$  and  $S_2$  are different (i.e.,  $A_1 - A_2$  is non-zero) may be important in determining the stresses around a wellbore. It suggests that horizontal bedding planes will be warped near the wellbore. If this warping is detectable, it could be used to help in determining the state of stress.

The complete stress history for introduction of a wellbore can now be written as follows:

$$\sigma_{ij}(t) = [H(t) - H(t - \tau_0)]\sigma'_{ij} + H(t - \tau_0)\sigma''_{ij} \quad (4-32)$$

where

$\tau_0$  = time at which the wellbore is introduced

$\sigma'_{ij}$  = initial state of stress

$\sigma''_{ij}$  = state of stress after introduction of the wellbore

The  $\sigma'_{ij}$  in cylindrical coordinates are:

$$\sigma'_{rr} = \frac{1}{2}[(S_1 + S_2) + (S_1 - S_2) \cos 2\theta]$$

$$\sigma'_{\theta\theta} = \frac{1}{2}[(S_1 + S_2) - (S_1 - S_2) \cos 2\theta]$$

$$\sigma'_{zz} = S_3 = \rho qz \quad (4-33)$$

$$\sigma'_{r\theta} = -\frac{1}{2}(S_1 - S_2) \sin 2\theta$$

$$\sigma'_{rz} = \sigma'_{\theta z} = 0$$

The  $\sigma''_{ij}$  are given by Equations 4-17, 4-29 and 4-31. The primary interest for this study is in radial strain at the wellbore wall, which depend on the normal components of stress only. The histories of the normal components are as follows:

$$\begin{aligned} \sigma_{rr}(t) = & \frac{1}{2}H(t)[(S_1 + S_2) + (S_1 - S_2)\cos 2\theta] \\ & - H(t - \tau_0) \left[ \frac{r_w^2}{r^2} (S_1 + S_2 - 2P_w) + \left( 4 \frac{r_w^2}{r^2} - 3 \frac{r_w^4}{r^4} \right) (S_1 - S_2)\cos 2\theta \right] \end{aligned}$$

$$\sigma_{\theta\theta}(t) = \frac{1}{2}H(t)[(S_1 + S_2) - (S_1 - S_2)\cos 2\theta] \quad (4-34)$$

$$+ H(t - \tau_0) \left[ \frac{r_w^2}{r^2} (S_1 + S_2 - 2P_w) - \frac{3r_w^4}{r^4} (S_1 - S_2)\cos 2\theta \right]$$

$$\sigma_{zz}(t) = H(t) S_3 - H(t - \tau_0) 2\nu \frac{r_w^2}{r^2} (S_1 - S_2)\cos 2\theta$$

2c. Viscoelastic Wellbore Deformation. The stress histories given by Equations 4-34 can now be used to determine the viscoelastic strain caused by drilling a vertical well. The constitutive relation for isotropic rock is found by using Equations 4-9 and 4-12 in Equation 4-8. The result for radial strain is as follows:

$$\epsilon_{rr}(t) = \int_0^t D(t-\tau) \frac{\partial}{\partial \tau} (\sigma_{rr}(t) - \nu[\sigma_{\theta\theta}(t) + \sigma_{zz}(t)]) d\tau \quad (4-35)$$

Differentiating the stress histories in Equation 4-34 with respect to time, inserting them in Equation 4-35, and performing the integration yields the following solution for strain:

$$\begin{aligned} \epsilon_{rr}(t) = & D(t) \{ \frac{1}{3}[(1-\nu)(S_1 + S_2) + (1+\nu)(S_1 - S_2)\cos 2\theta] - \nu S_3 \} \\ & + \frac{1}{3}D(t - \tau_0)(1+\nu) \left\{ -\frac{r_w^2}{r^2} (S_1 + S_2 - 2P_w) + [-4(1-\nu) \frac{r_w^2}{r^2} \right. \\ & \left. + 3 \frac{r_w^4}{r^4} \right\} (S_1 - S_2)\cos 2\theta \end{aligned} \quad (4-36)$$

The radial displacements at the wellbore wall can be found by integrating the strains and evaluating the result at  $r = r_w$ . For purposes of discussion, the term "wellbore deformation" will be defined as the change in diameter of the wellbore and is given by:

$$\begin{aligned} \gamma(t, \theta) = & \frac{u_r}{r_w} \Big|_{r=r_w} \\ = & D(t) \{ \frac{1}{3}[(1-\nu)(S_1 + S_2) + (1+\nu)(S_1 - S_2)\cos 2\theta] - \nu S_3 \} \\ & + \frac{1}{3}D(t - \tau_0)(1+\nu) \left[ (S_1 + S_2 - 2P_w) + (3 - 4\nu)(S_1 - S_2)\cos 2\theta \right] \end{aligned} \quad (4-37)$$

where

$u_r$  = radial displacement

$\gamma$  = wellbore deformation

A positive value for wellbore deformation refers to a decrease in wellbore diameter since compression has been taken as positive.

What is actually measured by the caliper log is more likely to be a change in wellbore deformation over a period of time, which would be given by:

$$\begin{aligned}\Delta\gamma &= \gamma(t_2, \theta) - \gamma(t_1, \theta) \\ &= \frac{1}{2}\bar{D}(1 + \nu)[(S_1 + S_2 - 2P_w) + (3 - 4\nu)(S_1 - S_2)\cos^2 2\theta]\end{aligned}\quad (4-38)$$

where  $\bar{D} = D(t_2 - \tau_0) - D(t_1 - \tau_0)$

Equation 4-38 has been derived with the following assumption:

$$D(t_1) = D(t_2) \quad (4-39)$$

Equation 4-39 will hold true if the rock is not undergoing significant creep prior to drilling the well.

The wellbore deformation can be related to the maximum and minimum horizontal stresses by first determining the maximum and minimum wellbore deformations. The deformations will occur at  $\theta = 0, \pi/2$ , respectively, as determined by the first and second derivations of Equation 4-38 with respect to  $\theta$ . The maximum and minimum deformations are given by:

$$\begin{aligned}\Delta\gamma_1 &= \Delta\gamma|_{\theta = 0} \\ &= \bar{D}(1 + \nu)[2(1 - \nu)S_1 - (1 - 2\nu)S_2 - P_w] \\ \Delta\gamma_2 &= \Delta\gamma|_{\theta = \pi/2} \\ &= \bar{D}(1 + \nu)[2(1 - \nu)S_2 - (1 - 2\nu)S_1 - P_w]\end{aligned}\quad (4-40)$$

Solving Equations 4-40 for the principal in situ stresses gives the primary result of this study:

$$S_1 = \frac{2(1 - \nu) \Delta\gamma_1 + (1 - 2\nu)\Delta\gamma_2}{\bar{D}(1 + \nu)(3 - 4\nu)} + P_w \quad (4-41)$$

$$S_2 = \frac{2(1 - \nu) \Delta\gamma_2 + (1 - 2\nu)\Delta\gamma_1}{\bar{D}(1 + \nu)(3 - 4\nu)} + P_w$$

These equations can be used to calculate stress magnitudes from the maximum and minimum wellbore deformations.

For situations where the mechanical properties in Equations 4-41 are not available, relative values of the horizontal stresses can still be determined. For example, the ratio given below can be helpful under certain conditions:

$$\frac{S_1 - P_w}{S_2 - P_w} = \frac{2(1 - \nu) \Delta\gamma_1 + (1 - 2\nu)\Delta\gamma_2}{2(1 - \nu) \Delta\gamma_2 + (1 - 2\nu)\Delta\gamma_1} \quad (4-42)$$

If the pressure in the wellbore and the pore pressure are equal and if  $\beta$  is approximately equal to one, then the two pressures cancel each other and the ratio between total stresses can be calculated from Equation 4-42. Another value that may be useful is the differential stress, which is directly proportional to the differential wellbore deformation, as seen in the following equation:

$$S_1 - S_2 = \frac{\Delta\gamma_1 - \Delta\gamma_2}{\bar{D}(1 - \nu)(3 - 4\nu)} \quad (4-43)$$

The change in differential stress between two points, a and b, along the wellbore can be calculated directly from the wellbore deformations without any other information, as follows:

$$\frac{S_{1a} - S_{2a}}{S_{1b} - S_{2b}} = \frac{\Delta\gamma_{1a} - \Delta\gamma_{2a}}{\Delta\gamma_{1b} - \Delta\gamma_{2b}} \quad (4-44)$$

Wellbore deformations may also be useful in extending knowledge of stresses at a particular point up and down the wellbore. If the stresses and the wellbore deformations are known at one point in a formation, then the mechanical properties can be calculated with the following equations:

$$\bar{D} = \frac{\Delta\gamma_1}{(1 + \nu)[2(1 - \nu) S_1 - (1 - 2\nu) S_2 - P_w]} \quad (4-45)$$

$$\nu = \frac{\Delta\gamma_2 (2S_1 - S_2 - P_w) - \Delta\gamma_1 (2S_2 - S_1 - P_w)}{2(\Delta\gamma_1 + \Delta\gamma_2)(S_1 - S_2)}$$

These values together with wellbore deformations from other points in the formation can be used in Equations 4-41 to calculate stress magnitudes at those other points.

Under most conditions the wellbore will decrease in diameter with time; however, there are situations where the diameter will increase in the direction of the minimum horizontal stress. The condition under which the minimum wellbore deformation will be less than zero can be determined from Equation 4-40. The result is as follows:

$$\frac{2(1 - \nu)}{(1 - 2\nu)} < \frac{S_1 - P_w}{S_2 - P_w} \quad (4-46)$$

When the stress ratio satisfies Equation 4-46, then the wellbore diameter will increase with time in the direction of the minimum horizontal stress. Table 4-1 gives some values of critical stress ratios for different Poisson's ratios.

The work presented here shows, theoretically at least, that the orientation and magnitudes of in situ stresses can be related to the viscoelastic deformation of a wellbore. For a vertical wellbore drilled perpendicular to a principal plane, the orientation of the greater horizontal principal stress will be parallel to the direction of maximum shortening of the wellbore diameter, and the orientation of the least stress will be parallel to the direction of minimum shortening. For cases where the ratio of stresses is relatively high, the wellbore may actually increase in diameter parallel to the least stress. The principal stress magnitudes can be calculated from measurements of the wellbore deformation using Equations 4-41. These equations also require information on the mechanical properties of the rock, specifically the creep compliance and Poisson's ratio. In

TABLE 4-1.  
CRITICAL STRESS RATIOS  
ABOVE WHICH THE WELLBORE DIAMETER  
WILL INCREASE WITH TIME.

Poisson's Ratio	Stress Ratio
.10	2.25
.15	2.42
.20	2.67
.25	3.00

situations where mechanical properties are not available or where only routine elastic properties have been measured, information can still be obtained on relative magnitudes of the principal stresses. The equations can also be used to determine how stresses are changing through a zone.

While this work shows the potential for stress determination from measurements of wellbore deformation and provides equations for calculating stress magnitudes, it is still limited in three ways: (1) knowledge of the creep compliance is required for calculation of stress magnitudes, (2) the equations apply only to a continuum and can not be used for wellbore shapes resulting from spalling in a particular directions, (3) the work is theoretical and has not been tested under controlled experimental conditions.

Overcoming the first limitation can be approached in two ways. First, if a third equation could be added to Equations 4-41 without adding an additional unknown, then the creep compliance could be eliminated from these equations. One potential candidate for the third equation would be one that includes the effect of a change in wellbore pressure. Measurement of the response to such a change should allow determination of the creep compliance. Another candidate may be obtained from Equation 4-31, which suggest that horizontal bedding planes may be deformed by introducing a vertical wellbore when the rate of increase of the two horizontal principal stresses is different.

A second approach to the first limitation is to examine the nature of the creep compliance for rock more closely. It may be that the sensitivity of the equations to practical variations in creep compliance is small compared to the sensitivity to other parameters. This examination could be based on existing creep recovery data on core that has been used for determining in situ stresses. Calculating stresses from creep recovery measurements involves three equations and three unknowns, two principal stresses and the creep compliance (Blanton, 1983). Usually the creep compliance is simply eliminated from the equations; however, it could be calculated. Data exists for several different rock types from different locations, so that the variation among different rocks could be determined (Teufel, 1981, Teufel, 1983, Blanton and Teufel, 1983, Teufel and Warpinski, 1984).

The second limitation could be overcome by including a failure criterion in the constitutive model. This would result in equations that could be used to analyze situations where wellbore breakouts occur.

The third limitation could be overcome by performing controlled laboratory experiments designed to test the theoretical equations. Two types of tests should be run: (1) mechanical property tests to characterize the viscoelastic properties and failure behavior of the materials to be used and (2) scaled wellbore deformation experiments under triaxial stress conditions, which would establish an empirical relation between states of stress and wellbore deformation.

As part of another project these equations were applied to wellbore caliper data obtained at the Nevada Test Site. The stresses

calculated from this data correlated well with measurements of stresses by hydraulic fracturing and overcoring. The details of this work may be found in Blanton and Teufel (1985).

## TASK 5. TECTONICS OF THE APPALACHIAN BASIN

### OBJECTIVE

The objective of this task is to develop a tectonic model of the Appalachian Basin that can be used as a basis for extrapolating from or interpolating between site specific data on the abundance and distribution of fractures and in situ states of stress.

### WORK PERFORMED

Work on this task has been carried out in three phases. First, hypotheses regarding the origin of fractures in the Devonian shales have been formulated. These hypotheses are drawn from existing eastern gas shales literature, as well as from the literature on plate tectonics of eastern North America. Using data from the gas shales literature and theories or models from plate tectonics, a tectonic history of the Appalachian basin has been constructed, with particular attention given to fracture forming episodes.

An analysis of the types of fracture systems that should be associated with the various structures in the basin is presented. This work draws primarily on the tectonophysics literature for conceptual models that have proven effective in analyzing fracture systems in the shallow crust. These models allow association of fracture systems with certain events. When a fracture system in a particular area can be associated with a tectonic event in the basin, then this provides a basis for extrapolation and/or interpolation of that fracture system.

Existing fracture data was collected from four sources (Evans, 1978, 1980, Cliffs, 1981, Mound, 1980), and was then re-analyzed in view of the models for fracture formation presented in the previous paragraph and the tectonic history of the basin. Various systems have been distinguished and different fracture domains have been associated with particular tectonic events.

### TECTONIC MODELS: EXISTING HYPOTHESES

In general, hypotheses for the origin of fractures fall into three categories: those associated with faulting, those associated with folding, and those associated with regional stress fields. In the faulting category there are two hypotheses regarding the origin of

fractures: thrust faulting (Gwinn, 1964, Dean, 1980) and basement faulting (Berger and Wheeler, 1979, Shumaker, 1982, Williams et al., 1982, Lavin et al., 1982).

The importance of low-angle detachment thrust faults to structures (particularly those forming hydrocarbon traps) in the eastern part of the basin has been shown in the classic paper by Gwinn. To be an important factor in Devonian shale production, the detachments would have to extend further west. Concrete evidence of this has not been found, but detachments would explain one peculiar aspect of the distribution of natural fractures noted in the work of Evans (1980): fractures were more abundant in black shales than in gray shales. In a package of sedimentary rocks exposed to deformation the more ductile rock usually contains fewer fractures, and the black shales have been shown to be more ductile than gray shales (Blanton et al., 1981). As pointed out by Gwinn, detachments tend to occur in the more ductile layers, thus concentrating the deformation in these layers. It may be possible that detachment in the ductile Salina salt begins to climb in the section where the salt pinches out and continues in the first suitably ductile Devonian Shale. In fact, this theory has been born out by the analyses in the following sections.

Basement faulting seems to have received more attention than thrust faulting. In most cases these theories involve the reactivation of pre-existing basement faults or zones of weakness. It should be pointed out that while the evidence seems strong in some instances for reactivation over a long period of time (e.g., Lavin et al., 1982, Gay, 1983), the mechanics of reactivation are not simple (Handin, 1969).

Folding is not particularly intense in the central and western parts of the Appalachian Basin where hydrocarbon potential is greatest for Devonian shales. Still, there are hypotheses of fracture formation that would fall into this category in the sense that they involve relatively broad flexures. Two examples are differential compaction (Hennington, 1980) and glacial loading (Clark, 1982).

Regional fracture trends have been related to regional stress fields. Engelder and Geiser (1980) relate regional joint sets in New York to trajectories of paleostress fields that existed during the development of the Appalachian Plateau. Another regional fracture system related to the contemporary ENE trending maximum compressive stress has been postulated by Engelder (1982) who drew evidence from New York, Ohio, Indiana, Michigan, and West Virginia. However, there is still some controversy regarding the relation. Scheidegger (1982) argues that many of the fractures in Engelder's study are shear fractures and thus could not be related to the contemporary stress field.

A more complete tectonic model is presented after an analysis of the fracture data has been given.

## NATURAL FRACTURE SYSTEMS

The purpose of this section is to outline the basic principles and definitions that will be used in analyzing the fracture data in the following section. There is still a great deal of controversy and a wide variety of terminology related to fractures in rock. The approach taken in this study has been developed over the years by geologists such as Hubbert, Griggs, Handin, Stearns, Sowers, Logan and Friedman. Most of the principles used can be found in Stearns and Friedman (1972).

Before discussing the different types of natural fracture systems, it is important to understand the basic relations between principal stress orientations and fracture patterns. There are two types of fractures that develop in rocks: extension fractures and shear fractures. Extension fractures form in a plane perpendicular to the least principal stress. If the least stress is tensile, then this is the same as a tensile fracture, but extension fractures can form under compression as well. Shear fractures can occur in one or both of two orientations. These are thirty degrees either side of the greatest principal stress and parallel to the intermediate principal stress. These orientations along with associated displacements are illustrated in Figure 5-1.

Natural fracture systems can be divided into regional orthogonal systems and structure related systems. While no satisfactory explanation of regional orthogonal systems has been made (e.g. see discussion in Stearns and Friedman, 1972), their occurrence in plateau regions has been recognized throughout the world. Their intersection is oriented perpendicular to bedding and they are not affected by local structures, unless that structure developed after their formation. While the actual event that leads to their development is not known, it is most likely that they are extension fractures that align with the principal stress directions at the time of formation.

Structure related fractures can be divided into those associated with faults and those associated with folds. Fracture patterns associated with faults fit the pattern in Figure 5-1, with the fault occupying one of the shear fracture positions. In basins where one of the principal stresses is vertical, there are three possible orientations for this pattern: one for strike slip faults, one for high-angle normal faults, and one for low-angle reverse faults. In the first two cases, most of the fractures would be vertical and all would have dips greater than forty-five degrees. In the last case, all fractures should have dips of less than forty-five degrees. These generalities will prove useful in analyzing fracture data in the following section. However, it should be recognized that there are exceptions. These usually occur when curved fault surfaces are involved, which of course implies a curved stress field. In particular, this study will be concerned with irregular surfaces associated with detachments.

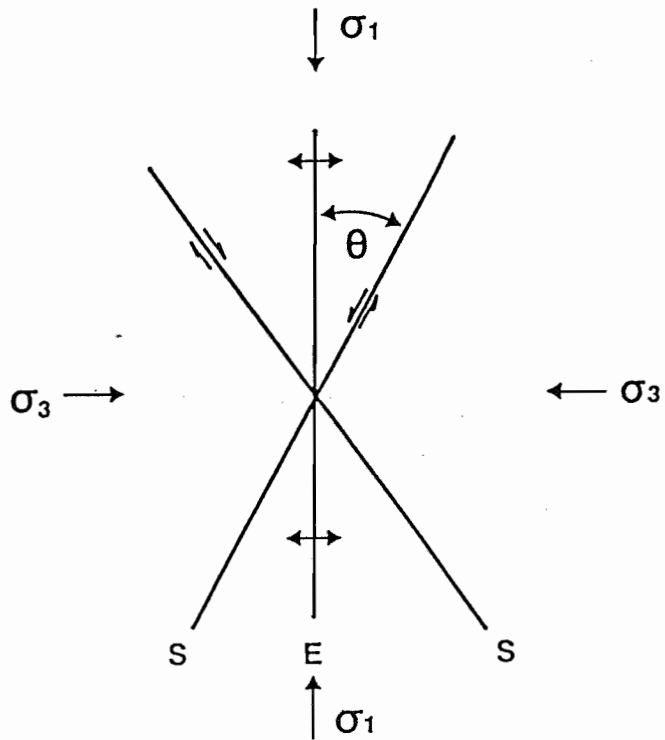


FIGURE 5-1. Relation between principal stress directions and orientations of extension and shear fractures.

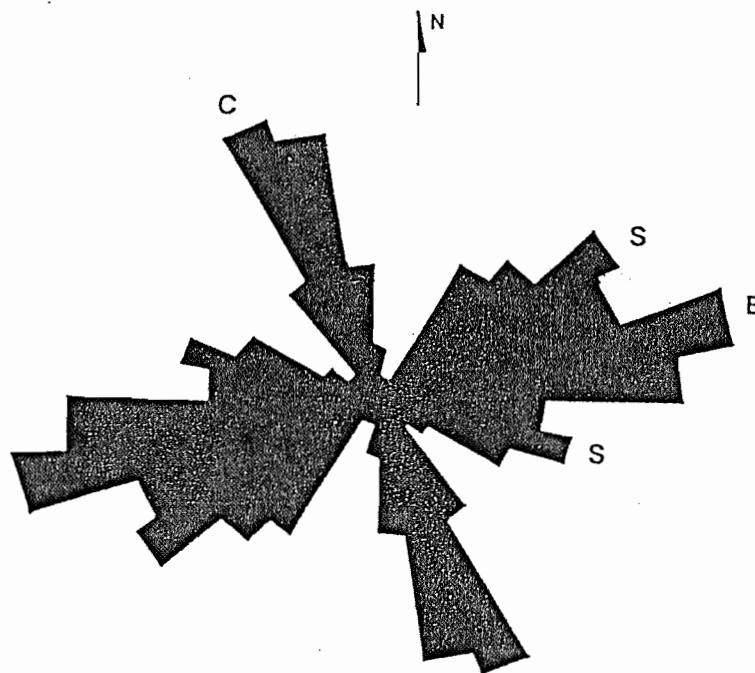


FIGURE 5-2. Rose diagram of orientations of type one and two fracture sets (Stearns, 1968).

Stearns (1968) has recognized five sets of fractures associated with folds. The most common sets are shown as types one and two in Figure 5-3. They develop in situations where the intermediate stress is vertical. Type one fractures develop early in folding whereas type two fractures develop after there has been more extension in the outer part of the folded layer. Type two fractures are also more localized on the fold, usually occurring along hinges that run subparallel to the axis of the fold. A rose diagram of the orientations of several thousand measurements of types one and two made on outcrops by Stearns (1968) is shown in Figure 5-2. There are two important points regarding this diagram. The first is that much information about fracture patterns is lost by lumping data onto one rose diagram. The second is that lumping the data does produce a pattern that can be used to analyze regional stresses at the time of formation and possibly even the amount of deformation that has been experienced. For example, if the type one set is dominant this would indicate that only low amplitude folding had occurred.

#### FRACTURE DATA

Fracture data has been collected from four sources (Evans, 1978, Evans, 1980, Cliffs, 1982, and Mound, 1982). The quality of the data varies considerably. The best quality data has been collected by Evans, but he did not analyze data from all the wells. The Cliffs report treats all the wells, but the amount of data recorded varies from well to well. In particular, the dips of fractures and faults were not recorded for some wells. In the Mounds report, it appears that in some, if not all, cases core-induced and natural fractures may not have been distinguished. Even after detailed records have been made, data in most reports were lumped together, yielding a confusing pattern. For example, Figure 5-4 shows what were considered to be the dominant fracture and fault orientations in the Mound report.

By working with all four reports as complete a picture as possible has been put together of the details necessary for the fracture analysis techniques discussed in the previous section. Care has been taken to insure that only natural fractures have been included in the data set. Whenever there has been some doubt, the data has been omitted. What are referred to as fractures or joints in the referenced reports are fractures with no apparent offset on them. These fractures can be either extension or shear fractures. All of these fractures are reported as having a high angle of dip with most being vertical. What are called faults are shear fractures with slickensides on them. Slickenside orientations were recorded in the referenced reports, but they have been excluded from this study. The reason for this is that they reflect only the very last few inches of movement, which can be, and often is, quite different from the net displacement on a fault. Unless they can be supported by other evidence they are not particularly useful.

Stearns (1968) has recognized five sets of fractures associated with folds. The most common sets are shown as types one and two in Figure 5-2. They develop in situations where the intermediate stress is vertical. Type one fractures develop early in folding whereas type two fractures develop after there has been more extension in the outer part of the folded layer. Type two fractures are also more localized on the fold, usually occurring along hinges that run subparallel to the axis of the fold. A rose diagram of the orientations of several thousand measurements of types one and two made on outcrops by Stearns (1968) is shown in Figure 5-3. There are two important points regarding this diagram. The first is that much information about fracture patterns is lost by lumping data onto one rose diagram. The second is that lumping the data does produce a pattern that can be used to analyze regional stresses at the time of formation and possibly even the amount of deformation that has been experienced. For example, if the type one set is dominant this would indicate that only low amplitude folding had occurred.

#### FRACTURE DATA

Fracture data has been collected from four sources (Evans, 1978, Evans, 1980, Cliffs, 1982, and Mound, 1982). The quality of the data varies considerably. The best quality data has been collected by Evans, but he did not analyze data from all the wells. The Cliffs report treats all the wells, but the amount of data recorded varies from well to well. In particular, the dips of fractures and faults were not recorded for some wells. In the Mounds report, it appears that in some, if not all, cases core-induced and natural fractures may not have been distinguished. Even after detailed records have been made, data in most reports were lumped together, yielding a confusing pattern. For example, Figure 5-4 shows what were considered to be the dominant fracture and fault orientations in the Mound report.

By working with all four reports as complete a picture as possible has been put together of the details necessary for the fracture analysis techniques discussed in the previous section. Care has been taken to insure that only natural fractures have been included in the data set. Whenever there has been some doubt, the data has been omitted. What are referred to as fractures or joints in the referenced reports are fractures with no apparent offset on them. These fractures can be either extension or shear fractures. All of these fractures are reported as having a high angle of dip with most being vertical. What are called faults are shear fractures with slickensides on them. Slickenside orientations were recorded in the referenced reports, but they have been excluded from this study. The reason for this is that they reflect only the very last few inches of movement, which can be, and often is, quite different from the net displacement on a fault. Unless they can be supported by other evidence they are not particularly useful.

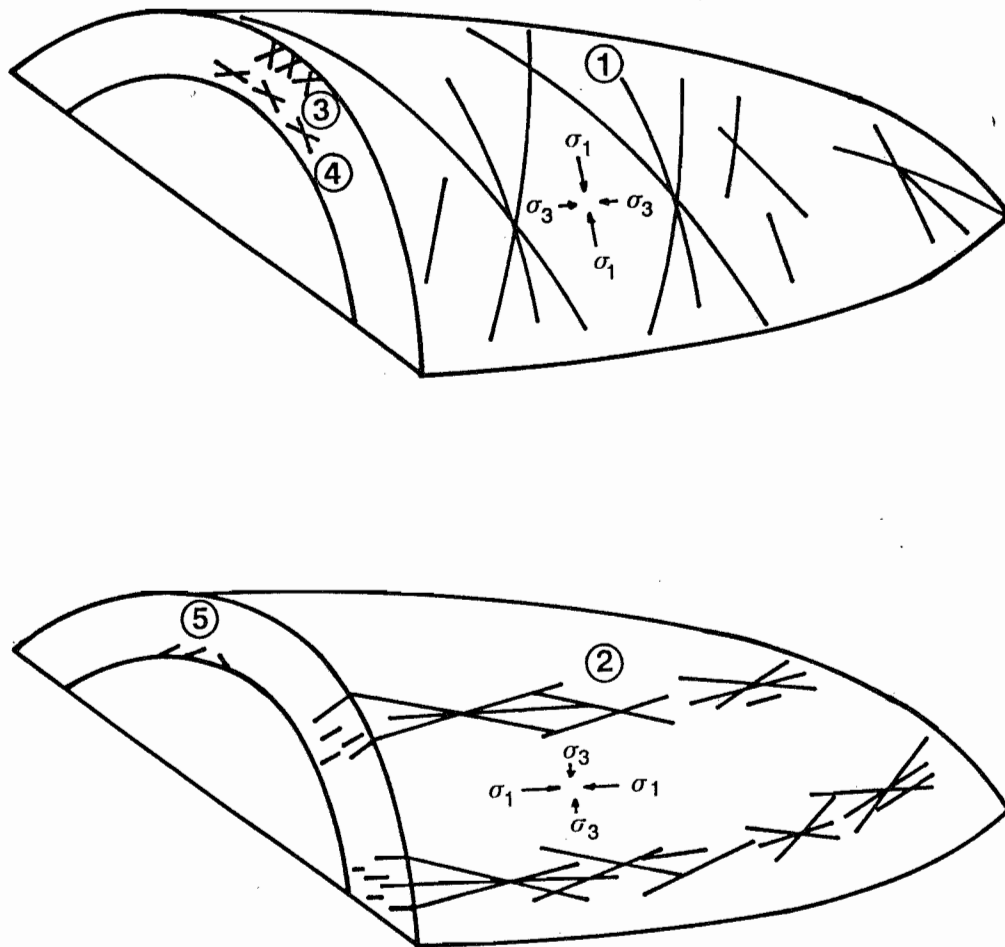


FIGURE 5-3. Location of different fracture sets on a typical fold (Stearn 1968 and Stearns and Friedman, 1972).

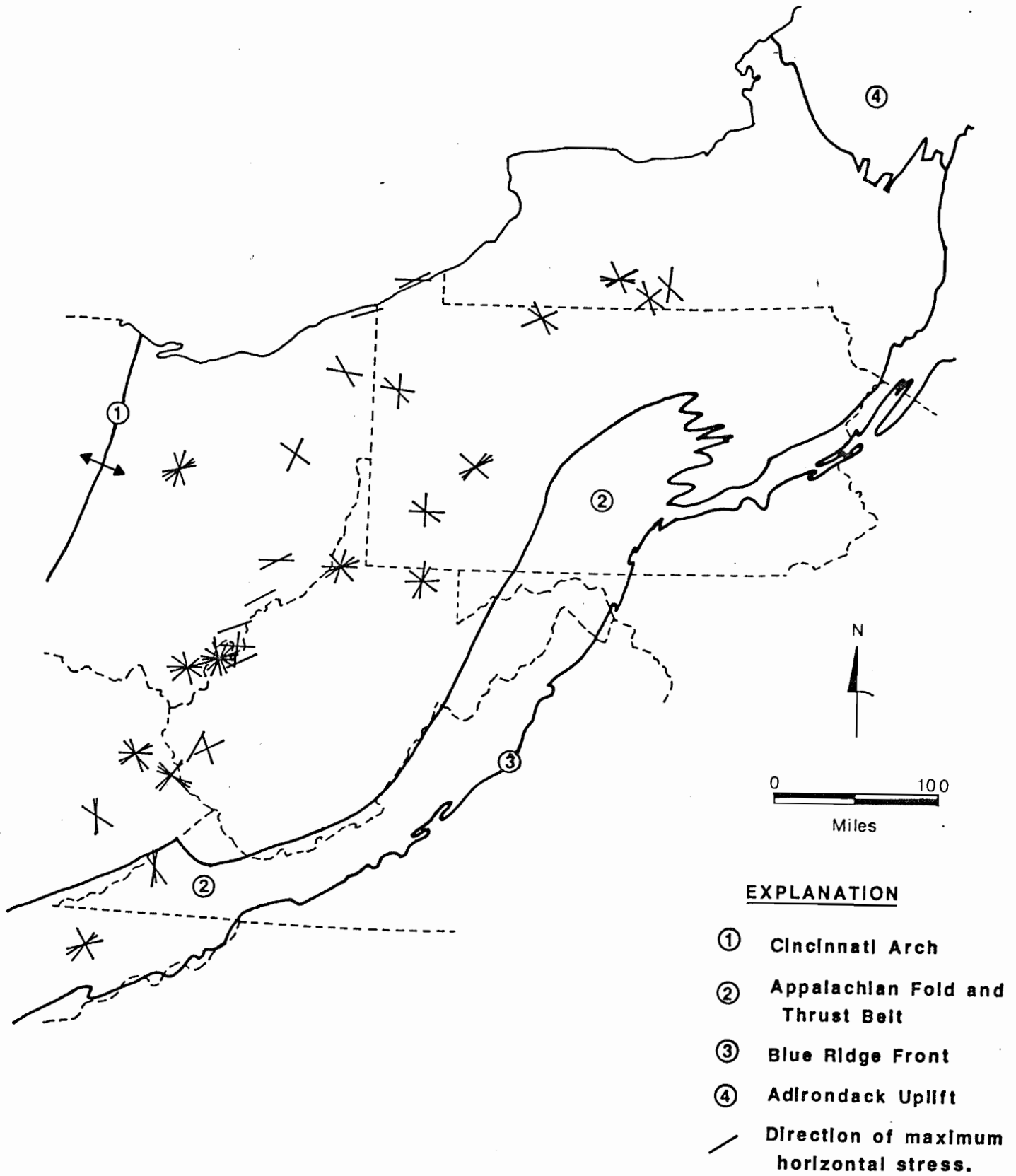


FIGURE 5-4. All fracture orientations from EGSP wells.

The data have been organized in Tables 5-1 through 5-6. Orientations are given in degrees east of north, or clockwise, from 0 to 180. This is followed by the number of fractures that had orientations within plus or minus fifteen degrees of the given orientation. Whenever there were more fractures or faults than the total of those associated with the dominant trends, the overall total number has been given in parentheses. As mentioned earlier, the fractures have high angles of dip and most are vertical. For the faults, dip information is given in the footnotes except where they are horizontal, in which case they are indicated by an "H".

The first distinctions to be made are between fractures and faults and between high and low-angle faults. Figure 5-5 shows all the fracture orientations, and Figure 5-6 shows the high-angle faults. The low-angle faults are shown in Figure 5-7 with particular attention given to the zones in which they occur.

#### TECTONIC MODELS: PLATE TECTONICS

The existing hypotheses for fracture development and the fracture data are best compared and evaluated if viewed in the context of the tectonic history of the Appalachian Basin. Dietz (1972) has outlined a history of the eastern continental margin from the point of view of plate tectonics. In Table 5-7, his outline is compared to the major orogenies in the Appalachians and events that influenced fracture formation in Devonian shales.

Three tectonic features stand out as being particularly important to fracture development in the shales. One is high-angle basement faulting, which seems to fit the pattern of a failed rift system. Another is the Appalachian orogeny which produced thrust faulting and associated folding and fracturing. Finally, there is the current regional stress field. Other events of possible importance such as the breakup of Pangaea and glacial loading will also be discussed.

#### Failed Rift System

High-angle faults and lineaments taken together seem to fit the pattern of a rift system. Evidence for this system, presented in Figure 5-8, consists of three parts: normal faulting, lineaments, and gravity anomalies. A sketch of one possible geometry for the rift system is given in the overlay.

The spreading centers are evidenced by normal faults and gravity highs. The Rough Creek fault system, which extends into Eastern Kentucky, and the faults in the Adirondacks are taken from King's (1969) Tectonic Map of North America. The Rome Trough has been discussed extensively in the gas shales literature (e.g. Kulander and Dean, 1978). While its general trend is northeast-southwest, in its southern part it merges in to an east-west trend with the Rough Creek

TABLE 5-1.  
KENTUCKY CORE DATA

WELL NO.	ZONE CORED	FRACTURES ORIEN./NO. (TOTAL)	FAULTS ORIEN./NO. (TOTAL)
KY-1	Berea		
	Cleveland		H/12
	Chagrin		
	U. & M. Huron		
KY-3	L. Huron		H/21, 175/6
	Olentangy		
	Composite		H/33, 175/6 <sup>1</sup>
KY-3	Cleveland	55/1	
	Chagrin	40/2, 105/1	
	U. & M. Huron	5/1, 35/1, 150/2	45/4
	L. Huron	125/4	75/3, 135/1
	Java (O. & P.C.)	125/1	115/1, 145/1
	Angola	35/1, 55/1, 105/1	85/1
	Rhinestreet	145/1	80/6, 155/4
	Composite	35/4, 125/5 (17)	80/10, 45/4, 150/6 (21) <sup>2</sup>
KY-4	Berea		5/4, 90/8, 145/5
	Bedford		H/1, 5/2, 35/5 (15)
	Cleveland	65/4	
	Chagrin		135/1
	U. & M. Huron	35/1	
	L. Huron	55/5	
	Olentangy		R/4
	Composite	60/10	5/6, 35/9, 90/10, 145/5 (36) <sup>3</sup>

<sup>1</sup>Of the six striking faults, four are near horizontal and the other two dip thirty and sixty degrees West.

<sup>2</sup>Faults dip twenty-five to sixty degrees. There appears to be a East-West striking conjugate set dipping about twenty-five and fifty degrees South. About five of these dip fifty degrees. All faults in the forty-five degree trend dip fifty degrees or more. Three of the one-hundred-fifty degree trend dip sixty degrees.

<sup>3</sup>Most faults dip thirty degrees or less, but two North-striking faults dipping steeply East. It appears to be a weak conjugate set suggesting a horizontal maximum compressive stress about one-hundred and fifty-five degrees. Notes indicate that these are microfaults with curving surfaces, which accounts for the variability in orientations.

TABLE 5-2.  
NEW YORK CORE DATA

WELL NO.	ZONE CORED	FRACTURES ORIEN./NO. (TOTAL)	FAULTS ORIEN./NO. (TOTAL)
NY-1	Dunkirk	90/3	
	Java(Han.&P.C.)	85/2	
	Angola	90/2	
	Rhinestreet	70/12, 100/8, 145/3	
	Sonyea	50/4, 155/1	
	Genesee	35/2, 60/4, 100/3	
	Composite	80/28, 150/4 (44)	
NY-3	Rhinestreet	5/2, 45/1	
NY-4	Genesee	55/1	H/2
	Upper Hamilton Gp.	not cored	
	Marcellus		H / 7 , 135 / 15
	Onondaga (top)	35/1, 105/1	H/2, 160/8, 120/5, 65/1
	Composite	45/2, 105/1	H/9, 140/21 (40) <sup>1</sup>

<sup>1</sup>Poles to all but four of these faults form a tight cluster whose peak indicates dips less than ten degrees Southwest. Of the four, three dip greater than fifty degrees.

TABLE 5-3.  
OHIO CORE DATA

WELL NO.	ZONE CORED	FRACTURES ORIEN./NO. (TOTAL)	FAULTS ORIEN./NO. (TOTAL)
OH-1	Fractures undifferentiated.		
OH-2	Fractures undifferentiated.		
OH-3	Cleveland Chagrin U. Huron M. Huron L. Huron Olentangy Onondaga	85/1, 165/1  60/3	  H/1
	Composite	70/4, 165/1	H/1
OH-4	Chagrin Dunkirk Java(Hn.&P.C.) Angola Rhinstreet Tully Mahantango Marcellus Onondaga	   70/1	
	Composite	70/1	
OH-5	No natural fracture or faults were found.		

TABLE 5-3 CON'T.  
OHIO CORE DATA

Well No.	Zone Cored	Fractures Orien./No. (Total)	Faults Orien./No. (Total)
OH-6-1	Cleveland		
	Chagrin	45/2	115/2
	L. Huron	55/7	
	Composite	50/9	115/2 <sup>1</sup>
OH-6-2	Bedford		130/4 (6)
	Cleveland		
	L. Huron	65/7, 5/1	115/1, 165/1
	Composite	65/7, 5/1	115/4, 165/4 <sup>2</sup>
OH-6-3	Bedford		
	Cleveland		
	L. Huron	5/1, 75/1	
OH-6-4	Bedford	135/1	50/8, 170/6 (19)
	Cleveland	65/1	
	Chagrin		
	U. Huron		
	M. Huron	80/16	
	L. Huron	70/38	5/3, 135/4
	Composite	75/56	0/8, 50/8, 140/7 (26) <sup>3</sup>
OH-6-5	Bedford		
	Cleveland	25/1	
	U. Huron		
	L. Huron	65/2	
	Olentangy		55/1
	Composite	25/1, 65/2	55/1 <sup>4</sup>
OH-6	Composite	5/1, 25/1, 70/76	0/11, 50/9, 135/19 (37)

<sup>1</sup>The faults dip forty-two degrees Northeast and fifteen degrees Southwest, suggesting a maximum compression plunging about fourteen degrees Northeast.

<sup>2</sup>Faults dip twenty-five to seventy degrees, but no record of the distribution can be found.

<sup>3</sup>Faults in Bedford dip twenty-five to thirty degrees. Faults in Lower Huron dip zero to thirty-four degrees.

<sup>4</sup>No mention of the dip of the fault.

TABLE 5-3 CON'T.  
OHIO CORE DATA

WELL NO.	ZONE CORED	FRACTURES ORIEN./NO. (TOTAL)	FAULTS ORIEN./NO. (TOTAL)
OH-7	Chagrin & Hur. Huron Java (Hn.&P.C.) Angola Rhinstreet Mahantango Marcellus Onondaga	105/1, 135/1	130/8 15/1, 35/1  115/1
	Composite	120/2	25/2, 130/9 <sup>1</sup>
OH-8	Chagrin Huron Java (Hn.&P.C.) Angola Rhinstreet  Mahantango Marcellus Onondaga	85/18 80/6, 125/1 85/1 65/1, 95/5	H/1, 45/1, 165/2 H/1  H/1, 60/4, 130/5, 175/1 H/1, 85/1
	Composite	80/29 (32)	H/4, 60/6, 130/5, 170/3 <sup>2</sup>
OH-9	L. Huron	70/13	75/1 <sup>3</sup>

<sup>1</sup>Vertical faults.

<sup>2</sup>Poles to these faults form a cluster whose peak indicates dips less than ten degrees Southeast.

<sup>3</sup>Dips twenty-five degrees Southeast.

TABLE 5-4.  
PENNSYLVANIA CORE DATA

WELL NO.	ZONE CORED	FRACTURES ORIEN./NO. (TOTAL)	FAULTS ORIEN./NO. (TOTAL)
PA-1	Angola		15/1
	Rhinestreet	155/2	
	Genesee	15/1, 155/1	70/3
	Geneseo		65/1
	Moscow		
	Ludlowville	125/4	
	Skaneateles	145/2	H/1, 65/2, 175/1
	Marcellus	80/3, 165/1	90/10
	Composite	80/3, 140/9 (14)	80/14 (19) <sup>1</sup>
PA-2	Genesee	105/2	45/11, 150/25
	Geneseo	125/1	
	Tully	135/1	25/1
	Mahantango		35/2, 175/5
	Marcellus	0/13, 85/6, 130/8 (36)	40/18, 150/30 (84)
		Composite	0/13, 90/8, 130/10 (40)
PA-3	Dunkirk	65/7	R/4 <sup>3</sup>
	Java (Hn.&P.C.)		
	Angola		
	Rhinestreet		
	Tully		
	Mahantango		
	Marcellus		
	Onondaga		

<sup>1</sup>Most of these faults dip about thirty degrees South. One East-West fault is nearly vertical, and one fifty-five degree trending fault dips about sixty-five degrees Northwest.

<sup>2</sup>Evans' report shows a majority of the faults with less than forty-five degree dips. No mention is made of the dips of the faults in the Cliffs report, but a significant number must have been near horizontal since the Genesee and Marcellus are said to contain decollements.

<sup>3</sup>No record of the dips of these faults could be found.

TABLE 5-4 CON'T.  
PENNSYLVANIA CORE DATA

WELL NO.	ZONE CORED	FRACTURES ORIEN./NO. (TOTAL)	FAULTS ORIEN./NO.(TOTAL)
PA-4	Sonyea	60/4, 120/20, 160/6	H/3, 35/1, 125/1
	Genesee	0/9, 125/14, (29)	H/11, 30/14 (27)
	Geneseo	120/8 (12)	H/3, 15/3
	Tully		
	Mahantango	15/1, 130/2	65/2
	Marcellus	125/5 (11)	H/7, 45/5 (15)
	Composite	60/5, 120/49, 170/19	H/24, 40/20 (55) <sup>1</sup>
PA-5	Java (Hn.&P.C.)		
	Angola		H/1, 135/4
	Rhinestreet	95/5, 135/2	0/8 (14)
	Sonyea	135/1	135/1
	Genesee		
	Geneseo		
	Tully		
	Mahantango	100/3, 140/3	H/1, 10/4 (9)
Marcellus			
Composite	95/8, 140/6	H/2, 5/12, 135/5 (29) <sup>2</sup>	

<sup>1</sup>Poles to most of these faults form a cluster whose peak indicates a dip of less than ten degrees. Two twenty degree trending faults are near vertical.

<sup>2</sup>Poles to most of these faults from a cluster whose peak indicates a dip of less than ten degrees. Two in the five degree trend and one in the one hundred thirty-five degree trend dip greater than sixty degrees.

TABLE 5-5.  
TENNESSEE AND VIRGINIA CORE DATA

WELL NO.	ZONE CORED	FRACTURES ORIEN./NO. (TOTAL)	FAULTS ORIEN./NO. (TOTAL)
TN-9	Cleveland	65/10, 140/14 (30)	0/6
	Chagrin		
	U. Huron	45/7, 130/11 (27)	H/4, 45/3
	M. Huron		
	L. Huron		
	Olentangy	75/4, 165/1	H/11, 60/16 (32)
	Rhinestreet	65/1, 155/1	H/19, 40/30 (87)
Composite	60/42, 140/67 (173)	H/87, 45/71 (196) <sup>1</sup>	
VA-1	Cleveland	25/1, 95/2	40/3
	Chagrin	R/6	50/7 (9)
	M. Huron	170/28	50/11 (16)
	L. Huron	135/26 (50)	45/50 (109)
	Composite	135/26, 170/28 (87)	45/71 (137) <sup>1</sup>

<sup>1</sup>Poles to these faults form a cluster whose peak indicates a dip of less than ten degrees.

TABLE 5-6.  
WEST VIRGINIA CORE DATA

WELL NO.	ZONE CORED	FRACTURES ORIEN./NO. (TOTAL)	FAULTS ORIEN./NO. (TOTAL)
WV-1	L. Ohio	45, 95, 165 <sup>1</sup>	
WV-2	L. Huron	55/77	165/3 <sup>2</sup>
WV-3	Ohio	60/34	
	U. & M. Huron	60/43, 145/32	165/2
	L. Huron	70/8, 145/2	H/1
	Java	75/3	45/2
	West Falls (Angola & Rhinstreet)	55/7	70/60 (106)
	Composite	65/95, 145/34	70/60 (111) <sup>3</sup>
WV-4	Ohio	25/49	
	M. Huron	5/1	
	L. Huron	30/20 (28)	30/4
	Angola	25/1	30/16 (20)
	Rhinstreet	25/4, 115/5	35/37 (83)
	Composite	25/74 (88)	35/57 (107) <sup>4</sup>

<sup>1</sup>Fractures were undifferentiated, but, notes indicate that there were concentrations of mineralized fractures at these orientations.

<sup>2</sup>These faults dip ten to thirty degrees Southwest.

<sup>3</sup>Poles to these faults form three distinct clusters dipping zero, forty Southeast, and forty Northwest.

<sup>4</sup>Poles to these faults form distinct clusters dipping twenty Northwest and twenty-five Southeast.

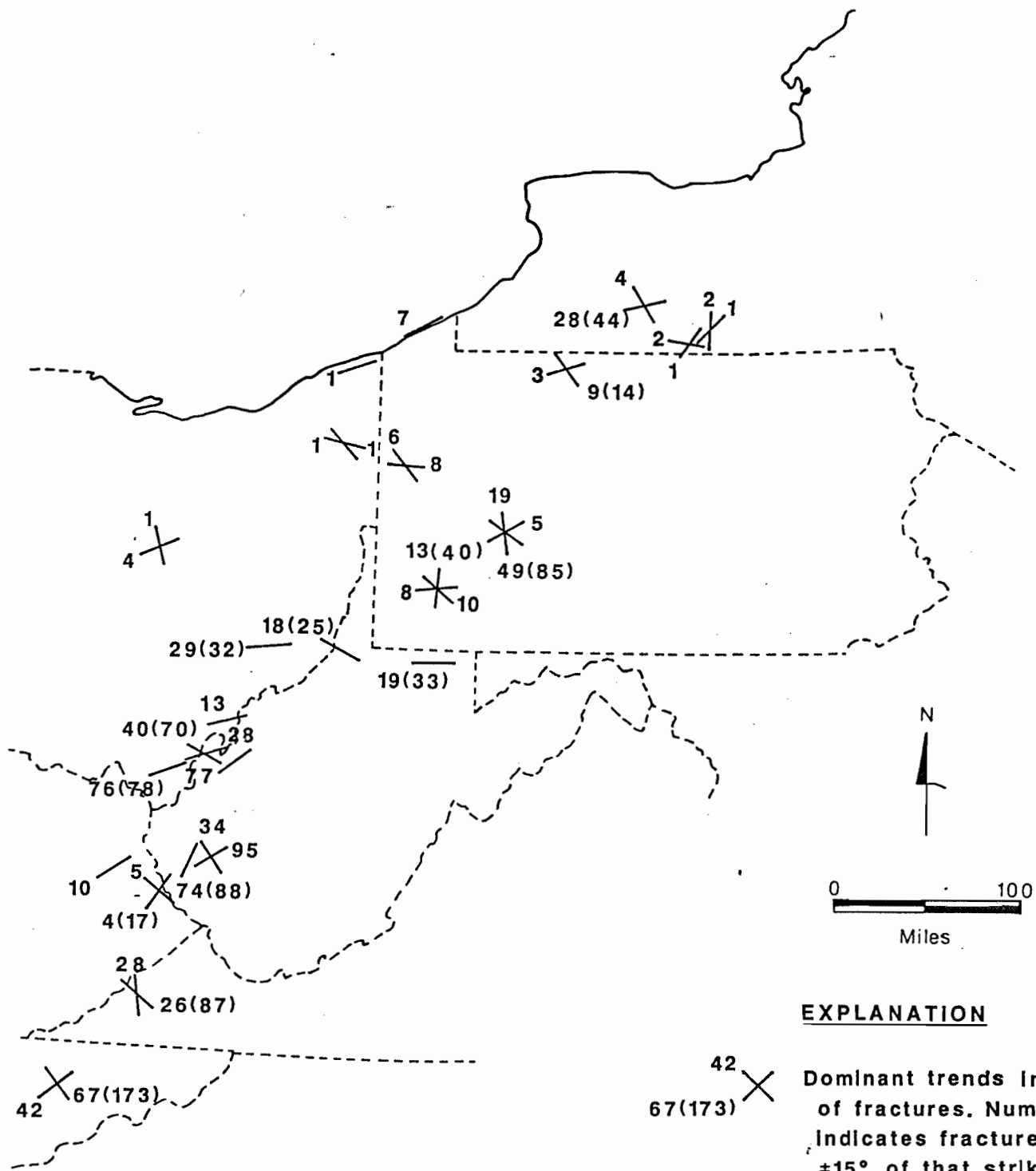
TABLE 5-6 CON'T.  
WEST VIRGINIA CORE DATA

WELL NO.	ZONE CORED	FRACTURES ORIEN./NO. (TOTAL)	FAULTS ORIEN./NO. (TOTAL)
WV-5	Chagrin		
	Huron	75/20, 120/39	160/3
	Hanover		
	Pipe Creek		5/1, 65/1, 160/3
	Angola	80/4	
	Rhinestreet	20/2, 80/2, 135/1	165/1
	Hamilton	55/1, 95/1	
	Composite	75/28, 120/40 (70)	5/1, 65/1, 160/7 <sup>1</sup>
WV-6	Tully	90/2	170/4
	Mahantango	40/2, 90/5, 135/2	75/4 (10)
	Marcellus	90/12 (22)	10/6, 70/3, 150/4(16)
	Onondaga		5/1, 135/1, 165/1
	Composite	90/19 (33)	5/7, 75/7 <sup>2</sup>
WV-7	Rhinestreet	30/2, 135/3	15/9, 135/7 (22)
	Sonyea Gp.		
	Genesee	125/1	25/11
	Geneseo	130/11	
	Mahantango	5/1	
	Marcelus	65/1, 120/2, 175/1	25/4, 125/1, 165/1
	Onondaga	25/1, 85/1, 115/1	20/2
	Composite	130/18 (25)	25/26 (41) <sup>3</sup>

<sup>1</sup>Poles to these faults form a distinct cluster indicating a dip of fifteen degrees Southwest.

<sup>2</sup>Poles to these faults form a distinct cluster indicating a dip of less than ten degrees East.

<sup>3</sup>Evans report shows poles forming a cluster suggesting mainly horizontal faults.



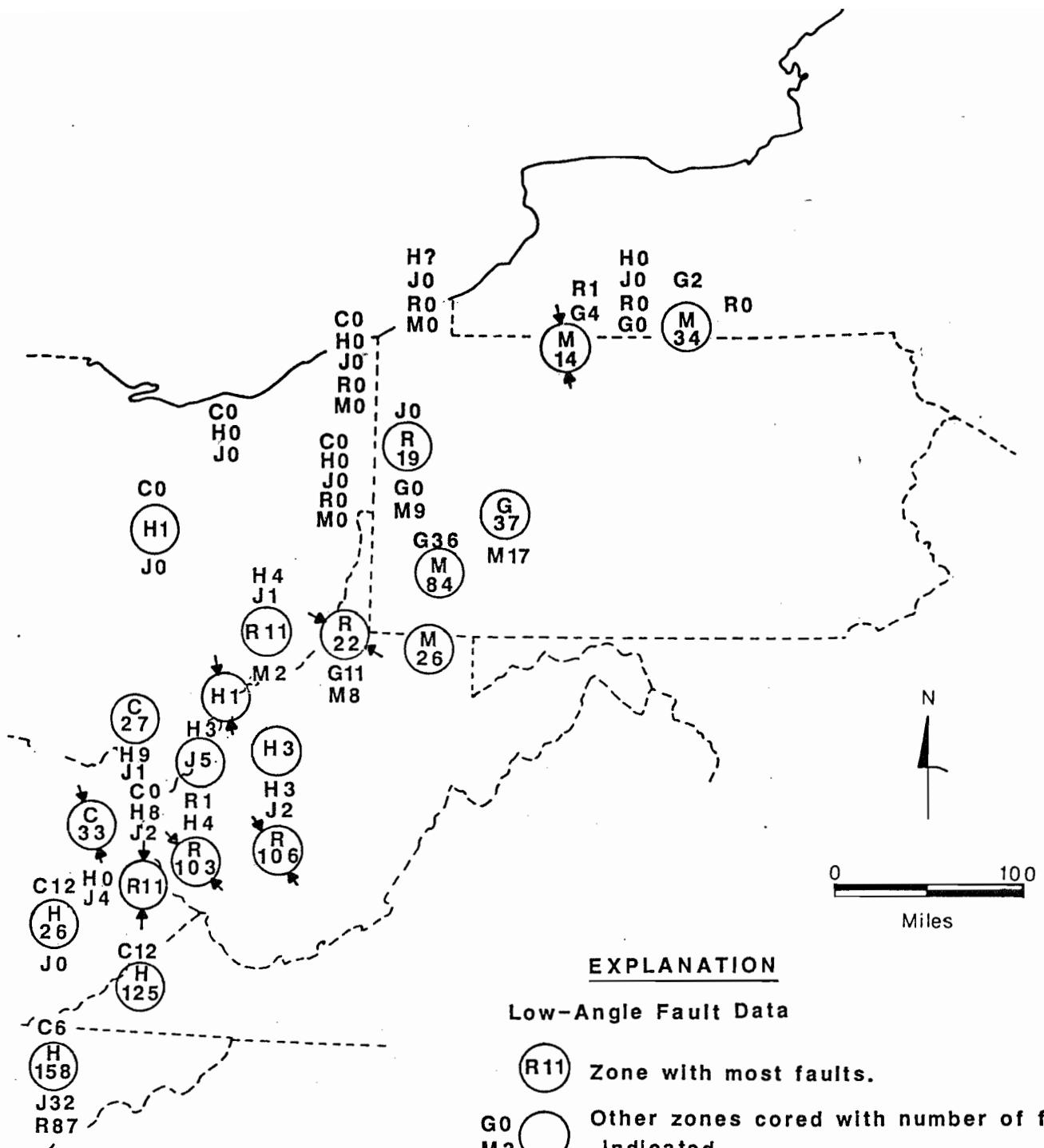
**EXPLANATION**

42 67(173) X

Dominant trends in strikes of fractures. Number indicates fractures within  $\pm 15^\circ$  of that strike. Total number of fractures at a site is given in parentheses when the number represented by the dominant trends is less than the total.

FIGURE 5-5. Dominant fracture trends.





**EXPLANATION**

**Low-Angle Fault Data**

- (R11) Zone with most faults.
- G0 ( ) Other zones cored with number of faults indicated.
- M3 ( ) Inferred direction of maximum compression from conjugate shear geometry.

**Decollement Zones with Dominant Detachment Zone Underlined.**

- C Chagrin, Cleveland, Bedford
- H Middle and Lower Huron
- J Java (Olentangy, Angola, Pipe Creek)
- R Rhinestreet
- G Genesee and Geneseo
- M Mahantange and Marcellus

FIGURE 5-7. Stratigraphic distribution of low angle faults.

TABLE 5-7.

TECTONIC HISTORY OF APPALACHIAN BASIN

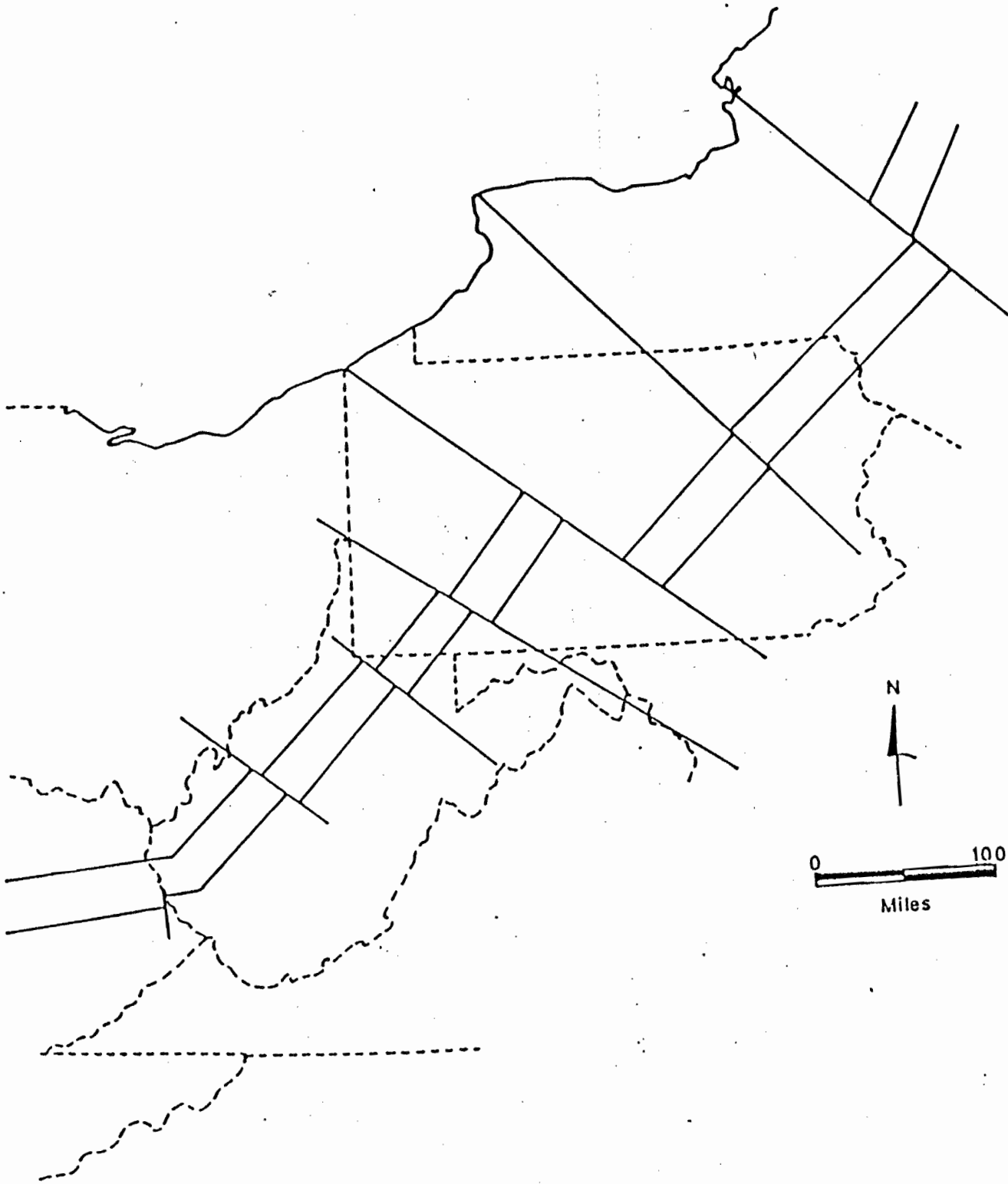
Periods (my's)	Dietz's Model	Orogenies	Events Related To Fracture Development
0			
T			
70			
100			
K			
136	S.A. breaks from Africa.		ENE extension fractures develop.
J			
195	Break-up of Pangaea, modern Atlantic forms.	Appalachian	Decollements and associated low-angle fractures form, intra-sheet extension fracturing perpendicular to thrust.
225			
P			
280			
300			
P			
320			
345			
M			
D	Atlantic closes, Pangaea forms.	Acadian	Re-activation of faults in fail rift, associated fracturing.
400			
S	Subduction of Atlantic plate under N.A. plate, collapse of eugeosyncline, volcanism, upthrust of ancient Appalachians.	Taconian	
440			
O	Atlantic begins to close.		
500			
500	Mio- & eugeosynclines form.		
570	Initial rift, ancestral Atlantic forms.		
600			Failed rift forms.
pE			

faults. It also aligns with a gravity high, as do the Adirondack faults. The significance of the gravity high is that most rift systems have anomalously high gravity because of dense mantle material rising beneath them. In a failed rift system this is no longer rising, but during rising crystallization of dense intrusives can emplace a permanent gravity high. Between the Rome Trough and the Adirondack faults, the spreading center is believed to follow the Scranton gravity high in Northeastern Pennsylvania.

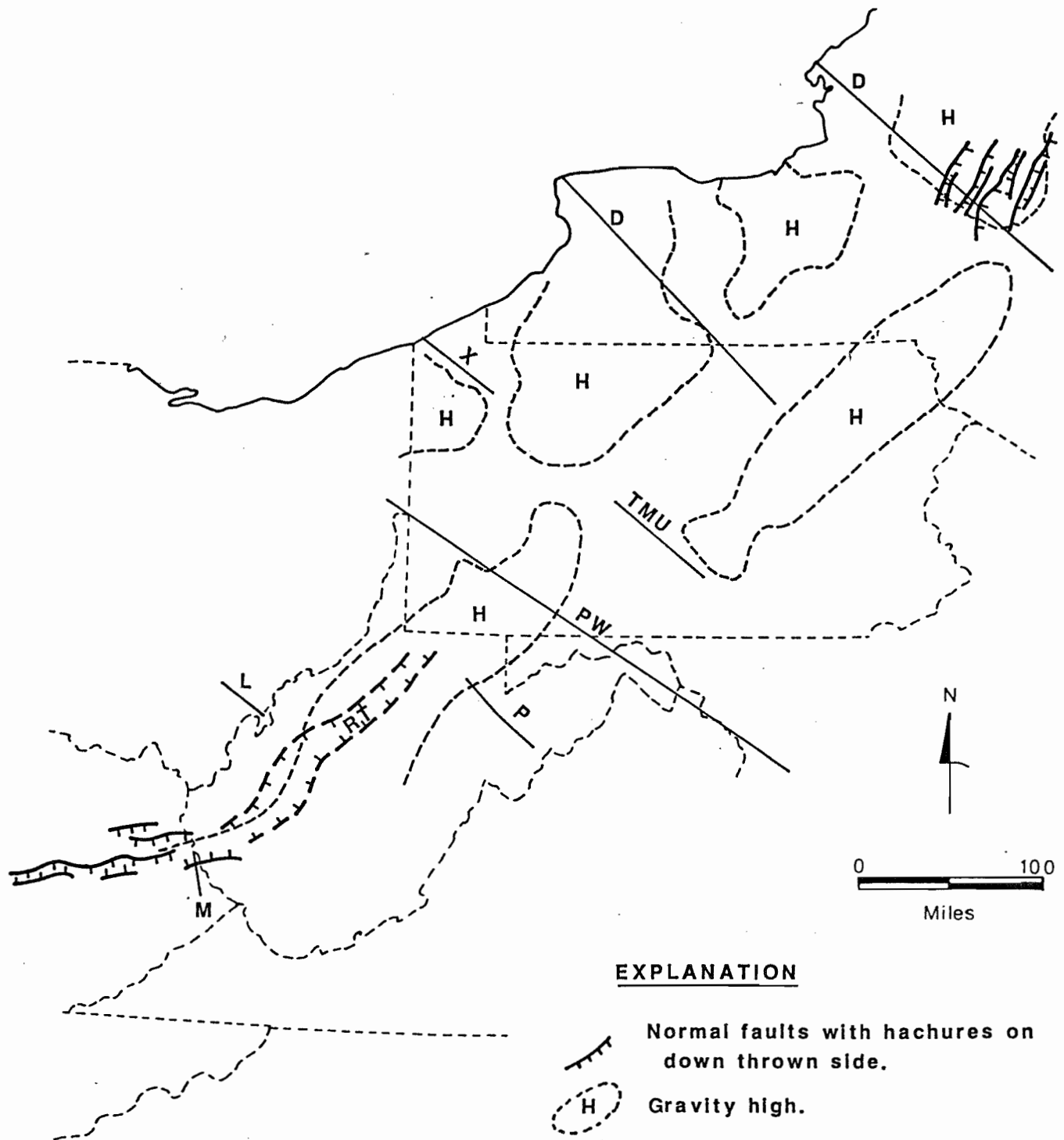
Evidence for the transform faults consists of lineaments and offsets in the gravity anomalies. The major lineaments in the Basin, those tens to hundreds of miles long, tend to be subparallel, trending N50-60W, and perpendicular to the axis of the spreading center. The two northernmost lineaments (D) are discussed in Diment et al. (1980). The Tyrone-Mount Union lineament (TMU) is a well-known feature in central Pennsylvania (Gold et al., 1973). Extensions of this lineament (X) have been found on LANDSAT images by Kowalik (1975) in Crawford County and Pees (1984) in Erie County. Lavin et al. (1982) discuss this lineament, as well as the Pittsburgh-Washington lineament (PW) and point out associated gravitational, magnetic, sedimentological and structural discontinuities. As can be seen in Figure 5-8, the TMU and Diment's lineaments are aligned with offsets in the gravitational field. Parson's lineament (P), or cross strike discontinuity, is discussed in Dixon and Wilson (1979). The lineament in Southeastern Ohio (L) is based on two sources. It appears on the Ohio Geological Survey's map of lineaments from LANDSAT. In addition, structure contours drawn on the base of the Lower Huron and the top of the Berea Sandstone have shown a strike-slip fault that is in line with this lineament in Meigs County, Ohio (SAI, 1984). Finally, the line marked "M" in Eastern Kentucky is a strike-slip fault in the Martin County field.

The timing of the rift is put at sometime prior to the formation of the ancestral Atlantic. The primary reason for this is that the faults in the system were known to have been active throughout the Paleozoic. Immediately prior to the Paleozoic, about 600 million years ago, a successful rifting was taking place just to the east that would form the ancestral Atlantic. The failed rift probably started first, then shifted to the east where it was successful.

For this system to have influenced fractures in the Devonian shales, it would have had to have been reactivated during the closing of the ancestral Atlantic and possibly during the breakup of Pangaea (See Table 5-7). The normal and strike-slip faulting in a rift system should produce fracture systems with high-angle dips. Fractures and faults that may be associated with the rift system are shown in Figure 5-9 with the overlay for comparison. Most of the fractures and faults are oriented perpendicular to the axis of the rift. These are interpreted as shear fractures oriented parallel to the transform faults, and in fact a number of them do show slickensides indicating that they have experienced shear. In Eastern Kentucky and Southwestern West Virginia there is a set of fractures and faults that parallels the Rome Trough. These are interpreted to be fractures associated with normal faulting in the extensional part of the rift.



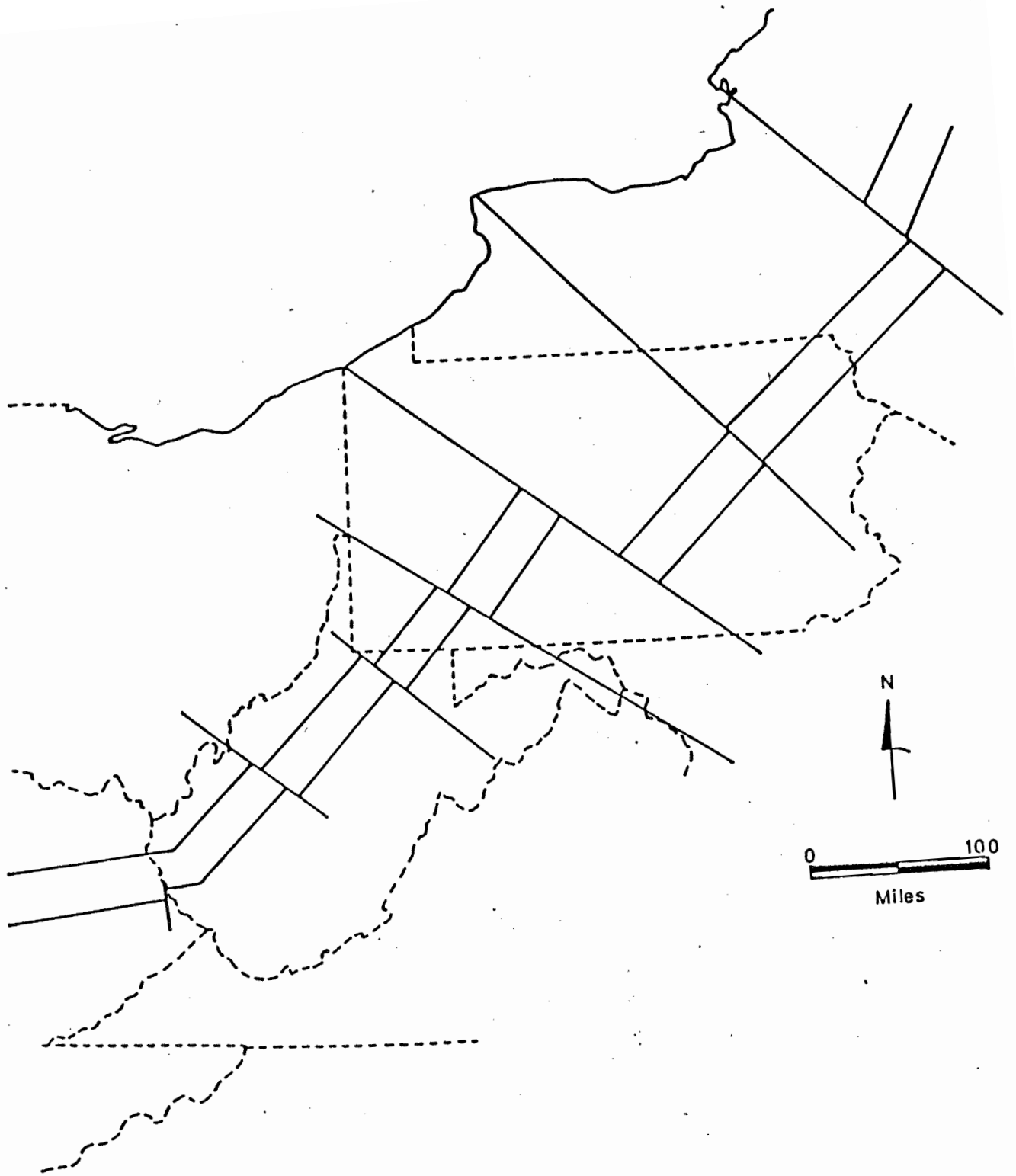
/// Spreading Center  
— Transform Fault



**EXPLANATION**

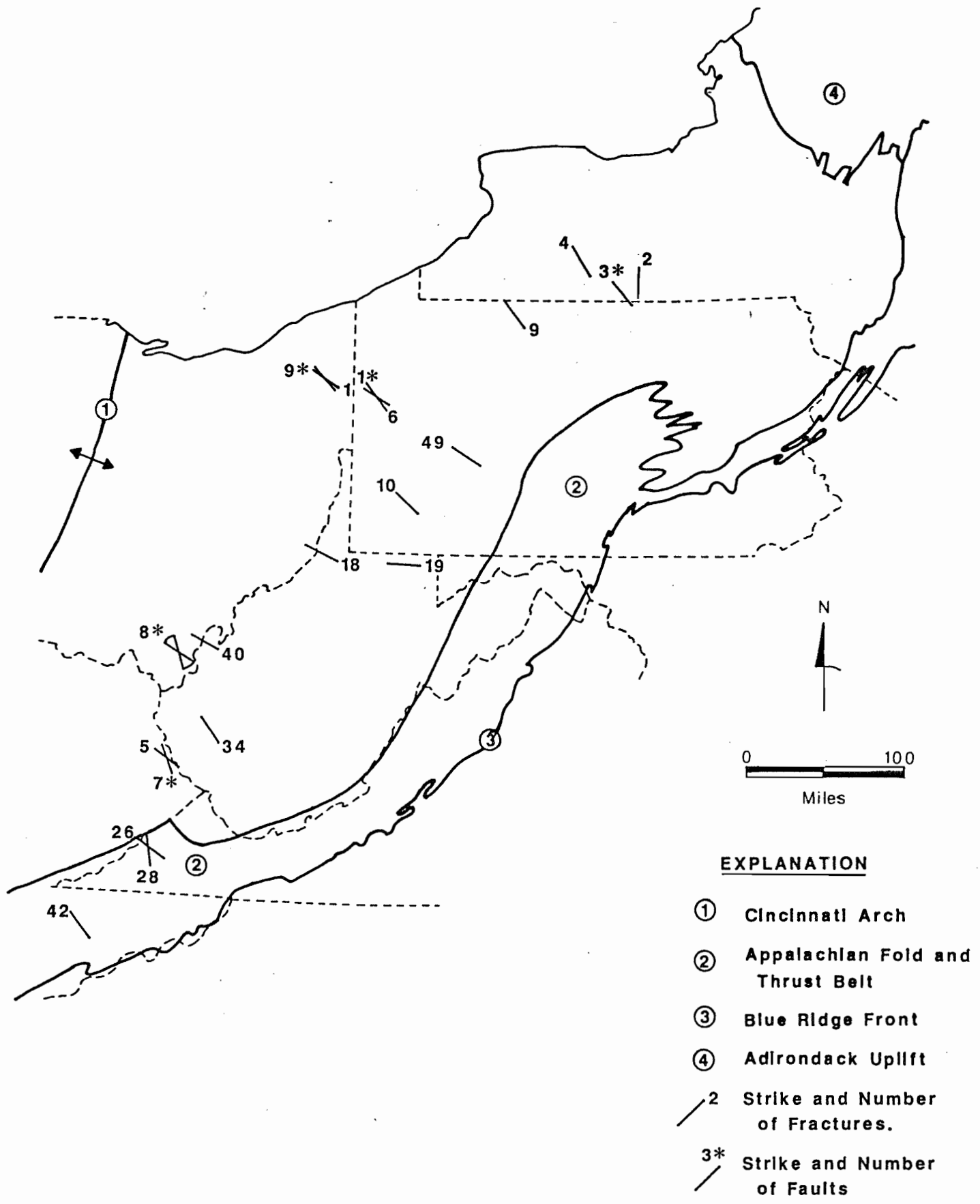
-  Normal faults with hachures on down thrown side.
-  Gravity high.
-  Lineaments.
- D** Discussed in Diment et al (1980)
- L** LANDSAT from Ohio Geological Survey.
- M** Martin County.
- P** Parson's.
- PW** Pittsburgh-Washington
- RT** Rome trough.
- TMU** Tyrone-Mt. Union.
- X** LANDSAT extension of TMU.

FIGURE 5-8. Evidence for a failed rift system.



/// Spreading Center

- Transform Fault



**EXPLANATION**

- ① Cincinnati Arch
- ② Appalachian Fold and Thrust Belt
- ③ Blue Ridge Front
- ④ Adirondack Uplift
- 2 Strike and Number of Fractures.
- 3\* Strike and Number of Faults

FIGURE 5-9. Fractures and faults that may be associated with the failed rift system.

## DEVONIAN DECOLLEMENTS

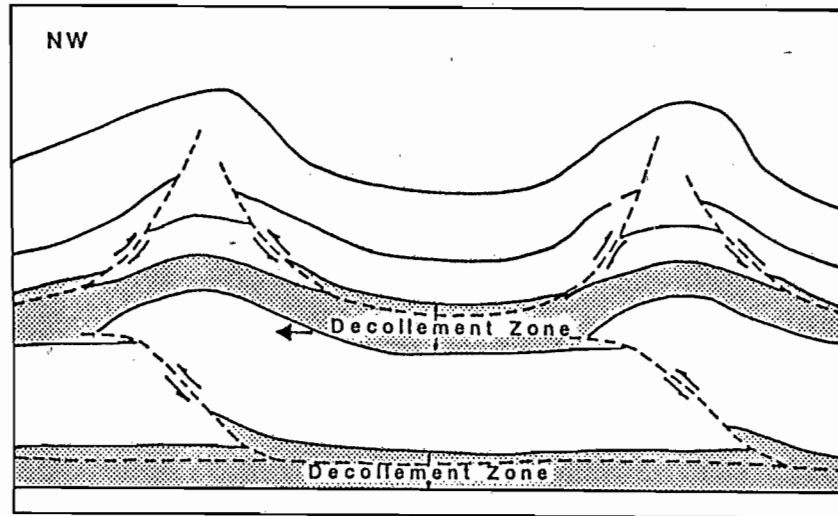
Classic papers by Rogers (1963) and Gwinn (1964) have established the importance of decollements in the eastern part of the Basin. Gwinn's model of the system is shown in Figure 5-10. An important feature of this model is that the horizontal portions of the detachment occur in relatively ductile layers and the fault climbs section rapidly through the more brittle layers, thus concentrating the faulting and fracturing in the more ductile layers. The question addressed here is how much further to the northwest does the decollement shown in Figure 5-10A extend after it climbs into the Devonian section.

The large number of low-angle faults shown in Figure 5-7 would suggest that thrusting is extensive in the Devonian section and that the decollement does extend a considerable distance to the northwest. Even more convincing are the facts that (1) the faults are concentrated in the more ductile black shales, as shown by Blanton et al. (1983), and (2) the detachment climbs section as it moves to the northwest. Both of these features are consistent with Gwinn's model.

The data in Figure 5-7 can be used to construct a detachment surface consistent with Gwinn's model. This construction has been carried out in Figure 5-11. The letters indicate the zone with the most horizontal faults at that site, except where they are in parentheses. The parentheses indicate that an adjacent site had a secondary number of low-angle faults in the indicated zone. The letter "N" indicates no horizontal faulting in the cored section. The area designated with an "S" is the region of detachment in the Silurian Salina salt as determined by Rogers (1963). There were no data for the area indicated by the (MG?); however, the model suggests that there should be a detachment in a Marcellus or Genessee equivalent in this area. The well to the northwest went directly from the Rhinestreet into the Onondaga limestone, but this does not mean that there could not be another black shale zone between the Rhinestreet and the Onondaga southeast of the Warfield anticline.

A less cluttered view of the decollement as it climbs section to the northwest is shown in Figure 5-12. A regional compression oriented northwest-southeast would have been associated with this detachment. Fractures and high-angle faults that may have resulted from this compression are shown in Figure 5-13. Some of these were also shown in Figure 5-9 as possibly being associated with the northwest trending transform faults. Unfortunately, in some parts of the basin orientation alone does not help distinguish between rift-related fractures and fractures related to the Appalachian orogeny. However, those that are faults, and thus have definitely undergone shear, are more probably related to the transforms.

A)



B)

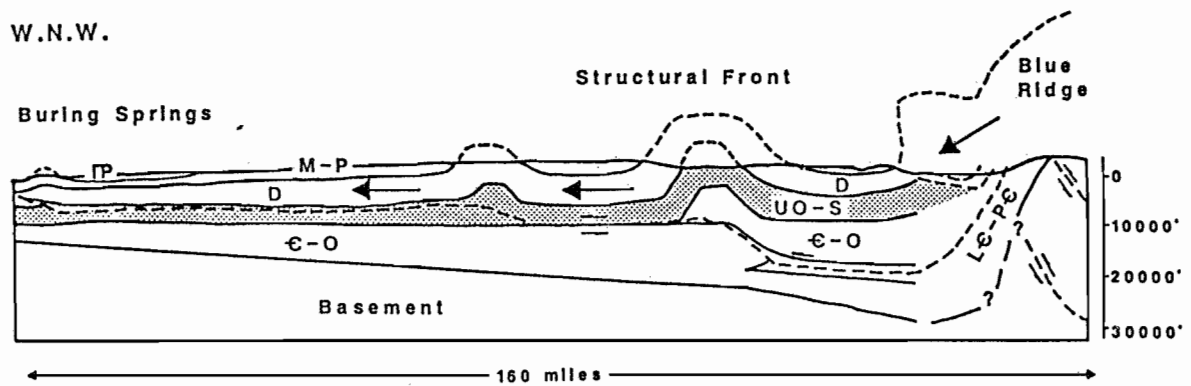


FIGURE 5-10. Model of a decollement. A.) Decollement in Silurian in the eastern part of the Appalachian Basin. B.) Structures associated with a decollement climbing section (after Gwinn, 1964).

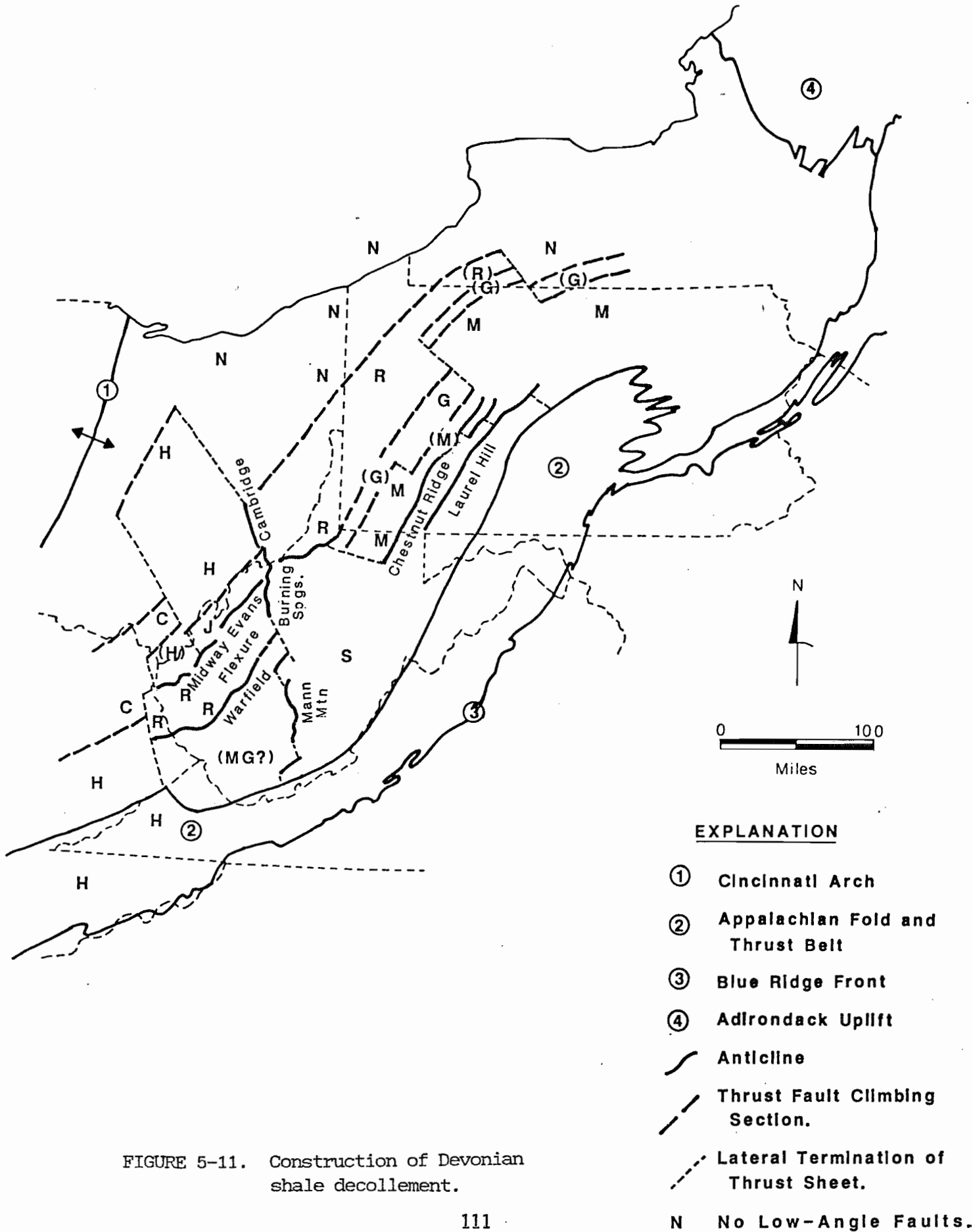
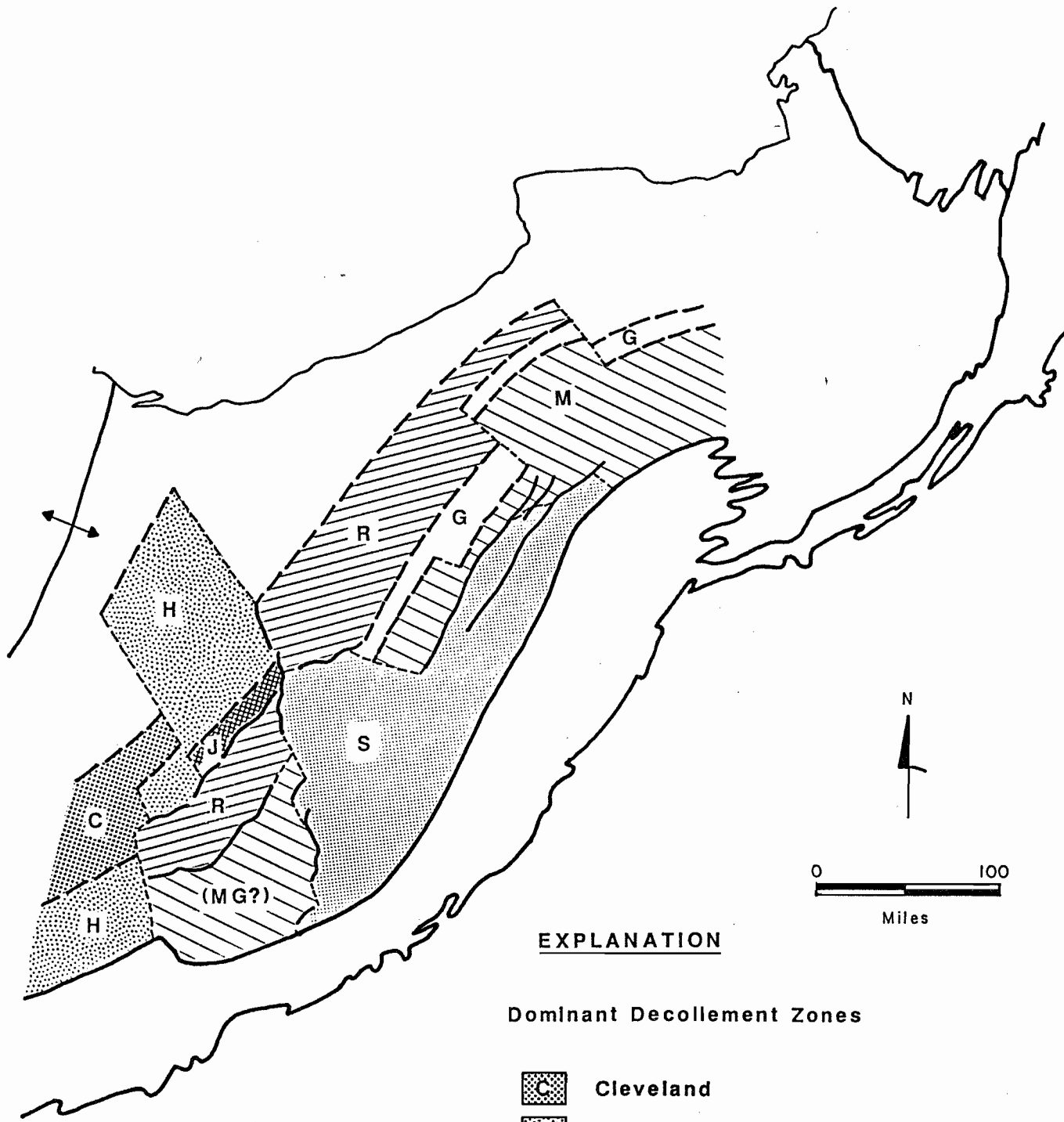


FIGURE 5-11. Construction of Devonian shale decollement.



**EXPLANATION**

**Dominant Decollement Zones**

-  **C** Cleveland
-  **H** Lower Huron
-  **J** Java
-  **R** Rhinestreet
-  **G** Genesee
-  **M** Marcellas
-  **S** Salina Salt (after Rogers, 1963)

FIGURE 5-12. Devonian shale decollement.

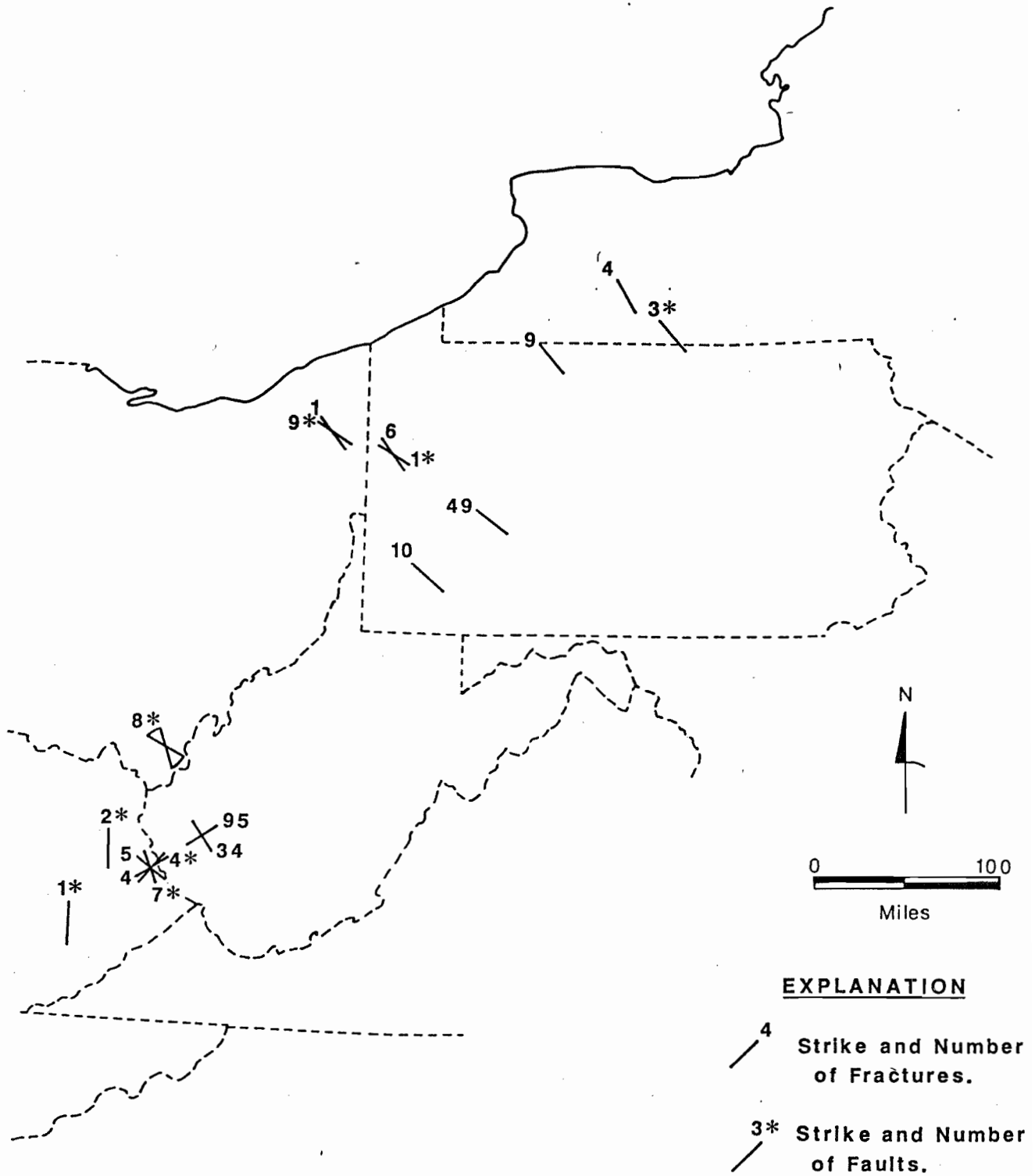


FIGURE 5-13. Fractures and faults that may be associated with the Appalachian orogeny.

## CURRENT REGIONAL STRESS FIELD

Fractures and faults that parallel the current regional stress field are shown in Figure 5-14 with an overlay of the stress orientations from Figure 4-1. The fractures seem to follow the stress orientations as they change from the east-northeast trend in the north and south to a more east-west trend in the Eastern Ohio and Western Pennsylvania region.

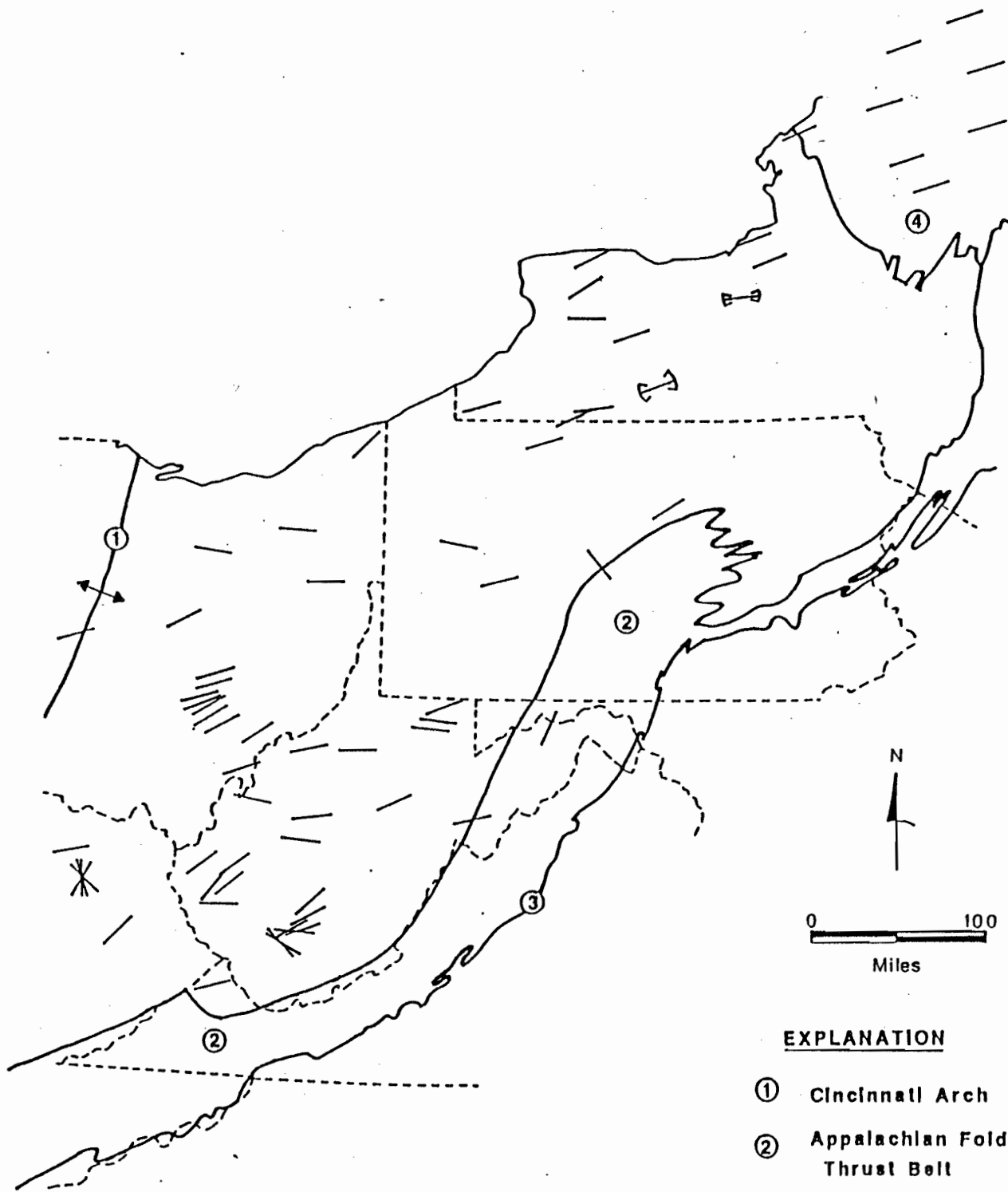
## OTHER FRACTURE TRENDS

Fracture trends which were not obviously related to any of the above tectonic features are shown in Figure 5-15. It is interesting that these odd fractures are not randomly oriented throughout the basin, but, instead seem to form a definite fracture domain in the central part of the basin with a north-south trend. Three explanations have been considered for this trend.

One explanation is that these are conjugate shears to the transform faults represented by the PW and TMU lineaments. (This explanation would seem to exclude the one fracture in Central Ohio.) For this to be true, at some point in time there would have had to have been right lateral movement on these two shear zones. Lavin et al. (1982) present strong evidence that the TMU lineament has experienced right lateral movement. However, they contend that the PW lineament is a left lateral displacement, although the evidence is not as convincing for the latter because it consists primarily of magnetic data in the coastal region.

Another possibility is that they are linked to a north-south trending fracture set found by Engelder and Geiser (1980) in Western New York. This set appeared to be independent of those fractures that were orthogonal to the Appalachian front. They attributed these fractures to a period of Appalachian deformation that had a more north-south component. This explanation is feasible for New York since the overall deformation trends are not that far from an east-west, north-south system, but it is not feasible for the fractures shown in Figure 5-15 because Appalachian trends are rotated forty-five degrees here. One possible explanation is that they are extensional features associated with the breakup of Pangaea. There are some north-south trends in the coastal regions of Virginia, Maryland, and New Jersey that probably developed during the breakup.

A final possibility is that they are related to glacial loading and unloading. The glacial limit trends East-Northeast through Eastern Ohio and Western Pennsylvania (Clark, 1982).



**EXPLANATION**

- ① Cincinnati Arch
- ② Appalachian Fold and Thrust Belt
- ③ Blue Ridge Front
- ④ Adirondack Uplift
- Direction of maximum horizontal stress
- ↔ Average and range of directions for maximum horizontal stress.



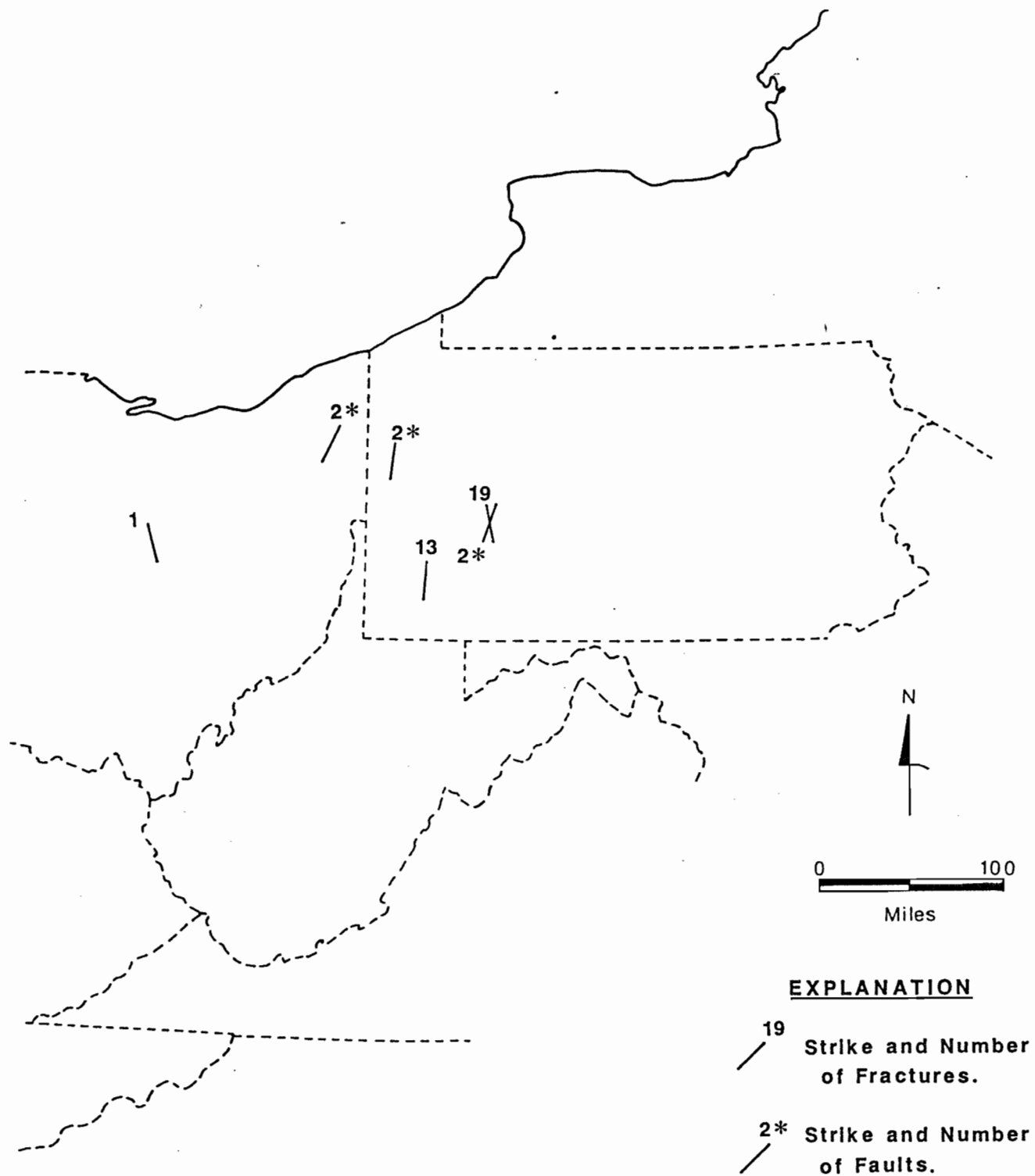


FIGURE 5-15. Fractures and faults not clearly associated with any of the tectonic features discussed.

TASK 6. INDUCED/NATURAL FRACTURE INTERACTION  
IN DEVONIAN SHALES OF THE APPALACHIAN BASIN

OBJECTIVE

The objective of this task was to synthesize the results of the laboratory studies and the investigative analysis into an approach to determine the type of fracture interaction that can be expected in different points of the Appalachian Basin.

LIMITS DEFINED BY INTERACTION CRITERIA

Based on the results of Tasks 1 and 2, two types of fracture interaction regions can be defined. The first, which will be referred to as Type I, consists of areas where all the natural fractures are oriented relative to the stress field such that they will tend to open and divert induced fractures. In these areas little can be gained from extending induced fractures beyond the first natural fracture encountered. The question of which stimulation to use depends on which is more economical: a small hydraulic treatment or a dynamic treatment. In Type II areas there exist natural fractures oriented relative to the stress field so that an induced fracture will cross them, given enough differential stress.

The division between Type I and Type II areas is made solely on the basis of angle of approach. A fifty degree limit has been selected by scaling the criterion from Task 1 for Devonian shales. Type I areas will then be those where the maximum horizontal compressive stress is oriented fifty degrees or less to the fracture system. By referring to Figures 1-8 and 1-9, it can be seen that for angles of approach less than forty-five degrees, opening interaction can be expected no matter what the differential stress. Between forty-five and fifty degrees differential stresses would have to be much higher (greater than 5500 psi) than exist in Devonian shale reservoirs to get crossing interaction, thus opening interaction can be expected for this range as well. In Type II areas, where angles of approach are greater than fifty degrees, it is possible for differential stresses to be high enough to cause crossing interaction.

## APPLICATION OF INTERACTION CRITERION IN THE APPALACHIAN BASIN

The Appalachian Basin has been divided into Type I and Type II regions by combining the stress orientation data from Task 4 with the fracture system data from Task 5. For each well site, the number of fractures and high-angle faults with strikes above and below fifty degrees from the orientation of the maximum horizontal compressive stress have been determined and are presented in Table 6-1. The numbers have also been plotted in Figure 6-1.

First it is apparent that in all but two cases there are some fracture systems that are oriented so as to open and divert an induced fracture. This does not necessarily mean that there will always be opening interaction. The numbers shown in Figure 6-1 are for all the fractures at each site. It is possible that the zone of interest may contain only fractures oriented so as to give a crossing interaction.

The boundaries shown in Figure 6-1 have been drawn by considering the domains of the fracture systems oriented to give a crossing interaction. These fractures appear to be associated with two of the tectonic features discussed in Task 5: the Precambrian rift system and the intrasheet extension fractures associated with the Appalachian orogeny.

The boundaries of the domain associated with the rift system are shown in Figure 6-2. Fractures oriented to give a crossing interaction appear to have developed only in the northern and southern parts of this domain. This is probably because these are the high energy parts of the system. The southern part is in the neighborhood of where the rift axis changes direction and may even be a failed triple juncture. The northern part is occupied primarily by the block bounded by the TMU and PW lineaments, which has been reactivated numerous times since the Precambrian.

The domain of intrasheet extension fractures associated with the Appalachian orogeny is shown in Figure 6-3. Again, fractures oriented to give a crossing interaction appear to have developed only in the northern and southern parts of this domain. In this case a change in the trend of the Appalachian front causes fractures in the central portion to be oriented so that opening rather than crossing interaction can be expected.

The boundaries in Figure 6-1 have been drawn by superposing the boundaries of the regions marked as Type II in Figures 6-2 and 6-3. It should be emphasized that just because one is stimulating a well in the Type II region, it does not follow that one will obtain crossing interaction but only that it is a possibility. Two things must be checked before designing for a crossing induced fracture. The first is that the natural fracture system oriented for crossing interaction exists in the zone of interest and that it has a significant influence on reservoir drainage. The second is that there is enough differential stress in the zone to produce a crossing interaction.

TABLE 6-1.

DIVISION OF FRACTURE SYSTEMS  
INTO TYPE I AND II AREAS

WELL NO.	MAX. STRESS ORIENTATION	TYPE I FRACTURES APPROACH ANGLE/NO.	TYPE II FRACTURES APPROACH ANGLE/NO.
KY-1	58		63/1
KY-3	58	13/4, 22/5, 23/4	67/5, 88/3
KY-4	58	2/10	53/2
NY-1	75	5/28	75/4
NY-3	75	30/1	70/2
NY-4	75	30/3	65/3
OH-3	85	15/4	80/1
OH-4	75	5/1	
OH-6	74	4/76, 49/1	69/1, 89/4
OH-7	94	26/2, 36/2	69/2
OH-8	69	11/29	
OH-9	70	0/13	
PA-1	70	10/5	70/9
PA-2	86	4/8, 44/10	86/3
PA-3	75	10/7	
PA-4	85	15/5, 35/49	65/2, 85/19
PA-5	94	1/8, 41/1, 46/6	89/2
TN-9	73	13/42	67/67
VA-1	73	62/26, 83/28	
WV-2	85	30/77	
WV-3	58	7/95	87/34
WV-4	58	33/74	
WV-5	85	10/28, 35/40	
WV-6	87	3/19	
WV-7	88	42/18	

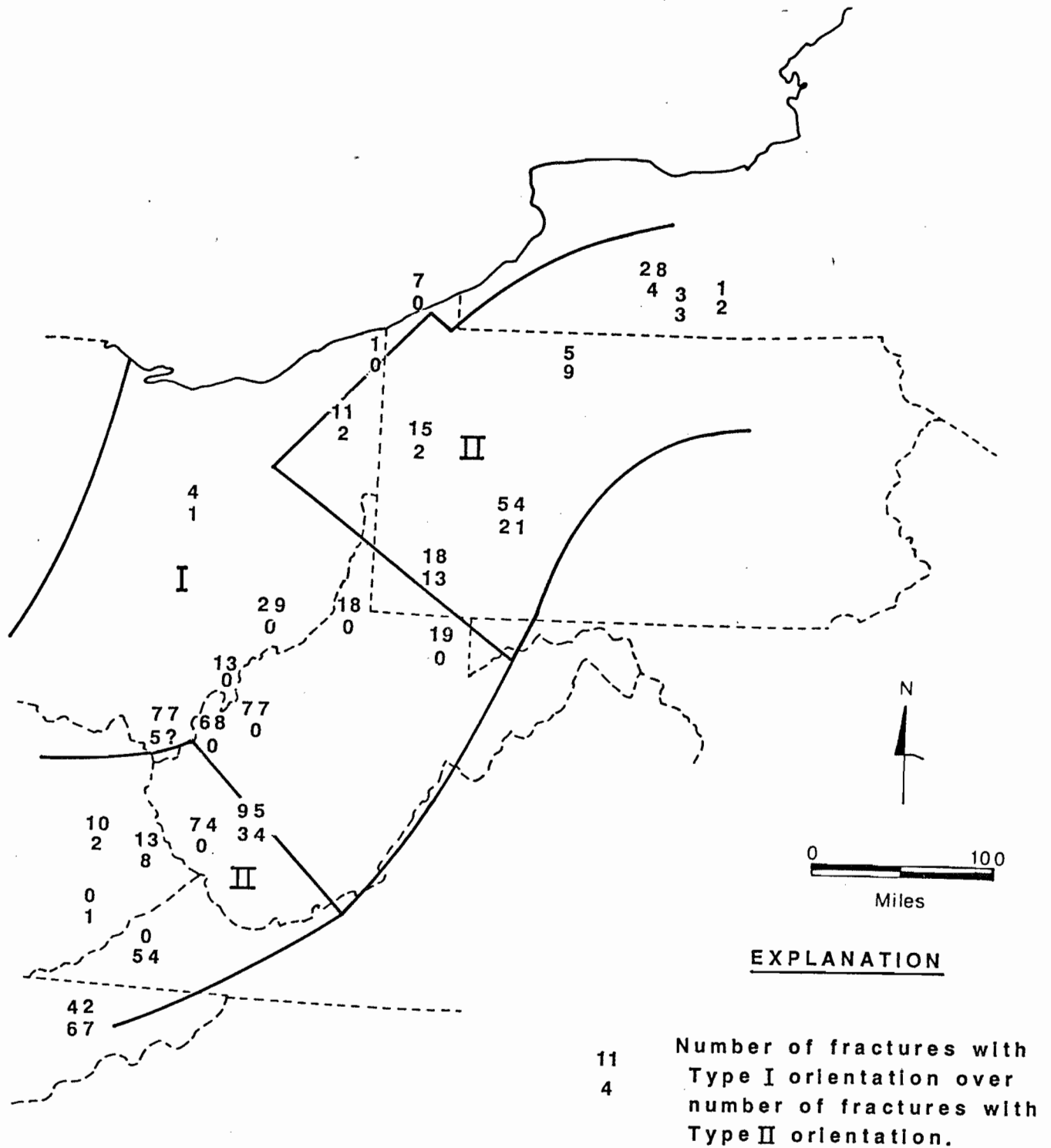


FIGURE 6-1. Number of fractures with Type I and II orientations, and boundaries of Type I and II regions.

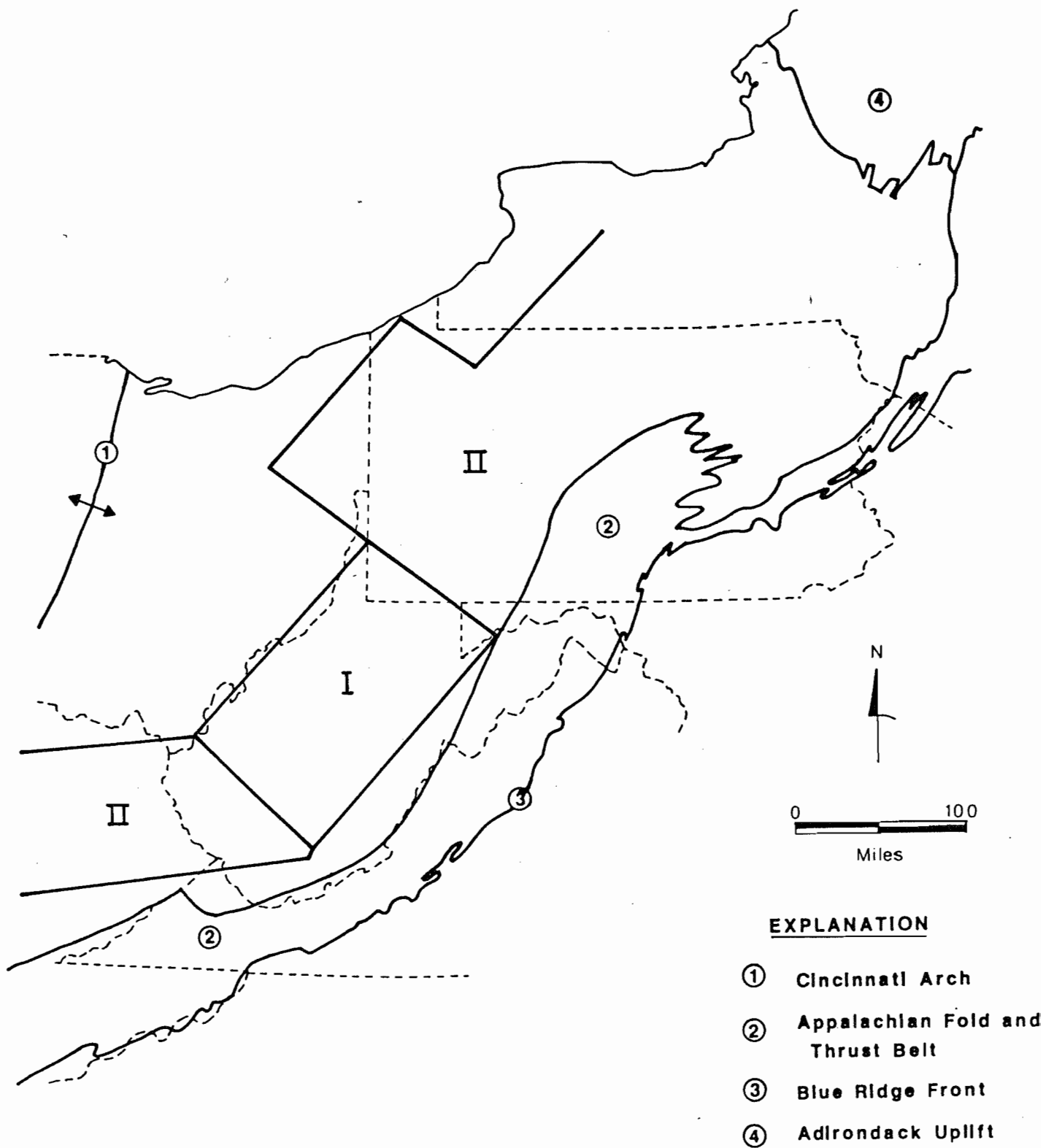


FIGURE 6-2. Domain of the failed rift system divided into Type I and II regions.

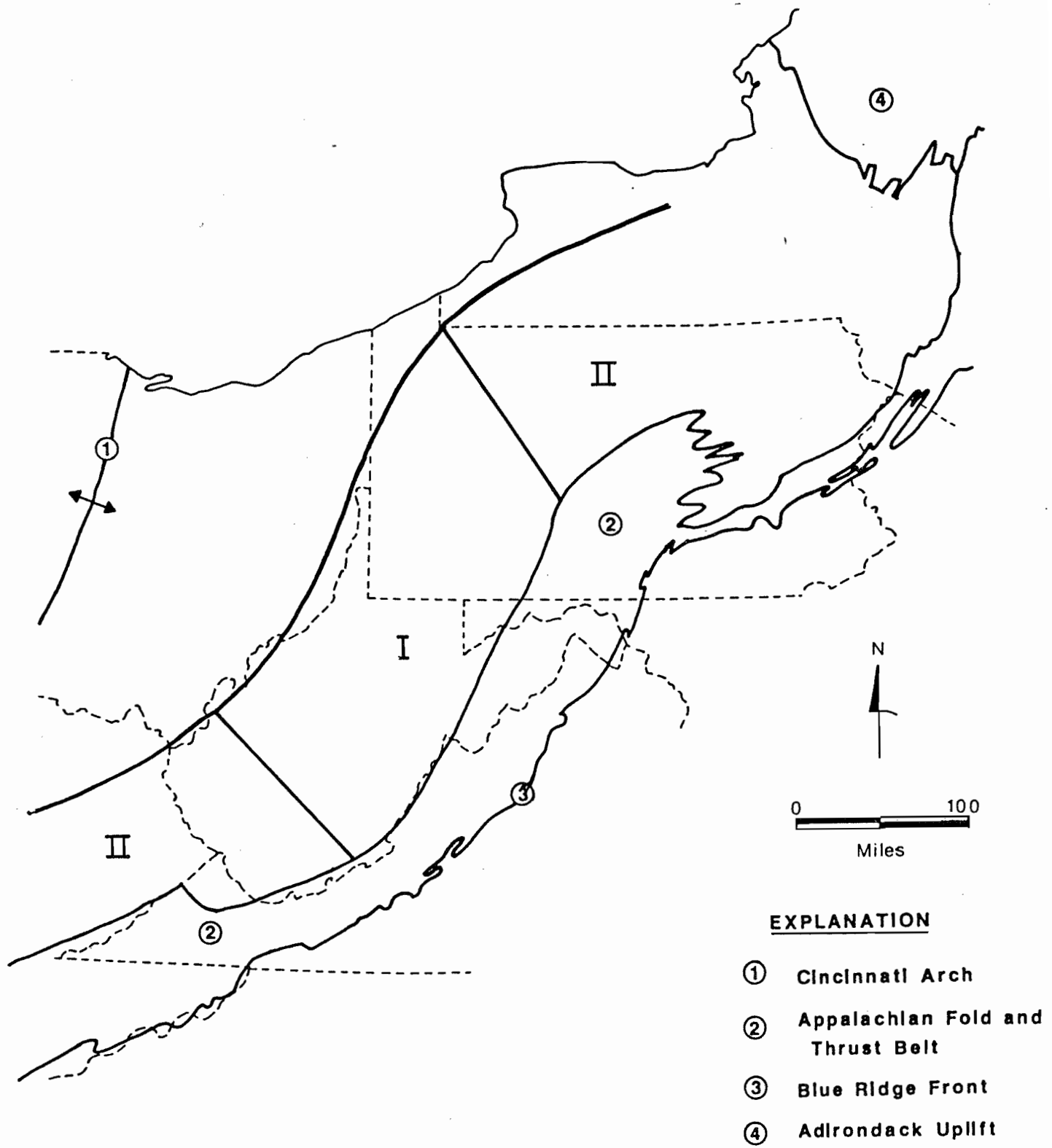


FIGURE 6-3. Domain of Appalachian orogeny divided into Type I and II regions.

APPENDIX A  
RESULTS OF  
HYDRAULIC FRACTURE INTERACTION TESTS  
(TASK 1)

TEST PT-1

TEST CONDITIONS

Maximum Horizontal Stress: 2000 psi  
Minimum Horizontal Stress: 1000 psi  
Vertical Stress: 1000 psi  
  
Differential Stress: 1000 psi

RESULTS

The hydraulic fracture produced in this solid block test was very asymmetrical, extending to the wall of the block in one direction and 5.4 inches in the other. Five extension/shut-in cycles were run, each cycle lasting forty seconds. Only four "shut-in" rings were obvious on the fracture surface.

COMMENTS

While drilling the borehole, a 0.5-inch length of drill bit broke off and remained at the bottom of the hole. The 1/8-inch borehole was then epoxied to a depth of 6.5 inches, 0.5 inches from the broken drill bit. It was observed that fluid penetrated the area around the bit and that the fracture propagated from the entire 1-inch "open" section of the borehole.

TEST PT-3

TEST CONDITIONS

Maximum Horizontal Stress: 2000 psi  
Minimum Horizontal Stress: 1000 psi  
Vertical Stress: 1000 psi  
  
Differential Stress: 1000 psi

RESULTS

A slightly asymmetrical hydraulic fracture outline was produced in this solid block test with wings extending 4.7 inches in one direction and 5.8 inches in the other. Only five rings were obvious on the fracture surface.

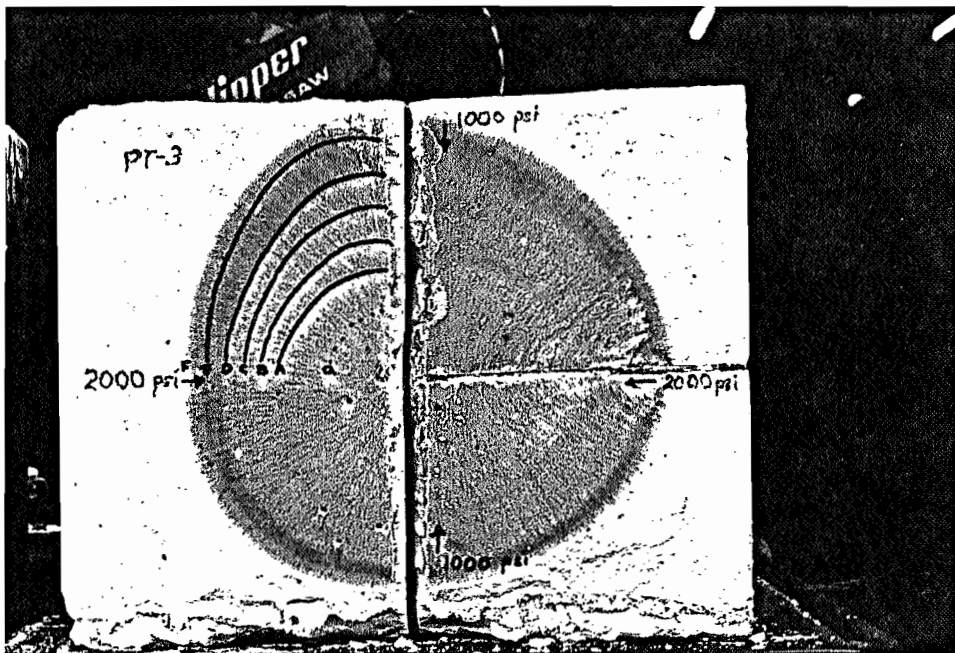


FIGURE A-1. Solid block test PT-3 showing "shut-in rings".

## TEST PT-4

### TEST CONDITIONS

Maximum Horizontal Stress:	2100 psi
Minimum Horizontal Stress:	600 psi
Vertical (Intermediate) Stress:	1350 psi
Differential Stress:	1500 psi
Angle of Approach:	90 degrees

### RESULTS

The hydraulic fracture created in this test is symmetrical with very little leakage into the pre-fractures. Crossing behavior is observed with wings extending beyond respective pre-fractures 1.9-inches and 2.3-inches. Fluid leakage into pre-fractures extended up to 0.7-inches and leakage through the borehole was slight.

### COMMENTS

This block was poured in four sections with the 1/8-inch borehole tube cemented into place. Initial hydraulic pressurization opened into the central crack - that is, the hydraulic fracture propagated along a pre-existing plane oriented in the direction of minimum principal stress. After disassembling the block, a 1/16-inch notch was cut into the central 1-inch section of the borehole oriented in the direction of maximum principal stress (to be applied in the succeeding trial). The 1/8-inch borehole tube was removed then epoxied into place. A fracture oriented in the direction of maximum principal stress was produced in the second trial. The actual distances from the borehole to pre-fracture by the hydraulic fracture are 2.9 inches and 3.1 inches.

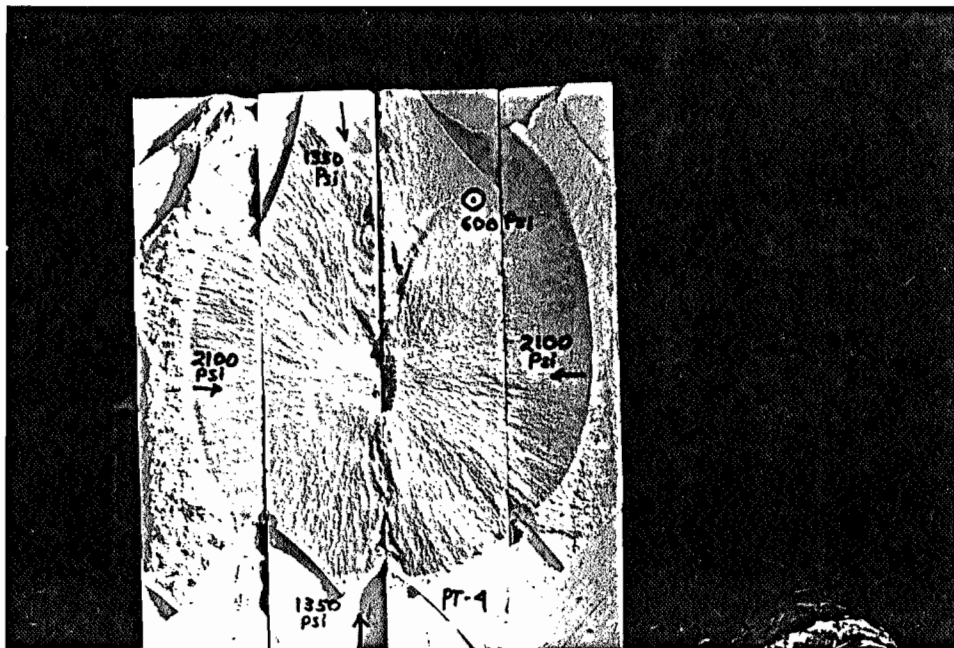


FIGURE A-2. Interaction test PT-4.

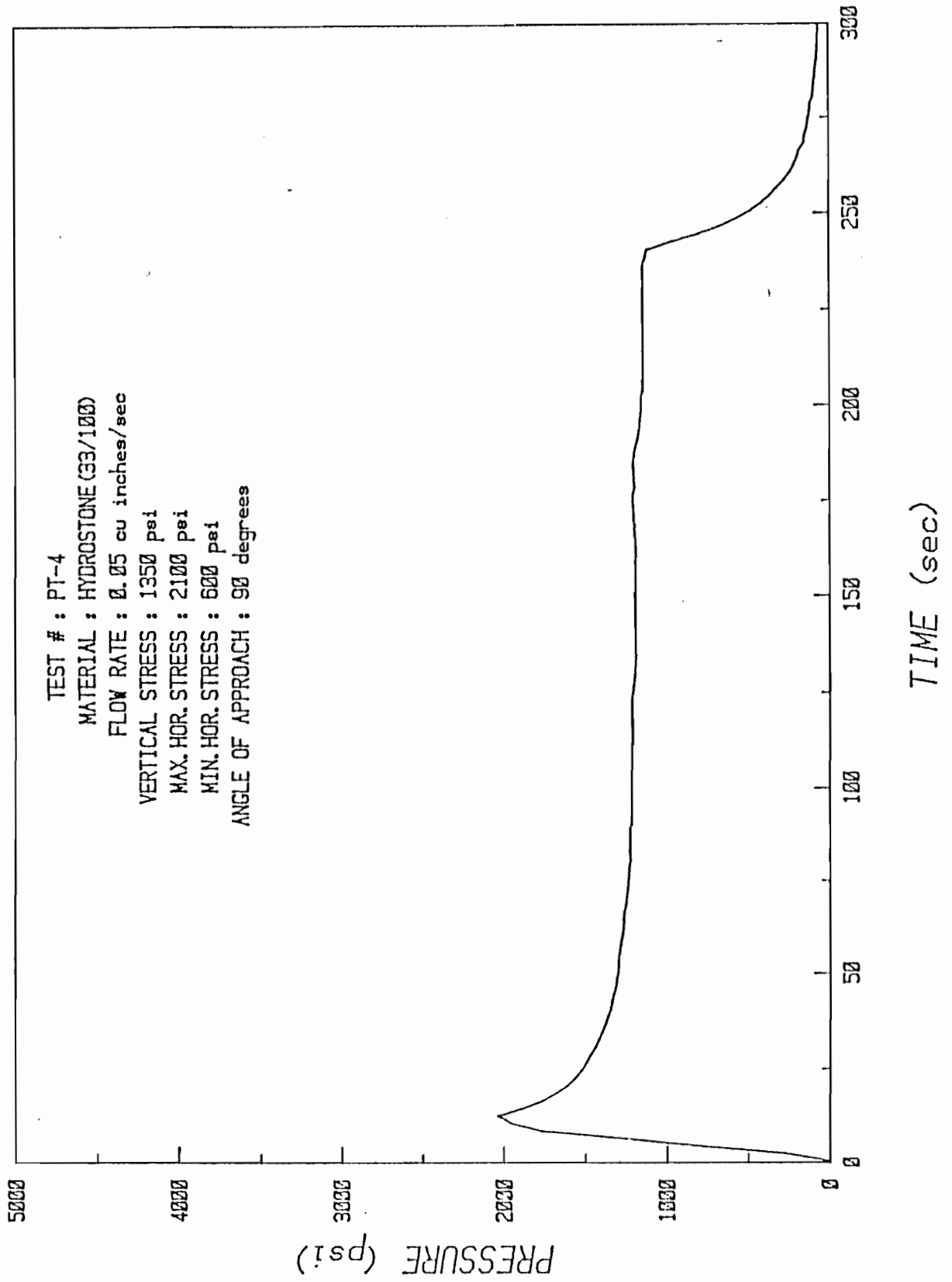


FIGURE A-3. Pressure time record for test PT-4.

TEST PT-5

TEST CONDITIONS

Maximum Horizontal Stress:	900 psi
Minimum Horizontal Stress:	600 psi
Vertical (Intermediate) Stress:	750 psi
Differential Stress:	300 psi
Angle of Approach:	90 degrees

RESULTS

The hydraulic fracture generated by this test is symmetrical with only moderate leakage (up to 1.9 inches) of fluid into pre-fractures. Crossing behavior occurred with wings extending beyond pre-fractures 1.9 inches and 2.5 inches.

COMMENTS

This block and all successive blocks were poured in three sections, using a paddle to initiate fracture. The borehole tube and paddle assembly is cemented in place. The actual distance from the borehole to a pre-fracture are 2.9 inches and 3.1 inches.

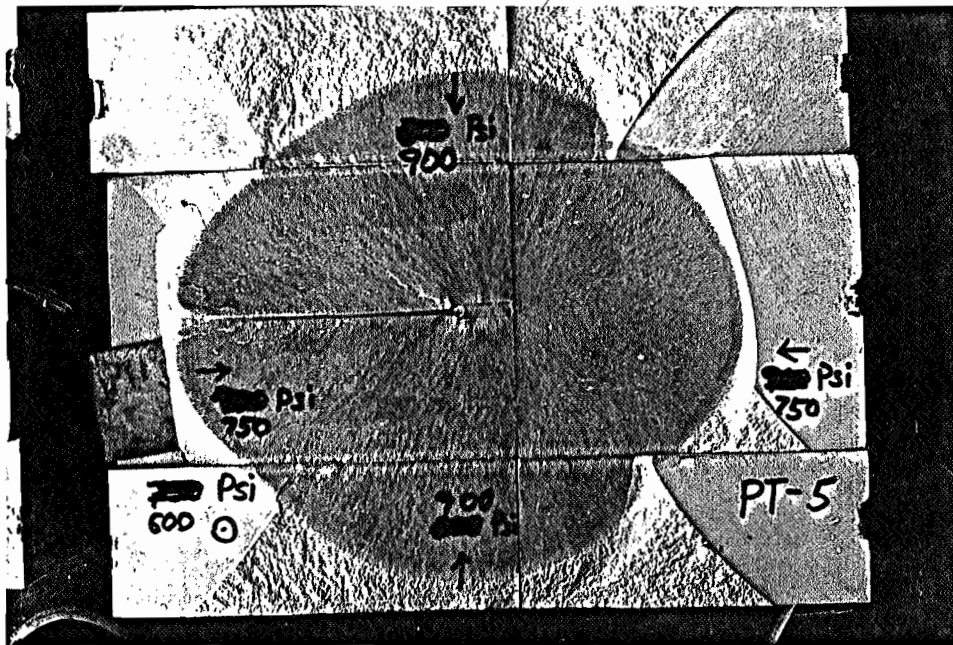
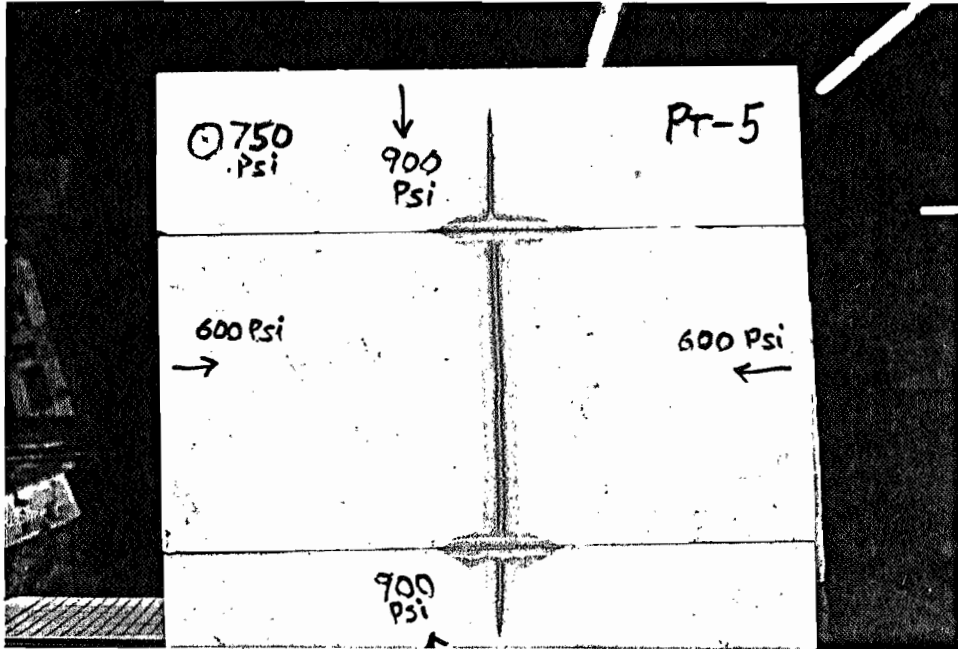


FIGURE A-4. Interaction test PT-5.

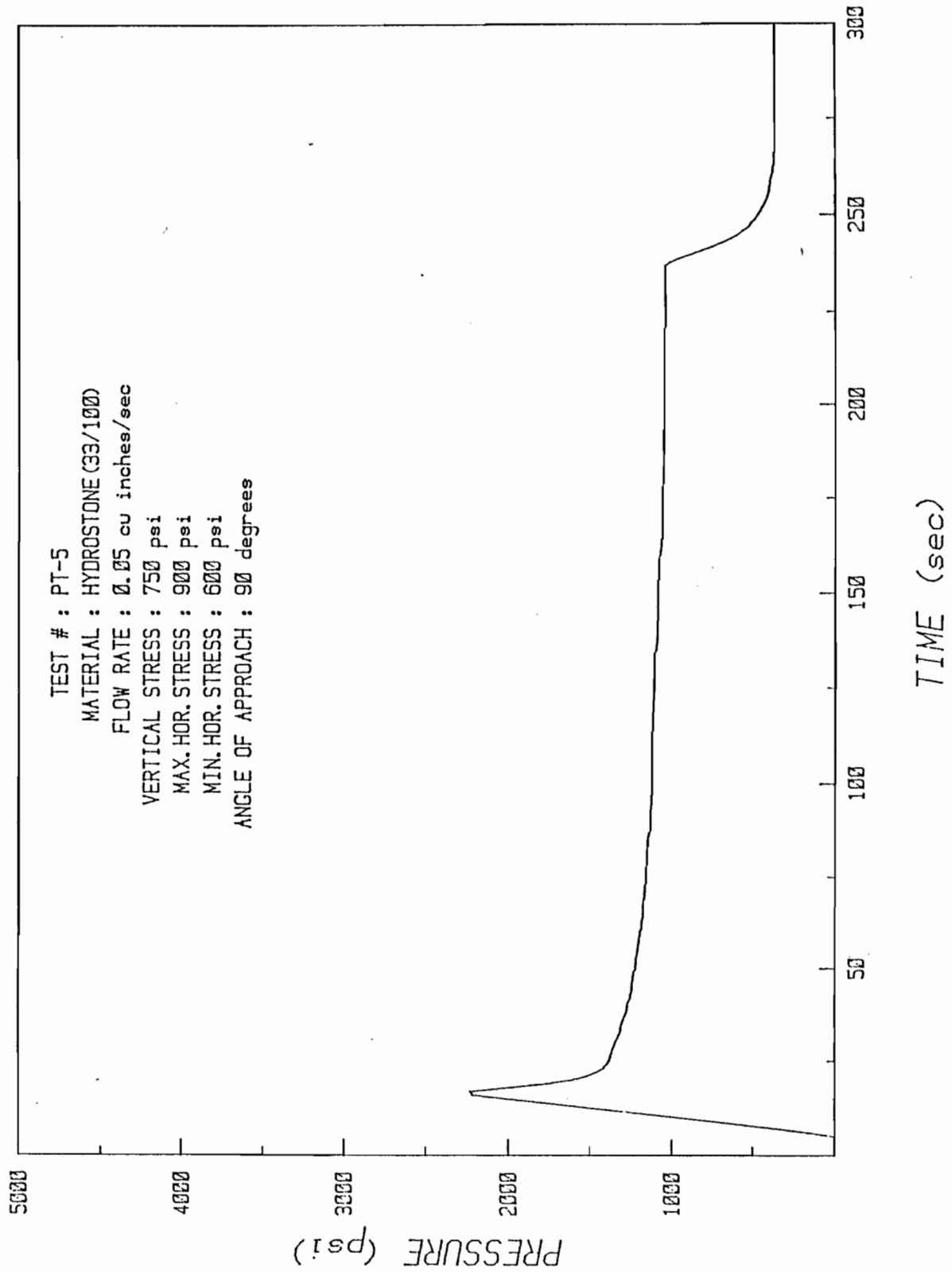


FIGURE A-5. Pressure time record for Test PT-5.

TEST PT-6

TEST CONDITIONS

Maximum Horizontal Stress:	1200 psi
Minimum Horizontal Stress:	600 psi
Vertical (Intermediate) Stress:	900 psi
Differential Stress:	600 psi
Angle of Approach:	30 degrees

RESULTS

Opening behavior is observed in this test with considerable flow into one pre-fracture and only moderate flow into the other. Leakage into pre-fractures extended 2.8 inches on one side of the borehole and 1.3 inches on the other. The actual distances between the borehole and a pre-fracture travelled by the hydraulic fracture are 2.8 inches and 2.9 inches.

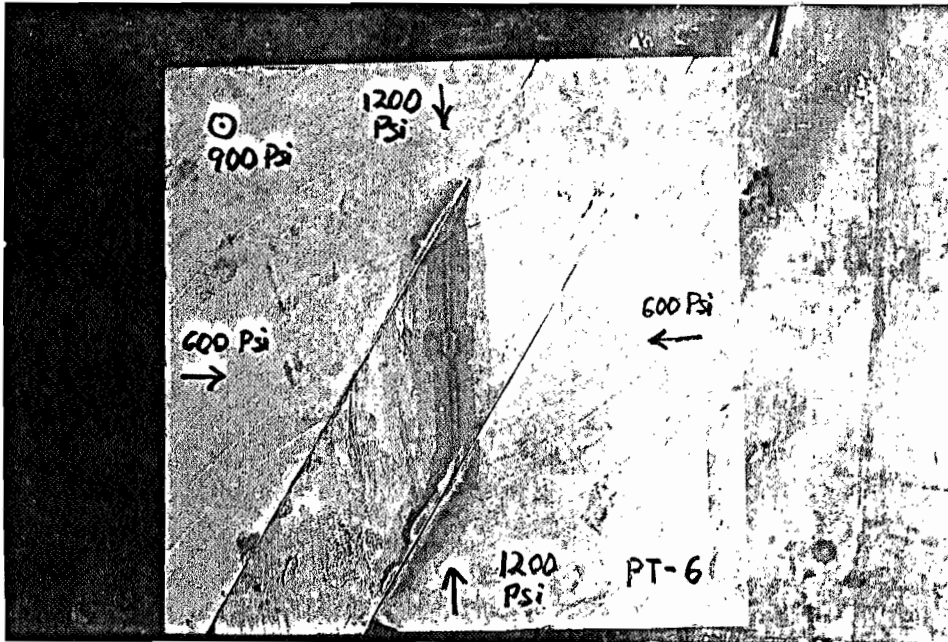


FIGURE A-6. Interaction test PT-6.

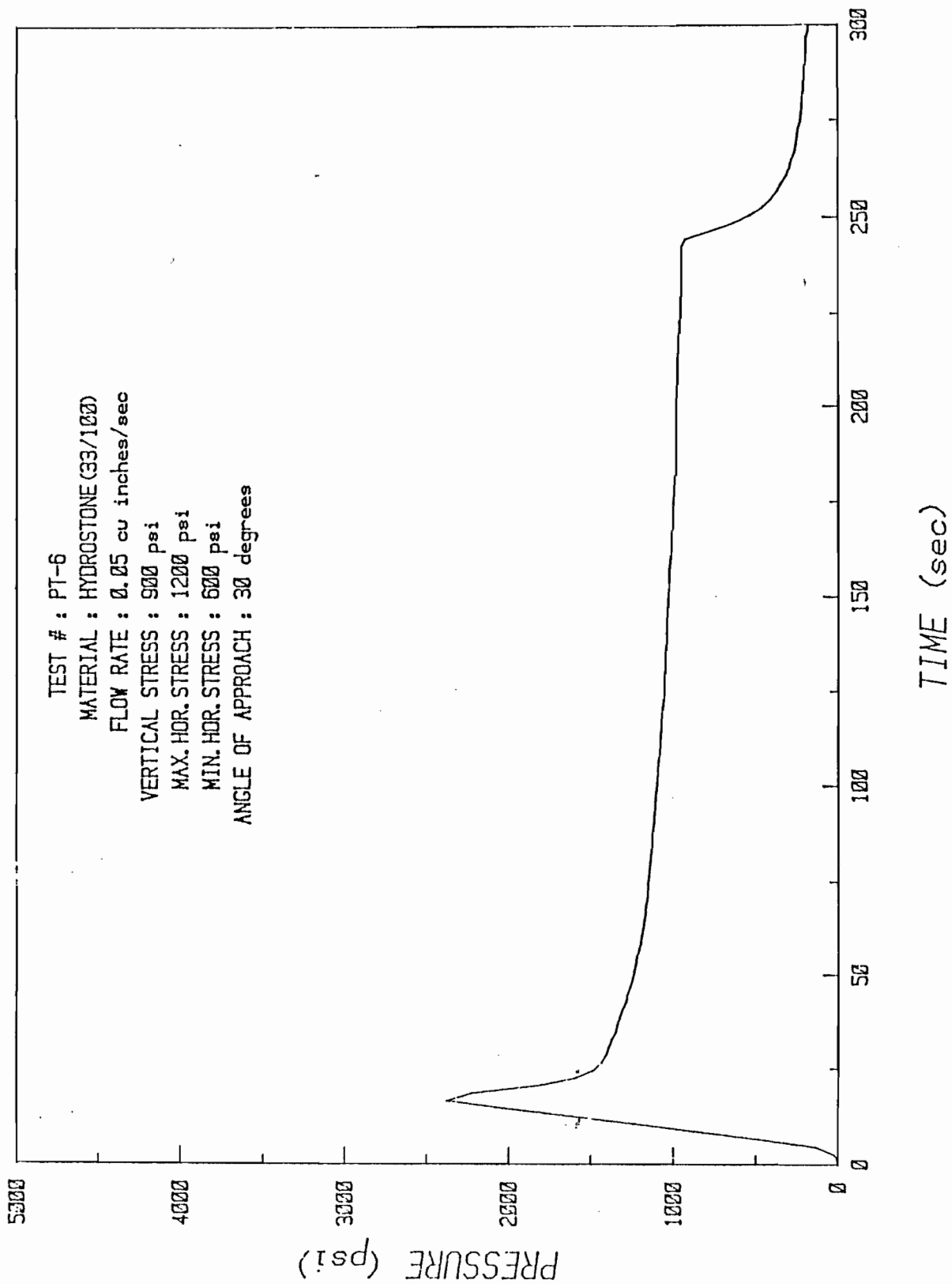


FIGURE A-7. Pressure time record for test PT-6.

TEST PT-7

TEST CONDITIONS

Maximum Horizontal Stress:	900 psi
Minimum Horizontal Stress:	600 psi
Vertical (Intermediate) Stress:	750 psi
Differential Stress:	300 psi
Angle of Approach:	60 degrees

RESULTS

The hydraulic fracture opened into pre-fractures with moderate flow into one and only slight flow into the other. Leakage extended 1.8 inches along one pre-fracture and 0.4 inches along the other. The actual distances between the borehole and a pre-fracture travelled by the hydraulic fracture are 2.7 inches and 2.8 inches.

COMMENTS

It was decided that the top surface of a block contained too many asperities to allow an even distribution of vertical stress. In order to provide a more regular top surface, cement was poured to approximately 1/4 inch. After testing, it was observed that a very small portion of cement had leaked into the pre-fractures away from the area of interaction. Clay was used in all successive trials to seal the trace of pre-fractures at the top surface. A "cement spacer" was utilized in all following trials. The conditions of this test were repeated in test PT-16.

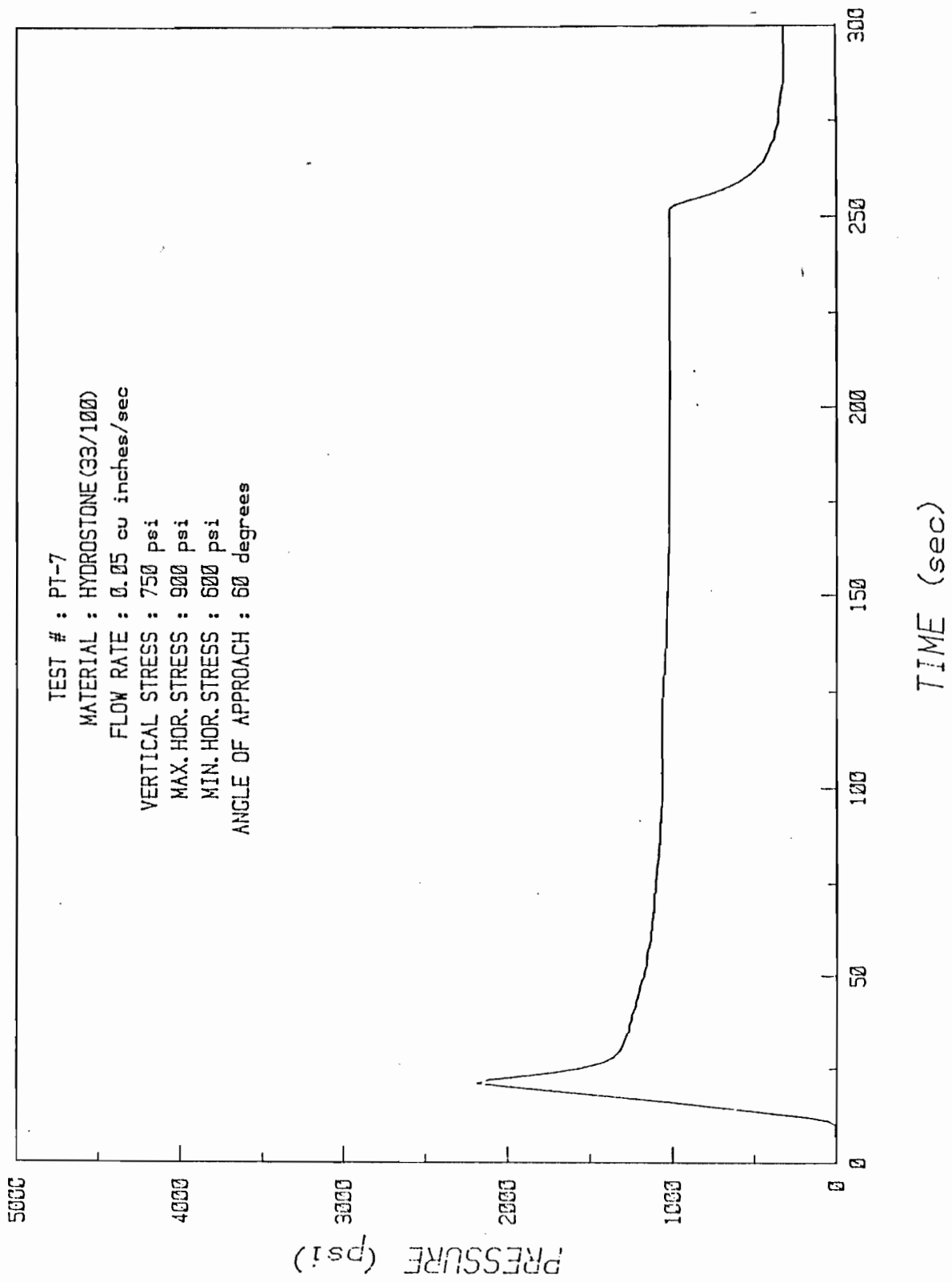


FIGURE A-8. Pressure time record for test PT-7.

## TEST PT-8

### TEST CONDITIONS

Maximum Horizontal Stress:	1500 psi
Minimum Horizontal Stress:	600 psi
Vertical (Intermediate) Stress:	1050 psi
Differential Stress:	900 psi
Angle of Approach:	90 degrees

### RESULTS

A very symmetrical hydraulic fracture outline was produced by this test. Crossing behavior is observed with wings extending beyond respective pre-fractures 2.0 inches and 2.1 inches. Leakage of fluid into pre-fractures was moderate, extending up to 1.3 inches.

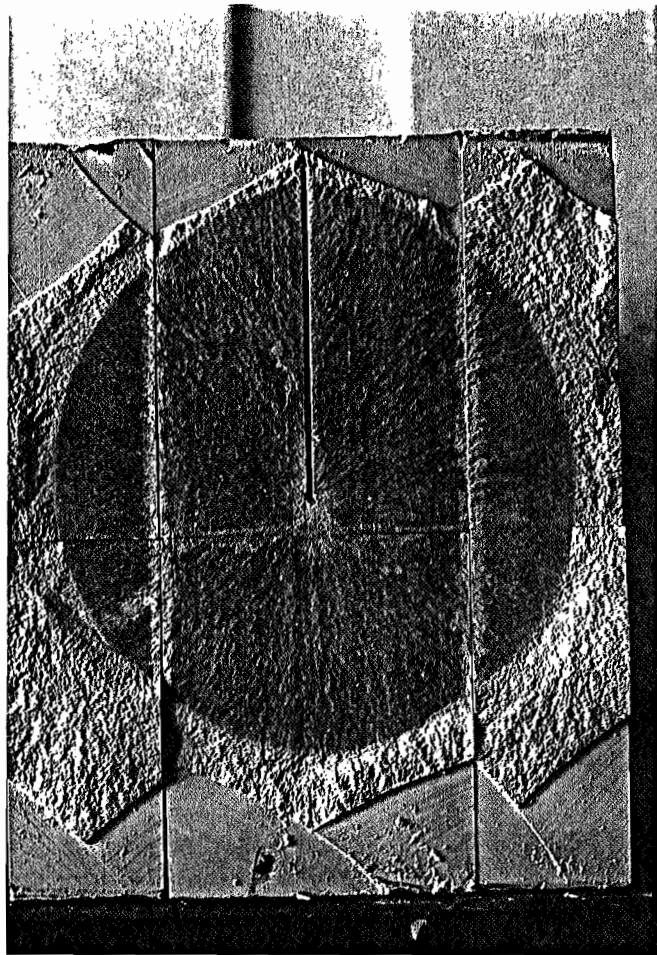
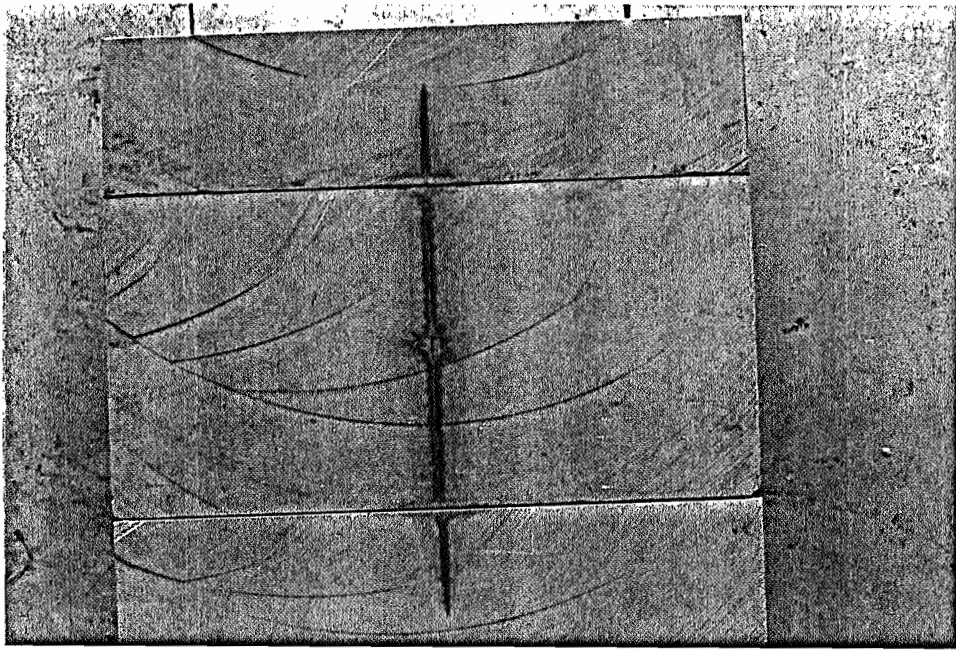


FIGURE A-9. Interaction test PT-8.

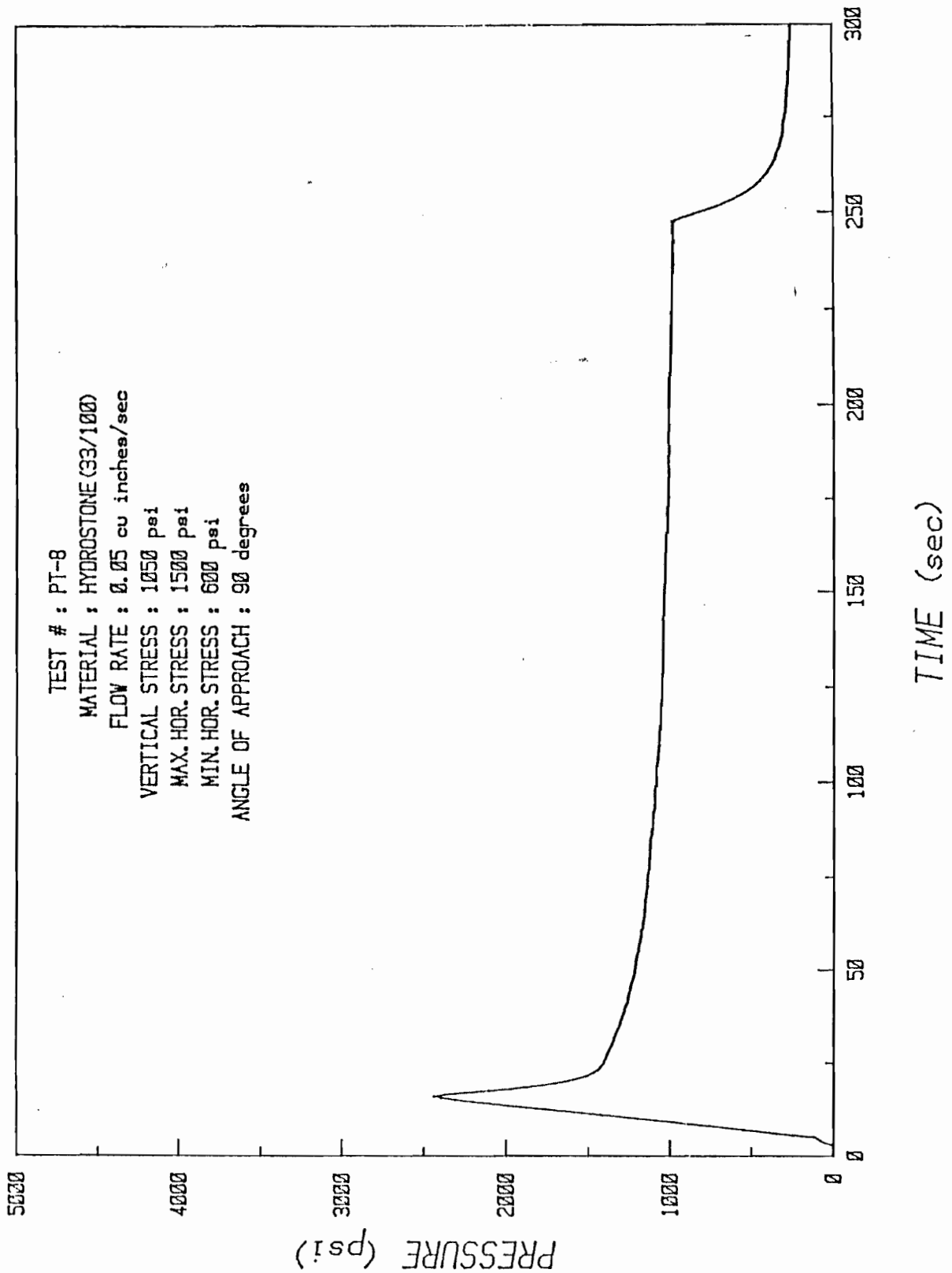


FIGURE A-10. Pressure time record for test PT-8.

TEST PT-9

TEST CONDITIONS

Maximum Horizontal Stress:	800 psi
Minimum Horizontal Stress:	600 psi
Vertical (Intermediate) Stress:	700 psi
Differential Stress:	200 psi
Angle of Approach:	90 degrees

RESULTS

This test created a highly asymmetrical hydraulic fracture outline with excessive leakage (3.8 inches) into one pre-fracture. The hydraulic fracture crossed one pre-fracture but did not extend far enough in the opposite direction to interact with the opposing pre-fracture. Wings extended 2.1 inches beyond the borehole and 2.8 inches beyond the pre-fracture respectively. An additional crossing fracture offset 0.8 inches from the major wing and extending 1.6 inches from the pre-fracture is also observed. Each crossing fracture surface shows abnormal contour beyond the pre-fracture. Actual distances from the borehole to pre-fractures are 2.9 inches to the uncrossed pre-fracture and 3.0 inches to the pre-fracture where crossing occurred.

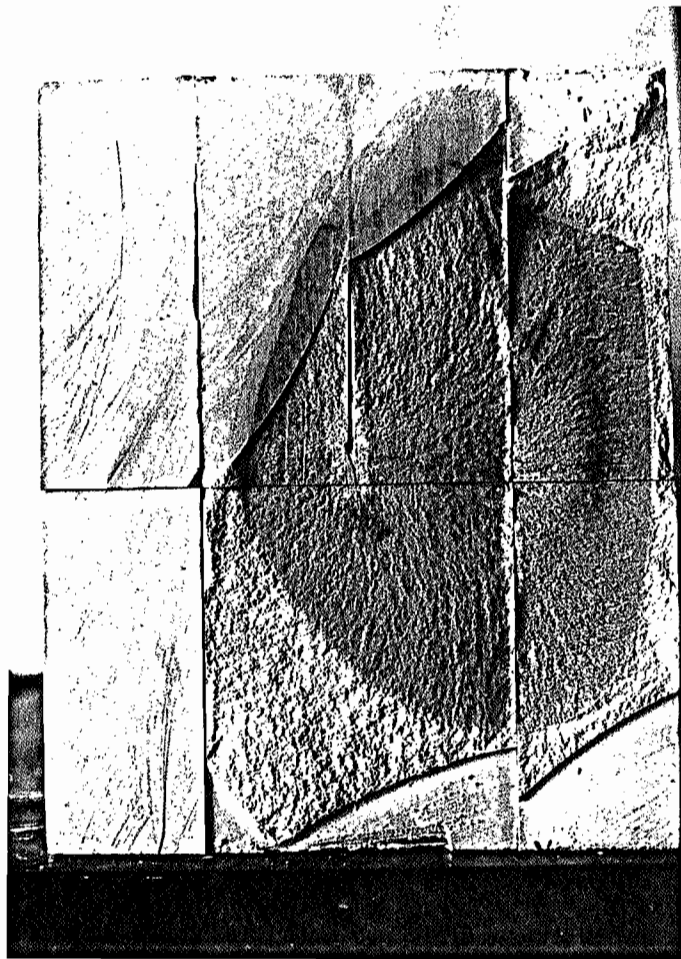
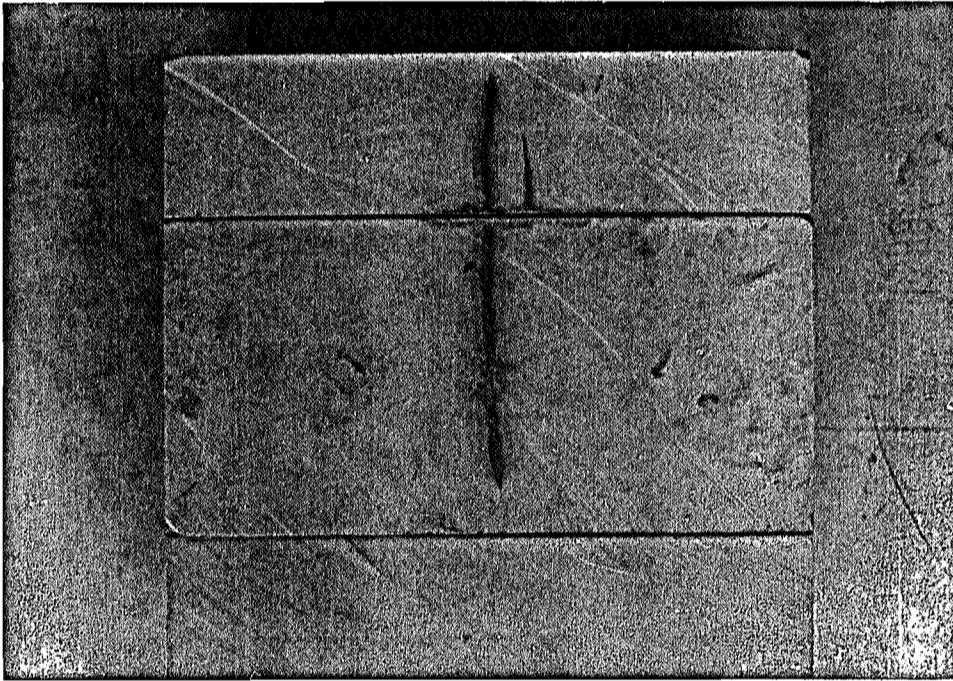


FIGURE A-11. Interaction test PT-9.

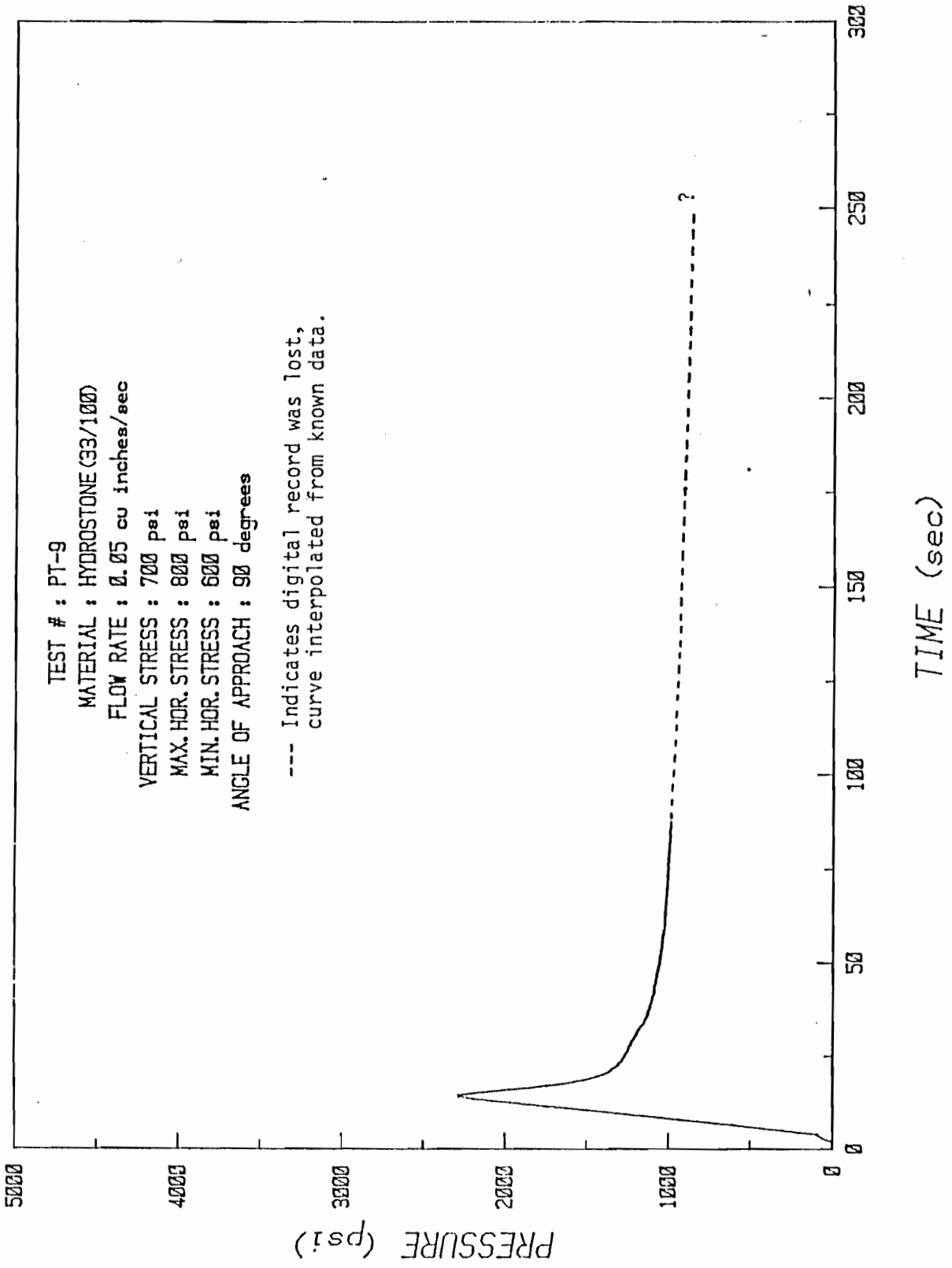


FIGURE A-12. Pressure time record for test PT-9.

## TEST PT-10

### TEST CONDITIONS

Maximum Horizontal Stress:	2100 psi
Minimum Horizontal Stress:	600 psi
Vertical (Intermediate) Stress:	1350 psi
Differential Stress:	1500 psi
Angle of Approach:	30 degrees

### RESULTS

The hydraulic fracture in this test opened into pre-fractures with fluid extending 1.0 inches into one pre-fracture and 1.5 inches into the other. The actual distance between the borehole and pre-fractures are 3.1 inches and 2.5 inches, respectively.

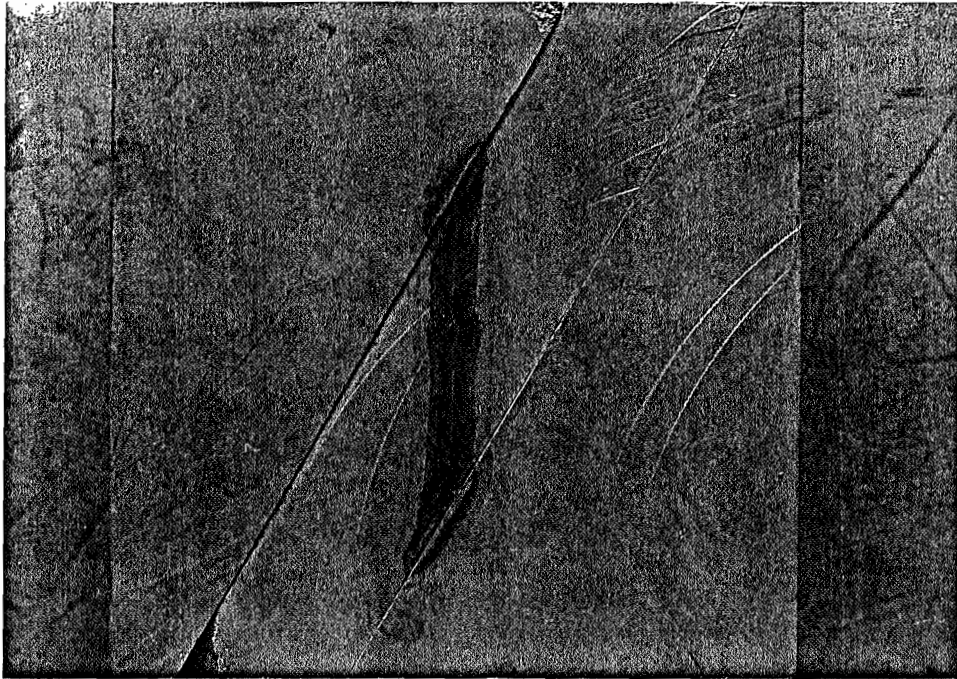


FIGURE A-13. Interaction test PT-10.

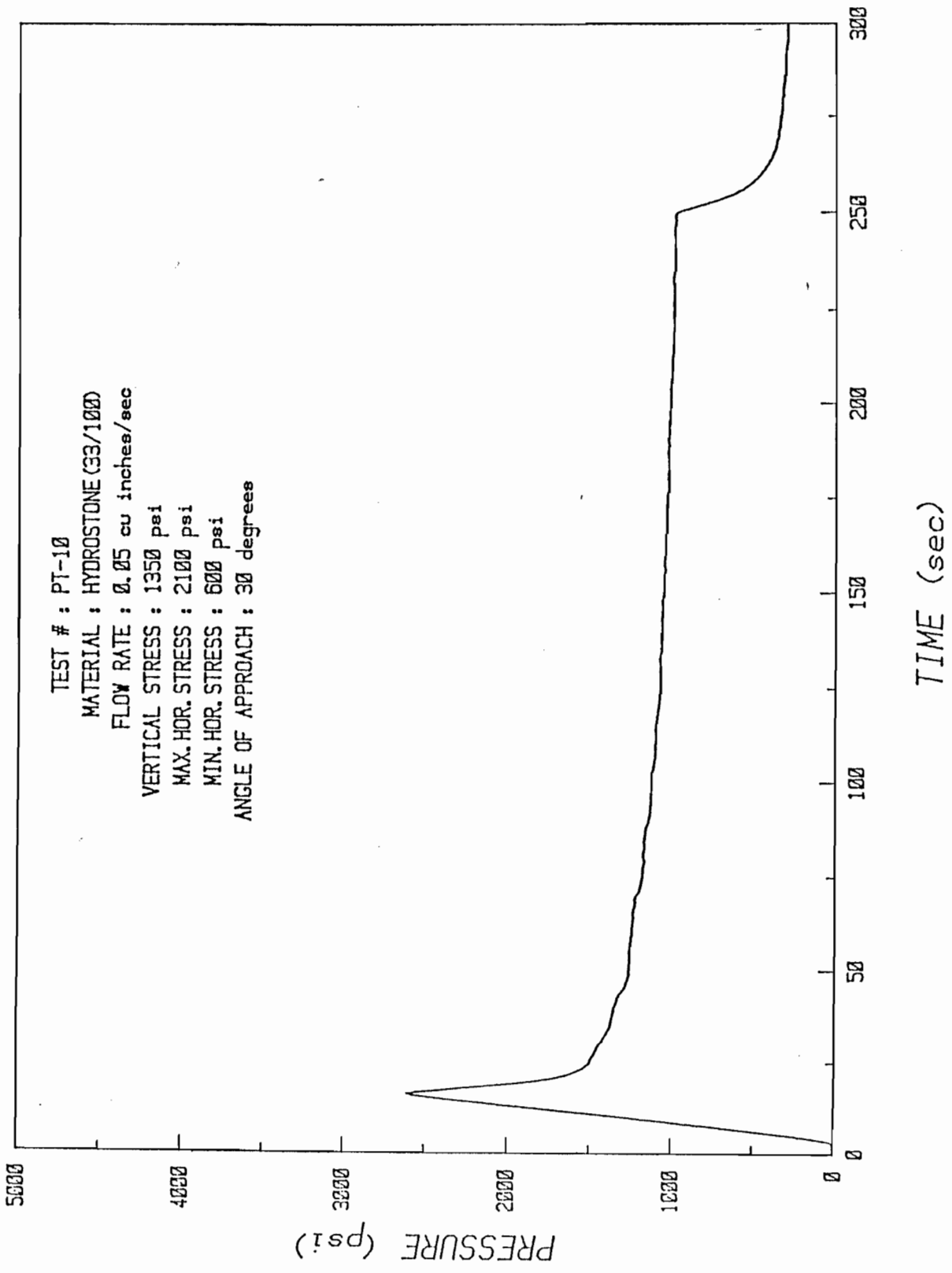


FIGURE A-14. Pressure time record for test PT-10.

## TEST PT-11

### TEST CONDITIONS

Maximum Horizontal Stress:	1800 psi
Minimum Horizontal Stress:	600 psi
Vertical (Intermediate) Stress:	1200 psi
Differential Stress:	1200 psi
Angle of Approach:	60 degrees

### RESULTS

A slightly asymmetrical hydraulic fracture surface was created in this test with moderate to high leakage into pre-fractures. Crossing behavior occurred, with wings extending beyond pre-fractures 1.0 inches and 1.9 inches. The hydraulic fracture at one interaction was offset 0.6 inches before extension continued. Fluid penetrated one pre-fracture 1.1 inch and the other 4.7 inches.

### COMMENTS

One pre-fracture contained an unusually rough area on each surface. This surface roughness was formed during sample preparation when two sections of the block fused together while curing. Fracture offset and excessive leakage into the pre-fracture were results of this surface irregularity. Since co-linear crossing is observed on the smooth pre-fracture, it was decided that duplicating the test would be unnecessary.

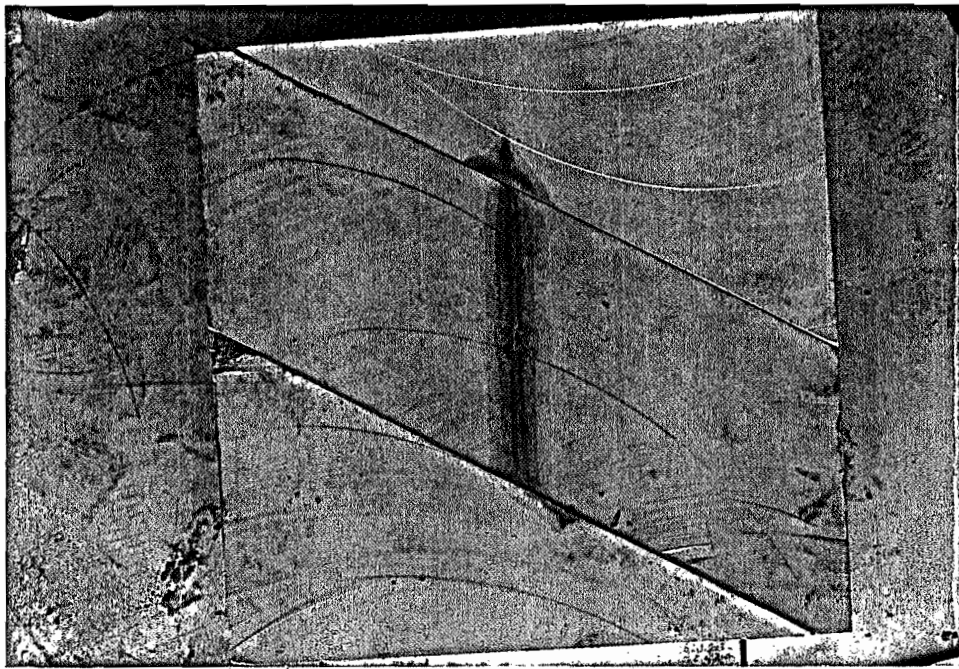


FIGURE A-15. Interaction test PT-11.

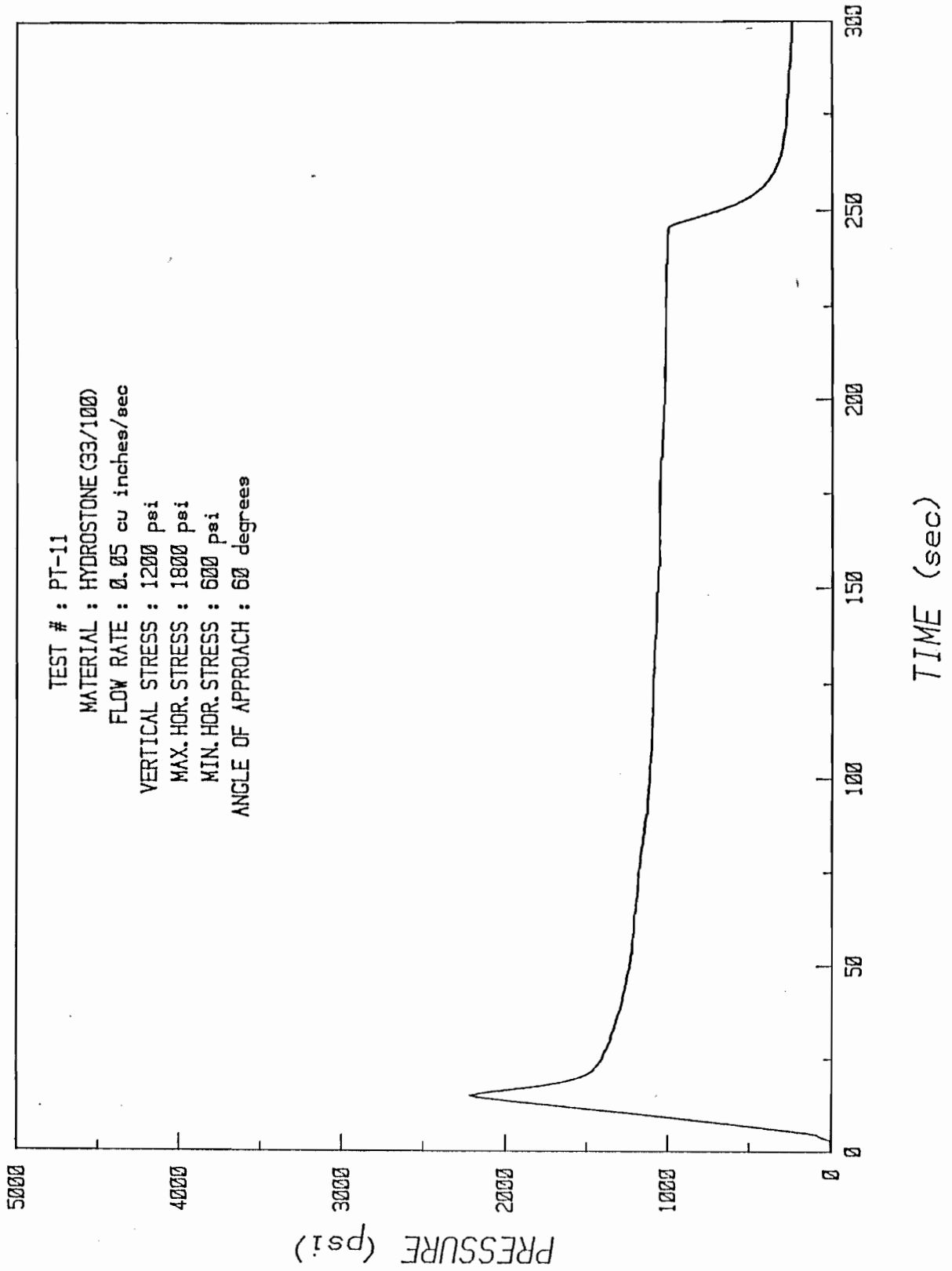


FIGURE A-16. Pressure time record for test PT-11.

## TEST PT-12

### TEST CONDITIONS

Maximum Horizontal Stress:	800 psi
Minimum Horizontal Stress:	600 psi
Vertical (Intermediate) Stress:	200 psi
Differential Stress:	200 psi
Angle of Approach:	90 degrees

### RESULTS

The hydraulic fracture produced in this test is slightly asymmetrical with a moderate amount of leakage (1.6 inches) into pre-fractures. Crossing behavior occurred with wings extending beyond pre-fractures 0.9 inches and 2.5 inches. The distance from the borehole to a pre-fracture was 3.0 inches in both directions.

### COMMENTS

During application of confining pressure, a slow leak developed in one flatjack. The test was run to completion with less than 20 psi pressure loss.

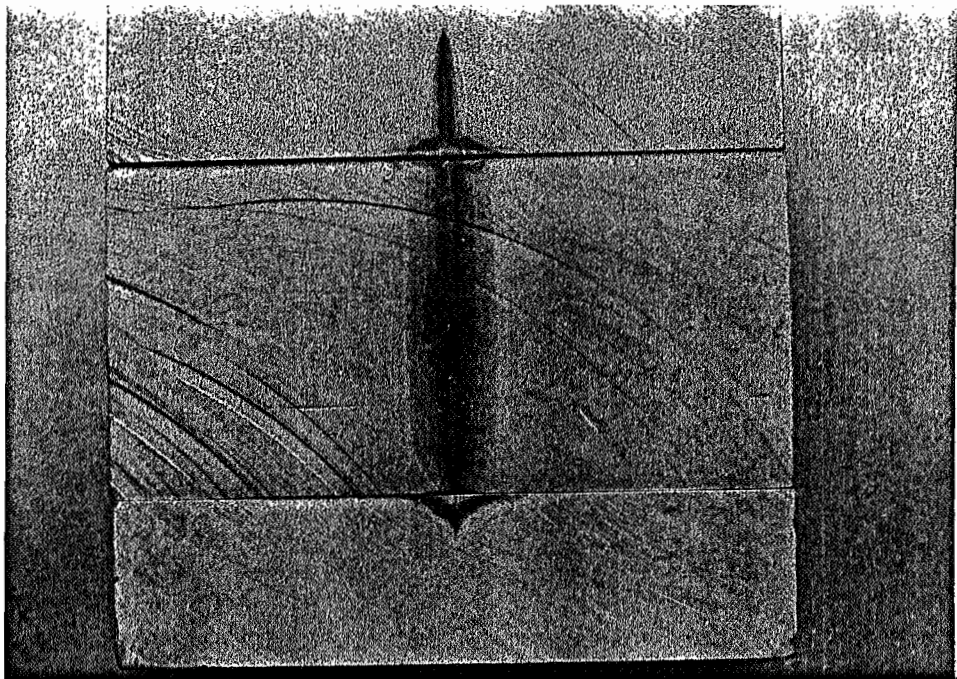


FIGURE A-17. Interaction test PT-12.

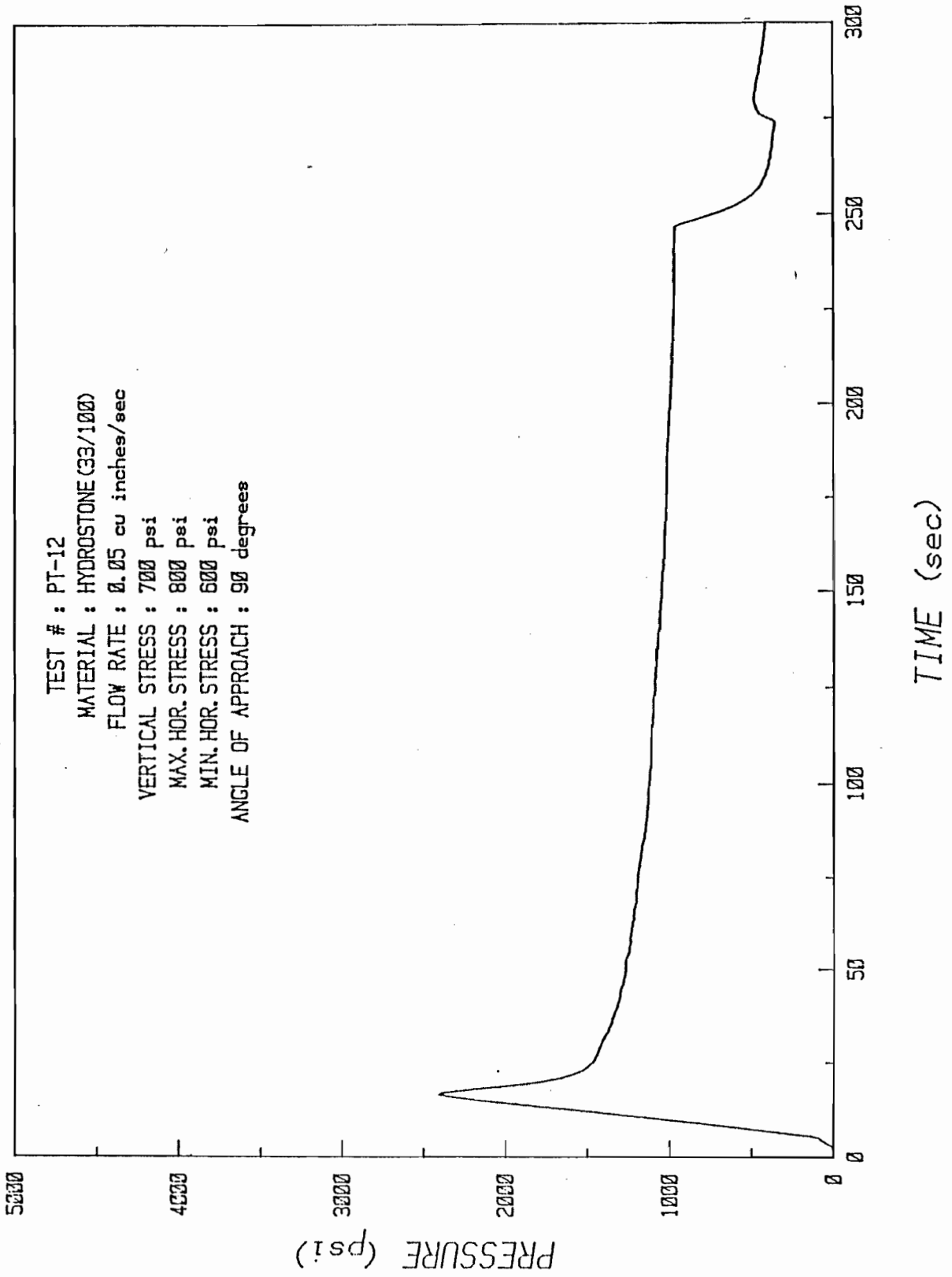


FIGURE A-18. Pressure time record for test PT-12.

## TEST PT-13

### TEST CONDITIONS

Maximum Horizontal Stress:	700 psi
Minimum Horizontal Stress:	600 psi
Vertical (Intermediate) Stress:	650 psi
Differential Stress:	100 psi
Angle of Approach:	90 degrees

### RESULTS

An asymmetrical fracture outline was produced in this test with moderate leakage (1.1 inch) into pre-fractures. Hydraulic fracture wings crossed pre-existing fractures, extending to the outside of the block on one side and 0.8 inches on the other side. The actual distances between the borehole and pre-fracture are 3.2 inches and 2.9 inches.

### COMMENTS

During assembly of the block for testing, it was noticed that the wellbore tube was loose in the borehole. An O-ring (Parker size 003) was forced onto the tube and placed on the borehole opening. Application of vertical pressure to the cement spacer sealed the borehole from fluid leakage.

It may be that the lack of lubrication on the contact between hydrostone and flatjack was the cause of abnormal hydraulic fracture extension in one direction. Excessive traction on a block surface may reduce fracture toughness significantly near the block surface.

A repaired flatjack was used in this trial for the first time. It appears that the original molds are rather weak and that flatjack repair is fast, inexpensive, and reliable.

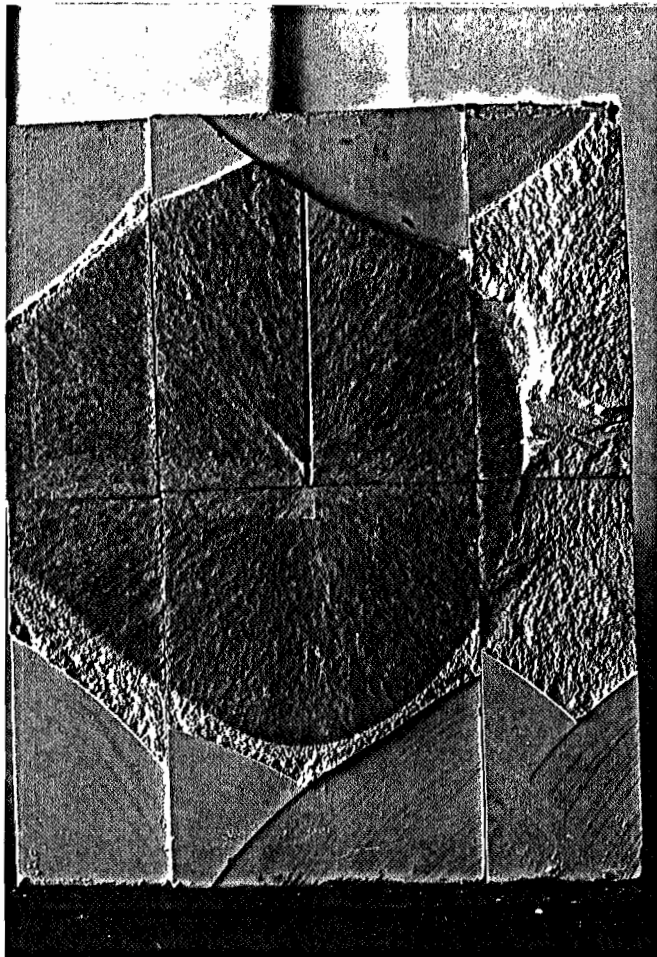
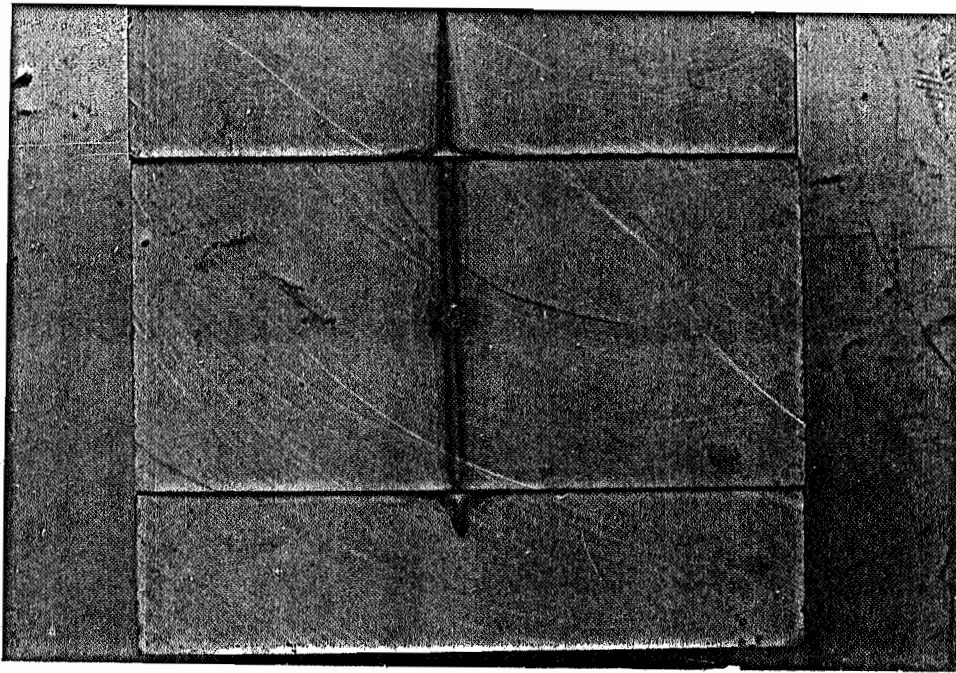


FIGURE A-19. Interaction test PT-13.

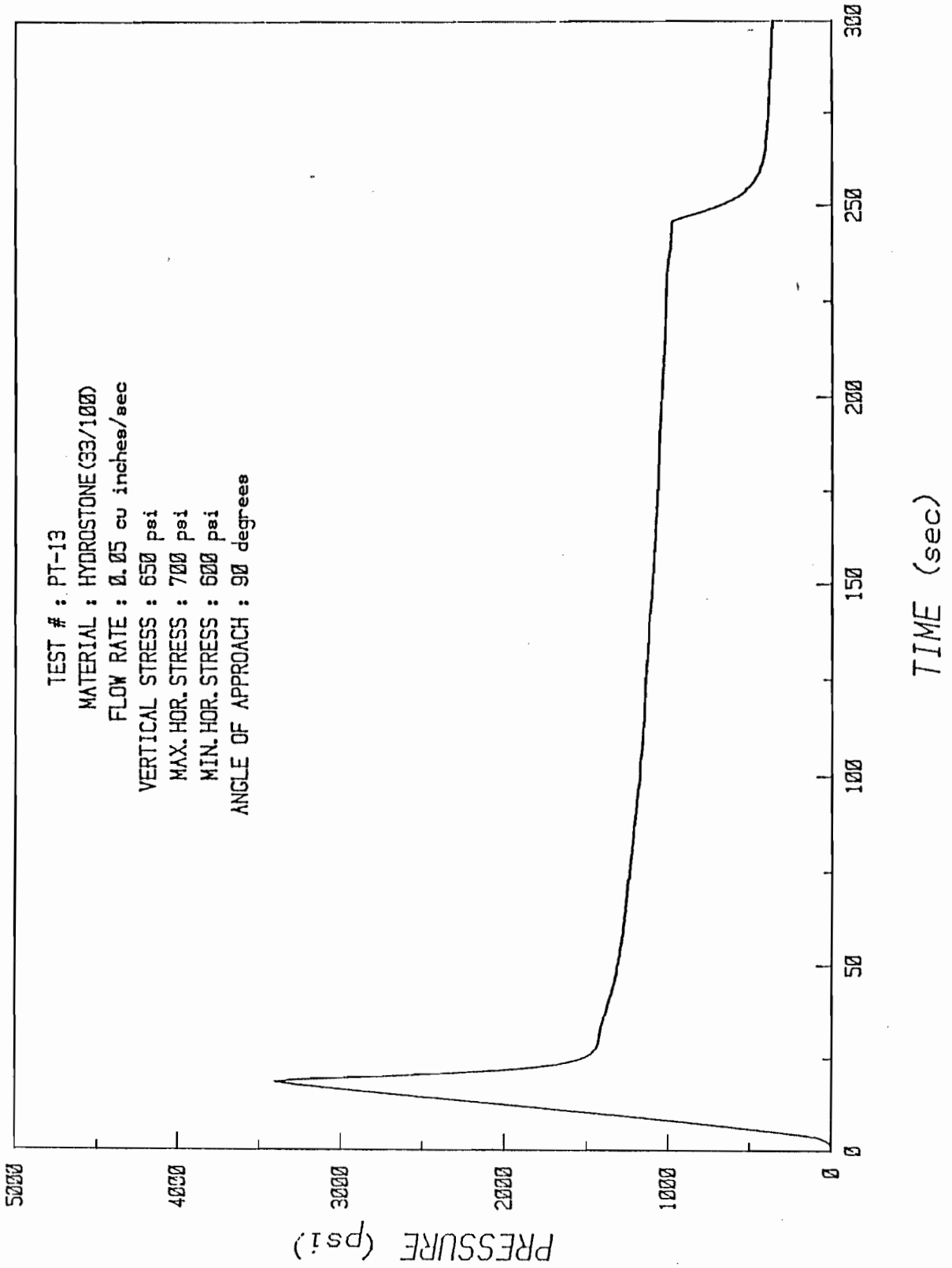


FIGURE A-20. Pressure time record for test PT-13.

TEST PT-14

TEST CONDITIONS

Maximum Horizontal Stress:	1500 psi
Minimum Horizontal Stress:	600 psi
Vertical (Intermediate) Stress:	1050 psi
Differential Stress:	900 psi
Angle of Approach:	60 degrees

RESULTS

The hydraulic fracture outline produced in this test is slightly asymmetrical with moderate leakage (1.5 inches) into pre-fractures. Fracture wings crossed both pre-fractures, extending 1.5 inches and 2.8 inches beyond pre-existing fractures. The actual distances between the borehole and pre-fractures are 3.0 inches and 2.9 inches.

COMMENTS

The block experienced two cycles of compression due to rupture of one flatjack during the first trial.

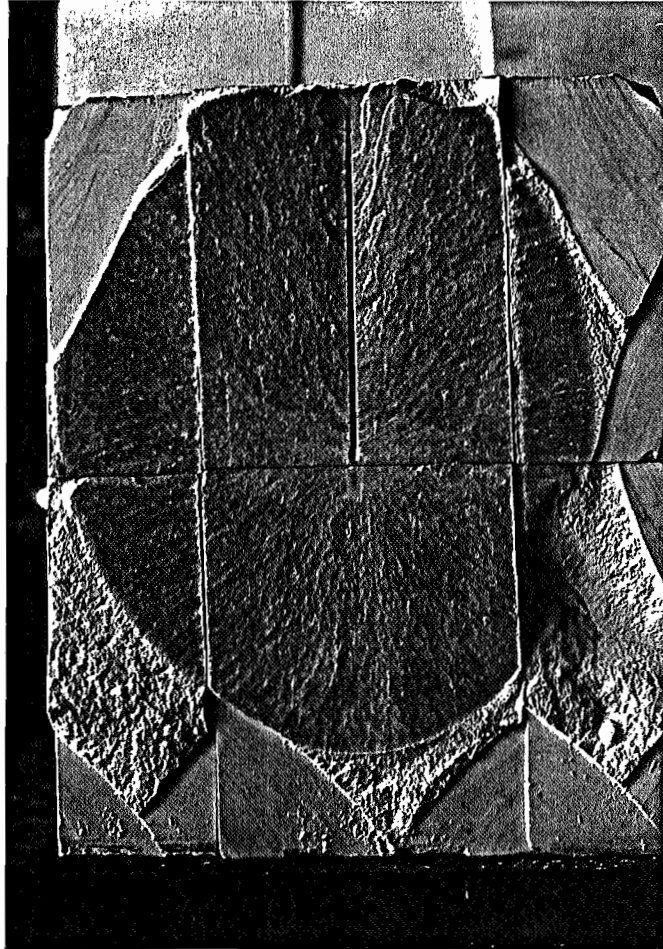
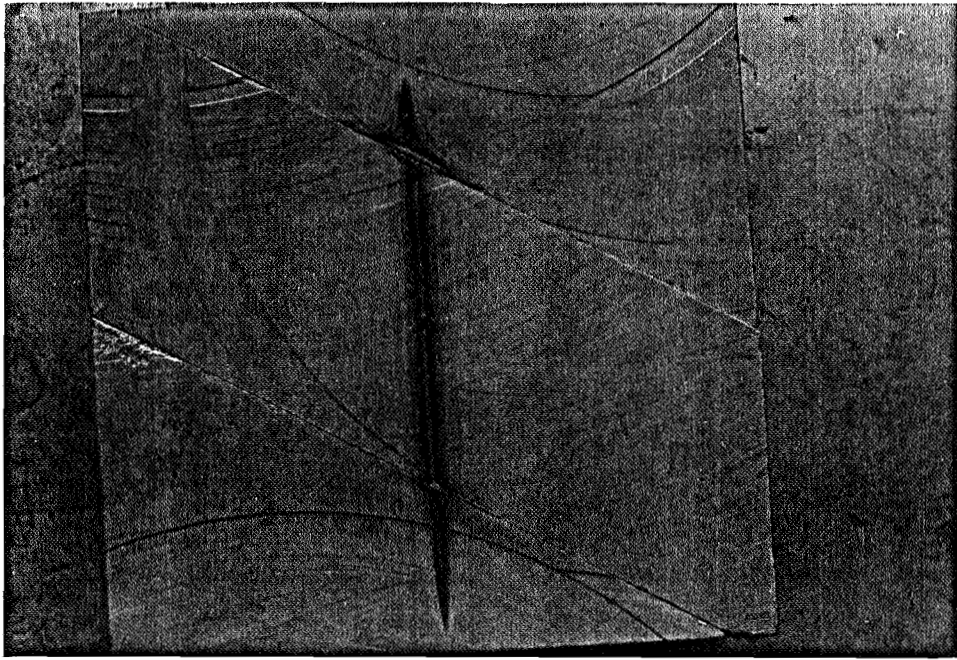


FIGURE A-21. Interaction test PT-14.

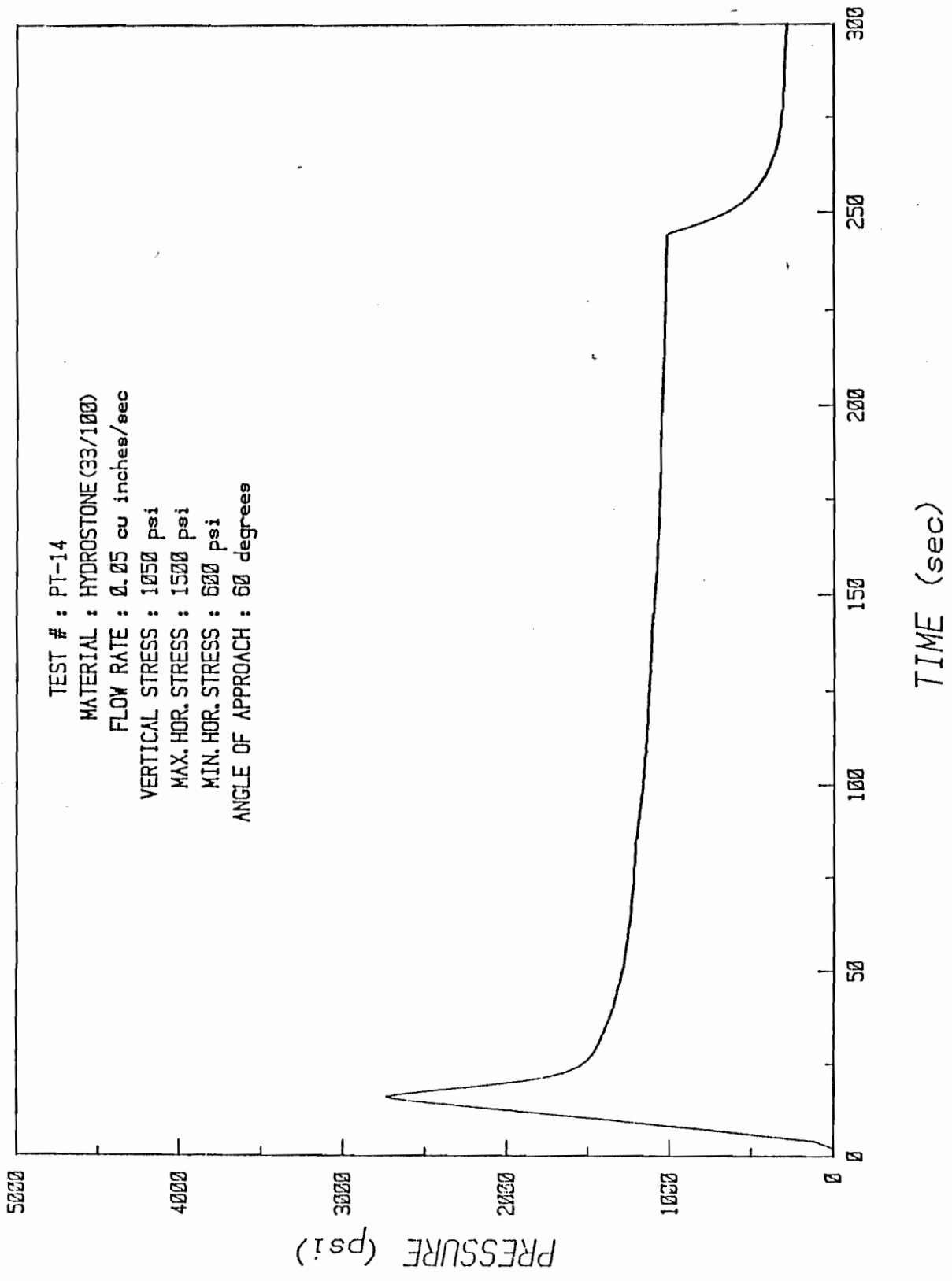


FIGURE A-22. Pressure time record for test PT-14.

TEST PT-15

TEST CONDITIONS

Maximum Horizontal Stress:	1200 psi
Minimum Horizontal Stress:	600 psi
Vertical (Intermediate) Stress:	900 psi
Differential Stress:	600 psi
Angle of Approach:	60 degrees

RESULTS

A symmetrical hydraulic fracture outline was created in this test with moderate leakage (1.5 inches) into pre-fractures. Crossing behavior is observed with one wing offset 0.2 inches along pre-fracturing and the other wing offset from 0 to 0.3 inches. Wings extended beyond pre-fractures 0.7 inches on one side and 0.9 inches on the other.

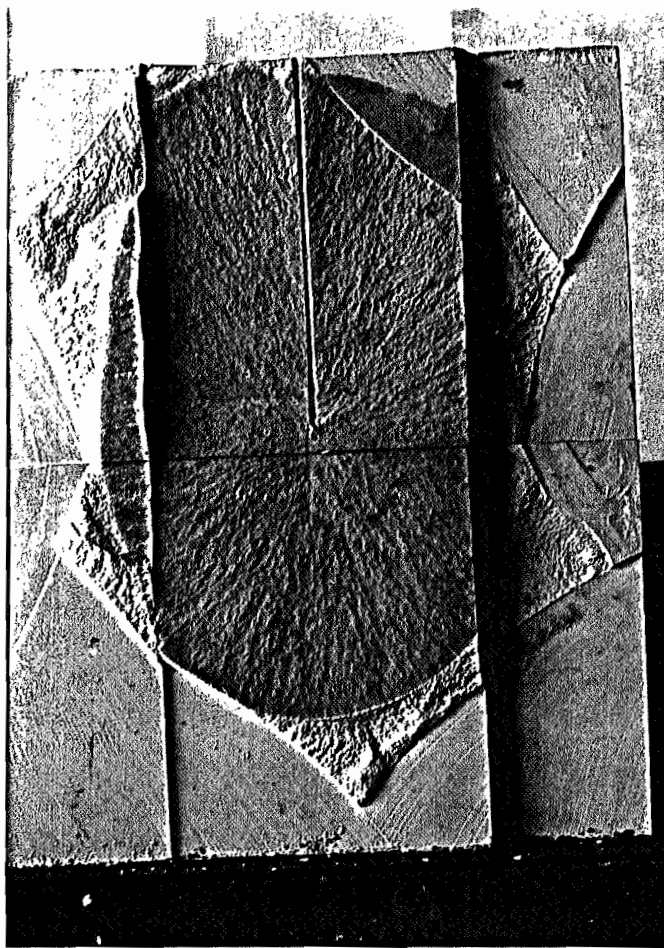
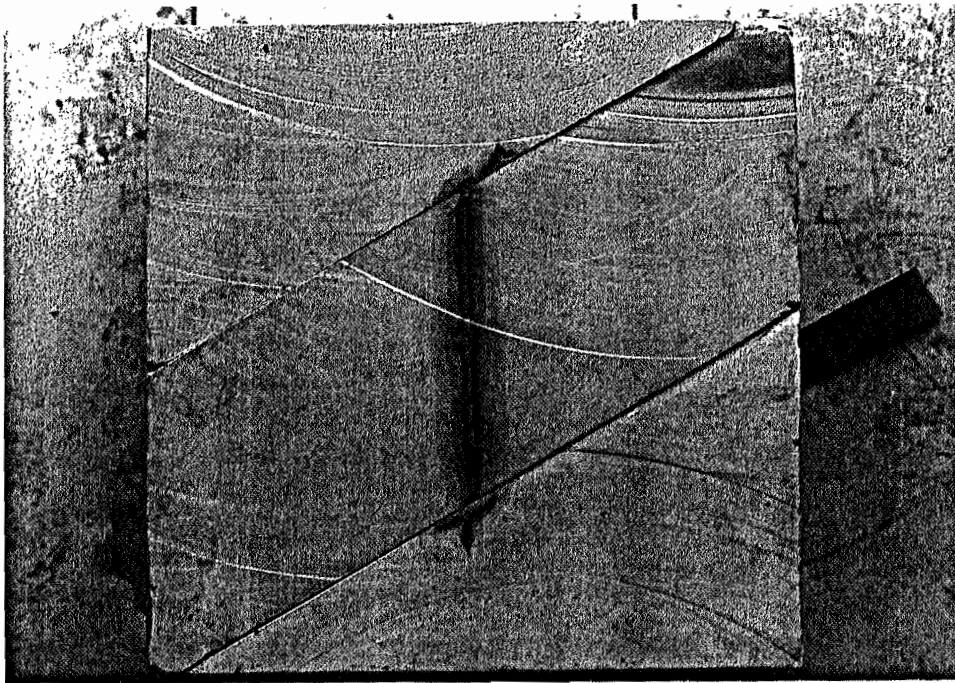


FIGURE A-23. Interaction test PT-15.

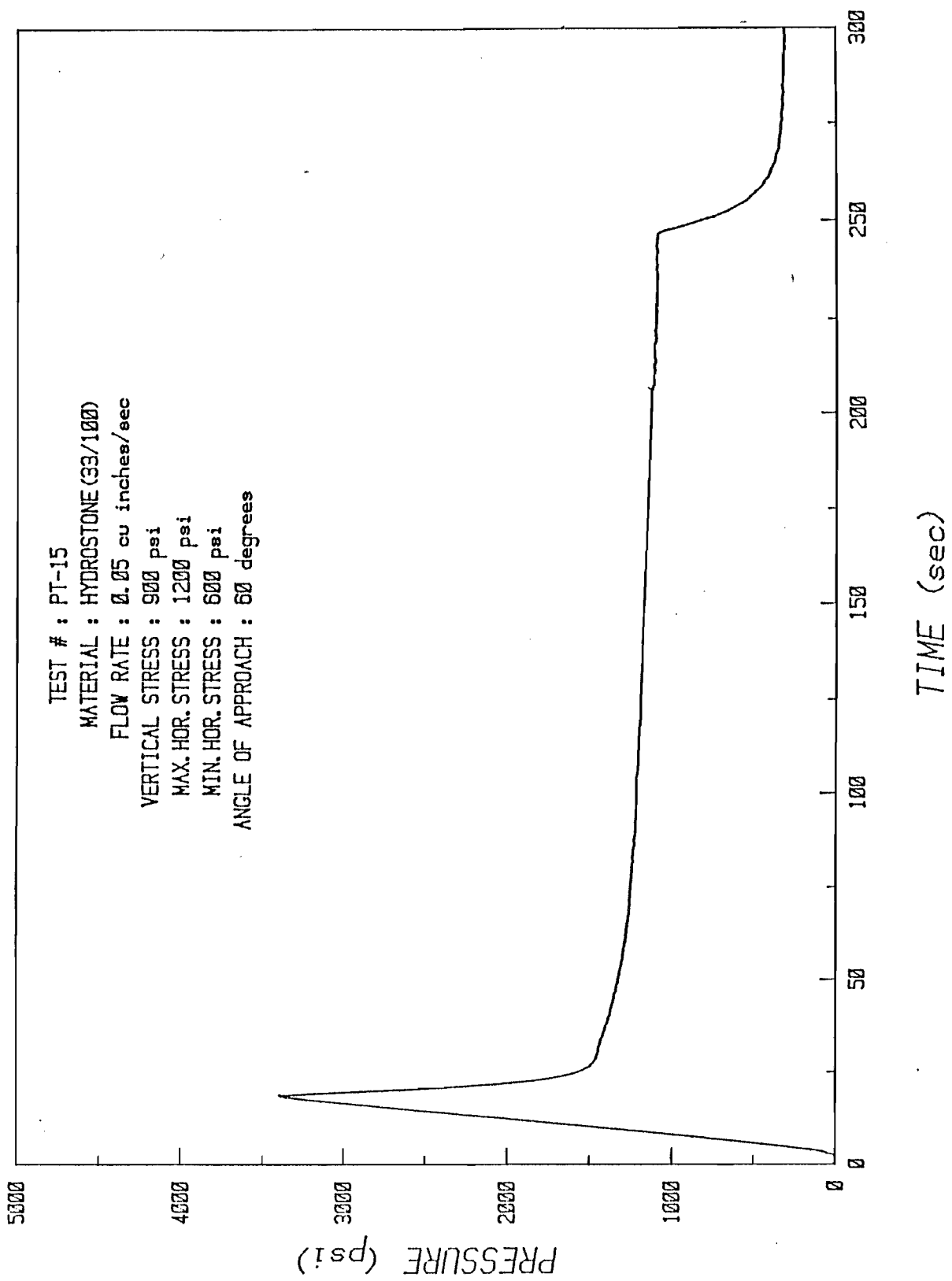


FIGURE A-24. Pressure time record for test PT-15.

TEST PT-16

TEST CONDITIONS

Maximum Horizontal Stress:	900 psi
Minimum Horizontal Stress:	600 psi
Vertical (Intermediate) Stress:	750 psi
Differential Stress:	300 psi
Angle of Approach:	60 degrees

RESULTS

Opening behavior occurred in the test with slight leakage into one pre-fracture and moderate leakage into the other. Fluid penetrated pre-fractures 0.7 inches and 2.1 inches. The actual distance between the borehole and a pre-fracture is 2.9 inches in each direction. This test repeats the conditions under which PT-7 was tested.

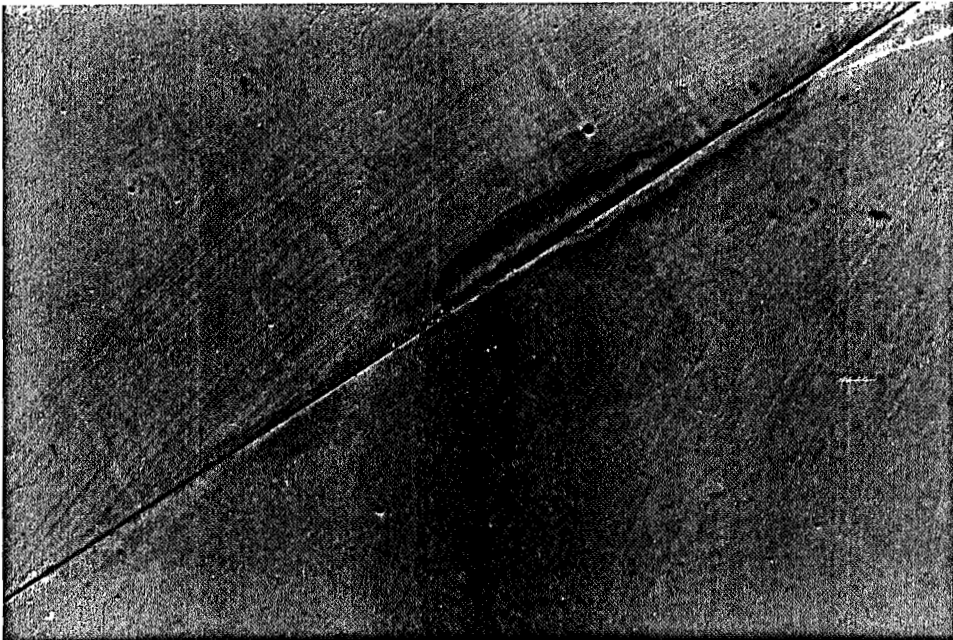
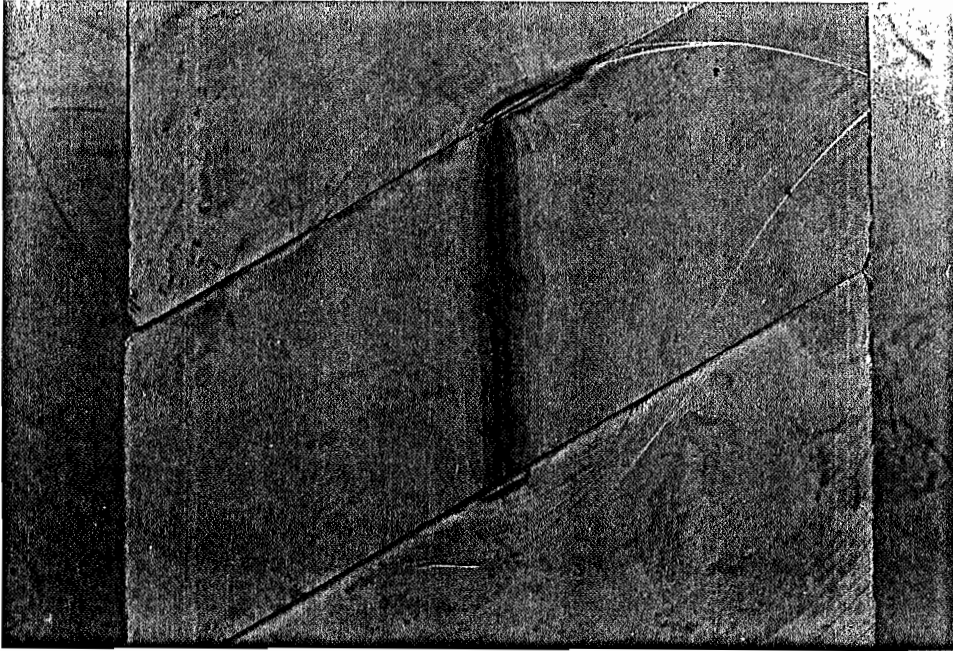


FIGURE A-25. Interaction test PT-16.

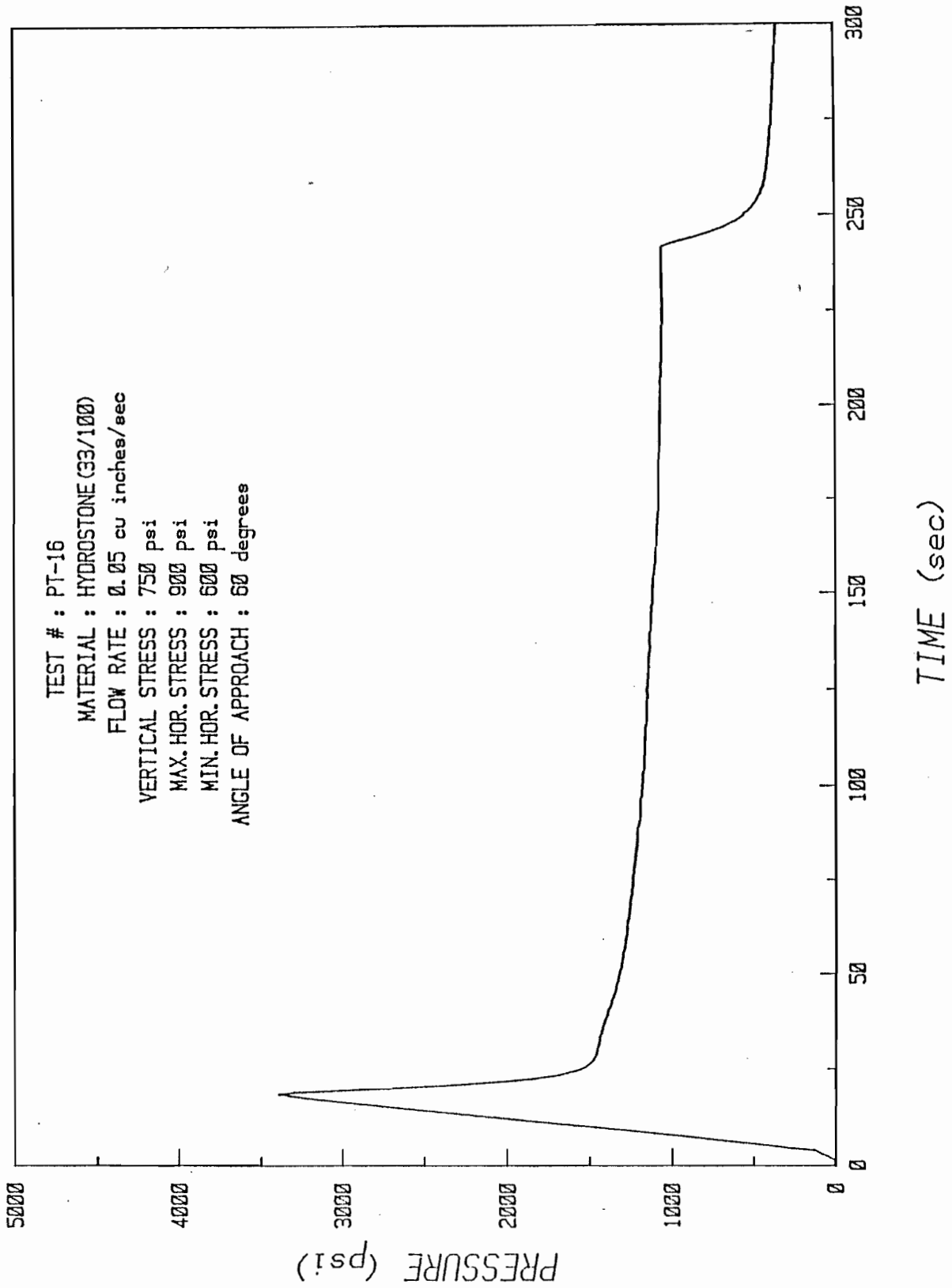


FIGURE A-26. Pressure time record for test PT-16.

## TEST PT-17

### TEST CONDITIONS

Maximum Horizontal Stress:	2200 psi
Minimum Horizontal Stress:	600 psi
Vertical (Intermediate) Stress:	1400 psi
Differential Stress:	1600 psi
Angle of Approach:	30 degrees

### RESULTS

Opening behavior occurred in this test with slight leakage into one pre-fracture and moderate leakage into the other. Fluid penetration respective pre-fractures 0.8 inches and 1.5 inches. The actual distance between the borehole and each pre-fracture is 2.9 inches in both directions.

### COMMENTS

This block experienced two cycles of compression due to failure of a hydraulic connection on the first trial.

In order to achieve 1600 psi differential stress, it was necessary to exceed 2200 psi maximum horizontal stress by as much as 1600 psi. Stress was transmitted through pre-existing fractures, causing slippage along these planes. Since an unstable situation existed under these conditions, no other attempts were made to test a 30-degree interaction above 1500 psi differential stress.

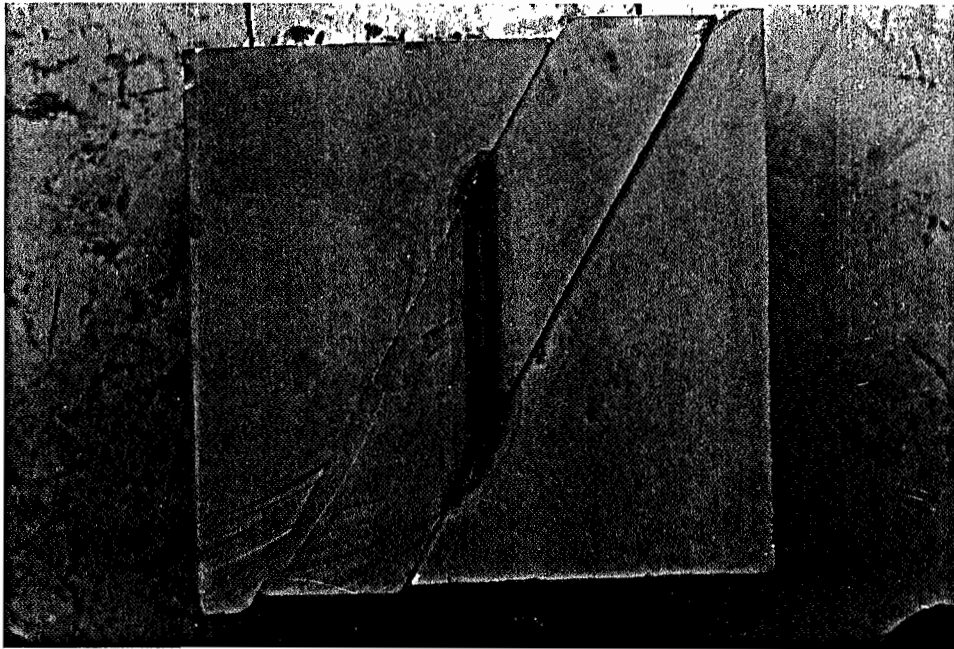


FIGURE A-27. Interaction test PT-17.

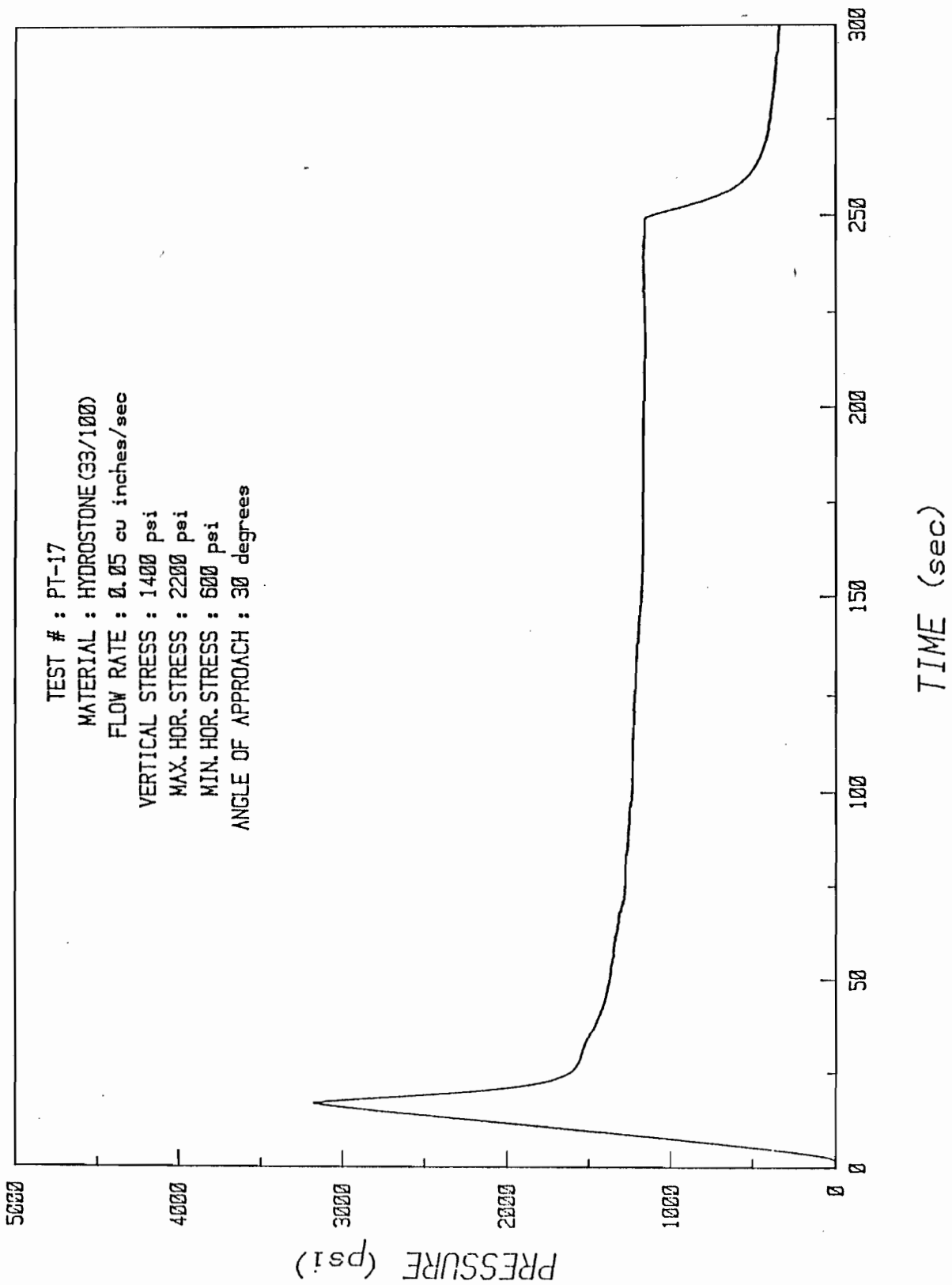


FIGURE A-28. Pressure time record for test PT-17.

TEST PT-18

TEST CONDITIONS

Maximum Horizontal Stress:	1200 psi
Minimum Horizontal Stress:	600 psi
Vertical (Intermediate) Stress:	900 psi
Differential Stress:	600 psi

RESULTS

The hydraulic fracture produced in this solid block test extended beyond the 1-inch open hole section of the central wellbore 2 1/8-inches in both directions. The cycle of pressurization continued to a time just after initial breakdown.

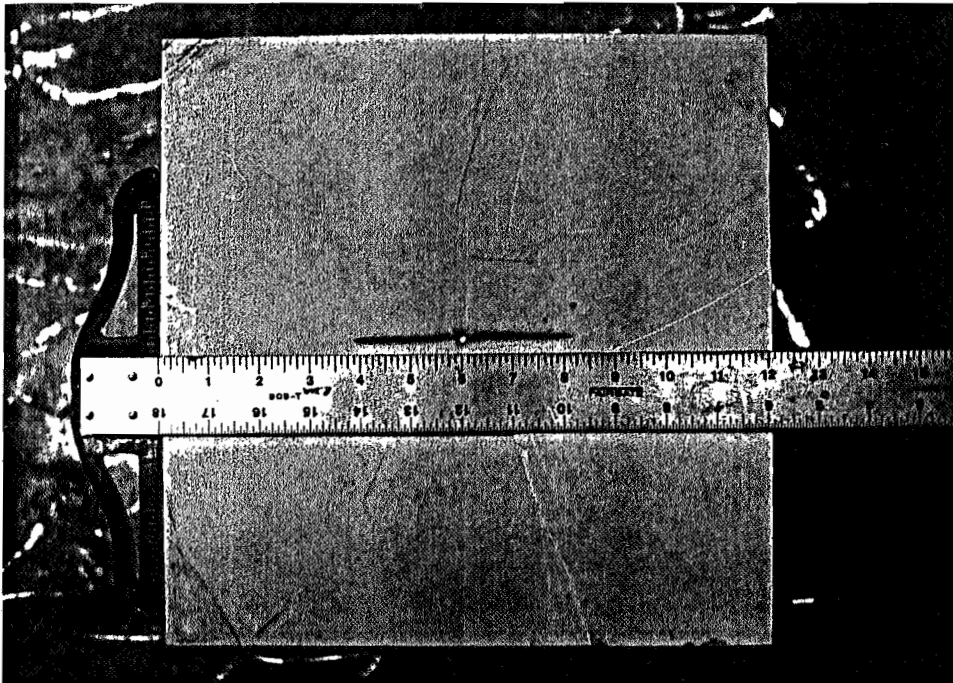


FIGURE A-29. Solid block test PT-18 showing extension of hydraulic fracture from an open hole after initial breakdown.

TEST PT-19

TEST CONDITIONS

Maximum Horizontal Stress:	1200 psi
Minimum Horizontal Stress:	600 psi
Vertical (Intermediate) Stress:	900 psi
Differential Stress:	600 psi

RESULTS

The hydraulic fracture produced in this solid block test extended beyond the central 1-inch fracture initiation device 2 1/8-inches in one direction and 2 1/4-inches in the other. The cycle of pressurization continued to a time just after initial breakdown.

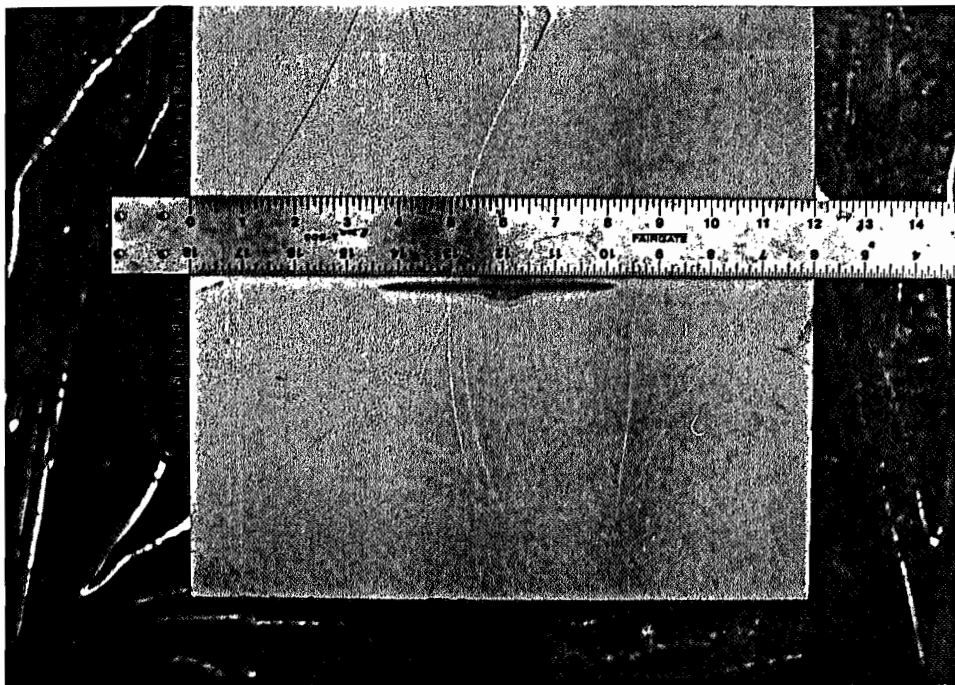


FIGURE A-30. Solid block test PT-19 showing extension of hydraulic fracture from a paddle after initial breakdown.

APPENDIX B  
RESULTS OF  
DYNAMIC FRACTURE TESTS

SOLID BLOCK TESTS

TABLE B-1.

## BLOCK TESTS

TEST	STRESS (MIN,MAX,VERT) (PSI)	HOLE DIAM (IN)	CHARGE TYPE SIZE (GM)		INITIATOR	FRACTURES/COMMENTS
DB-1	600,1200,900	0.25	4F	1.70	1xRP-2 EBW	Two (90:1 in, 270:1 in)
DB-2	600,900,750	0.375	4F	1.70	1xRP-2 EBW	One (80:3/8 in)/ double hole
DB-3	600,900,750	0.375	4F	2.50	1xRP-2 EBW	Two (90:2.5 in, 270:2 in)
DB-4	600,900,750	0.375	RDX 4F	1.07 0.25	1xRP-83 EBW	Two (90:1.5 in, 270:1 in) Curved fractures
DB-5	600,900,750	0.375	RDX 4F	2.14 0.25	2xRP-83 EBW	Five (0:1 in, 130:7 in, 200:1 in, 250:1 in, 310:3.25 in)/ Multiple at the hole
DB-6	600,900,750	0.375	RDX 4F	2.14 0.25	2xRP-83 EBW	Two (-10:0.75 in, 170:3.75 in)/Multiple at the hole
DB-7	600,1200,750	0.375	RDX 4F	2.14 0.25	2xRP-83 EBW	Two (80:2.25 in, 180:2.25 in)

Note: Stresses are principal with minimum and maximum perpendicular to hole.

Fractures given as (Orientation: Length, .....). Orientation is angle of trace to minimum principal stress

TEST DB-1

TEST CONDITIONS

Maximum Horizontal Stress: 1200 psi  
Minimum Horizontal Stress: 600 psi  
Vertical (Intermediate) Stress: 900 psi

Differential Stress: 600 psi  
Stress Ratio: 2:1

Hole Size: 1/4 inch  
Charge Configuration: 1.7 gm 4F black powder charge (4 inch length) initiated with single EBW detonator.

RESULTS

Two fractures developed perpendicular to the minimum principal stress. Both wings were about one inch long.

COMMENTS

This charge had given three inch multiple fractures in the unstressed pipe tests.

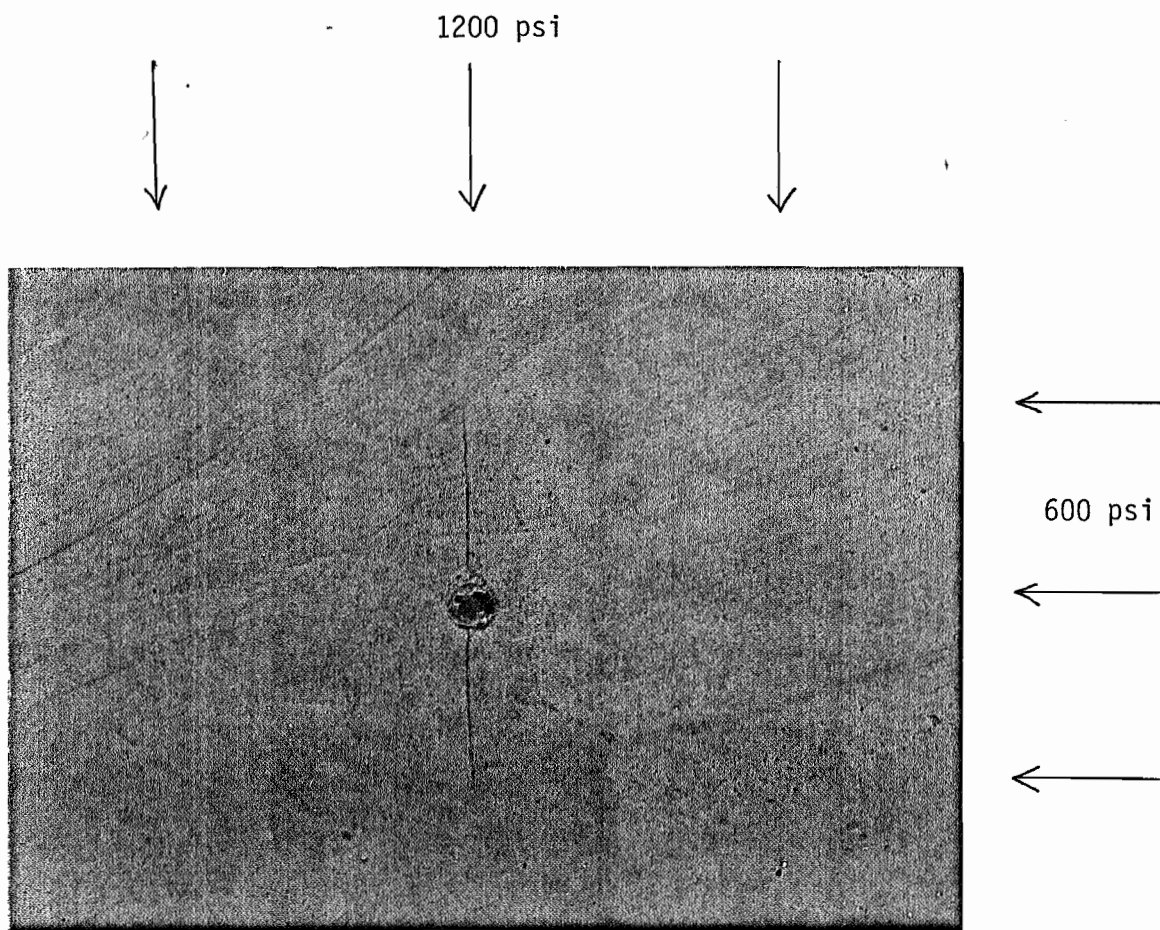


FIGURE B-1. Test DB-1.

TEST DB-2

TEST CONDITIONS

Maximum Horizontal Stress: 900 psi  
Minimum Horizontal Stress: 600 psi  
Vertical (Intermediate) Stress: 750 psi

Differential Stress: 300 psi  
Stress Ratio: 1.5:1

Hole Size: 3/8 inch  
Charge Configuration: 1.7 gm 4F black powder (1.125 in length)  
with single EBW initiation.

RESULTS

A single 3/8 inch fracture was developed nearly perpendicular to the minimum principal stress.

COMMENTS

A larger hole size was used in an attempt to concentrate the energy of the propellant over a smaller hole length. This block had already been prepared with a 1/4-inch hole, and this hole was increased in diameter by drilling. Wander in the drill bit gave a double hole at the charge position invalidating the results.

TEST DB-3

TEST CONDITIONS

Maximum Horizontal Stress: 900 psi  
Minimum Horizontal Stress: 600 psi  
Vertical (Intermediate) Stress: 750 psi

Differential Stress: 300 psi  
Stress Ratio: 1.5:1

Hole Size: 3/8 inch  
Charge Configuration: 2.5 gm 4F black powder (1.125 in length)  
with single EBW initiation.

RESULTS

Two fractures were developed perpendicular to the minimum principal stress. These had lengths of 2 and 2.5 inches.

COMMENTS

In this test the charge size and density were increased. The result was to drive longer fractures than in Test DB-1, but the fracture geometry was still that of a hydraulic or slow rise time fracture.

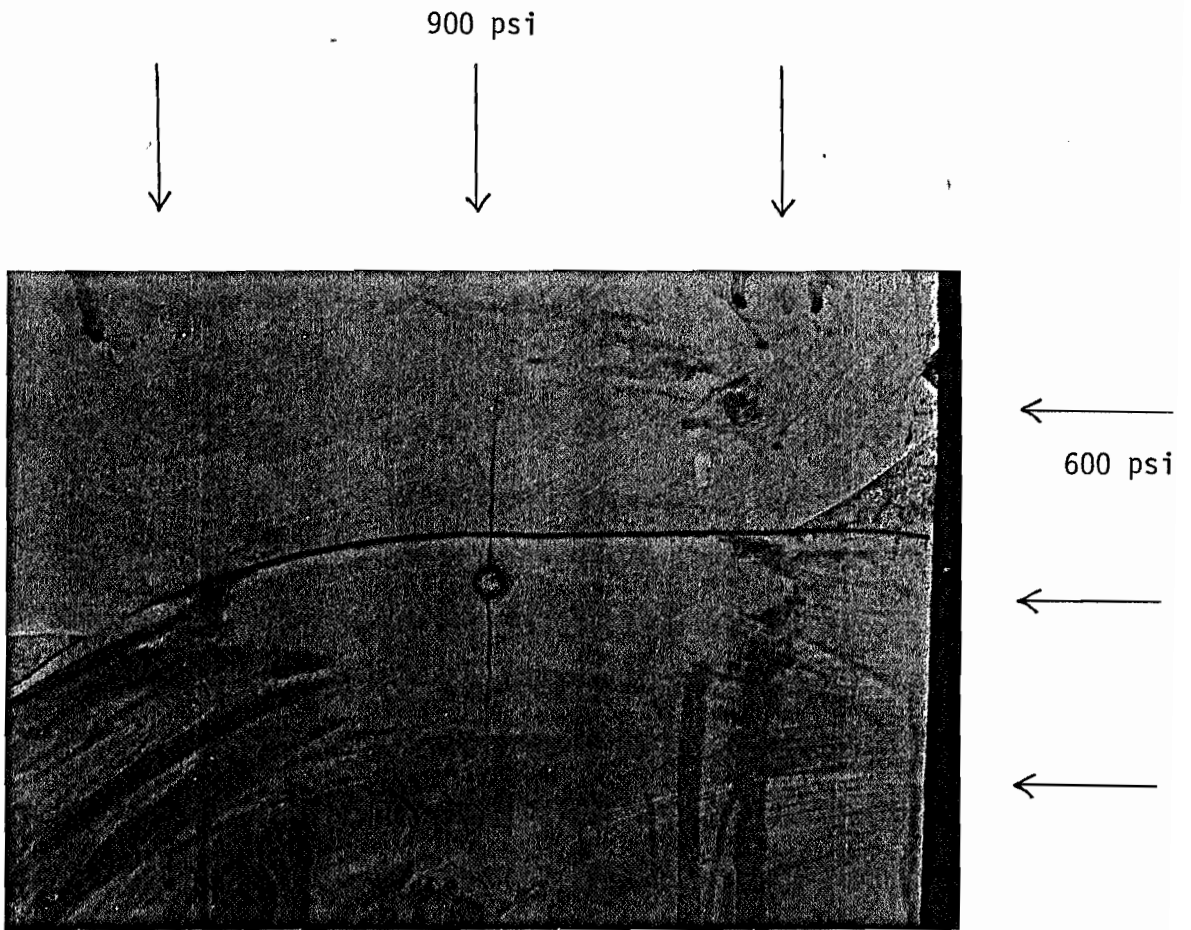


FIGURE B-2. Test DB-3.

## TEST DB-4

### TEST CONDITIONS

Maximum Horizontal Stress: 900 psi  
Minimum Horizontal Stress: 600 psi  
Vertical (Intermediate) Stress: 750 psi

Differential Stress: 300 psi  
Stress Ratio: 1.5:1

Hole Size: 3/8 inch  
Charge Configuration: 1.07 gm RDX in an aluminum RP-83 EBW detonator with 0.25 gm of 4F black powder. Total charge length was 1.25 inches. Single ended initiation with the EBW.

### RESULTS

Two fractures about 1 and 1.5 inches long were formed. These initiated at about 15 degrees to the perpendicular to the least principal stress, but curved rapidly to this perpendicular.

### COMMENTS

It appeared from this test that the faster rise time of the RDX was helping in driving fractures with orientations away from the perpendicular to the least principal stress, but that the charge size was insufficient to drive the fractures for a reasonable distance.

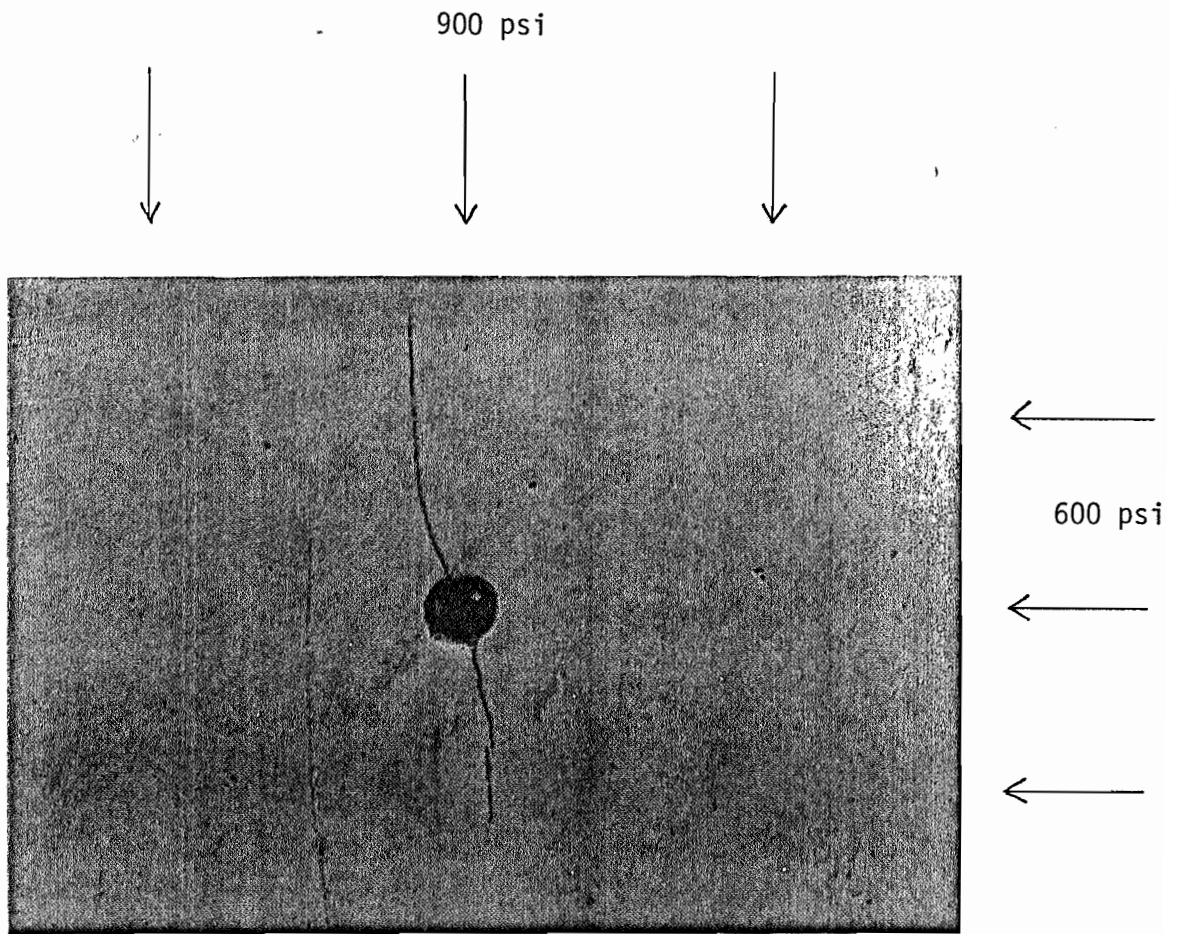


FIGURE B-3. Test DB-4.

## TEST DB-5

### TEST CONDITIONS

Maximum Horizontal Stress: 900 psi  
Minimum Horizontal Stress: 600 psi  
Vertical (Intermediate) Stress: 750 psi

Differential Stress: 300 psi  
Stress Ratio: 1.5:1

Hole Size: 3/8 inch  
Charge Configuration: 2.14 gm of RDX contained in two aluminum RP-83 EBW detonators with 0.25 gm 4F black powder. Total charge length was 2.5 inches. Initiation was at both ends simultaneously by the EBW detonators.

### RESULTS

Pulverization of the near hole region occurred. Numerous very short fractures were produced outside of this zone. Two long fractures were produced. These started at about 45 degrees to the minimum principal stress and curved slightly towards the maximum stress away from the hole. One fracture extended to the edge of the block, the other ran for about 3-1/4 inches.

### COMMENTS

This charge configuration appears capable of driving fractures which are not parallel to the maximum principal stress, and of driving them for a considerable distance. The orientation of the main fractures may be due to tensile reflections off the sides of the block.

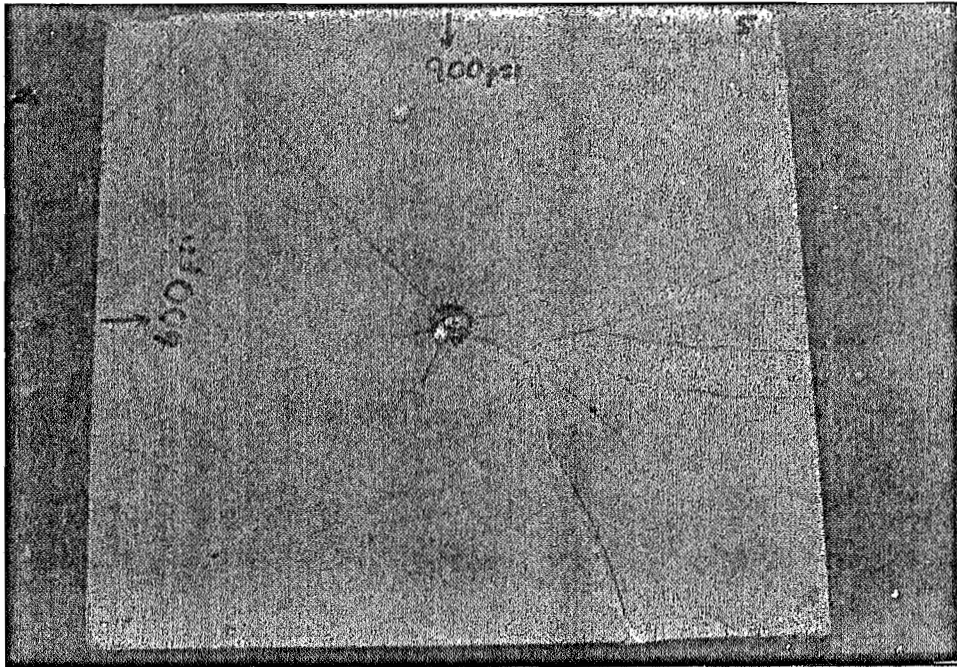


FIGURE B-4. Test DB-5.

## TEST DB-6

### TEST CONDITIONS

Maximum Horizontal Stress:	900 psi
Minimum Horizontal Stress:	600 psi
Vertical (Intermediate) Stress:	750 psi
Differential Stress:	300 psi
Stress Ratio:	1.5:1
Hole Size:	3/8 inch
Charge Configuration:	2.14 gm of RDX contained in two aluminum RP-83 EBW detonators with 0.25 gm 4F black powder. Total charge length was 2.5 inches. Initiation was at both ends simultaneously by the EBW detonators.

### RESULTS

Pulverization of the near hole region occurred at the level of the center of the charge. Numerous very short fractures were produced outside of this zone. At the level of the base of the charge (about 1 inch below the center) two fractures were observed sub-parallel to the minimum stress. One of these was about 3-3/4 inch long, the other about 3/4 inch long.

### COMMENTS

This test was intended as a duplication of Test 5. The results were somewhat different suggesting that the charges are not very reproducible, possibly because of slightly different initiation times of the two detonators. However, this charge configuration appears capable of driving fractures which are sub-parallel to the minimum principal stress, and of driving them for a considerable distance. It appears that the major propagation may be away from the center of the charge.

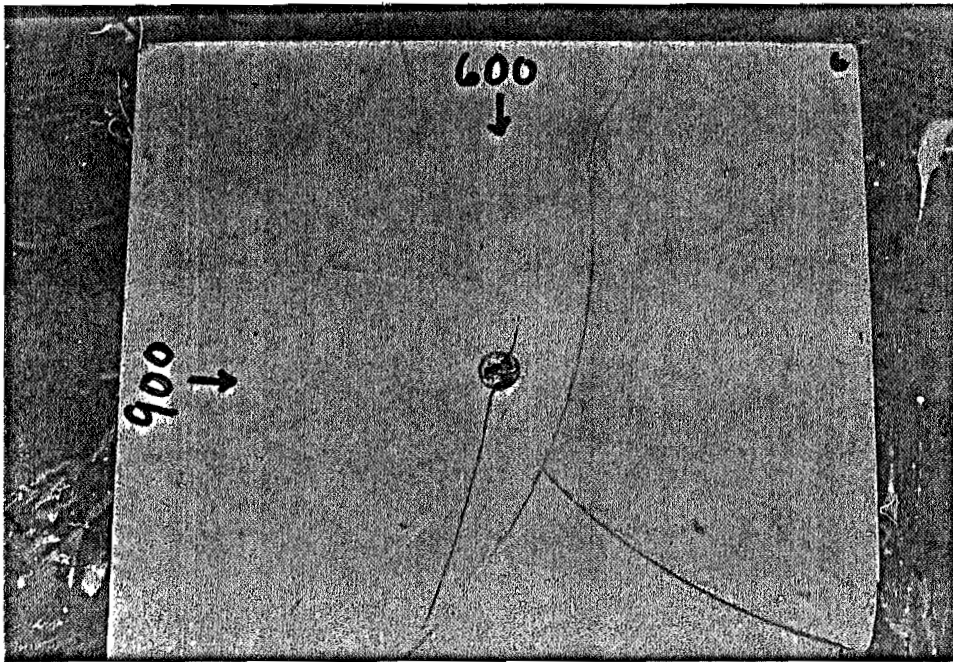


FIGURE B-5. Test DB-6.

## TEST DB-7

### TEST CONDITIONS

Maximum Horizontal Stress: 1200 psi  
Minimum Horizontal Stress: 600 psi  
Vertical (Intermediate) Stress: 900 psi

Differential Stress: 600 psi  
Stress Ratio: 2:1

Hole Size: 3/8 inch  
Charge Configuration: 2.14 gm of RDX contained in two aluminum RP-83 EBW detonators with 0.25 gm 4F black powder. Total charge length was 2.5 inches. Initiation was at both ends simultaneously by the EBW detonators.

### RESULTS

Pulverization of the near hole region occurred. Two primary fractures were produced, running sub-parallel to the maximum stress. These had lengths of 2-1/4 inches.

### COMMENTS

This test used the same charge configuration as Tests 5 and 6, but used a higher differential stress. It appears that under these more severe stress conditions this charge configuration is not capable of driving fractures which are not parallel to the maximum principal stress, and drives them for a shorter distance.

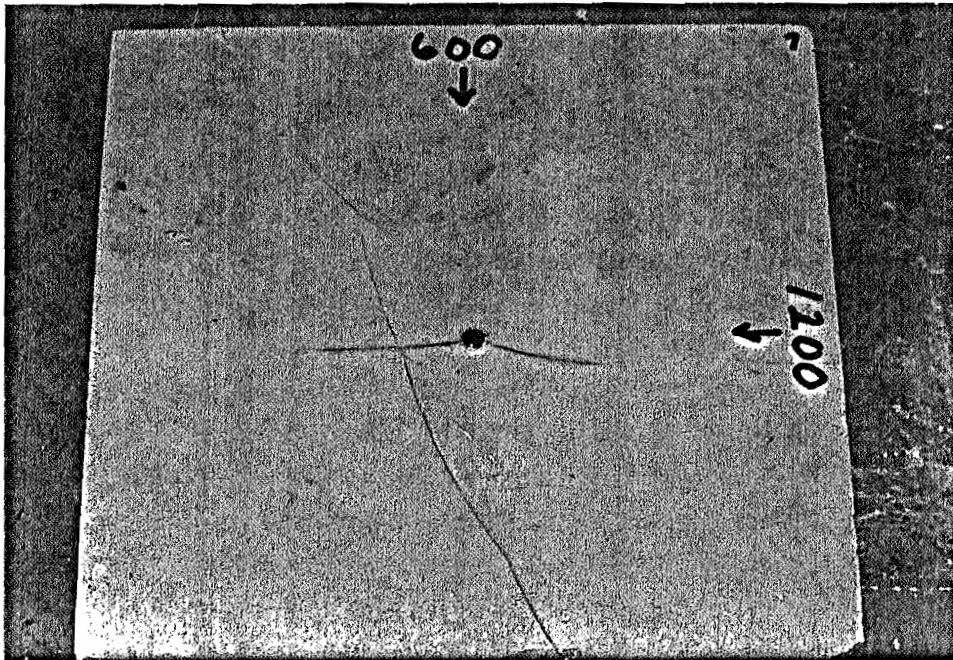


FIGURE B-6. Test DB-7.

SPLIT BLOCK TESTS

TABLE B-2.

## INTERACTION TESTS

TEST	STRESS (MIN, MAX, VERT) (PSI)	NATURAL FRACTURE ORIENTATION	COMMENTS
DS-1	600, 900, 750	Perpendicular	Two fractures @ 45 and 135 deg. intersected natural fractures. Did not cross.
DS-2	600, 900, 750	Perpendicular	Two/three fractures. One @ 15 deg. intersected natural fracture. Did not cross.
DS-3	600, 900, 750	60 degrees	Three fractures. One @ 45 deg. intersected natural fracture. Did not cross.
DS-4	600, 900, 750	60 Degrees	Pulverization and multiple short fraction. No intersection with natural fractures.

Note: All tests were conducted with 2.14 gm RDX and 0.25 gm 4F black powder in a 3/8 inch hole with double ended RP-83 EBW initiation.

Stresses are principal with minimum and maximum perpendicular to hole.

Natural and dynamic fracture orientation is angle of trace to relative to minimum principal stress axis.

## TEST DS-1

### TEST CONDITIONS

Maximum Horizontal Stress: 900 psi  
Minimum Horizontal Stress: 600 psi  
Vertical (Intermediate) Stress: 750 psi

Differential Stress: 300 psi  
Stress Ratio: 1.5:1

Natural Fractures: Perpendicular to the minimum stress.

Hole Size: 3/8 inch  
Charge Configuration: 2.14 gm of RDX contained in two aluminum RP-83 EBW detonators with 0.25 gm 4F black powder. Total charge length was 2.5 inches. Initiation was at both ends simultaneously by the EBW detonators.

### RESULTS

Pulverization of the near hole region occurred near the center of the charge. Thus, at the center, the 3/8-inch hole was enlarged to 3/4 inch. Outside of this zone numerous small fractures were seen, with five more major fractures up to about 3/4 inch long and fairly uniformly spaced. A single fracture at about sixty degrees to the least stress was seen in the block though this did not connect to the hole at this level, (Figure B-7A). Above the charge longer fractures are seen. Thus, at a level two inches above the center of the charge two primary fractures were produced. These fractures have orientations of about forty-five and one hundred thirty-five degrees to the least stress near the hole, and tend to curve towards the maximum stress away from the hole. The fractures tend to be discontinuous at this level, but presumably connect at other levels. One of these fractures intersects a simulated natural fracture, but does not cross it, (Figure B-7B).

### COMMENTS

As previously observed in the solid block tests it appears that the longer fractures occur at levels away from the center of the charge. The intersecting fracture approached the simulated natural fracture at about fifty degrees and did not cross. A small deposit of black powder residue was observed on the opposing face of the simulated fracture at the point where the intersection occurred.

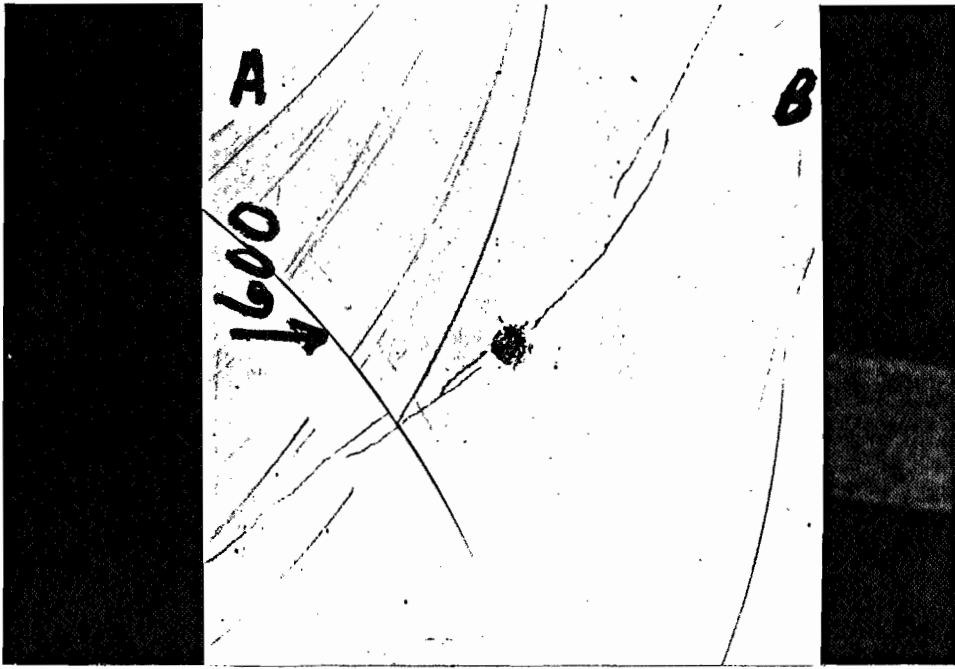


FIGURE B-7A. Test DS-1.



FIGURE B-7B. Test DS-1.

TEST DS-2

TEST CONDITIONS

Maximum Horizontal Stress: 900 psi  
Minimum Horizontal Stress: 600 psi  
Vertical (Intermediate) Stress: 750 psi

Differential Stress: 300 psi  
Stress Ratio: 1.5:1

Natural Fractures: Perpendicular to the minimum stress.

Hole Size: 3/8 inch  
Charge Configuration: 2.14 gm of RDX contained in two aluminum RP-83 EBW detonators with 0.25 gm 4F black powder. Total charge length was 2.5 inches. Initiation was at both ends simultaneously by the EBW detonators.

RESULTS

Pulverization of the near hole region occurred near the center of the charge. Thus, at the center, the 3/8-inch hole was enlarged to about 3/4 inch. Outside of this zone numerous small fractures were seen. Two major fractures occurred at about fifteen and one hundred thirty-five degrees to the least stress. The fifteen degree fracture intersected one of the simulated fractures. The one hundred thirty-five degree fracture did not intersect, and tended to curve towards the maximum stress direction further from the hole, (Figure B-8A). Below the charge, more long fractures are seen. Thus, at a level four inches below the center of the charge four primary fractures were produced. Two of these fractures are continuations of those seen at the higher level. The fifteen degree fracture appears very similar and again intersects the natural fracture. That at one hundred thirty-five degrees is similar to the higher level, but does not connect to the hole at this level. The two new fractures run at about ninety-five and one hundred seventy degrees to the maximum stress and have lengths of about 1-1/4 and 2-1/2 inches respectively, (Figure B-8B).

COMMENTS

The intersecting fracture approached the simulated natural fracture at about seventy to seventy-five degrees and did not cross. A small deposit of black powder residue was observed on the opposing face of the simulated fracture at the point where the intersection occurred.

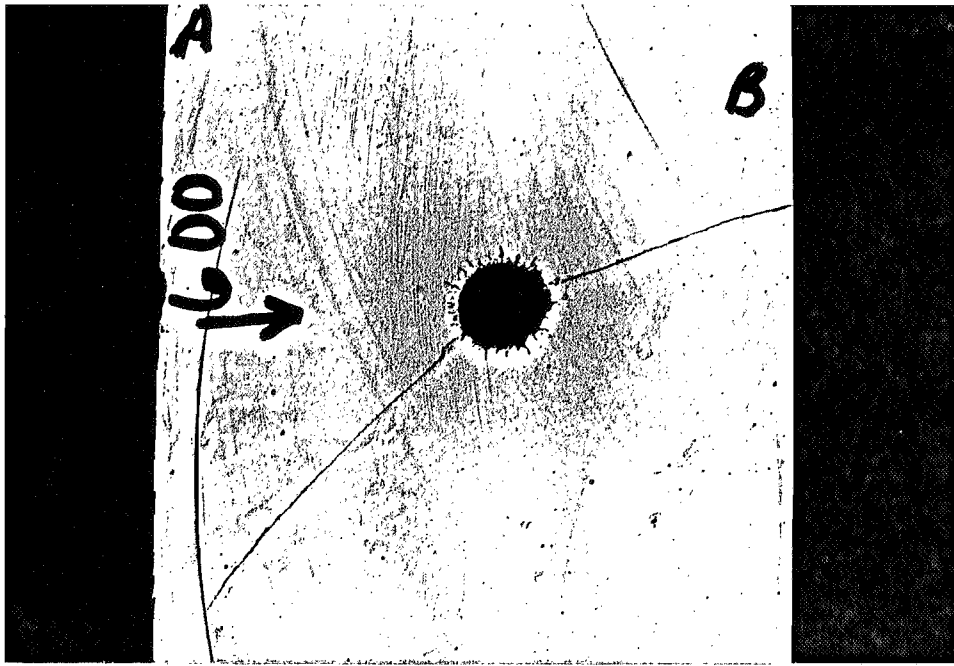


FIGURE B-8A. Test DS-2.

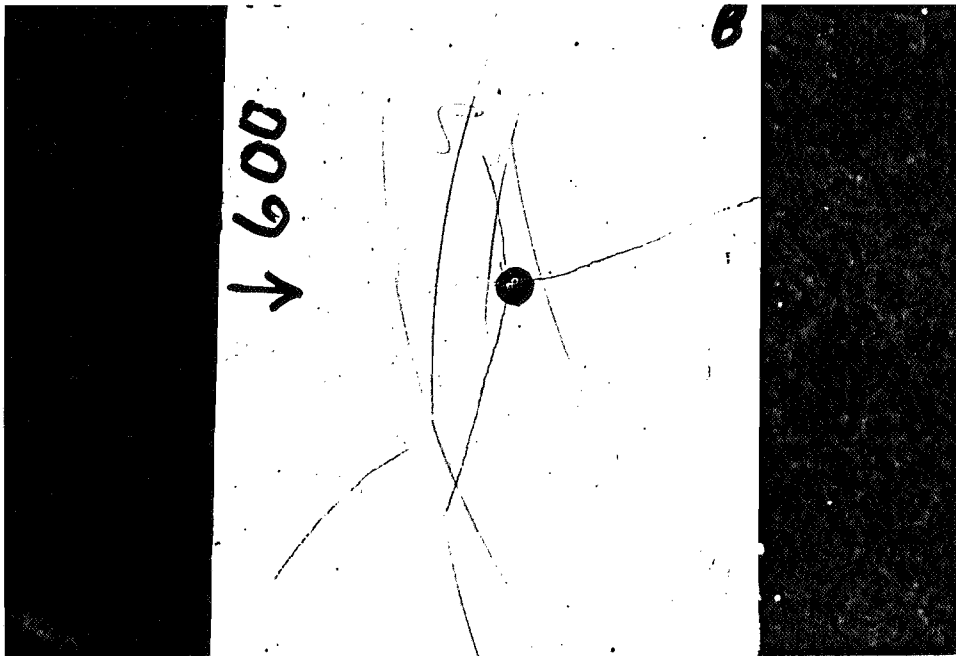


FIGURE B-8B. Test DS-2.

### TEST DS-3

#### TEST CONDITIONS

Maximum Horizontal Stress: 900 psi  
Minimum Horizontal Stress: 600 psi  
Vertical (Intermediate) Stress: 750 psi

Differential Stress: 300 psi  
Stress Ratio: 1.5:1

Natural Fractures: 60 degrees to the minimum stress.

Hole Size: 3/8 inch  
Charge Configuration: 2.14 gm of RDX contained in two aluminum RP-83 EBW detonators with 0.25 gm 4F black powder. Total charge length was 2.5 inches. Initiation was at both ends simultaneously by the EBW detonators.

#### RESULTS

Pulverization of the near hole region occurred near the center of the charge. Thus, at the center the 3/8-inch hole was enlarged to 3/4 inch. Outside of this zone numerous small fractures were seen. A single fracture occurred at about one hundred degrees to the least stress and extending through much of the block, though it did not connect to the hole at this level, (Figure B-9B). Above the charge, more longer fractures are seen. Thus, at a level three inches above the center of the charge three primary fractures were produced, (Figure B-9A). These fractures have orientations of about 105, 135 and 295 degrees to the least stress. The 105 degree fracture is a continuation of that seen at the center. At this level it reaches to the outside of the block, and tends to curve towards the maximum stress away from the hole. It does not intersect the natural fractures. The 295 degree fracture runs for about 2-1/2 inches and does not intersect any natural fractures. The 135 degree fracture intersects one of the simulated fractures, but does not cross it. Both the 105 and 135 degree fractures reached the top surface of the block and vented during the test.

#### COMMENTS

Again, it appears that the longer fractures occur at levels away from the center of the charge. The intersecting fracture approached the simulated natural fracture at about ninety degrees and did not cross. Again a small deposit of black powder residue was observed on the opposing face of the simulated fracture at the point where the intersection occurred.

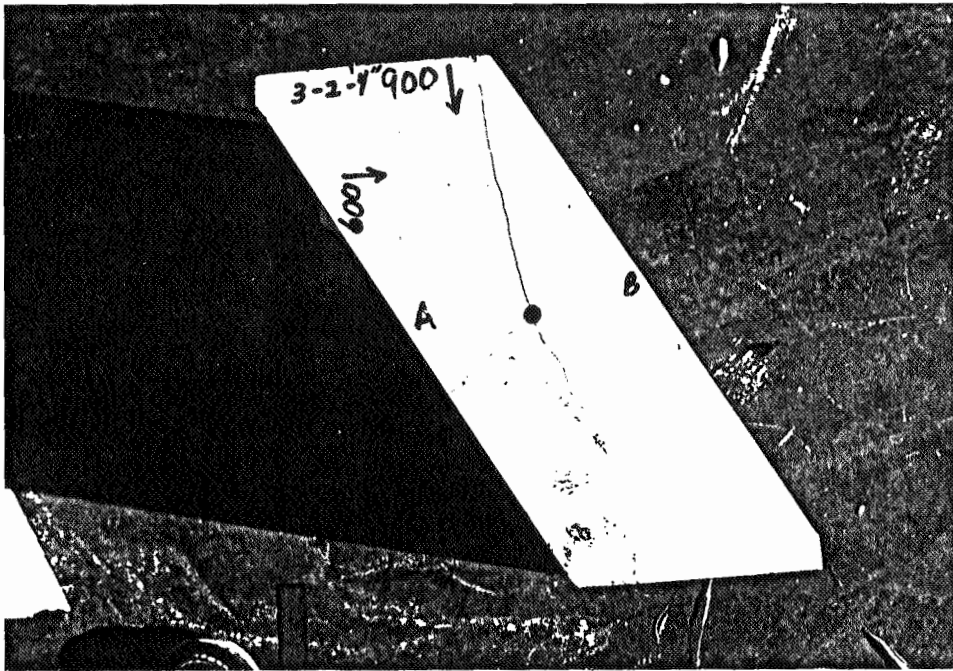


FIGURE B-9A. Test DS-3.

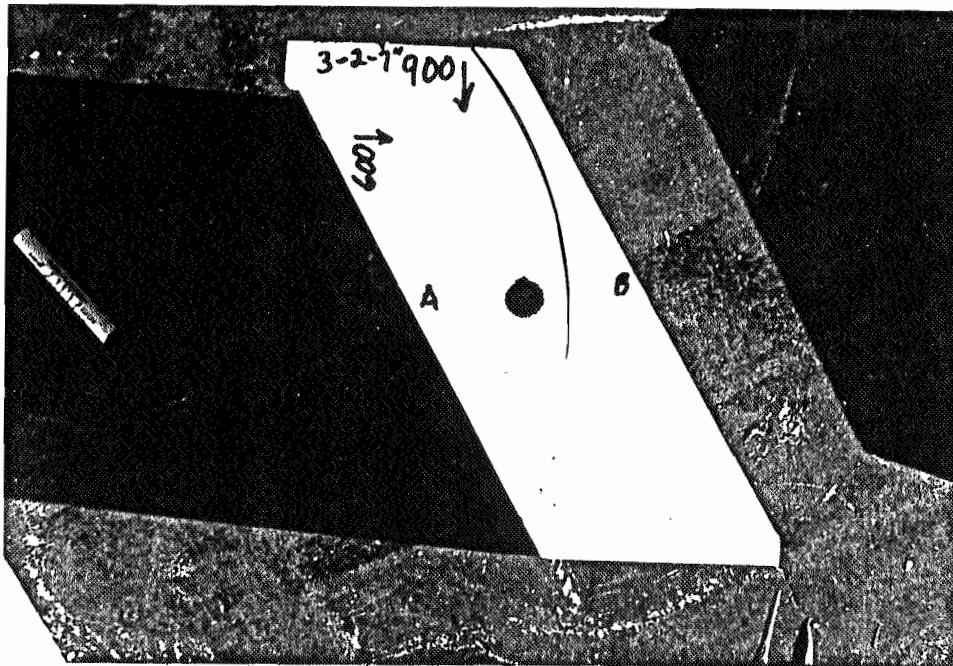


FIGURE B-9B. Test DS-3.

## TEST DS-4

### TEST CONDITIONS

Maximum Horizontal Stress: 900 psi  
Minimum Horizontal Stress: 600 psi  
Vertical (Intermediate) Stress: 750 psi

Differential Stress: 300 psi  
Stress Ratio: 1.5:1

Natural Fractures: 60 degrees to the minimum stress.

Hole Size: 3/8 inch  
Charge Configuration: 2.14 gm of RDX contained in two aluminum RP-83 EBW detonators with 0.25 gm 4F black powder. Total charge length was 2.5 inches. Initiation was at both ends simultaneously by the EBW detonators.

### RESULTS

Excessive pulverization of the near hole region occurred near the center of the charge. Thus, at a point one inch below the center, the 3/8-inch hole was enlarged to 7/8 inch. Outside of this zone numerous small fractures were seen, with five more major fractures up to about 1/2 inch long and fairly uniformly spaced. No longer fractures were seen at this or other levels.

### COMMENTS

Although this test was performed in the same way as the previous test it appears that the charge behaved differently giving more pulverization and no long fractures.

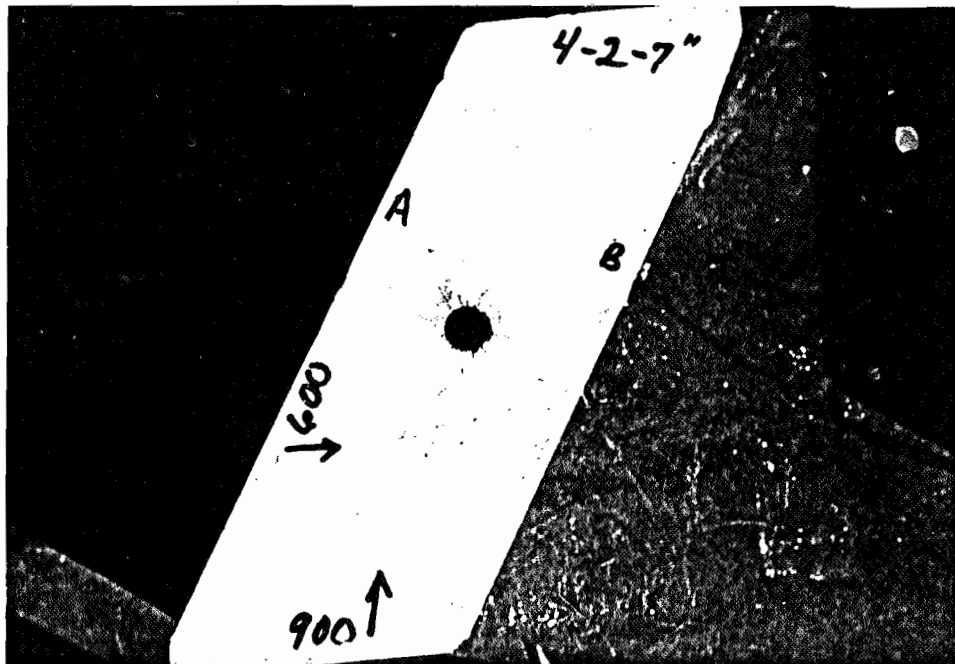


FIGURE B-10. Test DS-4.

## REFERENCES

- Babcock, E. A.: "Measurement of Subsurface Fractures From Dipmeter Logs," Am. Assoc. Petroleum Geol. Bull., v. 62, pp. 1111-1126, 1978.
- Bell, J. S.: "Northeast-Southwest Compressive Stress in Alberta: Evidence from Oil Wells," Earth Planet. Sci. Letters, v. 45, pp. 475-482, 1979.
- Berger, P. S.: "Late-Tectonic Extension Faulting in the Central Appalachians," Proc. Third Eastern Gas Shales Sym., pp. 51-61, 1979.
- Biot, M. A.: "Theory of Stress-Strain Relations in Anisotropic Viscoelasticity and Relaxation Phenomena," J. Applied Phys., v. 25, pp. 1385-1391, 1954.
- Blanton, T. L.: "An Experimental Study of Interaction Between Hydraulically Induced and Pre-existing Fractures," Proc. SPE/DOE UGR Sym., pp. 559-571, 1982.
- Blanton, T. L.: "The Relation Between Recovery Deformation and In Situ Stress Magnitudes," Proc. SPE/DOE Sym. on Low Perm., pp. 213-218, 1983a.
- Blanton, T. L.: unpublished work, 1983b.
- Blanton, T. L. and L. W. Teufel: "A Field Test of the Strain Recovery Method of Stress Determination in Devonian Shale," Proc. Eastern Regional Meeting, pp. 71-80, 1983.
- Blanton T. L. and L. W. Teufel: "In-Situ Stress Determination From Well-Bore Elongation," SPE/DOE 13877, Proc. SPE/DOE Symp. Low Perm. Reservoirs, p279-290, Denver, CO, 1985
- Blanton, T. L., S. A. Dishler and N. C. Patti: "Mechanical Properties of Devonian Shales from the Appalachian Basin," DOE/METC Report, 1981.
- Blanton T. L., S. A. Dishler, and N. C. Patti: "Mechanical Properties of Devonian Shales from the Appalachian Basin," Report to US DOE, Morgantown, 1981
- Brace, W. F., J. B. Walsh and W. T. Frangos: "Permeability of Granite under High Pressure," J. Geophys. Res., V 73, 2225-2236, 1968.
- Carroll, M. M.: "An Effective Stress Law for Anisotropic Deformation," J. Geophys. Res., v. 84, pp. 7510-7512, 1979.

- Carslaw, H. S. and J. C. Jaeger: "Conduction of Heat in Solids," Oxford Univ. Press, 1959.
- Chen, T. and P. W. Stagg: "Semilog Analysis of the Pulse-Decay Technique of Permeability Measurement," Soc. Pet. Eng. J., V --, 639-642, 1984.
- Clark J. A.: "Glacial Loading: A Cause of Natural Fracturing and a Control of The Present Stress State in Regions of High Devonian Shale Gas Production," Proc. SPE/DOE UGR Sym., pp. 87-97, 1982.
- Dean, C. S.: "Perspective on Devonian Shale Gas Exploration," Proc. SPE/DOE UGR Sym., pp. 237-241, 1980.
- Diment W. H., O. H. Muller and P. M. Lavin: " Basement Tectonics of New York and Pennsylvania as Revealed by Gravity and Magnetic Studies," Proc. "The Caledonides in the USA", p. 221-227, Virginia Polytechnic Inst. and State Univ., Blacksburg, VA, 1980
- Dietz R. S.: "Geosynclines, Mountains, and Continental Buliding," Sci. Am., V226, p. 30-38, 1972
- Dixon J. M. and Wilson T. H.: "The Parsons Cross Strike Structural Discontinuity Area for Fractured Gas Reservoirs," Proc. 3rd. Eastern Gas Shales Symp., 407-414, Morgantown, WV, 1979
- Engelder, T.: "Is There a Genetic Relationship Between Selected Regional Joints and Contemporary Stress Within the Lithosphere of North America?" Tectonics, v. 1, pp. 161-177, 1982.
- Evans, K. and T. Engelder: "Stress Ratio/Structure Studies and Testing in the Appalachian Basin," Unconventional Gas Recovery Contractor's Meeting, US DOE, Morgantown, WV, Nov 18-19, p. 6-8, 1986
- Engelder T. and P. Geiser: "On the Use of Regional Joint Sets as Trajectories of Paleostress Fields during the Development of the Appalachian Plateau, New York," J. Geoph. Res., V 85, p. 6319-6341, 1980
- Evans, M. A.: "Fractures in Oriented Devonian Shale Cores from the Appalachian Basin, Vol. I, DOE/METC Report, 1980.
- Fourney W. L., D. B. Barker and D. C. Holloway: "Model Studies of Well Stimulation Using Propellant Charges," Int. J. Rock Mech. Min. Sci., V20, p. 91-101, 1983
- Friedman, M. and H. C. Heard: "Principal Stress Ratios in Cretaceous Limestones from the Texas Gulf Coast," Am. Assoc. Petroleum Geol. Bull., v. 58, pp. 71-78, 1974.
- Gangarao, H. V. S., N. Rojanavanich and R. N. Velaga: "In Situ Stress Determination of Devonian Shales," DOE/METC Report, 1981.

- Gay, S. P.: "Basement Control of Lineaments, Faulting, Structure & Lithology of Petroleum Bearing Rocks in the Midcontinent, USA," Remote Sensing/Lineament Applications for Energy Extraction Workshop, 1983.
- Gold D. P., R. R. Parizek and S. S. Alexander: "Analysis and Applications of ERTS-1 Satellite Data for Regional Geologic Mapping," Symp. on Significant Results Obtained from the Earth Resources Technology Satellite-1, p. 231-246, NASA, Washington, DC, 1973
- Gwinn, W. E.: "Thin-Skinned Tectonics in the Plateau and Northwestern Valley and Ridge Provinces of the Central Appalachian," Geol. Soc. Am. Bull., v. 75, pp. 863-900, 1964.
- Haimson, B. C.: "The Hydraulic Fracturing Stress Measuring Method and Recent Field Results," IJRMMS&GA, v. 15, pp. 167-178, 1978.
- Haimson, B. C.: "Deep Stress Measurements in Three Ohio Quarries and Their Comparison to Near-Surface Tests," 23rd Sym. Rock Mech., pp. 190-202, 1982.
- Haimson, B. C. and C. Fairhurst: "Hydraulic Fracturing in Porous-Permeable Materials," J. Pet. Tech., pp. 811-817, July, 1969.
- Handin, J.: "On the Coulomb-Mohr Failure Criterion," Jour. Geophys. Res., v. 74, pp. 5343-5347, 1969.
- Hennington, W. M.: "Unconventional Exploration for Natural Fractures," Proc. SPE/DOE UGR Sym., pp. 265-270, 1980.
- King P. B., "Tectonic Map of North America," USGS, 1969
- Klyoncu R. S., W. G. Coppins, D. T. Hooie and M. J. Snyder: "Characterization and Analysis of Devonian Shale: I. Physical Characterization," Proc. 1st. Eastern Gas Shales Symp., p230-258, 1977.
- Komar, C. A. and T. Bolyard: "Structure/Stress Ratio Relationships Within the Appalachian Basin," METC-EGSP Map Series, 1981.
- Kowalik W. S., "Use of LANDSAT-1 Imagery in the Analysis of Lineaments in Pennsylvania," M.S. Paper, Penn. State Univ., University Park, PA, 1975
- Kulander B. R., S. L. Dean, R. E. Williams: "Correlations between Outcrop Fractures, Geophysics and Rome Trough Structure in Kanawha County, West Virginia," Proc. 1st. Eastern Gas Shales Symp., Morgantown, WV, p.484 - 495, 1978
- Lavin, P. M., D. L. Chaffin and W. F. Davis: "Major Lineaments and the Lake Erie-Maryland Crystal Block," Tectonics, v. 1, pp. 431-440, 1982.

- Lee, S. C., S. H. Advani, and J. K. Lee: "Thermoviscoelastic Finite Element Model Simulations Associated with Underground Coal Conversion," Proc. 25th Rock Mech., pp. 248-260, 1984.
- Lindner, E. N. and J. A. Halpern: "In Situ Stress in North America: A Compilation," IJRMMS&GA, v. 15, pp. 183-203, 1978.
- McKetta, S. F.: "Earth Stress Relationships in the Appalachian Basin," SPE/DOE UGR Sym., pp. 259-261, 1980.
- Obert, L. and W. I. Duvall: "Rock Mechanics and the Design of Structures in Rock," John Wiley, New York, 1967.
- Pees S. T.: "Subsurface Anomalies Expressed as Lineaments in the Northwest Pennsylvania Portion of the Appalachian Plateau," Workshop on Remote Sensing/Lineament Applications for Energy Extraction (Howard JF, Komar CA and Cooper IM, Editors), Morgantown, WV, p. 53-62, 1984
- Peng, S. S., W. H. Su and K. Matsuki: "Development of Ultrasonic Technique for Measuring In Situ Stresses at Great Depth," DOE/METC Report, 1980.
- Plumb R., " ": submitted to J. Geophys. Res., 1986  
Cliffs, 1981
- Rogers J.: "Mechanics of Appalachian Foreland Folding in Pennsylvania and West Virginia," Bull. Am. Assoc. Pet. Geol., V 47, p. 1527-1536, 1963.
- Schapery, R. A.: "Viscoelastic Behavior and Analysis of Composite Materials," In Composite Materials, Mechanics Volume, Academic Press, 1974.
- Scheidegger, A. E.: "Comment On: Is There a Genetic Relationship Between Selected Regional Joints and Contemporary Stress Within the Lithosphere of North America," Tectonics, v. 1, pp. 463-464, 1982.
- Science Applications Inc.: "Multiple Well Testing in Meigs County, Ohio," Report to GRI, 1984
- Shaffer, R. J., R. K. Thorpe, A. R. Ingraffea and F. E. Heuze: "Numerical and Physical Studies of Fluid-Driven Fracture Propagation in Jointed Rock," Proc. SPE/DOE/GRI Unconventional Gas Recovery Symposium, May, 1984.
- Shumaker, R. C.: "A Detailed Geologic Study of Three Fractured Devonian Shale Gas Fields in the Appalachian Basin," SPE/DOE UGR Sym., pp. 9-13, 1982.

- Simmons, G., R. W. Siegfried and M. Feves: "Differential Strain Analysis: A New Method of Examining Cracks in Rocks," Jour. Geophys. Res., v. 79, pp. 4383-4385, 1974.
- Stearns, D. W.: "Certain Aspects of Fracture in Naturally Deformed Rocks," NSF Advanced Science Seminar in Rock Mechanics, Boston College, Boston, MA, p. 97-116, 1968
- Stearns D. W. and M. Friedman: "Reservoirs in Fractured Rock," Am. Assoc. Pet. Geol. Mem. No.16,82-106, 1972.
- Stearns, D. W.: "Certain Aspects of Fracture in Naturally Deformed Rocks," NSF Advanced Science Seminar in Rock Mechanics, Boston College, Boston, MA, p. 97-116, 1968
- Stearns D. W. and M. Friedman: "Reservoirs in Fractured Rock," Am. Assoc. Pet. Geol. Mem. No.16,82-106, 1972.
- Strickland, F. G. and N. K. Ren: "Use of Differential Strain Curve Analysis in Predicting In Situ Stress State for Deep Wells," 21st Sym. Rock Mech., 1980.
- Swols, H. F., R. Lingle and J. M. Thomas: "Determination of the Strain Relaxation and Their Relation to Subsurface Stresses in Devonian Shale," Report to Columbia Gas, 1977.
- Teufel, L. W.: "Strain Relaxation Method for Predicting Hydraulic Fracture Azimuth from Oriented Core," Proc. SPE/DOE Low Perm. Sym., pp. 81-86, 1981.
- Teufel, L. W.: "Determination of In Situ Stresses from Anelastic Strain Recovery Measurements of Oriented Core," SPE/DOE Low Perm., Sym., 1983a.
- Teufel, L. W., and N. R. Warpinski: "Determination of In Situ Stresses from Anelastic Strain Recovery Measurements of Oriented Core: Comparison of Hydraulic Fracture Stress Measurements in the Rollins Sandstone, Piceance Basin, Colorado," Proc. 25th Rock Mech. Sym., pp. 176-186, 1984.
- Teufel, L. W.: personal communications, 1983b.
- Voight, B.: "Determination of the Virgin State of Stress in the Vicinity of a Borehole from Measurements of a Partial Anelastic Strain Tensor in Drill Cores," Felsmechanik u. Ingenieurgeol., v. 6, pp. 201-215, 1968.
- Walls, J. D., A. M. Nur and T. Bourbie: "Effects of Pressure and Partial Water Saturation on Gas Permeability in Tight Sands: Experimental Results," J. Pet. Tech., V ---, 930-936, 1982.
- Williams, R. T., J. E. Ruotsala, J. J. Kudla et al.: "Shallow Seismic Investigations of Devonian Shale Gas Production," DOE/METC Report, 1982.

Yang J.P. and Y. P. Aggarwal: "Seismotectonics of Northeastern United States and Adjacent Canada," J. Geophys. Res., V 86, pp 4981-4998, 1981

Zoback, M. L. and M. Zoback: "State of Stress in the Coterminous United States," Jour. Geophys. Res., v. 85, pp. 6113-6156, 1980.

Zoback M. and M. L. Zoback: "Preliminary Stress Map of North America," USGS Open File, 1985